Higgs production via weak boson fusion in the Standard Model and the MSSM

PALMER, SOPHY,ELIZABETH

Higgs production via weak boson fusion in the Standard Model and the MSSM

Sophy Palmer
Institute for Particle Physics Phenomenology, Durham University

A dissertation submitted to Durham University
for the degree of Doctor of Philosophy

Abstract

Higgs production via weak boson fusion (WBF) is an interesting and important process at both the LHC and a future linear collider. Not only is it a possible Higgs discovery channel, but it also allows us to study the properties of the Higgs boson and the mechanism of electroweak symmetry breaking. In this thesis this process is studied in detail for both the LHC and a future linear collider.

Results for light Higgs production via vector boson fusion at a linear collider, taking the Higgsstrahlung contribution into account, are obtained in the (s)fermion sector of the Standard Model and the MSSM.

Complete one loop results for weak boson fusion at the LHC in the Standard Model are presented. These include the effects of photon radiation and the full virtual electroweak corrections, as well as the QCD corrections (the latter are well known in the literature and have been taken from the code `VBFNLO` in this work). The electroweak corrections are found to be as important as the QCD corrections after the application of appropriate cuts – they are $\sim \mathcal{O}(-5\%)$ in the Higgs mass range of 100–200 GeV.

We present the dominant supersymmetric one loop corrections to neutral Higgs production, in the general case where the MSSM includes complex phases. These results are supplemented by all one loop corrections of Standard Model type and by the propagator type corrections from the Higgs sector of the MSSM, taking the dominant two loop contributions into account. In this way the most complete available result for weak boson fusion Higgs production in the MSSM is achieved. In the decoupling region, $M_A \gg M_Z$, where the light MSSM Higgs boson becomes Standard Model like, the difference between the MSSM loop corrections and those in the Standard Model (for an equivalent Higgs

mass) are, as expected, relatively small – generally $\mathcal{O}(-0.5\%)$. Larger SUSY loop corrections occur for the light Higgs in the non-decoupling regime – in the M_h^{max} scenario we see differences of $\sim \mathcal{O}(-5\%)$ between the total SM and MSSM loop corrections, and in the CPX scenario, differences of $\mathcal{O}(-5\%)$ are seen in the (s)fermion sector. In some regions of parameter space, production of the heavy MSSM Higgs boson is dominant, and in these regions loop corrections range between $\sim \pm 5\%$.

Our results have been implemented into the public Monte Carlo program `VBFNLO`, which should serve as a useful tool for performing experimental analyses. We make use of an effective Higgs coupling as a simple (and computationally efficient) method of including the Higgs vertex corrections, while the Standard Model type box and pentagon diagrams are incorporated in the standard way using squared matrix elements.

Finally, we also present parton level studies of (s)fermion corrections to Z boson production via weak boson fusion, in both the Standard Model and the MSSM. This process has the potential to be used in order to "calibrate" WBF Higgs production. Corrections to Z production are generally smaller than those to Higgs production, and are typically $\sim -0.8\%$.

Declaration

I declare that this thesis has not been submitted for another degree at this or any other university. The work in this thesis was funded by an STFC studentship, and the copyright of this work rests with the author.

Sophy Palmer
August 2009

Acknowledgements

Firstly, of course, I would like to thank my supervisor, Professor Georg Weiglein, for all of his help and support. I feel that special thanks are necessary for his acceptance of my deep and irrational suspicion of charge renormalisation, and for going over it with me just as patiently the fourteenth time as the first! I am also very grateful to Terrance Figy, for his invaluable help in understanding the mysteries of `VBFNLO`.

I have enjoyed my time at the IPPP enormously, and would like to thank everyone for providing such a brilliant place to work. My office mates have my thanks for providing me with help and entertainment, and for never once throwing things at me when I wailed "It's infinite *again*!" On that note, special thanks go to Karina Williams and Alison Fowler, for innumerable checks and re-checks of odd results, and for many hours commiserating over the vagaries of computers.

All of my friends in Durham have my gratitude for being so wonderful – especially Callum and Vicky for discussing *Merlin* just as seriously as supersymmetry, for Saturday nights of *Jonathan Creek* and Shakespeare, and of course for a goodly number of trebuchets. I feel that Allen deserves extra thanks for his helpful advice about sharks, tigers and ducks. I would also like to thank all of my many housemates for countless delicious meals, landing parties and exciting adventures, and especially Jon, for cheerfully rescuing me from various monsters on a daily basis and keeping me sane.

I'd like to mention my friends who are now scattered around the globe – especially Sarah, Giles and Lel – for putting up with my long silences when I'm buried in work, and for reminding me that there is a world outside of physics and Durham, and it's actually quite a nice place to visit! And of course, thanks go to Jane for many Book Buying Days (even if she is a terrible influence).

Finally, thanks go to my family. To my baby brother, for random text messages about the nature of light, and to my parents, for everything.

Contents

"While I'm still confused and uncertain, it's on a much higher plane, d'you see, and at least I know I'm bewildered about the really fundamental and important facts of the universe."

— Terry Pratchett

Chapter 1

Introduction

"It's very hard talking quantum mechanics in a language originally designed to tell other monkeys where the ripe fruit is."
— Terry Pratchett

1.1 Standard Model

The Standard Model (SM) is a quantum field theory that describes the fundamental particles in nature and the way in which they interact. Over the last four decades it has been rigorously tested in various collider experiments around the world, and has been confirmed to an astonishing degree of accuracy. It contains the matter fields – three generations of quarks and leptons. It also describes three fundamental forces – the electromagnetic force, the weak force and the strong force, which are carried by the (bosonic) exchange particles, the photon γ, the $W^{\pm}$ and Z bosons, and the gluon g respectively.

Strong interactions between quarks and gluons are described by Quantum Chromodynamics (QCD), which was developed in the 1970s [1–3]. The electromagnetic force is described by Quantum Electrodynamics (QED) – the manner in which photons and matter interact. Both QCD and QED rely on the principle of local gauge invariance. The Lagrangians describing free quarks and leptons are invariant under global phase rotations for the gauge groups $SU(3)_C$ and $U(1)_{em}$ respectively – i.e. under transformations of the type $\psi \rightarrow e^{i\theta}\psi$ where ψ is a spinor representing a fermion field and θ a real

number. To obtain the Lagrangians for QCD and QED, these global gauge invariances are promoted to local gauge invariances – i.e. the Lagrangians are forced to be invariant under the *local* transformation $\psi \rightarrow e^{i\theta(x)}\psi$, where the phase θ is now a function of the space-time point x. This is achieved by introducing the massless gauge bosons g and γ which also undergo gauge transformations such as $A_\mu \rightarrow A_\mu - \frac{1}{e}\partial_\mu\theta$, adding kinetic terms for the gauge bosons to the Lagrangian, and exchanging the partial derivatives acting on the fermion fields for covariant derivatives.

The Standard Model also contains the Glashow-Weinberg-Salam theory of electroweak interactions [4–6]. The symmetry $SU(2)_L \times U(1)_Y$ is broken at the weak scale by the Higgs mechanism leaving $U(1)_{em}$ as an unbroken gauge group.

1.1.1 The Higgs mechanism

The principle of local gauge invariance works very well for the strong and electromagnetic interactions. If we consider the weak force, however, we encounter problems as the gauge fields – the $W^\pm$ and Z bosons – are massive, but their mass terms in the Lagrangian are not invariant under local gauge transforms. We therefore need to consider spontaneous electroweak symmetry breaking, and in particular the Higgs mechanism [7–9], to give masses to the weak gauge bosons. The Higgs sector of the Lagrangian consists of the SU(2) complex doublet field ϕ

$$\begin{aligned} \phi &= \frac{1}{\sqrt{2}} \begin{pmatrix} \phi_1 + i\phi_2 \\ \phi_3 + i\phi_4 \end{pmatrix} \\ \text{where } \phi^\dagger\phi &= \frac{1}{2}\left(\phi_1^2 + \phi_2^2 + \phi_3^2 + \phi_4^2\right) \end{aligned} \tag{1.1}$$

with the scalar part of the Lagrangian

$$\mathcal{L} = \frac{1}{2}\left(\partial_\mu\phi\right)^\dagger\left(\partial^\mu\phi\right) - \mu^2\phi^\dagger\phi - \lambda\left(\phi^\dagger\phi\right)^2 \tag{1.2}$$

This is manifestly invariant under the global U(1) phase transformations, $\phi \rightarrow e^{i\theta}\phi$. We can make this invariant under local gauge transformations in the usual way by introducing the massless gauge fields, W_a^μ (where $a = \{1, 2, 3\}$) and B^μ, which transform such that the derivative below is covariant (note that τ_a are the $SU(2)_L$ generators, equal

to half of the Pauli matrices)

$$D_\mu = \partial_\mu - ig_2\frac{\tau_a}{2}W_\mu^a - ig_1\frac{1}{2}B_\mu \tag{1.3}$$

This leads us to the Lagrangian for the Higgs and gauge boson fields[1]

$$\begin{aligned}\mathcal{L} &= \left(\left[\partial_\mu - ig_2\frac{\tau_a}{2}W_\mu^a - ig_1\frac{1}{2}B_\mu\right]\phi\right)^\dagger\left(\left[\partial_\mu - ig_2\frac{\tau_a}{2}W_\mu^a - ig_1\frac{1}{2}B_\mu\right]\phi\right)\\ &\quad -\mu^2\phi^\dagger\phi - \lambda\left(\phi^\dagger\phi\right)^2 - \frac{1}{4}W_{\mu\nu}^a W_a^{\mu\nu} - \frac{1}{4}B_{\mu\nu}B^{\mu\nu}\end{aligned} \tag{1.4}$$

The field strengths are given by (summation over repeated indices is understood)

$$\begin{aligned}W_{\mu\nu}^a &= \partial_\mu W_\nu^a - \partial_\nu W_\mu^a + g_2\epsilon^{abc}W_\mu^b W_\nu^c\\ B_{\mu\nu} &= \partial_\mu B_\nu - \partial_\nu B_\mu\end{aligned} \tag{1.5}$$

We can now define new fields, H and ξ_a, that enable us to expand around a particular ground state that lies on a minimum of the potential (since the symmetry of the Lagrangian is a continuous symmetry, the minima lie on a circle). We choose a particular minimum along this circle, giving the Higgs doublet a vacuum expectation value (VEV), v.

$$\begin{aligned}\phi &= \frac{1}{\sqrt{2}}\exp\left[i\frac{\tau_a\cdot\xi^a}{v}\right]\begin{pmatrix}0\\ v+H\end{pmatrix}\\ \text{where } v^2 &= -\frac{\mu^2}{\lambda}\end{aligned} \tag{1.6}$$

This results in a Lagrangian describing a scalar particle (H) with mass $M_H^2 = -2\mu^2$, massless Goldstone bosons ξ_a and the couplings between the scalar, the Goldstones and the gauge bosons. By performing a gauge transformation to a unitary gauge, we can transform the Goldstone bosons so that $\xi_a^{'} = 0$. We also define the fields $W_\mu^\pm$ and Z_μ (the mass eigenstate fields) in terms of our original gauge fields $W_\mu^{1,2,3}$ and B_μ.

$$\begin{aligned}W_\mu^\pm &= \frac{1}{\sqrt{2}}\left(W_\mu^1 \mp iW_\mu^2\right)\\ Z_\mu &= \frac{g_2W_\mu^3 - g_1B_\mu}{\sqrt{g_2^2+g_1^2}}\end{aligned} \tag{1.7}$$

[1]Note that g_1 and g_2 are the coupling constants of $U(1)_Y$ and $SU(2)_L$.

We are then left with

$$\begin{aligned}\mathcal{L} &= \left(\frac{1}{2}(\partial_\mu H)(\partial^\mu H) - \lambda v^2 H^2\right) + \left(\frac{1}{4}g_2^2 v^2 W_\mu^+ W_-^\mu + \frac{1}{8}\left(g_1^2+g_2^2\right)v^2 Z_\mu Z^\mu\right) \\ &+ \left(\frac{1}{2}g_2^2 v H W_\mu^+ W_-^\mu + \frac{1}{4}\left(g_1^2+g_2^2\right)v H Z_\mu Z^\mu\right. \\ &+ \frac{1}{4}g_2^2 H^2 W_\mu^+ W_-^\mu + \frac{1}{8}\left(g_1^2+g_2^2\right)H^2 Z_\mu Z^\mu \\ &\left. -\lambda v H^3 - \frac{1}{4}\lambda H^4\right) + ... \end{aligned} \tag{1.8}$$

This Lagrangian describes a massive scalar particle, H, the massive gauge bosons, $W_\mu^\pm$ and Z_μ, and their interactions (the dots signify the expansion of the gauge boson field strength tensors).

The original complex doublet has four degrees of freedom. Three of these are "eaten", giving masses to the three gauge bosons, $W^\pm$ and Z, and we are left with one degree of freedom – the Higgs boson H. In the Standard Model the Higgs mechanism is thought to be responsible not only for giving masses to the gauge bosons, as above, but also for making the fermions massive. Initially, the fermions are considered to be massless, with Yukawa couplings to the Higgs. When the Higgs is "shifted", by the vacuum expection value v (i.e. by spontaneous symmetry breaking), the Yukawa term splits into two pieces – one which describes the Higgs–fermion interaction and one which is a mass term for the fermion.

The Higgs boson is the "missing piece" of the Standard Model – the only particle in the SM that we have not produced and studied experimentally. Thus far, we have only been able to put bounds on its properties. The Large Electron Positron collider (LEP) set a lower mass limit of 114.4 GeV (at the 95% confidence level) [10], and searches are continuing to be carried out at the Tevatron [11], which have already excluded a Standard Model Higgs with a mass between 160 GeV and 170 GeV at the 95% confidence level. Later this year, the Large Hadron Collider (LHC) should switch on and join the search.

There are several excellent text books and introductions to the Standard Model and gauge field theory. Ref. [12] provides a very basic, pedagogical introduction to elementary particle physics, and the Higgs Hunter's Guide [13] gives a good introduction to Higgs physics. More in-depth, technical and recent texts on the Standard Model and electroweak symmetry breaking include, for instance, Ref. [14–16].

1.1.2 Problems with the Standard Model

Despite its numerous successes, it is generally agreed that the Standard Model is not a "Theory of Everything", as it includes only three of the four fundamental forces – it does not include gravity. The Standard Model is instead thought to be an extremely accurate low energy effective theory, valid at the energy scales that we commonly observe and have been able to study in collider experiments. There are a large number of problems with the Standard Model, all of which hint that there is some deeper, high-energy theory that provides a more complete description of the particle content of the Universe. For one thing, the Standard Model provides no candidate for a dark matter particle (let alone any explanation of dark energy) and thus – for all its accuracy – it can only explain approximately 5% of the Universe's content (see [17–19] and references therein). The coupling constants for the strong, weak and electromagnetic forces do not (quite) unify at high energies in the Standard Model [20]. While CP-violation through the CKM matrix (which describes quark mixing) can account for a small amount of the observed matter-antimatter asymmetry, no other mechanism in the Standard Model exists in order to explain the remainder (see, e.g. [21], and references therein).

For our purposes, however, the most pertinent problem with the Standard Model is the so-called hierarchy problem. Since the Standard Model is a low energy effective theory, we must introduce a cut-off scale where gravity becomes important, the Planck scale. When calculating the one loop corrections to the Higgs mass from fermion diagrams, this Planck scale enters the calculation and quadratic divergences emerge. We can, of course, adjust our renormalisation procedures in order to eliminate these divergences, but the parameters involved then need to be carefully fine tuned in order to result in loop corrections leading to a weak scale Higgs mass, rather than a Planck scale Higgs mass, and this is thought to be unnatural.

1.2 Supersymmetry

Supersymmetry (SUSY) is one of the most popular extensions to the Standard Model. The underlying principle is that there is a symmetry between bosons and fermions [22–24][2]. Theoretically, supersymmetry is a very attractive idea, as it is a uniquely non-trivial extension of the Poincaré group (which describes external symmetries, such as

[2]For an excellent short history (and motivation) of SUSY, see [25].

gravity) to include a Lie algebra (which describes the internal symmetries exploited in quantum field theory) [26].

Supersymmetry predicts that every SM particle has a superpartner – SM bosons have fermionic partners, and SM fermions have bosonic partners. Since we have not observed any of the new SUSY particles, we know that supersymmetry must be broken – if it were not, the superpartners would have the same mass as their SM counterparts, in which case we would have already seen them in our experiments. The supersymmetric particles differ from their partners in two properties – their spin is different by one half, and their mass is larger. All other quantum numbers are the same.

Practically, supersymmetry has many advantages as well. One of the main attractions of supersymmetry is that it provides a solution to the hierarchy problem described above. The quadratic divergence involved in calculating corrections to the Higgs mass is cancelled out by a "new" divergence from the additional diagrams that are present in a supersymmetric theory – the divergences originating from top quark loops, for example, are cancelled by divergences from stop (the superpartner of the top quark) loops – see Fig. 1.1.

Additionally, supersymmetry introduces new sources of CP violation, and allows unification of the force coupling constants [20]. Also, since we generally impose R-parity on our theories (so that fast proton decay does not occur), the new SUSY particles can not decay only into Standard Model particles. This leaves us with a stable particle as the lightest supersymmetric particle, which is an excellent candidate for dark matter.

As with the Standard Model, there are many papers and textbooks providing an introduction to supersymmetry – see, for instance, Ref. [25, 27].

1.2.1 Particle content and parameters of the MSSM

The Minimal Supersymmetric Standard Model (MSSM) [28] is (as the name suggests) the simplest extension of the Standard Model into a supersymmetric theory. The supersymmetric partners of the SM matter fields – the fermions – are the sfermions (separated into sleptons and squarks). These are spin zero scalars, and are described by chiral superfields. The gauginos (superpartners of the gauge bosons) are spin half particles, described by vector superfields, and can be separated into gluinos, photinos, winos and zinos. Higgs bosons have spin half partners, called higgsinos. Electroweak symmetry breaking causes the gauginos and the higgsinos to mix to form the physical eigenstates

(charginos and neutralinos). These SUSY particles are usually denoted with a tilde – i.e. the stop squark is $\tilde{t}$, the gluino is $\tilde{g}$ and the charginos and neutralinos are $\tilde{\chi}^{\pm}$ and $\tilde{\chi}^{0}$ respectively.

The basic structure of the Lagrangian in the MSSM is

$$\mathcal{L}_{MSSM} = \mathcal{L}_{superpotential} + \mathcal{L}_{kinetic} + \mathcal{L}_{soft} + \mathcal{L}_{gauge-fix} + \mathcal{L}_{ghost} \tag{1.9}$$

The mass and interaction terms are contained within the superpotential part of the Lagrangian. The terms which break SUSY are contained in $\mathcal{L}_{soft}$. Much effort has been put into developing a realistic model of supersymmetry breaking, but the MSSM simply parametrises how SUSY is broken in a general manner, without describing the underlying theory (while this allows us to study the phenomenology that results from a specific theory in a simple way, it does lead to over 100 free parameters). In the MSSM, supersymmetry is broken softly, so that the relations between the dimensionless couplings are unchanged and no quadratic divergences are introduced. Scalar and gaugino mass terms, along with trilinear scalar interactions, are all contained in $\mathcal{L}_{soft}$. The final two terms in the Lagrangian involve the Faddeev-Popov ghosts [29] and the gauge fixing terms.

Although in general the parameters of the MSSM are taken to be real, there is no *a priori* reason why complex parameters cannot be used. For example, the higgsino mass parameter, μ, and the trilinear coupling parameters $A_{t,b,..}$ can be complex and this leads to some very interesting and non-excluded phenomenology, particularly in the Higgs sector. In this thesis, we will study scenarios in the MSSM with both real and complex parameters.

1.2.2 The Higgs sector in the MSSM

The Higgs sector in the MSSM is somewhat more complicated than that in the Standard Model. In the SM, the Higgs VEV, together with the Yukawa interaction terms, give rise to the masses of both the up-type and down-type fermions. These terms, however, depend on the conjugate Higgs field. In a supersymmetric theory, the superpotential (from which Yukawa terms originate) must be an analytic function of left chiral superfields, and so this conjugate field is not allowed. Consequently, we need two Higgs doublets $\mathcal{H}_1$ and $\mathcal{H}_2$ in the MSSM – one to give masses to the up-type fermions and one to the down-type. We also need two Higgs doublets to ensure anomaly cancellation. These

two doublets have 8 degrees of freedom between them – three of which are used to give masses to the gauge bosons $W^{\pm}$ and Z. We are left with 5 degrees of freedom and 5 physical Higgs bosons. At lowest order, the Higgs sector is CP conserving and contains

$$h, H, A, H^{+}, H^{-}$$

The Higgs bosons h and H are CP even, with $M_h < M_H$, the A Higgs boson is CP odd and $H^{\pm}$ are charged. This can give rise to some very interesting phenomenology, especially when one takes mixing between the neutral Higgs bosons into account. For a detailed account of the Higgs sector in the MSSM, see for example Ref. [13, 30, 31].

The Higgs potential V_H is given by

$$\begin{aligned} V_H &= m_1^2|\mathcal{H}_1|^2 + m_2^2|\mathcal{H}_2|^2 - m_{12}^2\left(\epsilon_{ab}\mathcal{H}_1^a\mathcal{H}_2^b + \text{h.c}\right) \\ &\quad \frac{1}{8}\left(g_1^2 + g_2^2\right)\left(|\mathcal{H}_1|^2 + |\mathcal{H}_2|^2\right)^2 + \frac{1}{2}g_2^2|\mathcal{H}_1^{\dagger}\mathcal{H}_2|^2 \end{aligned} \tag{1.10}$$

where

$$\begin{aligned} m_{1,2,12} &= \text{soft SUSY breaking parameters} \\ \epsilon_{12} &= -1 \\ g_1 &= \frac{e}{\cos\theta_W} = \text{U(1) coupling constant} \\ g_2 &= \frac{e}{\sin\theta_W} = \text{SU(2) coupling constant} \end{aligned}$$

The Higgs doublet fields are decomposed as

$$\mathcal{H}_1 = \begin{pmatrix} \mathcal{H}_1^0 \\ \mathcal{H}_1^- \end{pmatrix} = \begin{pmatrix} v_1 + \frac{1}{\sqrt{2}}\left(\phi_1^0 + i\chi_1^0\right) \\ -\phi_1^- \end{pmatrix} \tag{1.11}$$

$$\mathcal{H}_2 = \begin{pmatrix} \mathcal{H}_1^0 \\ \mathcal{H}_1^- \end{pmatrix} = \begin{pmatrix} \phi_2^+ \\ v_2 + \frac{1}{\sqrt{2}}\left(\phi_2^0 + i\chi_2^0\right) \end{pmatrix} \tag{1.12}$$

The VEVs of the neutral components of the Higgs doublets are v_1 and v_2.

The tree level Higgs mass spectrum can be defined by two supersymmetric parameters: $\tan\beta$, the ratio of the vacuum expectation values of the two Higgs doublets (v_2/v_1), and M_A, the mass of the CP odd Higgs boson (for the real MSSM). In the MSSM with complex parameters we use $M_{H^{\pm}}$, the mass of the charged Higgs boson, instead of M_A as an input parameter. This is because when working in the MSSM with complex pa-

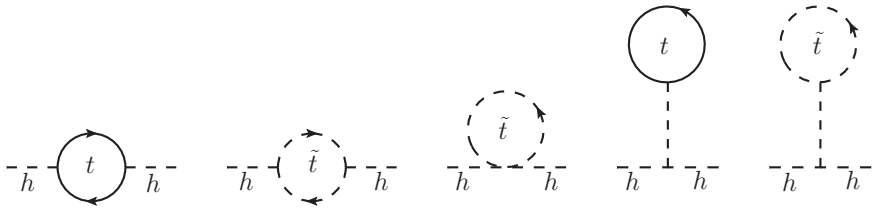

Figure 1.1: Dominant contributions to the lightest Higgs boson mass corrections.

rameters the mass of the CP odd Higgs M_A is no longer a mass eigenstate at higher orders, owing to the mixing between all three of the neutral Higgs bosons.

At tree level, the masses of the neutral CP even Higgs bosons are given by the mass matrix

$$m^2_{h,H} = \frac{1}{2}\begin{pmatrix} M_A^2 \sin^2\beta + M_Z^2\cos^2\beta & -(M_A^2+M_Z^2)\sin\beta\cos\beta \\ -(M_A^2+M_Z^2)\sin\beta\cos\beta & M_A^2\cos^2\beta + M_Z^2\sin^2\beta \end{pmatrix} \tag{1.13}$$

The eigenvalues of this matrix give the tree level masses:

$$m^2_{h,H} = \frac{1}{2}\left(M_A^2 + M_Z^2 \mp \sqrt{(M_A^2+M_Z^2)^2 - 4M_Z^2M_A^2\cos^2 2\beta}\right) \tag{1.14}$$

At first glance, this appears to present a problem as – in the decoupling limit when the mass of the CP odd Higgs boson M_A is large (i.e. $M_A \gg M_Z$) – the upper bound for the mass of the lightest Higgs boson h is

$$\begin{aligned} m_h^2 &< M_Z^2\cos^2 2\beta \\ \Rightarrow m_h^2 &< M_Z^2 \end{aligned} \tag{1.15}$$

Clearly, if the lightest Higgs boson was SM like and had a mass of less than that of the Z boson, it would have been observed by now [32]. It turns out, however, that the radiative corrections to the Higgs mass are extremely large. They are dominated by the diagrams shown in Fig. 1.1 – contributions from the top quark and the stop squark loops (owing to the large Yukawa coupling involved in this subset of diagrams). Note that throughout this work, a lower case m for Higgs masses will denote tree level masses, whereas an upper case M will signify the corrected mass.

The tree level mass eigenstates (h, H) can be related to the Higgs fields (ϕ_1, ϕ_2) using the following matrix:

$$\begin{pmatrix} h \\ H \end{pmatrix} = \begin{pmatrix} -\sin\alpha & \cos\alpha \\ \cos\alpha & \sin\alpha \end{pmatrix} \begin{pmatrix} \phi_1^0 \\ \phi_2^0 \end{pmatrix} \tag{1.16}$$

where the Higgs mixing angle α is given by

$$\begin{aligned} \tan 2\alpha &= \frac{m_h^2 + m_H^2}{M_A^2 - M_Z^2} \tan 2\beta \\ &= \frac{M_A^2 + M_Z^2}{M_A^2 - M_Z^2} \tan 2\beta \end{aligned} \tag{1.17}$$

The masses of the charged Higgs and the gauge bosons are given by

$$\begin{aligned} M_{H^\pm} &= M_A^2 - M_W^2 \\ M_W^2 &= \frac{1}{2} g_2^2 \left(v_1^2 + v_2^2\right) \\ M_Z^2 &= \frac{1}{2} \left(g_1^2 + g_2^2\right) \left(v_1^2 + v_2^2\right) \end{aligned} \tag{1.18}$$

1.2.3 Sfermions: masses and mixing

In order to define our notation, we briefly outline the masses and mixings in the sfermion sector of the MSSM. The relevant parts of the Lagrangian are (using the notation in [33])

$$\begin{aligned} \mathcal{L}_{soft}^{\tilde{q}_{mass}} &= -M_L^2 \left(\tilde{u}_L^\dagger \tilde{u}_L + \tilde{d}_L^\dagger \tilde{d}_L\right) - M_{\tilde{u}_R}^2 \tilde{u}_L^\dagger \tilde{u}_L - M_{\tilde{d}_R}^2 \tilde{d}_L^\dagger \tilde{d}_L \\ &\quad - \left(\lambda_u A_u v_2 \tilde{u}_L \tilde{u}_L^\dagger + \lambda_d A_d v_1 \tilde{d}_L \tilde{d}_L^\dagger + \text{hermitian conjugate}\right) \end{aligned} \tag{1.19}$$

and the squark mass matrix is given by

$$M_{\tilde{q}}^2 = \tag{1.20}$$
$$\begin{pmatrix} M_L^2 + m_q^2 + M_Z^2 \cos 2\beta \left(I_3^q - Q_q \sin^2\theta_W\right) & m_q X_q^* \\ m_q X_q & M_{\tilde{q}R}^2 + m_q^2 + M_Z^2 \cos 2\beta Q_q \sin^2\theta_W \end{pmatrix}$$

Here, M_L and $M_{\tilde{q}R}$ are soft SUSY breaking masses, Q is the fermion charge and I_3^q is the third isospin component, and (recalling that A is the trilinear coupling and μ the

higgsino mass parameter, which can – in the complex MSSM – have a non-zero phase)

$$\begin{aligned} X_{d,\tau} &= A_{d,\tau} - \mu^* \tan\beta \\ X_u &= A_u - \mu^* \cot\beta \\ I_3^{d,\tau} &= -\frac{1}{2} \\ I_3^u &= \frac{1}{2} \end{aligned} \tag{1.21}$$

Finding the eigenvalues of this matrix allows us to obtain the sfermion masses:

$$\begin{aligned} m^2_{\tilde{q}_{1,2}} = m_q^2 + \frac{1}{2}\Big(M_L^2 + M_{\tilde{q}R}^2 + I_3^q M_Z^2 \cos 2\beta \mp \\ \sqrt{\left([M_L^2 - M_{\tilde{q}R}^2 + M_Z^2 \cos 2\beta \left(I_3^q - 2Q_q \sin^2\theta_W\right)\right]^2 + 4m_q^2 |X_q|^2}\Big) \end{aligned} \tag{1.22}$$

The sfermion mass matrix can be diagonalised using the mixing matrix $U_{\tilde{q}}$:

$$\begin{aligned} \begin{pmatrix} \tilde{q}_1 \\ \tilde{q}_2 \end{pmatrix} &= U_{\tilde{q}} \begin{pmatrix} \tilde{q}_L \\ \tilde{q}_R \end{pmatrix} \\ &= \begin{pmatrix} \cos\theta_{\tilde{q}} & \sin\theta_{\tilde{q}} \\ -\sin^*\theta_{\tilde{q}} & \cos\theta_{\tilde{q}} \end{pmatrix} \begin{pmatrix} \tilde{q}_L \\ \tilde{q}_R \end{pmatrix} \end{aligned} \tag{1.23}$$

In this matrix, $\cos\theta_{\tilde{q}}$ is taken to be real and $\sin\theta_{\tilde{q}}$ is complex – they obey the relation $\cos^2\theta_{\tilde{q}} + |\sin\theta_{\tilde{q}}|^2 = 1$. The components of the mixing matrix are given by

$$\cos\theta_{\tilde{q}} = \frac{\sqrt{M_L^2 + m_q^2 + M_Z^2 \cos 2\beta \left(I_3^q - Q_q \sin^2\theta_W\right) - m^2_{\tilde{q}_2}}}{\sqrt{m^2_{\tilde{q}_1} - m^2_{\tilde{q}_2}}} \tag{1.24}$$

$$\sin\theta_{\tilde{q}} = \frac{m_q X_q^*}{\sqrt{M_L^2 + m_q^2 + M_Z^2 \cos 2\beta \left(I_3^q - Q_q \sin^2\theta_W\right) - m^2_{\tilde{q}_2}}\sqrt{m^2_{\tilde{q}_1} - m^2_{\tilde{q}_2}}} \tag{1.25}$$

1.3 Theory and experiment: event generators

The study of the Standard Model, and the searches for the Higgs boson and new physics beyond the Standard Model, have been going on for many years. Later this year, the

Large Hadron Collider (LHC) at CERN will switch on, allowing us to access higher energies than ever before. At Fermilab, near Chicago, the Tevatron (completed in 1983) is colliding protons with antiprotons in pursuit of new physics – in 1995 both detectors at the Tevatron announced the discovery of the top quark. At CERN, the Large Electron Positron collider (LEP) made extremely precise measurements of the Standard Model parameters – most notably the masses of the $W^{\pm}$ and Z gauge bosons.

There is, however, a large difference between the quantum field theory (and Feynman diagram calculations) describing the basic interactions between fundamental particles and the data we get from the experiments. Bremsstrahlung radiation from the particles involved in the initial interaction (e.g. a photon radiating from an electron $e \rightarrow e + \gamma$, or a gluon from a quark $q \rightarrow q + g$) means that the number of final state particles (that the detector will see) can be increased. We also need to take into account the fact that the coloured quarks and gluons are confined – we cannot observe a single quark. For hadron colliders, the structure of the incoming particle (a proton in the case of the LHC), from which the quark or gluon that takes part in a "hard" interaction originates, must be considered, as well as the process of hadronisation (whereby the quarks and gluons become jets of colourless hadrons).

Consequently, in order to make useful predictions that can be tested in colliders, we need to use event generators. These provide a link between theory and experiment, and aim to take a process and generate events from it as they would be seen in a detector. The basic principle is to split the complete calculation into more manageable pieces: the fundamental interaction is input, parton showers are generated, and the final products are allowed to hadronise[3].

1.3.1 Monte Carlo

A major challenge involved in calculations is the evaluation of complicated, multi-dimensional phase space integrals. Computationally, this is achieved using Monte Carlo techniques – these set each variable randomly (or at least as randomly as possible), according to an appropriate probability distribution. These techniques also allow us to perform calculations when the complexity of the situation is increased by the introduction of cuts. Several general purpose event generators exist – see for instance, Ref. [34]

[3]In practice, of course, the task of producing suitable code to enable a computer to do this is very complicated, but the basic structure is relatively simple.

for an overview. Most of the publicly available event generators do not include any virtual corrections[4].

In its broadest sense, a Monte Carlo (MC) technique is defined as a technique which makes use of random numbers in order to solve a problem. These techniques are ideal for simulations of particle physics as they can replicate the random, statistical behaviour that quantum mechanics describes. Random numbers between 0 and 1 (with a flat distribution) are generated and used to "choose" a point x such that $f(x)\mathrm{d}x$ (where f is some known distribution function) is proportional to the probability of a given x in the small interval $\mathrm{d}x$.

As stated, the multi-dimensional phase space integrals occuring in the calculations of particle physics events are in general evaluated using Monte Carlo integration. Algorithms performing MC integration are effective as they can provide a reliable estimate of the numerical error involved and the convergence rate is independent of the dimension of the integral. In addition, non-continuous functions can be evaluated.

Chapter 4 of the `Pythia` manual [35] provides a good, practical introduction to Monte Carlo techniques, and Ref. [36] provides a more detailed examination of the subject.

1.3.2 Jet algorithms

As has been stated, it is well known that coloured partons (quarks and gluons) cannot be observed singly – instead, they hadronise to form jets (collections of large numbers of colourless hadrons, photons and leptons). We use jet algorithms to take single particles (the final–state partons in our calculation, and calorimeter towers or hadrons in experimental analyses) and group them together into jets. The kinematic properties of the jet should allow us to deduce the properties of the original partons.

Two of the principle requirements for jet algorithms are that they must be both IR and collinear "safe". In other words, the presence of soft radiation in an event should not affect the jets found by the algorithm, and the same jets must be found for one particle with energy E as for two collinear particles with a combined energy E.

[4]The real corrections on their own are not IR finite – cuts are used to avoid the divergent region of phase space.

There are many different types of jet algorithms – see Ref. [37] for a review. One of the most popular classes of algorithms are the "k_T algorithms" – in this technique, pairs of particles are merged successively, in order of their transverse momentum, up to a certain "size" of jet (determined by the parameter R_{jj} defined in Section 2.2). The k_T algorithm has the advantage of a close link between theory and experiment – jets reconstructed from individual hadrons, leptons and photons are closely related to jets reconstructed from calorimeter data. Several different implementations of this class of jet algorithm have been proposed (and used) by the community.

1.4 Thesis outline

In this work we focus on a specific Higgs production channel – weak boson fusion (WBF) – in both the Standard Model and the MSSM (with real and complex parameters). In Chapter 2 the process of Higgs production via weak boson fusion will be studied in detail, describing the motivation behind the investigation, the experimental cuts, existing limits and future experimental capabilities. The work already available in the literature will be examined here as well.

Chapter 3 will present the details of the higher order calculations. For reference, all the necessary counterterms and renormalisation constants will be explicitly stated, and the renormalisation procedure for evaluating quantities involving UV, soft and collinear divergences will be outlined. In this Chapter we also examine the mixing between the neutral Higgs bosons, and how these effects can be included in our results (as they must be in order to make our results phenomenologically relevant).

The following chapter will study weak boson fusion of a Higgs boson at a linear collider, in both the Standard Model and the MSSM. The total cross sections, including corrections from the fermion and sfermion sectors, are calculated and analysed.

Chapters 5 and 6 will present the total and partonic cross sections of neutral Higgs production via weak boson fusion at the LHC, using a Monte Carlo program that has been modified to include the full one loop corrections in the Standard Model. We also study the corrections to this important process in the MSSM, in the general case of complex parameters, and combine the dominant SUSY corrections with the full SM result.

In Chapter 7, a possible reference process is investigated, which could help us to identify and understand Higgs production via WBF. The conclusions reached are presented in Chapter 8.

Chapter 2

Weak boson fusion

"Research is the process of going up alleys to see if they are blind."
— Marston Bates

2.1 Motivation and signal process

If all goes according to plan, the Large Hadron Collider will be switching on later this year and will begin to search for a Higgs boson. Discovering a candidate for the Higgs is, however, only the first step: we need to study it carefully and determine its properties – such as its mass, its couplings (especially to gauge bosons), its spin, and its CP behaviour. Production of a Higgs at the LHC has therefore received a considerable amount of attention in the literature (see, for example, [38–41] and references therein). In the Standard Model, the cross sections for the various Higgs production mechanisms are shown in Fig. 2.1 (reproduced from Reference [41]).

As can be seen from Fig. 2.1, the largest Higgs production cross section at the LHC is expected to be gluon fusion (labelled $gg \to h$) in the Standard Model (and, for a large region of parameter space, in the MSSM as well). In this process, gluons fuse via a loop (primarily top loops in the Standard Model, owing to the large Higgs-top quark coupling, and top and stop loops in the MSSM) to form a Higgs (Fig. 2.2). While gluon fusion is predicted to produce large numbers of Higgs bosons, it has the disadvantage of also having relatively large theoretical uncertainties $\mathcal{O}(10-20\%)$, even when the next-to-next-to-leading order (NNLO) QCD corrections are included –see Ref. [42–46].

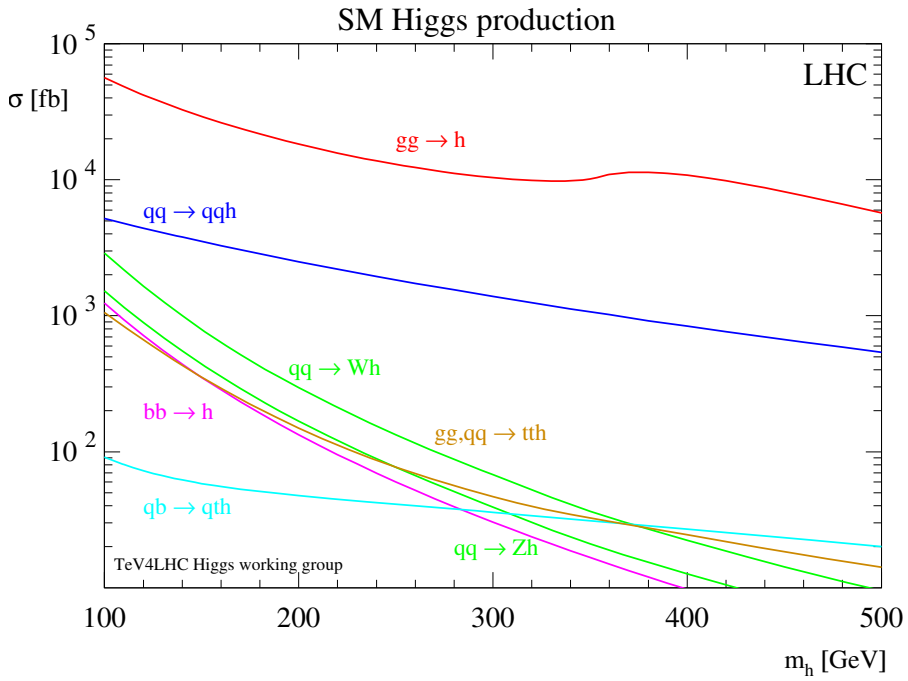

Figure 2.1: Production cross sections for a Standard Model Higgs at the LHC, reproduced from Ref. [41].

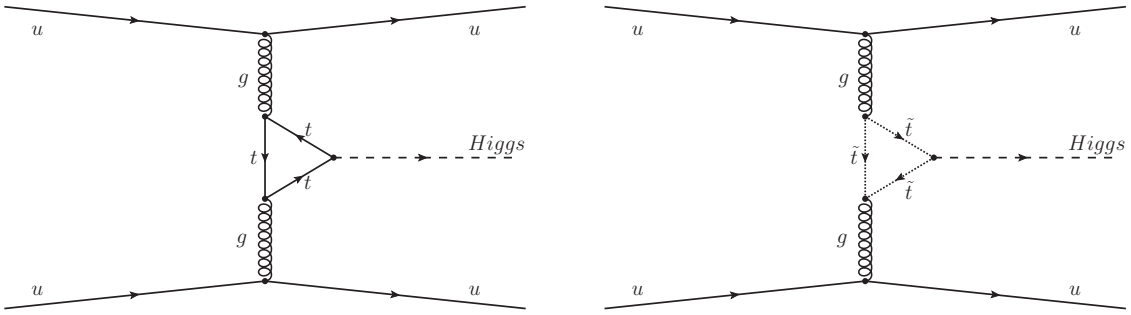

(a) Standard Model (b) MSSM

Figure 2.2: Leading order diagrams for gluon fusion in the SM and the MSSM.

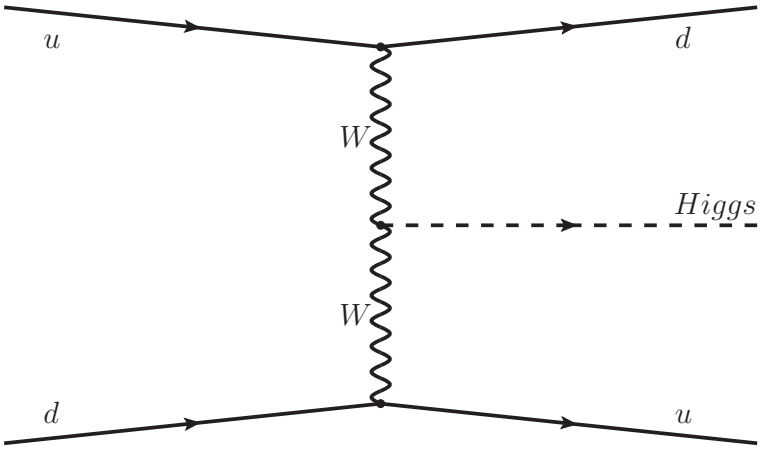

Figure 2.3: Leading order diagram for weak boson fusion.

Weak boson fusion (WBF) is one of the most promising methods of Higgs production. The process, shown in Fig. 2.3 and labelled as $qq \to qqh$ in Fig. 2.1, is expected to be the second largest contributor to Higgs production in the Standard Model at the LHC (smaller only than gluon fusion). Unlike gluon fusion, however, its QCD NLO corrections are relatively small – typically $\mathcal{O}(5\%)$ – and are theoretically well under control, and the Parton Density Function (PDF) errors and scale variations are not large in the relevant areas of phase space [47]. WBF also has the advantage of having a very clear signature of two energetic, strongly forward jets and a central Higgs, which can be used to isolate the signal from the backgrounds (see Section 2.2). Due to this, we can use weak boson fusion to study the important trilinear coupling between a Higgs and a pair of weak bosons (see Section 2.4), thus shedding light on the mechanism of electroweak symmetry breaking.

The amount of hadronic activity between the jets is small due to the fact that weak boson fusion is a colourless t-channel exchange process. There is therefore a greatly reduced amount of gluon radiation in the central region. This is in contrast to the gluon fusion process, which naturally involves the exchange of coloured particles. Gluon fusion of a Higgs with two additional jets and a large rapidity gap between them experiences Sudakov suppression (see Ref. [48]), and so has a reduced contribution.

The tagging jets of weak boson fusion are produced predominately at small angles (i.e. with large rapidity), as the momentum transfer is much less than the quark jets' energy. The dijet mass spectrum of weak boson fusion is much harder than that of gluon fusion, as the PDFs mean that the external legs for weak boson fusion are likely to be quarks (for gluon fusion, the external particles are far more likely to be gluons – hence

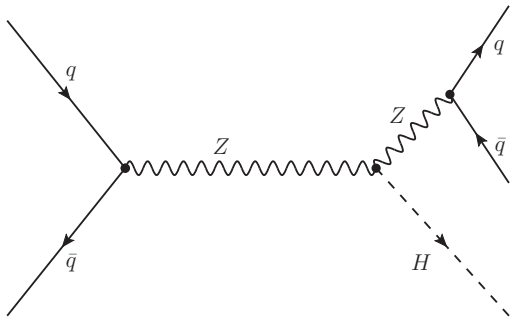

Figure 2.4: Higgsstrahlung contribution to the Higgs + 2 jets process.

the softer dijet mass spectrum). A useful reference describing the kinematics of weak boson fusion is Ref. [49].

2.2 Backgrounds and cuts

Higgs production via weak boson fusion results in two jets plus the Higgs[1]. There are, however, several other process that give rise to the same signature. The most important of these processes is gluon fusion (shown in Fig. 2.2), as can be seen from the cross section graph of Fig. 2.1. Another important Higgs plus two jets process is Higgsstrahlung, shown in Fig. 2.4, an s-channel process where a Higgs is radiated from a W or Z gauge boson (these channels are labelled $qq \to Wh$ and $qq \to Zh$ in Fig. 2.1).

In order to extract the WBF signal, various cuts on different observables have to be made. The coordinate system used in this work (which follows the same conventions as the LHC detector ATLAS) is shown in Figure 2.5. The z-axis is along the beam direction, the x-axis points towards the centre of the LHC ring and the y-axis points upwards. The azimuthal angle ϕ is measured from the positive x-axis and the polar angle θ is measured from the z-axis. The transverse momentum p_T is defined as the momentum of a particle perpendicular to the beam direction (the z-axis).

The experimentally measured quantities that are cut on include the transverse momentum p_T of the final jets, the rapidity y (and the pseudorapidity η), and the dijet invariant mass M_{jj}. The magnitude of the transverse momentum p_T is given by $\sqrt{p_x^2 + p_y^2}$. The pseudorapidity η is the coordinate that describes the angle of a particle relative to

[1]The Higgs will then decay, although this part of the full process is not considered here.

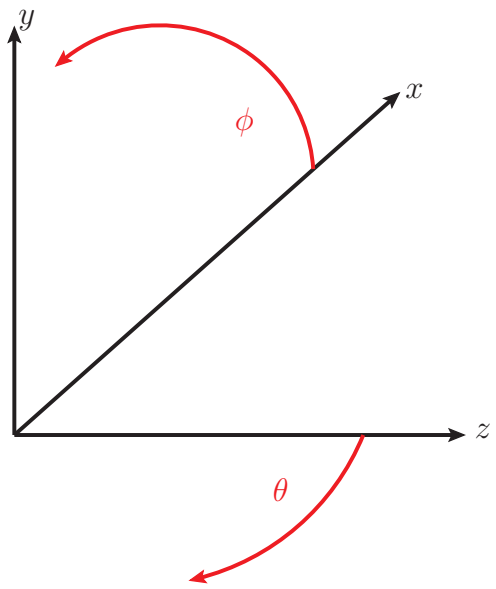

Figure 2.5: Coordinate system used to define the cuts.

the beam (z-) axis. It is defined as

$$\begin{aligned} \eta &= -\ln\left[\tan\frac{\theta}{2}\right] \\ &= \frac{1}{2}\ln\left(\frac{|\vec{p}|+p_z}{|\vec{p}|-p_z}\right) \end{aligned} \tag{2.1}$$

The rapidity of a particle is given in terms of its 4-momentum p_μ by

$$y = \frac{1}{2}\ln\left(\frac{p_0+p_z}{p_0-p_z}\right) \tag{2.2}$$

In the limit of zero mass, the rapidity and pseudorapidity coincide.

The dijet invariant mass is given by

$$M_{jj}^2 = (p_{j1}+p_{j2})^2 \tag{2.3}$$

where $p^\mu_{j1,j2}$ are the 4-momenta of the two jets. We also make a cut on the observable R_{jj}, the separation of the two jets in the pseudorapidity versus azimuthal angle plane,

which is defined as follows[2]:

$$R_{jj} = \sqrt{\Delta\eta_{jj}^2 + \phi_{jj}^2} \tag{2.4}$$

Weak boson fusion typically has two energetic tagging jets in the forward regions of the detector (i.e. two jets with a large rapidity gap), with a central Higgs and very little additional hadronic activity between the tagging jets. As was mentioned in the previous section, we can use this distinctive signature to devise a set of cuts, using the above quantities, which will effectively isolate the process from the various backgrounds. This will allow us not only to study the Higgs production cross section, but also to focus on the important Higgs–weak boson trilinear coupling.

In order to take advantage of the unique signature of WBF we demand a large rapidity gap (as there is little central hadronic activity) and a high dijet mass, which will eliminate much of the QCD background and the gluon fusion (with its soft dijet mass spectrum) process, as well as avoiding the threshold at the W/Z boson mass in the Higgsstrahlung channel. We also cut on the rapidity of the tagging jets, since they generally have a high rapidity in WBF. This leads to the following standard set of cuts used in the literature (see, e.g. [50]), which are employed throughout this thesis unless specifically stated otherwise.

$$\begin{aligned} p_{T_j} &> 20 \text{ GeV} \\ |\eta_j| &< 5 \\ R_{jj} &> 0.8 \\ \Delta\eta_{jj} = |\eta_{j_1} - \eta_{j_2}| &> 4 \\ \eta_{j_1} \cdot \eta_{j_2} &< 0 \\ M_{jj} &> 600 \text{ GeV} \end{aligned} \tag{2.5}$$

The cut $\eta_{j_1} \cdot \eta_{j_2} < 0$ ensures that the tagging jets lie in opposite detector hemispheres.

[2] $\Delta\eta_{jj}$ is the difference in rapidity between the two jets, and ϕ_{jj} is the difference in azimuthal angle - see Figure 2.5.

2.3 Previous work

Owing to the potential importance of the process of Higgs production via weak boson fusion at the LHC, it has already received a large amount of attention in the literature. The next to leading order (NLO) QCD corrections in the Standard Model (which are typically $\mathcal{O}(5\%)$ after WBF cuts) have been known for some time (see, for example, Ref. [47, 50, 51]), and there are two public Monte Carlo codes – `VBFNLO` (see Ref. [52, 53] and Section 2.5) and `VV2H` [54] – available that provide a useful tool enabling predictions of WBF cross sections and distributions to be made.

In addition, the one loop electroweak corrections in the Standard Model have been published [55]. These contributions were found to be of approximately the same size as the QCD corrections, and so should not be neglected in NLO predictions for the LHC. This paper reported the results of using a Monte Carlo code to study Higgs plus two jets production, and also included the effects of s-channel contributions (the Higgsstrahlung process – Fig. 2.4), as well as interference between t- and u-channel processes. The combined effects of these (s-channel and t-u channel interference) contributions was at most $\mathcal{O}(0.6\%)$ at next to leading order and $\mathcal{O}(0.007\%)$ at leading order after the weak boson fusion cuts were applied, and are not included in any of the LHC results presented in this thesis.

The specifically supersymmetric contributions (i.e. loops involving, for example, sleptons but not their leptonic partners) to the total cross section of the lightest CP even Higgs boson h production via gauge boson fusion and Higgsstrahlung have also been investigated [56]. If we are working in the (s)fermion sector at the one loop level, separating the Standard Model and SUSY contributions is of course simple as R-parity conservation ensures that there is no mixing between the SM type particles and their supersymmetric partners. If, however, we move beyond this sector to the full MSSM, this trivial separation is not possible owing to the different structure of the Higgs sector in the MSSM (see Section 1.2.2) – there is not simply one supersymmetric partner for the SM Higgs. The authors of Ref. [56] have chosen to define the SUSY contribution as:

$$\sigma^{SUSY} = \sigma^{MSSM} - \sigma^{SM} \sin^2(\beta - \alpha) \tag{2.6}$$

Naturally, the factor $\sin^2(\beta-\alpha)$ is only appropriate for the production of the light Higgs – if we were considering the heavy Higgs boson H, we would need to use $\cos^2(\beta - \alpha)$. This is discussed in more detail in Chapter 6, Section 6.4.1.

We have studied the complete electroweak corrections to neutral Higgs production via weak boson fusion in the Standard Model and supplemented these results with the dominant loop corrections in the MSSM, in the general case where non-vanishing complex phases are included (thus allowing the study of possible CP violating behaviour). Our results have been implemented into the public Monte Carlo code `VBFNLO`, providing a useful tool for experimental analyses.

A comparison of the published results with our work has been carried out, and agreement has been found.

2.4 Formfactors and azimuthal angle distributions

2.4.1 Effective Lagrangians and the HVV coupling

In the Standard Model, the tree level trilinear coupling between the Higgs and the gauge bosons ($vHV_\mu V^\mu$) originates from the kinetic energy term $(D_\mu\phi)^\dagger (D^\mu\phi)$ of the symmetry breaking field ϕ, when this scalar field acquires a vacuum expectation value v ($\phi \to \frac{1}{\sqrt{2}}(v+H)$: see Section 1.1.1). Ascertaining the existence of this vacuum expectation value (VEV) is crucial if we are to confirm the mechanism of electroweak symmetry breaking. If the VEV were zero, the trilinear term would not be present and we would be left with only quartic and higher couplings.

A trilinear coupling can also be loop-induced – for instance, the effective coupling between the gluons and a Higgs that is used when studying gluon fusion. By considering gauge invariance, however, it can be seen that these loop-induced couplings will involve a very different structure to the tree level value, and will include the operators

$$HV_{\mu\nu}V^{\mu\nu},\ H\tilde{V}_{\mu\nu}V^{\mu\nu} \tag{2.7}$$

where

$$\begin{aligned} V^{\mu\nu} &= \partial^\mu V^\nu - \partial^\nu V^\mu = \text{ field strength tensor} \\ \tilde{V}^{\mu\nu} &= \frac{1}{2}\epsilon^{\mu\nu\rho\sigma}V_{\rho\sigma} = \text{ dual field strength tensor} \end{aligned}$$

One would in general expect that a loop-induced coupling should be far smaller than a tree level coupling, but this is not necessarily the case. For instance, new, unknown

and unexpected physics could suppress the tree level coupling or enhance the loop-induced coupling, or the signature observed at the LHC may have a larger Higgs decay branching ratio than expected. A loop induced coupling is generally expected to lead to small deviations from the tree level coupling (hence the need for precise measurements and theoretical predictions), but if the tree level coupling is heavily suppressed (or even vanishes) – as is the case in several beyond the Standard Model scenarios – the loop induced coupling can become dominant. Consequently, it is crucial that this coupling is studied in some detail. To do this, an effective Lagrangian $\mathcal{L}_{eff}$ can be written describing the interaction between the Higgs and a pair of weak bosons (here, V stands for either the $W^{\pm}$ or the Z boson), including the corresponding part of the Standard Model Lagrangian as well as higher dimensional operators $\mathcal{O}_i^{(5)}$ and $\mathcal{O}_i^{(6)}$. This can be used to quantify observed deviations from the Standard Model. The Lagrangian below describes an effective theory that is valid only up to some energy scale Λ, and is consequently written as an expansion in $\frac{1}{\Lambda}$ up to the second order.

$$\mathcal{L}_{eff} = \mathcal{L}_{SM} + \sum_i \frac{g_i^{(5)}}{\Lambda}\mathcal{O}_i^{(5)} + \sum_i \frac{g_i^{(6)}}{\Lambda^2}\mathcal{O}_i^{(6)} \tag{2.8}$$

The g_i quantities are dimensionless coupling constants, generally $\mathcal{O}(1)$.

A description of higher dimensional operators, up to dimension 6, is given in [57]. We consider the operators that result in[3]

$$\begin{aligned}\mathcal{L}_{eff} \;=\; & g_{SM}^{HWW} H W_\mu^+ W_-^\mu + g_{SM}^{HZZ} H Z_\mu Z^\mu + \frac{g_e^{HWW}}{\Lambda_e} H W_{\mu\nu}^+ W_-^{\mu\nu} + \frac{g_o^{HWW}}{\Lambda_o} H \tilde{W}_{\mu\nu}^+ W_-^{\mu\nu} + \\ & \frac{g_e^{HZZ}}{2\Lambda_e} H Z_{\mu\nu} Z^{\mu\nu} + \frac{g_o^{HZZ}}{2\Lambda_o} H \tilde{Z}_{\mu\nu} Z^{\mu\nu}\end{aligned} \tag{2.9}$$

Since $V^{\mu\nu}$ is even under CP transformations, the term $HV_{\mu\nu}V^{\mu\nu}$ is also CP even for a Standard Model (or any other CP even) Higgs boson. Conversely, $\tilde{V}^{\mu\nu}$ is odd under these transforms and so the fourth and sixth terms in the above equation are also CP odd for a Standard Model type Higgs[4].

Expanding this Lagrangian term by term will allow us to arrive at an effective, general coupling between the Higgs field and the two weak bosons. In order to keep the formulae

[3]Note that these are dimension 5 operators, which originate from the corresponding dimension 6 operators when the symmetry breaking scalar field is expanded. Also, in order to be as general as possible, two scales Λ_e and Λ_o are used.

[4]The subscripts o and e indicate this behaviour.

as clear as possible (and avoid additional indices), in this derivation the two weak bosons (either a pair of W bosons, W^+W^-, or a pair of Z bosons, ZZ) are termed P and Q, and have momenta p and q respectively. First, considering the CP even term (the arrow signifies switching to momentum space):

$$\begin{aligned} HP_{\mu\nu}Q^{\mu\nu} &= H\left(\partial_\mu P_\nu - \partial_\nu P_\mu\right)\left(\partial^\mu Q^\nu - \partial^\nu Q^\mu\right) \\ &\rightarrow -H\left(p_\mu P_\nu - p_\nu P_\mu\right)\left(q^\mu Q^\nu - q^\nu Q^\mu\right) \\ &= -\left(Hp_\mu q^\mu P_\nu Q^\nu - Hp_\mu q^\nu P_\nu Q^\mu - Hp_\nu q^\mu P_\mu Q^\nu + Hp_\nu q^\nu P_\mu Q^\mu\right) \\ &= -\left((p\cdot q)g^{\mu\nu} - p^\nu q^\mu - p^\nu q^\mu + (p\cdot q)g^{\mu\nu}\right) HP_\mu Q_\nu \\ &= -2\left((p\cdot q)g^{\mu\nu} - q^\mu p^\nu\right) HP_\mu Q_\nu \end{aligned} \tag{2.10}$$

Now turning to the CP odd operator[5]:

$$\begin{aligned} H\tilde{P}_{\mu\nu}Q^{\mu\nu} &= \frac{1}{2}H\epsilon_{\mu\nu\rho\sigma}P^{\rho\sigma}Q^{\mu\nu} \\ &= \frac{1}{2}H\epsilon_{\mu\nu\rho\sigma}\left(\partial^\rho P^\sigma - \partial^\sigma P^\rho\right)\left(\partial^\mu Q^\nu - \partial^\nu P^\mu\right) \\ &\rightarrow -\frac{1}{2}H\epsilon_{\mu\nu\rho\sigma}\left(p^\rho P^\sigma q^\mu Q^\nu - p^\rho P^\sigma q^\nu Q^\mu - p^\sigma P^\rho q^\mu Q^\nu + p^\sigma P^\rho q^\nu Q^\mu\right) \\ &= -\frac{1}{2}\left(-\epsilon_{\mu\nu\rho\sigma} - \epsilon_{\mu\nu\rho\sigma} - \epsilon_{\mu\nu\rho\sigma} - \epsilon_{\mu\nu\rho\sigma}\right)p^\rho q^\sigma HP^\mu Q^\nu \\ &= 2\epsilon_{\mu\nu\rho\sigma}p^\rho q^\sigma HP^\mu Q^\nu \end{aligned} \tag{2.11}$$

Putting these two terms together, it can be seen that

$$\mathcal{L}_{eff} = T^{\mu\nu}HV_\mu V_\nu \tag{2.12}$$

where the general, effective coupling $T^{\mu\nu}$ is given by

$$\begin{aligned} T^{\mu\nu}(q_1,q_2) &= a_1(q_1,q_2)g^{\mu\nu} + \\ &\quad a_2(q_1,q_2)\left((q_1.q_2)g^{\mu\nu} - q_1^\mu q_2^\nu\right) + \\ &\quad a_3(q_1,q_2)\epsilon^{\mu\nu\rho\sigma}q_{1\rho}q_{2\sigma} \end{aligned} \tag{2.13}$$

Here, q_1 and q_2 are the momenta of the weak bosons, and $a_{1,2,3}$ are Lorentz invariant formfactors, which can be related back to the Lagrangian in Equation 2.9 and expressed

[5]Several lines of working are not explicitly written, as they involve only index manipulation.

in the following manner.

$$\begin{aligned} a_1 &= \text{SM type coupling} \\ a_2 &= -\frac{2}{\Lambda_e} g_e^{HVV} \\ a_3 &= \frac{2}{\Lambda_o} g_o^{HVV} \end{aligned} \tag{2.14}$$

Using this general form $T^{\mu\nu}$ of the $HV^{\mu}V_{\mu}$ coupling, deviations in this coupling from the Standard Model expectations can easily be parametrised in a simple, gauge invariant manner.

2.4.2 Determining the structure of the HVV coupling

Studying weak boson fusion at the LHC can in principle provide information not only about the strength of the coupling HVV between a pair of weak bosons and a Higgs, but also about its tensor structure. As explained in the previous section, this information is important, as it will be needed to confirm the mechanism of electroweak symmetry breaking. One method that has been proposed [58] to enable us to study the structure of $T^{\mu\nu}$, the effective HVV coupling, is to analyse the azimuthal angle distribution.

A comparison of the differing distributions obtained when the HVV coupling is described by only a_1, only a_2 or only a_3 is shown in Fig. 2.6, which was generated using the code `VBFNLO` (see Section 2.5 and later Chapters)[6].

If only a_3 (the CP odd formfactor) has a non-zero value, then the coupling (and hence the cross section) will vanish if the tagging jets are back-to-back or collinear in the transverse plane as the Levi-Civita symbol $\epsilon_{\mu\nu\rho\sigma}$ will force the coupling to zero. Consequently, as seen in Fig. 2.6, if the HVV coupling is described only by a CP odd formfactor there are approximate zeroes at 0 and π in the azimuthal angle distribution[7].

If only the anomalous CP even formfactor a_2 has a non-zero value, the azimuthal angle distribution has (approximate) zeroes at $\pm\frac{\pi}{2}$. The matrix element in this case is (note that the lower indices in the following equations indicate which of the particles we

[6]Note that the values of the couplings were fixed such that they would produce total cross sections of (roughly) the same size.

[7]Note that, due to the manner in which the results are binned, the distribution will not go to exactly zero as the bin at e.g. π spans angles in the range $\pi \pm x$, where x is some small value.

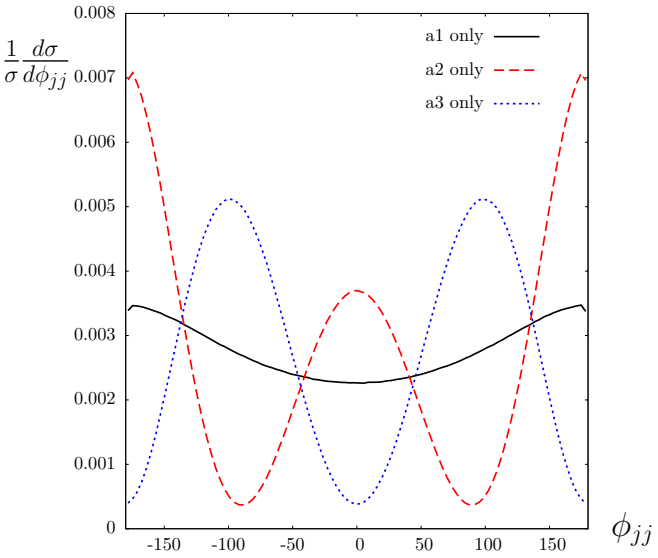

Figure 2.6: Azimuthal angle ϕ_{jj} distribution with standard WBF cuts, showing distinctions between SM type and anomalous CP even and CP odd coupling structures.

are referring to (1 or 2), and upper indices indicate the current or 4-momentum index):

$$\begin{aligned}\mathcal{M}_e &\propto \frac{1}{\Lambda_e} J_1^\mu J_2^\nu \left(g_{\mu\nu}(q_1 \cdot q_2) - q_{2,\mu} q_{1,\nu}\right) \\ &\propto \frac{1}{\Lambda_e} \left[\left(q_1^0 q_2^0 - q_1^i q_2^i\right)\left(J_1^0 J_2^0 - J_1^i J_2^i\right)\right. \\ &\quad \left. - q_1^0 J_2^0 \left(q_2^0 J_1^0 - q_2^i J_1^i\right) + q_1^i J_2^i \left(q_2^0 J_1^0 - q_2^i J_1^i\right)\right] \end{aligned} \tag{2.15}$$

Here, q and J are the momentum and current of the weak bosons, the index $i = \{1, 2, 3\}$ and is summed over. If we assume that the external quarks only experience a small energy loss (i.e. we use the approximation that $q^{0,3} = 0$), the matrix element becomes

$$\mathcal{M}_e \propto \frac{1}{\Lambda_e} \left[-q_1^k q_2^k \left(J_1^0 J_2^0 - J_1^i J_2^i\right) + q_1^k J_2^k \left(-q_2^k J_1^k\right)\right] \tag{2.16}$$

Here, the index $k = \{1, 2\}$ $(= x, y)$ and is summed over. If we then make the further approximation that the momentum component of the tagging jets in the z (beam) direction is much greater than the components in the x or y directions, $|p_z| \gg |p_{x,y}|$ (i.e. that $J^{1,2} = 0$), the matrix element becomes:

$$\mathcal{M}_e \propto \frac{1}{\Lambda_e} \left[-q_1^k q_2^k \left(J_1^0 J_2^0 - J_1^3 J_2^3\right)\right] \tag{2.17}$$

We can re-write this in terms of the transverse momenta of the tagging jets, which is $p_T^{tag} = (p_{T,x}, p_{T,y})$, and will (by momentum conservation) be equal to the transverse momenta of the weak bosons $q_{1,2}$ above.

$$\begin{aligned} \mathcal{M}_e &\sim \frac{1}{\Lambda_e}\left(J_1^0 J_2^0 - J_1^3 J_2^3\right) p_T^{tag1} \cdot p_T^{tag2} \\ &\sim \frac{1}{\Lambda_e}\left(J_1^0 J_2^0 - J_1^3 J_2^3\right) |p_T^{tag1}||p_T^{tag2}| \cos\phi_{jj} \end{aligned} \tag{2.18}$$

This leads to the distribution shown in red in Fig. 2.6, with zeroes when $\phi_{jj} = \pm\frac{\pi}{2}$ (i.e. where $\cos\phi_{jj} = 0$).

This distribution cleanly distinguishes between purely anomalous (non zero a_2 or non zero a_3) couplings and a purely Standard Model (non zero a_1) coupling. It can also determine whether there is a CP even a_2 coupling in addition to a Standard Model coupling. As it stands, however, a coupling that is a combination of anomalous CP even and CP odd contributions of similar strengths could easily closely resemble a Standard Model structure as the dips we observe for purely a_2 or purely a_3 couplings will cancel one another out.

Consequently, a new definition of the azimuthal angle was proposed [59] that includes a sign which takes the correlation of the tagging jets with the beam directions into account. $\Delta\phi$ is defined as the azimuthal angle of the "away" tagging jet minus the azimuthal angle of the "toward" tagging jet[8]. If we define $p_{T,+}$ and $p_{T,-}$ as the momenta of the tagging jets, which point into the same detector hemisphere as the (normalised) beam momenta b_+ and b_- respectively (as is shown in Fig. 2.7), then the azimuthal angle $\Delta\phi$ is given by:

$$\begin{aligned} \epsilon_{\mu\nu\rho\sigma} b_+^\mu p_+^\nu b_-^\rho p_-^\sigma &= 2|p_{T,+}||p_{T,-}| \sin\left(\phi_+ - \phi_-\right) \\ &= 2|p_{T,+}||p_{T,-}| \sin\left(\Delta\phi\right) \end{aligned} \tag{2.19}$$

$$|p_{T,+}||p_{T,-}| \cos\Delta\phi = p_{T,+} \cdot p_{T,-} \tag{2.20}$$

This allows us to define the sign of $\Delta\phi$ and, if it is used instead of the "standard" ϕ_{jj} (which is, effectively, $|\Delta\phi|$), interference effects between a_1, a_2 and a_3 can be observed. The Standard Model type and CP even type amplitudes are even functions of the quantity $\Delta\phi$, whereas the CP odd type amplitude is odd. If this definition of the azimuthal

[8]When viewing the azimuthal angles from the opposite beam direction, the "away" and "toward" tagging jets will obviously be switched, but so too will the forward and backward beam directions, so the sign of $\Delta\phi$ will be preserved.

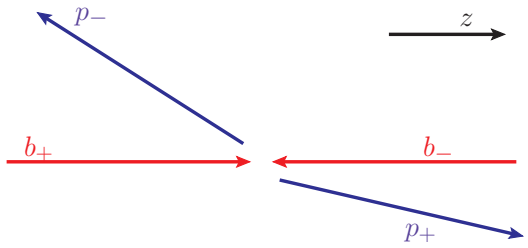

Figure 2.7: Direction of beam and tagging jet momenta for the new azimuthal angle $\Delta\phi$ definition.

angle is used, we can distinguish a coupling that contains contributions from a_2 and a_3 from a Standard Model type coupling a_1.

Since at leading order, gluon fusion can be considered to be governed by an effective ggH CP even coupling ($G^{\mu\nu}G_{\mu\nu}H$), there should be a dip in the azimuthal angle distribution at $\pm\frac{\pi}{2}$. This shape, however, is largely washed out by gluon radiation at next to leading order. Due to this decorrelation effect, doubts were expressed [60] about whether the clear structure seen in Fig. 2.6 of the azimuthal angle distribution of weak boson fusion would survive at NLO. It has been explicitly shown [50], however, that – due to the colour singlet t-channel exchange of WBF – gluon radiation in the central region is heavily suppressed and the characteristic dips at $\pm\frac{\pi}{2}$ are still present at NLO.

2.4.3 Experimental limits and capabilities

At the Large Electron Positron Collider (LEP), the search for a Higgs boson was undertaken primarily by looking for a Higgs produced via Higgsstrahlung (shown in Fig. 2.4). Owing to the energy of the LEP collisions, this channel could (kinematically) only produce a Higgs if its mass were less than ~ 115 GeV. Although LEP did not discover a Higgs boson, the studies performed meant that we could put limits on the properties of a Higgs. Experimental limits on the anomalous CP even HVV couplings derived from the LEP data were presented by the L3 collaboration in Ref. [61]. A different effective Lagrangian was used to the one described in previous sections: the relevant parts of the parametrisation used in Ref. [61], that contribute to a_2, are:

$$\begin{aligned}\mathcal{L}_{eff} &= g^{(1)}_{HWW}\left(W^+_{\mu\nu}W^{\mu}_{-}\partial^{\nu}H + W^-_{\mu\nu}W^{\mu}_{+}\partial^{\nu}H\right) + g^{(2)}_{HWW}HW^+_{\mu\nu}W^{\mu\nu}_{-} \\ &\quad + g^{(1)}_{HZZ}Z_{\mu\nu}Z^{\mu}\partial^{\nu}H + g^{(2)}_{HZZ}HZ_{\mu\nu}Z^{\mu\nu}\end{aligned} \tag{2.21}$$

where

$$\begin{aligned} g^{(1)}_{HWW} &= \frac{gM_W}{M_Z^2}\Delta g_1^Z \\ g^{(2)}_{HWW} &= \frac{g}{M_W}d \\ g^{(1)}_{HZZ} &= \frac{g}{M_W}\left(\Delta g_1^Z \cos 2\theta_w + \Delta\kappa_\gamma \tan^2\theta_w\right) \\ g^{(2)}_{HZZ} &= \frac{g}{2M_W}\left(d\cos^2\theta_w + d_B \sin^2\theta_w\right) \end{aligned} \tag{2.22}$$

Here, g is the $SU(2)_L$ coupling constant, and d, d_B, Δg_1^Z and $\Delta\kappa_\gamma$ are dimensionless parameters, the latter two of which are used when parametrising the anomalous triple gauge coupling (for limits set by LEP on these parameters, see Ref. [62]). We have explicitly verified that this Lagrangian is equivalent to the CP even part of the Lagrangian displayed earlier in Equation 2.9. The coefficients in each Lagrangian are related in the following manner:

$$\begin{aligned} g_e^{HWW} &= \Lambda_e\left(g^{(2)}_{HWW} + g^{(1)}_{HWW}\right) \\ g_e^{HZZ} &= \Lambda_e\left(2g^{(2)}_{HZZ} + g^{(1)}_{HZZ}\right) \end{aligned} \tag{2.23}$$

Ref. [63] converted the published L3 limits into limits on g_e^{HVV} for Higgs masses of 120 GeV and 160 GeV, assuming the limits to be uncorrelated, for a scale of $\Lambda_e = 480$ GeV [9]. These limits are reproduced in Table 2.1, along with a conversion to limits on the formfactor a_2.

Ref. [63] used these limits from LEP and extrapolated in order to estimate the ability of the ATLAS detector to identify anomalous couplings between a Higgs candidate and a pair of weak bosons. The authors used `VBFNLO` to generate the signal at leading order, `PYTHIA` [35, 64] to generate the background, and `ATLFAST` [65] to simulate the detector. They found that they would have the sensitivity to exclude purely anomalous couplings for a Higgs of mass 160 GeV (using $H \to W^+W^- \to ll\nu\nu$) to a level of $\sim 5\sigma$ for 10 fb^{-1} of data[10]. A lighter Higgs boson presents more difficulties, but using $H \to \tau^+\tau^-$ a Higgs of mass 120 GeV with purely anomalous couplings could be excluded at the $\sim 2\sigma$ confidence level with 30 fb^{-1}.

[9] This scale, with $g_e^{HWW} = \cos^2\theta_W g_e^{HZZ} = 1$, gives a total cross section for a purely anomalous CP even or CP odd coupling that is approximately equal to the cross section in the Standard Model.

[10] Note that this analysis was performed assuming an LHC energy of 14 TeV, instead of the 7 TeV that is likely to be used in the first phase of the LHC.

Table 2.1: Limits from LEP on anomalous HVV couplings at 95% confidence level, from [63].

M_H [GeV]	120	160
$\mathbf{d}$	-0.19 .. 0.19	-0.5 .. 0.4
$\boldsymbol{d_B}$	-0.06 .. 0.06	-0.13 .. 0.14
$\boldsymbol{\Delta g_1^Z}$	-0.051 .. 0.034	-0.051 .. 0.034
$\boldsymbol{\Delta\kappa_\gamma}$	-0.105 .. 0.069	-0.105 .. 0.069
$\boldsymbol{g_e^{HWW}}$	-0.78 .. 0.73	-2.0 .. 1.5
$\boldsymbol{g_e^{HZZ}}$	-0.63 .. 0.55	-1.6 .. 1.3
$\boldsymbol{a_2^{HWW}}$	-0.00304 .. 0.00325	-0.00625 .. 0.00833
$\boldsymbol{a_2^{HZZ}}$	-0.00229 .. 0.00263	-0.00542 .. 0.00667

The expected experimental precision for a combination of SM type and anomalous CP even type HVV couplings was also studied and, with 30 fb^{-1} of data, the following values of Δg_e^{HZZ} (the standard deviation of g_e^{HZZ}) were reported[11]:

$$\begin{aligned} \Delta g_e^{HZZ} = 0.11 \quad &\Rightarrow \Delta a_2^{HZZ} = 0.000458 \text{ for } M_H = 160 \text{ GeV} \\ \Delta g_e^{HZZ} = 0.24 \quad &\Rightarrow \Delta a_2^{HZZ} = 0.001 \text{ for } M_H = 120 \text{ GeV} \end{aligned} \tag{2.24}$$

2.5 The public code VBFNLO

The correction at next to leading order in α_s to the inclusive cross section of weak boson fusion has been known for almost 20 years to have a relatively small K-factor and scale dependence [51]. Monte Carlo generators (see Section 1.3) are ideal for simulating weak boson fusion, and have been used to check that these small K-factors and scale dependences extend to the distributions and phase space regions that will be accessible at the LHC [47]. VBFNLO [52] is one such publically available code: it is a fully flexible parton-level program that simulates weak boson fusion at next to leading order in QCD in the Standard Model. We have used this code as a base on which to implement the electroweak corrections to neutral Higgs production via weak boson fusion in both the Standard Model and the MSSM (the production of any of the three neutral Higgs bosons can be simulated using the adapted code). In this section we will describe the abilities of the public VBFNLO, as well as outlining the methods used by the code.

[11] These were converted to the formfactors used in this work using Equation 2.14.

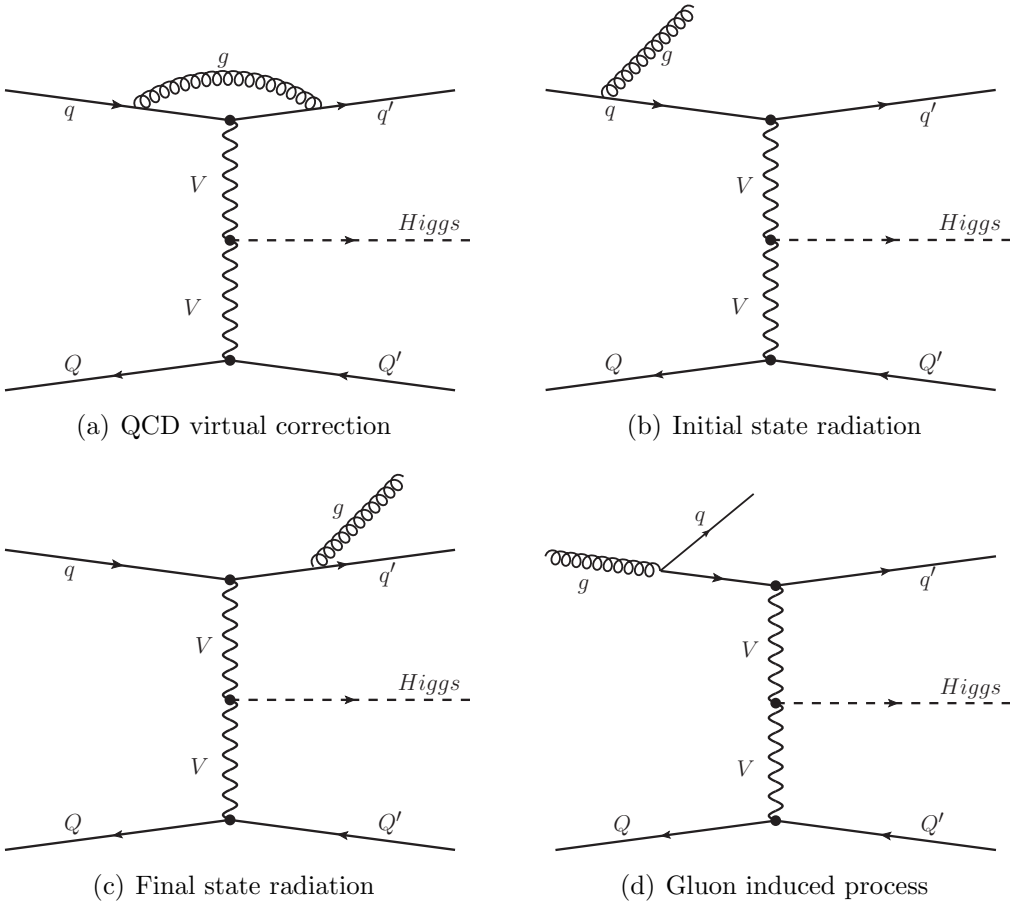

(a) QCD virtual correction (b) Initial state radiation

(c) Final state radiation (d) Gluon induced process

Figure 2.8: The next to leading order QCD corrections to weak boson fusion that are included in the public code `VBFNLO`.

The public `VBFNLO` includes the implementation of Higgs plus two jet production, which is described in Ref. [47]. After appropriate cuts, the t-channel exchange of a weak boson between two external quark lines is the dominant method of production, and consequently in `VBFNLO` the s-channel contributions (Higgsstrahlung) are not included. `VBFNLO` does not include same flavour quarks on the upper and lower external lines. The interference contributions between u- and t-channels are also neglected, as these are strongly kinematically suppressed. The decay of the Higgs is simulated using a narrow width approximation.

All tree level amplitudes are calculated numerically, using the helicity formalism described in Ref. [66, 67]. The next to leading order QCD Feynman diagrams that are incorporated into `VBFNLO` are shown in Fig. 2.8.

Since the exchanged weak boson is a colour singlet, `VBFNLO` does not consider interference between diagrams with a gluon attached to the upper and lower external quark

lines, as these will be identically zero at $\mathcal{O}(\alpha_s)$ for non-crossed diagrams. The three parton phase space integral that occurs when calculating the contribution of the next to leading order diagrams involves both soft and collinear divergences. In `VBFNLO` the divergent phase space integrals are evaluated using the subtraction method of Catani and Seymour (see Ref. [68]) by subtracting a "counterterm" from the integral, leaving a finite phase space integral which is integrated numerically in four dimensions. The divergent terms are integrated analytically using Dimensional Reduction in `VBFNLO` (see Section 3.1) in $4 - 2\epsilon$ dimensions. A broadly equivalent method was implemented to calculate the photon corrections in our modified `VBFNLO`, which is described in detail in Section 3.6.

Two independent Monte Carlo integrations (see Section 1.3) are performed (this is necessary, of course, because the phase spaces involved in the leading order and next to leading order diagrams are distinct – the NLO diagrams involve an extra particle) using the algorithm VEGAS [69]. Jet reconstruction is performed using the k_T algorithm (as described in Ref. [70]).

`VBFNLO` is a very flexible program, and many options determining its running parameters are available. Several relevant processes are coded: as well as Higgs production via weak boson fusion, it can also simulate production of a W or Z boson via WBF, as well as double and triple vector boson production. A variety of Higgs and weak boson decays are included as well. Moving beyond weak boson fusion in the Standard Model, both CP even and CP odd Higgs production via gluon fusion, in a general two Higgs doublet model, can be studied at leading order (i.e. one loop level) with the full top/bottom quark dependence in the loop. Furthermore, a warped Higgsless extra dimension model can be simulated, and anomalous couplings between a Higgs and a pair of weak bosons can be included. We use this particular ability to incorporate anomalous HVV couplings in order to implement the higher order electroweak corrections.

All of the cut parameters can be determined by the user (although, of course, if these are altered too much from the set of "standard" weak boson fusion cuts described in Section 2.2, they will not give an accurate idea of what to expect from the LHC), and renormalisation and factorisation scales can also be chosen. `VBFNLO` can be interfaced with `lhapdf` [71] to supply the PDFs, and the CTEQ6 [72] parton density functions are "hard-wired" into the code as well. The Standard Model parameters (such as the Higgs mass and value of the electromagnetic coupling constant) can obviously be controlled, and the Higgs width and branching ratios are calculated. Additionally, the effects of external bottom quarks can be included for the neutral currents (Z boson fusion).

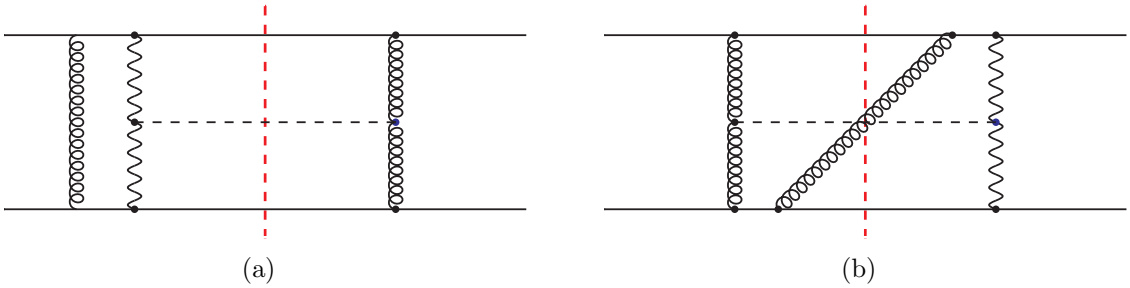

Figure 2.9: Example interference diagrams between gluon fusion and Z boson fusion, at one loop level.

Finally, the total cross section and a range of distributions is output, in a format that can be easily analysed by `ROOT`, `gnuplot` or `topdrawer`.

2.6 Higher order QCD-type contributions

In the Standard Model, higher order QCD contributions that are not considered in the present work have been studied and found to be negligible. These include two loop contributions from gluon induced weak boson fusion [73, 74] and the loop level interference effects between weak boson fusion and gluon fusion [75, 76].

Generally, the interference effects between gluon fusion and weak boson fusion are neglected in predictions for the LHC. At leading order, these contributions require a t $\leftrightarrow$ u channel crossing and so suffer a kinematic suppression and moreover only occur when we have identical quarks. The kinematic suppression comes about as a result of the structure of weak boson fusion (and the WBF cuts that are used to exploit that structure) filter out all but high energy, very forward jets. The contribution from an uncrossed diagram behaves like $\frac{1}{t^2}$ or $\frac{1}{u^2}$, whereas the crossed diagram is $\propto \frac{1}{tu}$. Since the cuts mean that t and u cannot both be small, the crossed diagram is always suppressed with respect to the uncrossed diagram.

At loop level $\mathcal{O}(\alpha^2\alpha_s^3)$, however, these restrictions are lifted and interference diagrams between gluon fusion and Z boson fusion survive that are not suppressed by flavour or crossing, and are not forbidden by colour conservation. Examples of these diagram types are shown in Fig. 2.9.

These diagrams are of order $\mathcal{O}(\alpha^2\alpha_s^3)$ and could potentially be numerically important, as the arguments that allowed us to neglect the interference contribution at lower orders

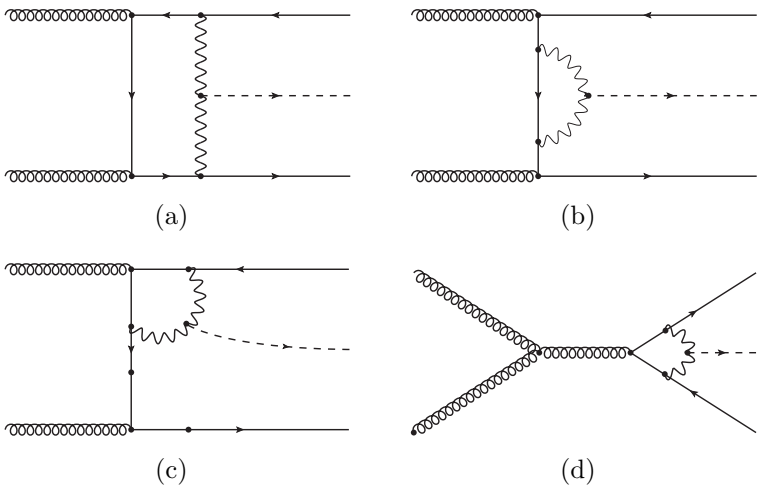

Figure 2.10: Gluon initiated NNLO QCD corrections to weak boson fusion.

do not apply here. The authors of Ref. [75] explicitly calculated these contributions, and found them to be small. This smallness was the result of a combination of a cancellation between flavours and helicities[12], the complex phases of the full one loop calculation and an accidental cancellation between sea and valence quarks. The authors concluded that the loop level interference contributions are not sufficient to destroy the purity of the obtained weak boson fusion signal.

Ref. [73] considers various categories of next to next to leading order (NNLO) QCD corrections and focuses on the subset of diagrams consisting of gluon induced processes (examples of which are shown in Fig. 2.10). This subset can be considered separately because it is gauge invariant, as well as both UV and IR finite (without the need for real radiation to cancel the IR divergences). The high gluon luminosity expected at the LHC means that these diagrams are potentially important and – since they involve a net colour exchange that is not suppressed by crossing – could lead to additional sources of hadronic activity, thus polluting the WBF sample. It was found, however, that owing to the kinematic structure of these types of diagrams, the weak boson fusion cuts strongly suppress the NNLO contribution from gluon induced weak boson fusion[13], which is formally $\mathcal{O}(\alpha^3\alpha_s^2)$. Other sets of NNLO corrections are not expected to have a significant effect on either the total cross section or the shapes of the distributions.

[12] Since the interference term is not squared, but is rather $\propto 2\mathrm{Re}(\mathcal{M}_{loop}\mathcal{M}^*_{tree})$, the sign of the coupling between the external quark pair and the Z boson becomes relevant.

[13] The WBF cuts suppress this NNLO contribution by a factor of ~ 30, compared to a factor of $\sim 2-3$ for the LO and NLO corrections shown in Fig. 2.8.

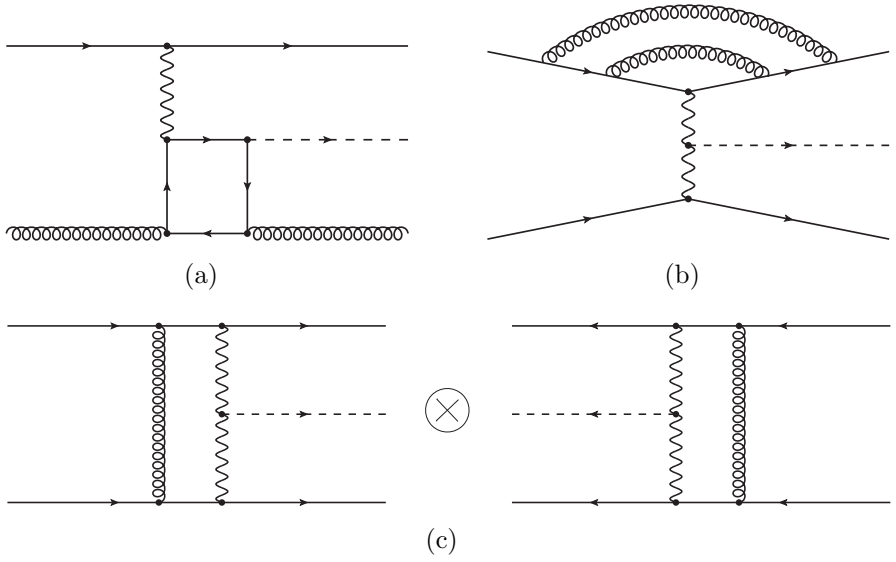

Figure 2.11: Quark loops, quark vertex and gluon exchange NNLO QCD corrections to weak boson fusion.

Diagrams of the type shown in Fig. 2.11(a), with closed quark loops, do not involve any net colour exchange between the external particles and so, following earlier arguments, additional hadronic activity in the central region is expected to be minimal.

Another set of NNLO virtual diagrams are analogous to those considered at NLO - corrections to the quark vertex, as seen in Fig. 2.11(b). The authors of Ref. [73] postulate that these can be estimated from corrections to the deep inelastic scattering process [77] and are thought to cause no appreciable reduction in the purity of the WBF signal.

As has been explained, at next to leading order diagrams of gluon exchange between the external quark lines are neglected in `VBFNLO`, as these are heavily suppressed by the necessity of crossing amplitudes. At NNLO, however, because the two exchanged gluons can form a colour singlet, interference with an uncrossed tree amplitude is possible and this suppression does not occur (see Fig. 2.11(c)). The authors of Ref. [73] postulate that, since the net colour exchange is zero (the two exchanged gluons form a colour *singlet*), there should be no significant increase in jet activity in the important central region of the detector, thus leaving the WBF signal relatively pure.

These investigations into the higher order QCD type contributions show that the theoretical uncertainty involved in calculating weak boson fusion is well under control, and the likelihood of NNLO corrections causing significant deviations from the predicted cross sections and distributions is slim. The NNLO diagrams calculated in Ref. [73]

amount to less than 0.3% of the leading order cross section after WBF cuts have been applied. The interference at one loop level between gluon fusion and weak boson appears to be even smaller, having less than a 0.03% effect on the $\Delta\phi$ distribution.

Using these results as guidelines, it appears safe to assume that these higher order contributions are small and consequently they are not taken into account in this work.

Chapter 3

Higher order calculations

"Here there be dragons."
— Anon

In this chapter we review the procedures used to renormalise all the processes considered in this thesis, explicitly stating all relevant counterterms and renormalisation constants. We will also discuss the methods used to implement the various higher order calculations into a modified version of the public code `VBFNLO`, as well as the checks imposed on the final results.

3.1 Renormalisation in the Standard Model and the MSSM

The calculation of loop corrections to weak boson fusion will involve tensor integrals over the loop momentum, which can be simplified via Passarino–Veltman reduction into scalar integrals [78]. These scalar integrals contain quadratic, linear and logarithmic divergences. Several schemes have been developed that allow us to analyse these divergences. The most well known of these methods is dimensional regularisation (DREG) [79], where we analytically continue the integrals into $D = 4 - 2\epsilon$ dimensions in order to perform the integration, where ϵ is some infinitesimal value. The original

divergence is regained in the limit of 4 dimensions – i.e. $\epsilon \to 0$. In other words

$$\int \frac{d^4q}{(2\pi)^4} \to \mu_{ren}^{4-D} \int \frac{d^Dq}{(2\pi)^D} \tag{3.1}$$

Here μ_{ren} is the regularisation scale – an arbitrary reference mass, which is needed to keep the couplings dimensionless. For the scalar integral A_0, the pole at $D = 4$ can be seen in the following:

$$\begin{aligned} A_0(m^2) &= \frac{(2\pi\mu_{ren})^{4-D}}{i\pi^2} \int d^Dq \frac{1}{q^2 - m^2 + i\varepsilon} \\ &= m^2 \left(\Delta - \ln\left(\frac{m^2}{\mu_{ren}^2}\right) + 1 \right) + \mathcal{O}(D-4) \end{aligned} \tag{3.2}$$

where

$$\begin{aligned} \Delta &= \frac{2}{4-D} - \gamma_E + \ln(4\pi) \\ \text{and } \gamma_E &= \text{Euler-Mascheroni constant} \end{aligned} \tag{3.3}$$

Dimensional regularisation is commonly used when working in the Standard Model, as it preserves both Lorentz and gauge invariance. Since the fields considered are D-dimensional rather than 4-dimensional, the number of bosons no longer equals the number of fermions – in other words, dimensional regularisation does not respect supersymmetry.

An alternative to DREG, which is normally used when supersymmetric calculations are being performed, is Dimensional Reduction (DRED)[1]. In this method, the fields are kept four-dimensional, while the loop integration is again performed in D dimensions, thus avoiding explicit SUSY breaking. It has been shown that DRED is mathematically consistent and that it preserves supersymmetry up to at least the two loop level for matter fields [80].

The divergences that occur during loop calculations are cancelled using a renormalisation procedure. The original parameters in the Lagrangian are considered to be the "bare" parameters, which are divergent (and hence unphysical). Renormalisation both allows us to eliminate the divergences that occur when calculating higher order corrections, and also allows us to define the physical meaning of a parameter beyond lowest

[1]Note that it is possible to use DREG in supersymmetric calculations, but in this case symmetry restoring counterterms must be used.

order. The bare parameters are replaced by physical parameters (which are finite, and referred to as "renormalised" parameters), plus a counterterm. Thus, for a parameter p and a field ϕ, the renormalisation transformation is typically:

$$p^{bare} = p^{ren} + \delta p \tag{3.4}$$

$$\phi^{bare} = \phi^{ren}\,(1 + \delta Z_\phi) \tag{3.5}$$

The renormalised parameters are fixed by the choice of renormalisation scheme, of which there are several. One choice is the Minimal Subtraction (MS) scheme, which makes use of DREG and cancels out only the divergences in the loop integrals (i.e. the first term in Equation 3.3), leaving all finite pieces alone. In the modified Minimal Subtraction ($\overline{MS}$) scheme, dimensional regularisation is again used, but in this case all terms proportional to Δ (defined in Equation 3.3) are cancelled by the counterterms, not only the divergences. The modified Dimensional Reduction ($\overline{DR}$) scheme is similar to $\overline{MS}$, as it is concerned with the terms in Δ, but makes use of dimensional reduction. One further scheme that is commonly used is the on-shell (OS) scheme. Here, all renormalised masses correspond directly to the physical masses (i.e. the real part of the pole of the particle's propagator), and the residue of the propagator is required to be 1.

We use the program `LoopTools` [81, 82] to evaluate the loop integrals that occur in our calculations.

3.2 Corrections to weak boson fusion

There are both real and virtual corrections to weak boson fusion that need to be considered. These corrections have been divided into groups in order to make the calculations clearer.

Firstly, there are real corrections to weak boson fusion, shown in Fig. 3.1. These consist of both gluon and photon emission from the external quark lines, as well as photon or gluon induced processes. While the QCD contributions have been studied in detail previously [47, 83], and the publicly available `VBFNLO` code includes these corrections, the QED contributions have only been studied in Ref. [55]. The real photonic corrections have now been included into our modified `VBFNLO` [84].

The virtual corrections to weak boson fusion fall into five different categories, shown in Fig. 3.2. These include corrections to the Higgs–weak boson vertex (HVV), correc-

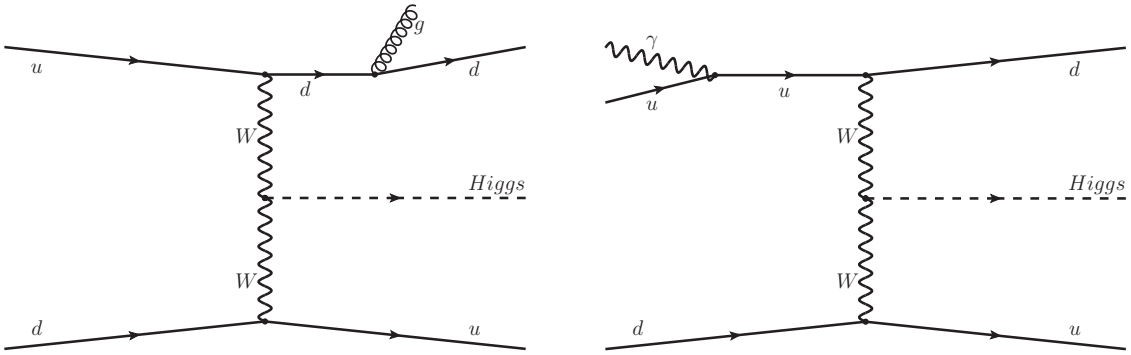

(a) QCD corrections (b) QED corrections

Figure 3.1: Examples of real corrections to the weak boson fusion process.

tions to the weak boson self energy (VV), corrections to the vertex between the external quarks and the weak bosons (qqV), and box and pentagon diagrams.

When only fermion (and sfermion) loop corrections are being considered, no box or pentagon diagrams contribute, and there are no loops present at the qqV vertex between the external quarks and the weak boson, although there is a counterterm diagram here. In the full Standard Model, or MSSM, these types of diagram (boxes, pentagons, loops at the qqV vertex) need to be considered as well.

Throughout this work, the external quarks are considered to be light and consequently radiation of a Higgs from the external legs is not considered. Non-zero masses are kept only where they are needed to regulate divergences at intermediate steps.

3.3 Renormalisation transformations and constants

In the following section we describe the renormalisation transformations and conditions we impose, along with the renormalisation constants to which they lead. We follow the SM conventions of [85]. One thing that should be noted is that the MSSM typically uses a different sign convention for the SU(2) covariant derivative (Equation 1.3) to the Standard Model as described in Ref. [85]. In practice, this means that any $\sin\theta_W$ in the Standard Model is replaced by $(-\sin\theta_W)$ in the MSSM, and a minus sign is included for every Higgs field in the MSSM couplings. Unless it is specifically stated otherwise, the renormalisation constants here use the MSSM convention – for completeness, the corresponding constants in the Standard Model are stated in Appendix A.

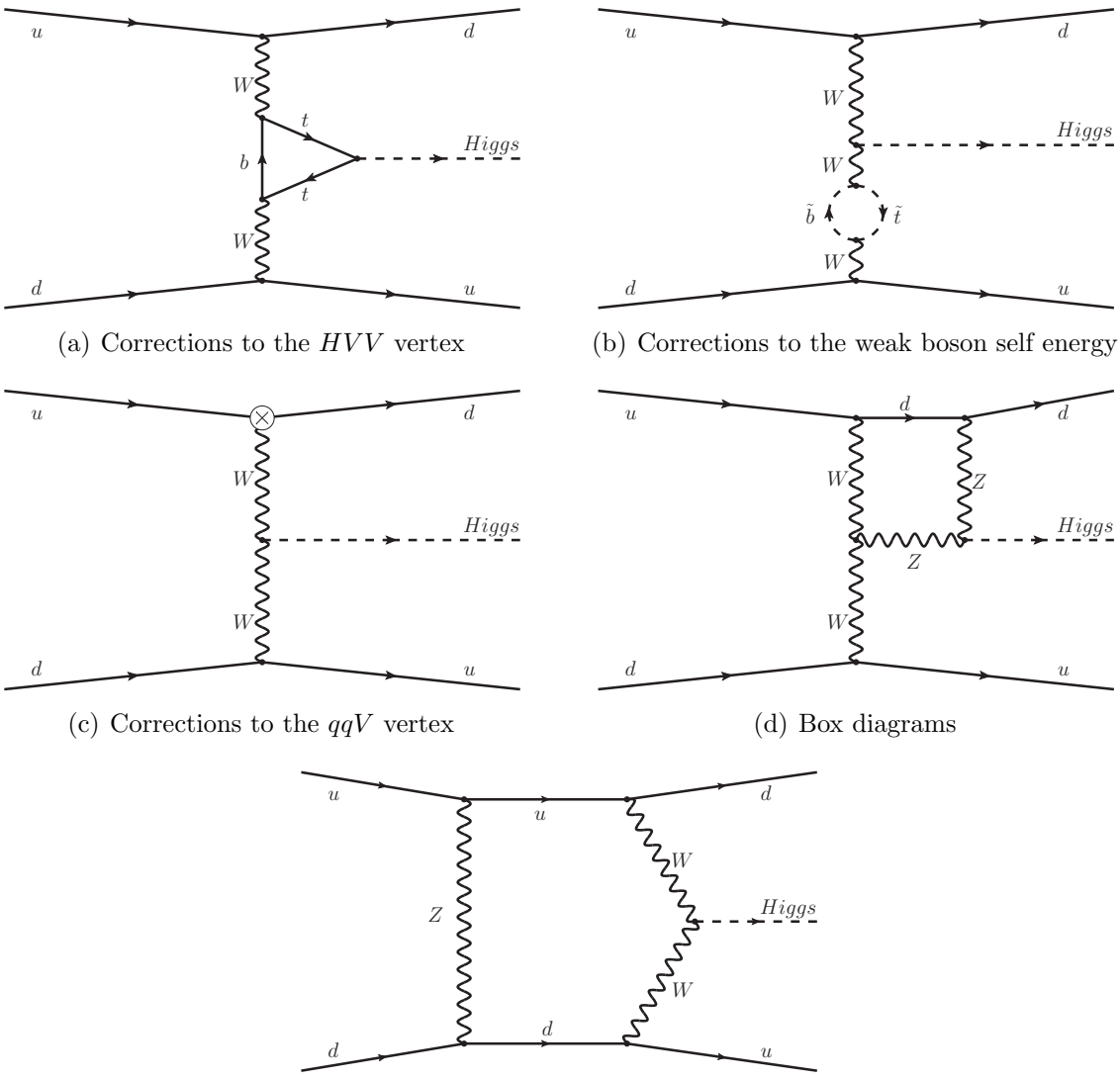

(a) Corrections to the HVV vertex

(b) Corrections to the weak boson self energy

(c) Corrections to the qqV vertex

(d) Box diagrams

(e) Pentagon diagrams

Figure 3.2: Types of virtual corrections to the weak boson fusion process.

In this work, a renormalisation scheme is used where the electroweak sector is renormalised on-shell, which means that the renormalised transverse self energies and the derivative of the renormalised self energy with respect to the square of the momentum p must vanish at $p^2 = m^2_{ren}$. For the field renormalisation constants, an on-shell condition means that, for external particles that are on-shell, the one particle irreducible two point functions are diagonal once renormalised. In this way we ensure that all renormalised masses of the gauge bosons correspond to the physical, measured masses and their propagators' poles are equal to 1. The renormalisation transforms of the gauge bosons are given by (where V stands for either the W or the Z boson):

$$M_V^2 \rightarrow M_V^2 + \delta M_V^2 \tag{3.6}$$

$$W \rightarrow \left(1 + \frac{1}{2}\delta Z_{WW}\right) W \tag{3.7}$$

$$\begin{pmatrix} Z \\ \gamma \end{pmatrix} \rightarrow \begin{pmatrix} \left(1 + \frac{1}{2}\delta Z_{ZZ}\right) & \frac{1}{2}\delta Z_{Z\gamma} \\ \frac{1}{2}\delta Z_{\gamma Z} & \left(1 + \frac{1}{2}\delta Z_{\gamma\gamma}\right) \end{pmatrix} \begin{pmatrix} Z \\ \gamma \end{pmatrix} \tag{3.8}$$

Imposing the on-shell renormalisation conditions described above, the renormalisation constants are seen to be

$$\delta M_V^2 = \mathrm{Re}\left(\Sigma^T_{VV}(M_V^2)\right) \tag{3.9}$$

$$\delta \sin\theta_W = -\frac{1}{2}\frac{\cos^2\theta_W}{\sin\theta_W}\left(\frac{\delta M_Z^2}{M_Z^2} - \frac{\delta M_W^2}{M_W^2}\right) \tag{3.10}$$

$$\delta Z_{VV} = -\mathrm{Re}\left(\Sigma'_{VV}(M_V^2)\right) \tag{3.11}$$

$$\delta Z_{\gamma Z} = -\frac{2}{M_Z^2}\mathrm{Re}\left(\Sigma_{\gamma Z}(M_Z^2)\right) \tag{3.12}$$

$$\delta Z_{Z\gamma} = \frac{2}{M_Z^2}\Sigma^T_{\gamma Z}(0) \tag{3.13}$$

Here, the prime (Σ') signifies that the derivative with respect to momentum p^2 is taken, and the superscript T denotes the transverse part of the self energy. The transverse (and longitudinal – denoted by the superscript L) parts of a self energy are defined according to:

$$\Sigma^{\mu\nu}(p) = \Sigma^T(p^2)\left(-g^{\mu\nu} + \frac{p^\mu p^\nu}{p^2}\right) - \frac{p^\mu p^\nu}{p^2}\Sigma^L(p^2) \tag{3.14}$$

Note that the renormalisation constant for the electroweak mixing angle ($\delta \sin\theta_W$) is found by considering the relation $M_Z \cos\theta_W = M_W$ – i.e. it is not an independent parameter and thus does not need to receive its own renormalisation transform.

The field renormalisation of the fermions is also performed on-shell, with a transform and constant given by:

$$f_X \rightarrow f_X \left(1 + \frac{1}{2}\delta Z_{f_X}\right) \tag{3.15}$$

$$\delta Z_{f_X} = -\mathrm{Re}\Sigma^X_{ff} - m_f^2 \frac{\partial}{\partial p^2} \mathrm{Re}\left[\Sigma^L_{ff}(p^2) + \Sigma^R_{ff}(p^2) + 2\Sigma^S_{ff}(p^2)\right]\Big|_{p^2=m_f^2} \tag{3.16}$$

Here, the superscripts L, R and S denote the left, right and scalar parts, and X is either L or R.

3.3.1 Higgs renormalisation

For the Higgs transform we impose one renormalisation transformation for each Higgs doublet, following Ref. [31]:

$$\mathcal{H}_i \rightarrow \left(1 + \frac{1}{2}\delta Z_{\mathcal{H}_i}\right)\mathcal{H}_i \qquad \text{where } i = 1,\, 2 \tag{3.17}$$

This means that the field renormalisation matrix (in the basis of the mass eigenstates) is given by:

$$\tan\beta \rightarrow \tan\beta\,(1 + \delta\tan\beta) = \tan\beta\left(1 + \frac{1}{2}\left[\delta\mathcal{H}_2 - \delta\mathcal{H}_1\right]\right) \tag{3.18}$$

$$\begin{pmatrix} h \\ H \\ A \end{pmatrix} \rightarrow \begin{pmatrix} \left(1 + \frac{1}{2}\delta Z_{hh}\right) & \frac{1}{2}\delta Z_{hH} & \frac{1}{2}\delta Z_{hA} \\ \frac{1}{2}\delta Z_{hH} & \left(1 + \frac{1}{2}\delta Z_{HH}\right) & \frac{1}{2}\delta Z_{HA} \\ \frac{1}{2}\delta Z_{hA} & \frac{1}{2}\delta Z_{HA} & \left(1 + \frac{1}{2}\delta Z_{AA}\right) \end{pmatrix} \begin{pmatrix} h \\ H \\ A \end{pmatrix} \tag{3.19}$$

Note that we are neglecting mixing between the neutral Higgs bosons and the Goldstone bosons[2]. The field renormalisation constants themselves are thus:

$$\begin{aligned}
\delta Z_{hh} &= \sin^2\alpha\ \delta Z_{\mathcal{H}_1} + \cos^2\alpha\ \delta Z_{\mathcal{H}_2} && (3.20)\\
\delta Z_{HH} &= \cos^2\alpha\ \delta Z_{\mathcal{H}_1} + \sin^2\alpha\ \delta Z_{\mathcal{H}_2} && (3.21)\\
\delta Z_{AA} &= \sin^2\beta\ \delta Z_{\mathcal{H}_1} + \cos^2\beta\ \delta Z_{\mathcal{H}_2} && (3.22)\\
\delta Z_{hH} &= \sin\alpha\cos\alpha\,(\delta Z_{\mathcal{H}_2} - \delta Z_{\mathcal{H}_1}) && (3.23)
\end{aligned}$$

The renormalisation constants δZ_{hA} and δZ_{HA} are both zero, due to the fact that the Higgs sector is CP conserving at tree level.

We renormalise the Higgs fields using the $\overline{DR}$ scheme in the following manner, where the superscript *div* signifies those terms which are proportional to Δ (see Equation 3.3). The $\overline{DR}$ scheme has been shown to be numerically stable [86] and has been found to be a convenient choice for Higgs field renormalisation when considering higher order corrections to the Higgs masses. The correct on-shell properties of the external Higgs are ensured by finite wavefunction normalisation factors. These so-called "Z-factors" are a convenient way of taking higher order corrections (which are, in the Higgs sector, typically large) into account, and are described in detail in Section 3.4. Since $\tan\beta$ corresponds directly to no obvious physical observable, there is no problem using $\overline{DR}$ for the field renormalisation.

$$\begin{aligned}
\delta Z_{hh} &= -\left[\mathrm{Re}\Sigma'_{hh}(m_h^2)\right]^{div} && (3.24)\\
\delta Z_{HH} &= -\left[\mathrm{Re}\Sigma'_{HH}(m_H^2)\right]^{div} && (3.25)\\
\delta Z_{hH} &= \delta Z_{Hh} = \frac{\sin\alpha\cos\alpha}{\cos 2\alpha}\,(\delta Z_{hh} - \delta Z_{HH}) && (3.26)\\
\delta\tan\beta &= \frac{1}{2\cos 2\alpha}\,(\delta Z_{hh} - \delta Z_{HH}) && (3.27)
\end{aligned}$$

Note that the Higgs masses used in these formulae are the tree level masses[3]. In the Standard Model, the Higgs field renormalisation is defined in the on-shell scheme:

$$\delta Z_{HH} = -\mathrm{Re}\left(\Sigma'_{HH}(m_H^2)\right) \qquad (3.28)$$

[2]In general, of course, this contribution cannot be neglected. In our case, as we are only interested in weak boson fusion and there is no coupling between a pair of weak bosons and a Goldstone boson, it is safe to neglect it.

[3]Recall that, throughout this work, lower case m_{Higgs} will refer to tree level masses, while upper case M_{Higgs} refers to loop corrected masses.

The renormalisation transformation for the Higgs masses, for the original ϕ and χ fields, is

$$M_{\phi\phi\chi} \to M_{\phi\phi\chi} + \delta M_{\phi\phi\chi} \tag{3.29}$$

Switching to the basis of mass eigenstates of the lowest order Higgs field, we obtain:

$$\begin{aligned} \delta M_{hHA} &= U \delta M_{\phi\phi\chi} U^\dagger \\ &= \begin{pmatrix} \delta m_h^2 & \delta m_{hH}^2 & \delta m_{hA}^2 \\ \delta m_{hH}^2 & \delta m_H^2 & \delta m_{HA}^2 \\ \delta m_{hA}^2 & \delta m_{HA}^2 & \delta m_A^2 \end{pmatrix} \end{aligned} \tag{3.30}$$

The Higgs mass renormalisation constants are then

$$\begin{aligned} \delta m_h^2 &= \delta m_A^2 \cos^2(\beta-\alpha) + \delta M_Z^2 \sin^2(\alpha+\beta) + \\ &\quad \frac{e}{2 M_Z \sin\theta_W \cos\theta_W} \big(\delta T_H \cos(\alpha-\beta) \sin^2(\alpha-\beta) + \\ &\qquad \delta T_h \sin(\alpha-\beta) \left[1 + \cos^2(\alpha-\beta) \right] \big) + \\ &\quad \delta \tan\beta \sin\beta \cos\beta \left[m_A^2 \sin\left(2(\alpha-\beta)\right) + M_Z^2 \sin\left(2(\alpha+\beta)\right) \right] \end{aligned} \tag{3.31}$$

$$\begin{aligned} \delta m_H^2 &= \delta m_A^2 \sin^2(\beta-\alpha) + \delta M_Z^2 \cos^2(\alpha+\beta) - \\ &\quad \frac{e}{2 M_Z \sin\theta_W \cos\theta_W} \big(\delta T_H \cos(\alpha-\beta) \left[1 + \sin^2(\alpha-\beta) \right] + \\ &\qquad \delta T_h \sin(\alpha-\beta) \cos^2(\alpha-\beta) \big) - \\ &\quad \delta \tan\beta \sin\beta \cos\beta \left[m_A^2 \sin\left(2(\alpha-\beta)\right) + M_Z^2 \sin\left(2(\alpha+\beta)\right) \right] \end{aligned} \tag{3.32}$$

$$\begin{aligned} \delta m_{hH}^2 &= \frac{1}{2} \left[\delta m_A^2 \sin\left(2(\alpha-\beta)\right) - \delta M_Z^2 \sin\left(2(\alpha+\beta)\right) \right] + \\ &\quad \frac{e}{2 M_Z \sin\theta_W \cos\theta_W} \big(\delta T_H \sin^3(\alpha-\beta) - \delta T_h \cos^3(\alpha-\beta) \big) - \\ &\quad \delta \tan\beta \sin\beta \cos\beta \left[m_A^2 \cos\left(2(\alpha-\beta)\right) + M_Z^2 \cos\left(2(\alpha+\beta)\right) \right] \end{aligned} \tag{3.33}$$

The renormalisation constants δT_h and δT_H are the tadpole renormalisation. The tadpoles $T_{h,H}$ are the coefficients of the linear terms in the Higgs potential, and must vanish at zeroth order to ensure that the VEVs of the Higgs potential are stationary points. Their renormalisation transform is given by

$$T_{h,H} \to T_{h,H} + \delta T_{h,H} \tag{3.34}$$

Since the tadpole coefficients are required to vanish, it follows that

$$T_{h,H}^{1-loop} + \delta T_{h,H} = 0 \tag{3.35}$$

In the MSSM with real parameters, the CP odd Higgs boson A is renormalised on-shell, whereas in the complex MSSM the charged Higgs $H^{\pm}$ is required to be on-shell. This follows the decision of which of the two masses is used as the independent parameter input – in the MSSM with complex parameters, M_A is not a mass eigenstate at higher orders, due to mixing with the other neutral Higgs bosons, and consequently $M_{H^{\pm}}$ is used as the input. Thus, for $i = A$ for the real MSSM and $i = H^{\pm}$ for the complex MSSM:

$$\delta m_i^2 = \mathrm{Re}\Sigma_{ii}(M_i^2) \tag{3.36}$$

and

$$\delta m_A^2 = \delta m_{H^+}^2 - \delta M_W^2 \tag{3.37}$$

3.3.2 Charge renormalisation

The counterterms needed[4] for the calculation of higher order corrections to weak boson fusion include the charge renormalisation constant, δZ_e. A renormalisation condition for the charge can be arrived at by defining the electric charge e as being equal to the full $ee\gamma$ vertex for on-shell external particles when the photon momentum tends to zero (this is known as the Thompson limit). The renormalisation transformation is

$$e \longrightarrow e\,(1 + \delta Z_e) \tag{3.38}$$

The renormalised charge is then identified with the physical charge in the Thompson limit

$$e(0) = \sqrt{4\pi\alpha(0)} \tag{3.39}$$

where $\alpha(0)$ is the fine structure constant [87]:

$$\alpha(0) = \frac{1}{137.035999679} \tag{3.40}$$

[4]The counterterms are described in Section 3.5.

The precise form of the renormalisation constant δZ_e is derived (for the derivation, see, for example, Reference [85]), by imposing the condition that the loop corrections to the vertex $ee\gamma$ vanish in the Thompson limit. Note that during this section we will work with the Standard Model convention for the SU(2) covariant derivative.

$$\begin{aligned}\delta Z_e &= \frac{1}{2}\Pi_\gamma(0) - \frac{\sin\theta_W}{\cos\theta_W}\frac{\sum_{\gamma Z}^{T}(0)}{M_Z^2} \\ &= \frac{1}{2}\frac{\partial}{\partial q^2}\sum\nolimits_{\gamma\gamma}\left(q^2\right)|_{q^2=0} - \frac{\sin\theta_W}{\cos\theta_W}\frac{\sum_{\gamma Z}^{T}(0)}{M_Z^2}\end{aligned} \tag{3.41}$$

Difficulties can be encountered, however, when calculating $\Pi^\gamma(0)$, as it involves large contributions from a logarithmic term involving the fermion masses. This leads to problems as the masses of the light quarks are not well defined. In order to avoid dependence on the light quark masses, the quantity $\Delta\alpha$ can be used.

$$\begin{aligned}\Delta\alpha &= \Pi_\gamma^{light}(0) - \mathrm{Re}\Pi_\gamma^{light}(M_Z^2) \\ \Rightarrow \Pi_\gamma^{light}(0) &= \Delta\alpha + \mathrm{Re}\Pi_\gamma^{light}(M_Z^2) \\ &= \Delta\alpha + \frac{1}{M_Z^2}\mathrm{Re}\left(\Sigma_{\gamma\gamma}^{light}\left(M_Z^2\right)\right)\end{aligned} \tag{3.42}$$

The $\Pi_\gamma(0)$ in Equation 3.41 can thus be split into its light (i.e. all leptons and all quarks except the top) and heavy (the top quark, bosons and any SUSY particles) parts and $\Delta\alpha$ can be used to replace the light particles' contribution to $\Pi^\gamma(0)$ in the following way.

$$\begin{aligned}\delta Z_e &= \frac{1}{2}\Pi_\gamma^{light}(0) + \frac{1}{2}\Pi_\gamma^{heavy}(0) - \frac{\sin\theta_W}{\cos\theta_W}\frac{\sum_{\gamma Z}^{T}(0)}{M_Z^2} \\ &= \frac{1}{2}\left(\Delta\alpha + \mathrm{Re}\Pi_\gamma^{light}(M_Z^2)\right) + \frac{1}{2}\Pi_\gamma^{heavy}(0) - \frac{\sin\theta_W}{\cos\theta_W}\frac{\sum_{\gamma Z}^{T}(0)}{M_Z^2} \\ &= \frac{1}{2}\left(\Delta\alpha + \frac{1}{M_Z^2}\mathrm{Re}\left[\sum\nolimits_{\gamma\gamma}^{light}(M_Z^2)\right]\right) + \frac{1}{2}\Pi_\gamma^{heavy}(0) - \frac{\sin\theta_W}{\cos\theta_W}\frac{\sum_{\gamma Z}^{T}(0)}{M_Z^2}\end{aligned} \tag{3.43}$$

$\Delta\alpha$ can be split into its component parts – the contribution from the leptons, which has been calculated at three loop level [88] to be $\Delta\alpha^{leptons} = 0.031497686$, plus the contributions from the light quarks (i.e. all quarks but the top). The quark contribution has been determined experimentally using a dispersion relation, and is given by $\Delta\alpha_{5flav}^{hadron} = 0.02755 \pm 0.0023$ [89].

We can also choose to absorb the $\Delta\alpha$ contribution into the tree level matrix element and parametrise using $\alpha(M_Z^2)$:

$$\alpha(M_Z^2) = \frac{\alpha(0)}{1-\Delta\alpha} \tag{3.44}$$

This means that δZ_e needs to be replaced by $\delta Z_e^{\alpha(M_Z^2)}$ in the following way (up to higher order terms)

$$\begin{aligned} e &\longrightarrow e(0)\,(1+\delta Z_e) \\ &= e(0)\left(1+\frac{\Delta\alpha}{2}\right)\left(1+\delta Z_e-\frac{1}{2}\Delta\alpha\right) \\ &= e(M_Z^2)\left(1+\delta Z_e^{\alpha(M_Z^2)}\right) \\ &\quad \text{where} \\ \delta Z_e^{\alpha(M_Z^2)} &= \delta Z_e-\frac{1}{2}\Delta\alpha \end{aligned} \tag{3.45}$$

In this way, $\Delta\alpha$ drops out of the charge renormalisation constant $\delta Z_e^{\alpha(M_Z^2)}$. Note that an alternative method of evaluating the charge renormalisation constant when the lowest order coupling has been reparametrised to $\alpha(M_Z^2)$ is to use effective masses for the light quarks. These masses are set to values that will reproduce $\delta Z_e^{\alpha(M_Z^2)}$ as above when the quantity $\Pi_\gamma(0)$ is calculated.

A third option is to parametrise the lowest order coupling via the Fermi constant G_F. The Fermi constant, determined from muon decay, is related to the fine structure constant $\alpha(0)$ according to

$$G_F = \frac{\alpha(0)\pi}{\sqrt{2}M_W^2\sin^2\theta_W}\,(1+\Delta r) \tag{3.46}$$

The quantity Δr summarises the higher order corrections to muon decay and at one loop order it can be written as

$$\Delta r = \Delta\alpha - \frac{\cos^2\theta_W}{\sin^2\theta_W}\Delta\rho + (\Delta r)_{remainder} \tag{3.47}$$

In this equation, $\Delta\alpha$ contains the large logarithmic corrections from the light fermions and $\Delta\rho$ involves the leading quadratic correction from the large mass of the top quark. The dependence on the Higgs mass originates from the remainder term.

The reparametrisation of the lowest order coupling in terms of the Fermi constant yields a corresponding shift in the charge renormalisation constant.

$$\delta Z_e^{G_F} = \delta Z_e - \frac{1}{2}\Delta r \tag{3.48}$$

When only loop contributions from fermions (or fermions and sfermions in the MSSM) are being considered, only counterterms and the loop diagrams for the W boson self energy in muon decay contribute to Δr, as there are no vertex or box loop diagrams. In this approximation, we arrive at the simple expression below, which comes directly from Equation 3.46:

$$\delta Z_e^{G_F,(s)fermion} = \frac{\delta \sin\theta_W}{\sin\theta_W} - \frac{1}{2}\left(\frac{\sum_{WW}^{T}(0) - \delta M_W^2}{M_W^2}\right) \tag{3.49}$$

In the full Standard Model, however, once the vertex and box diagrams have been computed, the expression for Δr (and hence $\delta Z_e^{G_F}$) is more complicated (owing to the additional diagrams), although it is still relatively compact [90–92].

$$\begin{aligned}
\Delta r^{1-loop,SM} &= \Pi_\gamma(0) - \frac{\cos^2\theta_W}{\sin^2\theta_W}\left(\frac{\delta M_Z^2}{M_Z^2} - \frac{\delta M_W^2}{M_W^2}\right) + \frac{\sum_{WW}(0) - \delta M_W^2}{M_W^2} \\
&\quad +2\,\frac{\cos\theta_W}{\sin\theta_W}\frac{\sum_{\gamma Z}^{T}(0)}{M_Z^2} + \frac{\alpha}{4\pi\sin^2\theta_W}\left(6 + \frac{7-4\sin^2\theta_W}{2\sin^2\theta_W}\ln\left(\cos^2\theta_W\right)\right) \\
&= \Pi_\gamma(0) - 2\,\frac{\delta\sin\theta_W}{\sin\theta_W} + \frac{\sum_{WW}(0) - \delta M_W^2}{M_W^2} + \frac{\cos\theta_W}{\sin\theta_W}\,\delta Z_{Z\gamma} + \\
&\quad \frac{\alpha}{4\pi\sin^2\theta_W}\left(6 + \frac{7-4\sin^2\theta_W}{2\sin^2\theta_W}\ln\left(\cos^2\theta_W\right)\right)
\end{aligned} \tag{3.50}$$

Accordingly, in the Standard Model, reparametrisation of the lowest order coupling by the Fermi constant yields the corresponding replacement of the charge renormalisation

constant by:

$$\begin{aligned}
\delta Z_e^{G_F,SM} &= \frac{1}{2}\Pi_\gamma(0) - \frac{\sin\theta_W}{\cos\theta_W}\delta Z_{Z\gamma} - \frac{1}{2}\Pi_\gamma(0) + \frac{\delta\sin\theta_W}{\sin\theta_W} - \frac{\sum_{WW}(0) - \delta M_W^2}{M_W^2} - \\
&\quad \frac{\cos\theta_W}{\sin\theta_W}\delta Z_{Z\gamma} - \frac{\alpha}{8\pi\sin^2\theta_W}\left(6 + \frac{7-4\sin^2\theta_W}{2\sin^2\theta_W}\ln\left(\cos^2\theta_W\right)\right) \\
&= \frac{\delta\sin\theta_W}{\sin\theta_W} - \frac{\sum_{WW}(0) - \delta M_W^2}{M_W^2} - \frac{1}{\sin\theta_W\cos\theta_W}\delta Z_{Z\gamma} - \\
&\quad \frac{\alpha}{8\pi\sin^2\theta_W}\left(6 + \frac{7-4\sin^2\theta_W}{2\sin^2\theta_W}\ln\left(\cos^2\theta_W\right)\right) \qquad (3.51)
\end{aligned}$$

Due to the extra diagrams that need to be considered in the full MSSM (see, for example, Ref. [93]), the expression corresponding to Equation 3.51 in the MSSM has a somewhat more complicated structure. It is not needed in this thesis, since here we consider the parametrisation of the lowest order coupling in terms of the Fermi constant only for the special case of pure (s)fermionic loop corrections.

3.4 Higgs mixing in the MSSM

In order to perform phenomenologically relevant studies of the Higgs sector of the MSSM, the masses and mixings of the Higgs particles need to be accurately known. In the Feynman diagrammatic approach, in the real MSSM, the full one loop correction is known, as well as two loop results for the $\mathcal{O}(\alpha_s\alpha_t)$, $\mathcal{O}(\alpha_t^2)$, $\mathcal{O}(\alpha_s\alpha_b)$, $\mathcal{O}(\alpha_t\alpha_b)$ and $\mathcal{O}(\alpha_b^2)$ contributions[5]. In the complex MSSM the full one loop corrections are also known, as is the $\mathcal{O}(\alpha_s\alpha_t)$ contribution at two loop level. These corrections are incorporated into the public code `FeynHiggs` [31, 94–97], which in this work we use to calculate the properties of the MSSM Higgs sector. In the improved effective potential approach, the complete two loop result is known [98, 99].

The corrected masses of the Higgs bosons are found by calculating the poles of the Higgs propagator matrix $\mathbf{\Delta}(\mathbf{p^2})$ in the h, H, A basis. Since these poles are in general complex, the physical mass is taken to be the real part of the pole (Equation 3.62, below). When calculating the loop corrected masses, the effects of mixing between the neutral Higgs bosons needs to be taken into account[6]. This corresponds to finding the

[5] Note that $\alpha_{t,b} = \frac{h_{t,b}^2}{4\pi}$, where $h_{t,b}$ are the Yukawa couplings of the top and bottom quarks.

[6] Note that, strictly speaking, mixing between the Higgs bosons and the Z boson and Goldstone boson should be considered, but since these are sub-leading at the two loop level they are neglected here.

three solutions to

$$\frac{1}{|\mathbf{\Delta}(\mathbf{p^2})|} = 0 \tag{3.52}$$

The propagator matrix $\mathbf{\Delta}(\mathbf{p^2})$ is related to the 2-point functions $\hat{\mathbf{\Gamma}}_{hHA}(p^2)$ via

$$\frac{-1}{\mathbf{\Delta}(\mathbf{p^2})} = \hat{\mathbf{\Gamma}}_{hHA}(p^2) = i\left(p^2 - \mathbf{M}(\mathbf{p^2})\right) \tag{3.53}$$

where the mass matrix is written in terms of the renormalised Higgs self energies, $\hat{\Sigma}$:

$$\mathbf{M}(\mathbf{p^2}) = \begin{pmatrix} m_h^2 - \hat{\Sigma}_{hh}(p^2) & -\hat{\Sigma}_{hH}(p^2) & -\hat{\Sigma}_{hA}(p^2) \\ -\hat{\Sigma}_{hH}(p^2) & m_H^2 - \hat{\Sigma}_{HH}(p^2) & -\hat{\Sigma}_{HA}(p^2) \\ -\hat{\Sigma}_{hA}(p^2) & -\hat{\Sigma}_{HA}(p^2) & m_A^2 - \hat{\Sigma}_{AA}(p^2) \end{pmatrix} \tag{3.54}$$

The renormalised self energies are calculated from the following formulae (in the first equation, $i = h, H$ or A):

$$\hat{\Sigma}_{ii}(p^2) = \Sigma_{ii}(p^2) + \delta Z_i\left(p^2 - m_i^2\right) - \delta m_i^2 \tag{3.55}$$

$$\hat{\Sigma}_{hH}(p^2) = \Sigma_{hH}(p^2) + \delta Z_{hH}\left(p^2 - \frac{1}{2}\left[m_h^2 + m_H^2\right]\right) - \delta m_{hH}^2 \tag{3.56}$$

$$\hat{\Sigma}_{hA}(p^2) = \Sigma_{hA}(p^2) + \delta m_{hA}^2 \tag{3.57}$$

$$\hat{\Sigma}_{HA}(p^2) = \Sigma_{HA}(p^2) + \delta m_{HA}^2 \tag{3.58}$$

Inverting the mass matrix gives the (diagonal) Higgs propagator in the same form as if there were no mixing, but with the usual self energy replaced by an effective self energy:

$$\Delta_{ii} = \frac{i}{p^2 - m_i^2 + \hat{\Sigma}_{ii}^{eff}(p^2)} \tag{3.59}$$

$$\hat{\Sigma}_{ii}^{eff}(p^2) = \hat{\Sigma}_{ii}(p^2) - i\left(\frac{2\hat{\Gamma}_{ij}\hat{\Gamma}_{jk}\hat{\Gamma}_{ki} - \hat{\Gamma}_{ki}^2\hat{\Gamma}_{jj} - \hat{\Gamma}_{ij}^2\hat{\Gamma}_{kk}}{\hat{\Gamma}_{jj}\hat{\Gamma}_{kk} - \hat{\Gamma}_{jk}^2}\right) \tag{3.60}$$

The irreducible vertex functions Γ_{ij} are defined in Equation 3.53, using the mass matrix of Equation 3.54. Note that Γ_{ij} are functions of momentum p^2, although this is not explicitly stated in the equation above, simply due to space considerations.

The complex poles ($\mathcal{M}_i$) of the propagator are solutions of the equation:

$$\mathcal{M}_i - m_i^2 + \hat{\Sigma}_{ii}^{eff}(\mathcal{M}_i^2) = 0 \tag{3.61}$$

We can write the complex pole as

$$\mathcal{M}^2 = M^2 - iM\Gamma \tag{3.62}$$

where M is the real (loop corrected) mass of the Higgs boson, and Γ is the width parameter. Expanding around M^2 we obtain an equation for the corrected, physical mass in terms of the real and imaginary parts of the effective self energy.

$$M_i^2 - m_i^2 + \mathrm{Re}\hat{\Sigma}_{ii}^{eff}(M_i^2) + \frac{\mathrm{Im}\hat{\Sigma}_{ii}^{eff}(M_i^2)\,\mathrm{Im}\hat{\Sigma}_{ii}^{eff\prime}(M_i^2)}{1 + \mathrm{Re}\hat{\Sigma}_{ii}^{eff\prime}(M_i^2)} = 0 \tag{3.63}$$

If we are considering a process with an external Higgs boson (such as weak boson fusion), we need to ensure that the outgoing Higgs has the correct on-shell properties and the S matrix is properly normalised by insisting that the propagator residues are equal to 1. In order to achieve this, we include finite wavefunction renormalisation factors (known as Z factors), which are composed of the renormalised self energies of the Higgs bosons[7]. These finite Z factors can be arranged into a (non-unitary) matrix. The one-particle vertex functions are thus modified for the physical Higgs bosons ($h_{1,2,3}$) as given in Equation 3.64[8]

$$\begin{aligned}
\begin{pmatrix} \hat{\Gamma}_{h_1} \\ \hat{\Gamma}_{h_2} \\ \hat{\Gamma}_{h_3} \end{pmatrix} &= \hat{\mathbf{Z}} \begin{pmatrix} \hat{\Gamma}_h \\ \hat{\Gamma}_H \\ \hat{\Gamma}_A \end{pmatrix} = \begin{pmatrix} \hat{Z}_{hh} & \hat{Z}_{hH} & \hat{Z}_{hA} \\ \hat{Z}_{Hh} & \hat{Z}_{HH} & \hat{Z}_{HA} \\ \hat{Z}_{Ah} & \hat{Z}_{AH} & \hat{Z}_{AA} \end{pmatrix} \begin{pmatrix} \hat{\Gamma}_h \\ \hat{\Gamma}_H \\ \hat{\Gamma}_A \end{pmatrix} \\
&= \begin{pmatrix} \sqrt{Z_h} & \sqrt{Z_h}Z_{hH} & \sqrt{Z_h}Z_{hA} \\ \sqrt{Z_H}Z_{Hh} & \sqrt{Z_H} & \sqrt{Z_H}Z_{HA} \\ \sqrt{Z_A}Z_{Ah} & \sqrt{Z_A}Z_{AH} & \sqrt{Z_A} \end{pmatrix} \begin{pmatrix} \hat{\Gamma}_h \\ \hat{\Gamma}_H \\ \hat{\Gamma}_A \end{pmatrix}
\end{aligned} \tag{3.64}$$

[7] These Z factors are an approximation that is used in an effort to compensate for the fact that we're treating the unstable Higgs as an external particle. Technically, the entire production and decay process should be considered. In principle, we could avoid the need for the Z factors by using an on-shell renormalisation for the Higgs fields, but – as mentioned previously – the $\overline{DR}$ scheme turns out to be more convenient.

[8] For convenience, we define the factors $\hat{Z}_{ij}$ here too.

If we consider, for instance, the vertex between the lightest Higgs boson and a pair of W bosons, h_1WW [9],

$$\hat{\Gamma}_{h_1WW} = \sqrt{Z_h}\left(\hat{\Gamma}_{hWW} + Z_{hH}\hat{\Gamma}_{HWW} + Z_{hA}\hat{\Gamma}_{AWW}\right) \tag{3.65}$$

The factor $\sqrt{Z_h}$ here gives an overall normalisation factor, which is dependent on the 3-particle mixing corrected hh propagator. The factors Z_{ij} are calculated from $\frac{\Delta_{ij}}{\Delta_{ii}}$. These factors take account of diagrams where an h_2 or h_3 tree level propagator is connected directly to the W bosons, as opposed to an h_1 tree level propagator.

Explicitly, we can write the Z factors in terms of the Higgs self energies [31]. For the real MSSM, we only need to consider mixing between h and H, the CP even Higgs bosons ($i, j = h, H$: these indices are not summed over).

$$Z_i = \left[1 + \mathrm{Re}\left(\hat{\Sigma}'_{ii}(p^2)\right) - \mathrm{Re}\left(\frac{\left(\hat{\Sigma}_{ij}(p^2)\right)^2}{p^2 - m_j^2 + \hat{\Sigma}_{jj}(p^2)}\right)'\right]^{-1}\Bigg|_{p^2=M_i^2} \tag{3.66}$$

$$Z_{ij} = -\frac{\hat{\Sigma}_{ij}(M_i^2)}{M_i^2 - m_j^2 + \hat{\Sigma}_{jj}(M_i^2)} \tag{3.67}$$

In the complex MSSM, the mixing of h and H with the CP odd Higgs boson A also needs to be considered, so the formulae become more complicated ($i, j, k = h, H, A$).

$$Z_i = \frac{1}{1 + \left(\mathrm{Re}\hat{\Sigma}^{eff}_{ii}\right)'(M_i^2)} \tag{3.68}$$

$$Z_{ij} = \frac{\hat{\Sigma}_{ij}(M_i^2)\left(M_i^2 - m_k^2 + \hat{\Sigma}_{jk}(M_i^2)\hat{\Sigma}_{ki}(M_i^2)\right)}{\hat{\Sigma}^2_{jk}(M_i^2) - \left(M_i^2 - m_j^2 + \hat{\Sigma}_{jj}(M_i^2\right)\left(M_i^2 - m_k^2 + \hat{\Sigma}_{kk}(M_i^2\right)} \tag{3.69}$$

The Higgs masses and Z factors used in the numerical analysis presented here have been obtained using the code `FeynHiggs`, working at two loop level.

[9] Note that the coupling AWW is of course zero - it is included in this equation in order to show the general form of the propagator corrections.

3.4.1 Effective couplings using the U_{Higgs} matrix

One can define effective couplings of the Higgs bosons in a $p^2 = 0$ approximation [31], where

$$\begin{aligned} \hat{\Sigma}_{ii}(p^2) &\rightarrow \hat{\Sigma}_{ii}(0) \\ \hat{\Sigma}_{ij}(p^2) &\rightarrow \hat{\Sigma}_{ij}(0) \end{aligned} \tag{3.70}$$

In this approximation, a unitary matrix U_{Higgs} can be defined that will diagonalise the Higgs mass matrix $\mathbf{M}$ (given in Equation 3.54), i.e.

$$U_{Higgs}\mathrm{Re}\left[\mathbf{M}(0)\right]U_{Higgs}^{\dagger} = \begin{pmatrix} M^2_{h_1,p^2=0} & 0 & 0 \\ 0 & M^2_{h_2,p^2=0} & 0 \\ 0 & 0 & M^2_{h_3,p^2=0} \end{pmatrix} \tag{3.71}$$

An effective coupling can then be defined as in Equation 3.65, where U_{Higgs} is used instead of the Z matrix.

The Z factors are needed for external Higgs bosons in order to ensure the correct on shell properties. Since the Z matrix is not unitary, however, it cannot be used if one wants effective couplings for internal particles (in particular within loops). The U_{Higgs} matrix can be used for these effective couplings, but in this case one must be careful that UV finiteness and gauge cancellations are maintained.

3.5 Counterterms for vertices and self energies in WBF

In order to produce the matrix elements needed for the calculations performed in this thesis, the public programs `FeynArts` [100–102] and `FormCalc` [103–106] are used.

For the main process of Higgs production via WBF, three sets of counterterms need to be considered – for the weak boson self energy VV, the vertex between the quarks and the weak bosons qqW, and the vertex between the Higgs and the weak bosons HVV. Additionally, a counterterm for the vertex between two W bosons and a Z boson is needed, as well as the vertex between two leptons and a weak boson. We neglect quark

mixing, and consequently the CKM matrix is assumed to be diagonal throughout this work. We follow the conventions used in [85], as implemented in `FeynArts`.

The `FeynArts` model files contain the counterterms in the Standard Model, but not in the MSSM. Consequently, the MSSM model file was altered to include the necessary counterterms, following the convention for the SU(2) covariant derivative described previously. The counterterms used are given below in the MSSM convention – the corresponding counterterms in the Standard Model are stated in Appendix A.

The first two sets of counterterms have equivalent forms in the Standard Model and the MSSM. The following equations give the couplings for the weak boson self energy, where V can be either W or Z and p is the momentum of the weak bosons

$$\Gamma^{CT}_{VV} = i \begin{pmatrix} \delta Z_{VV} \\ M_V^2 \delta Z_{VV} + \delta M_V^2 \\ -\delta Z_{VV} \end{pmatrix} \cdot \begin{pmatrix} g^{\mu\nu} p_1 \cdot p_2 \\ g^{\mu\nu} \\ p_1^\nu p_2^\mu \end{pmatrix} \tag{3.72}$$

In the notation used in this work (following the conventions of `FeynArts`), the coupling between the quarks and the weak bosons is denoted by

$$\Gamma_{q\bar{q}V_\mu} = \left\{ \begin{array}{l} \gamma_\mu \frac{1}{2}(1-\gamma_5) \\ \gamma_\mu \frac{1}{2}(1+\gamma_5) \end{array} \right\} \tag{3.73}$$

Following this notation, the left and right handed parts of the coupling between the external quarks and a W boson at tree level (indicated by the superscript 0) and the counterterm (superscript CT) are given by[10]

$$\Gamma^0_{u\bar{d}W} = \left\{ \begin{array}{l} \frac{-ie}{\sqrt{2}\sin\theta_W} \\ 0 \end{array} \right\} \tag{3.74}$$

$$\Gamma^{CT}_{u\bar{d}W} = \left\{ \begin{array}{l} \frac{-ie}{\sqrt{2}\sin\theta_W} \left(\delta Z_e + \frac{\delta \sin\theta_W}{\sin\theta_W} + \frac{1}{2}\delta Z_{WW} + \frac{1}{2}\left(\delta Z^*_{fL}(\bar{d}) + \delta Z_{fL}(u) \right) \right) \\ 0 \end{array} \right\} \tag{3.75}$$

The explicit form of the renormalisation constants used above was given in Section 3.3. The only difference between this coupling and the coupling $d\bar{u}W$ is that the quark

[10]Note that this coupling describes the interaction $u + \bar{d} \to W^-$.

field renormalisation constants (δZ_f) in the equation above need to be conjugated. The coupling between the external quarks and a Z boson is given by

$$\Gamma^0_{\bar{q}qZ} = ie \left\{ \begin{array}{c} g_{Lq} \\ g_{Rq} \end{array} \right\} \tag{3.76}$$

$$\Gamma^{CT}_{\bar{q}qZ} = ie \left\{ \begin{array}{c} \frac{g_{Lq}}{2}\delta Z_{ZZ} + \delta g_{Lq} - \frac{1}{3}\delta Z_{AZ} + \frac{1}{2}g_{Lq}\left(\delta Z_{fL}(q) + \delta Z^*_{fL}(q)\right) \\ \frac{g_{Rq}}{2}\delta Z_{ZZ} + \delta g_{Rq} - \frac{1}{3}\delta Z_{AZ} + \frac{1}{2}g_{Rq}\left(\delta Z_{fR}(q) + \delta Z^*_{fR}(q)\right) \end{array} \right\} \tag{3.77}$$

where q can be either up-type or down-type and

$$g_{Ru} = \frac{2}{3}\frac{\sin\theta_W}{\cos\theta_W} \tag{3.78}$$

$$g_{Rd} = -\frac{1}{3}\frac{\sin\theta_W}{\cos\theta_W} \tag{3.79}$$

$$g_{Lu} = -\frac{1}{\sin\theta_W\cos\theta_W}\left(\frac{1}{2} - \frac{2}{3}\sin^2\theta_W\right) \tag{3.80}$$

$$g_{Ld} = -\frac{1}{\sin\theta_W\cos\theta_W}\left(-\frac{1}{2} + \frac{1}{3}\sin^2\theta_W\right) \tag{3.81}$$

and

$$\delta g_{Ru} = \frac{2\sin\theta_W}{3\cos\theta_W}\left(\delta Z_e - \frac{1}{\sin\theta_W\cos^2\theta_W}\delta\sin\theta_W\right) \tag{3.82}$$

$$\delta g_{Rd} = -\frac{\sin\theta_W}{3\cos\theta_W}\left(\delta Z_e - \frac{1}{\sin\theta_W\cos^2\theta_W}\delta\sin\theta_W\right) \tag{3.83}$$

$$\begin{aligned}\delta g_{Lu} = & -\frac{1}{2\sin\theta_W\cos\theta_W}\left(\delta Z_e - \left(\frac{\sin^2\theta_W - \cos^2\theta_W}{\sin\theta_W\cos^2\theta_W}\right)\delta\sin\theta_W\right) \\ & + \frac{2\sin\theta_W}{3\cos\theta_W}\left(\delta Z_e - \frac{1}{\sin\theta_W\cos^2\theta_W}\delta\sin\theta_W\right)\end{aligned} \tag{3.84}$$

$$\begin{aligned}\delta g_{Ld} = & \frac{1}{2\sin\theta_W\cos\theta_W}\left(\delta Z_e - \left(\frac{\sin^2\theta_W - \cos^2\theta_W}{\sin\theta_W\cos^2\theta_W}\right)\delta\sin\theta_W\right) \\ & - \frac{\sin\theta_W}{3\cos\theta_W}\left(\delta Z_e - \frac{1}{\sin\theta_W\cos^2\theta_W}\delta\sin\theta_W\right)\end{aligned} \tag{3.85}$$

The supersymmetric counterterm for the Higgs vertex, however, is different from that in the Standard Model, owing to the increased complexity of the Higgs sector in

the MSSM. In the Standard Model, the couplings and counterterms are given by

$$\Gamma^0_{H_{SM}WW} = \frac{ieM_W}{\sin\theta_W} \tag{3.86}$$

$$\Gamma^0_{H_{SM}ZZ} = \frac{ieM_W}{\sin\theta_W \cos^2\theta_W} \tag{3.87}$$

$$\Gamma^{CT}_{H_{SM}WW} = \frac{ieM_W}{\sin\theta_W}\left(\delta Z_e - \frac{\delta \sin\theta_W}{\sin\theta_W} + \frac{\delta M_W^2}{2M_W^2} + \frac{1}{2}\delta Z_{HH} + \delta Z_{WW}\right) \tag{3.88}$$

$$\begin{aligned}\Gamma^{CT}_{H_{SM}ZZ} = {} & \frac{ieM_W}{\sin\theta_W \cos^2\theta_W}\left(\delta Z_e + \frac{\left(2\sin^2\theta_W - \cos^2\theta_W\right)}{\sin\theta_W\cos^2\theta_W}\delta\sin\theta_W\right. \\ & \left. + \frac{\delta M_W^2}{2M_W^2} + \frac{1}{2}\delta Z_{HH} + \delta Z_{ZZ}\right)\end{aligned} \tag{3.89}$$

In the MSSM, counterterms need to be considered for both the light and heavy CP-even Higgs bosons, h and H. In general, in the complex MSSM, we would need to include mixing between all three neutral Higgs bosons, but in the process studied in this thesis – since there is no tree level coupling between the CP odd Higgs and a pair of weak bosons – there is no AVV counterterm that needs to be considered.

$$\Gamma^0_{hWW} = \frac{ieM_W \sin(\beta-\alpha)}{\sin\theta_W} \tag{3.90}$$

$$\Gamma^0_{HWW} = \frac{ieM_W \cos(\beta-\alpha)}{\sin\theta_W} \tag{3.91}$$

$$\begin{aligned}\Gamma^{CT}_{hWW} = {} & \frac{ieM_W}{\sin\theta_W}\sin(\beta-\alpha)\left(\delta Z_e + \frac{1}{2}\frac{\delta M_W^2}{M_W^2} + \delta Z_{WW}\right. \\ & \left. + \frac{\delta\sin\theta_W}{\sin\theta_W} + \frac{1}{2}\delta Z_{hh} + \sin\beta\cos\beta\,\frac{\cos(\beta-\alpha)}{\sin(\beta-\alpha)}\delta\tan\beta\right) \\ & + \frac{1}{2}\frac{ieM_W}{\sin\theta_W}\cos(\beta-\alpha)\delta Z_{Hh}\end{aligned} \tag{3.92}$$

$$\begin{aligned}\Gamma^{CT}_{HWW} = {} & \frac{ieM_W}{\cos\theta_W}\cos(\beta-\alpha)\left(\delta Z_e + \frac{1}{2}\frac{\delta M_W^2}{M_W^2} + \delta Z_{WW}\right. \\ & \left. + \frac{\delta\sin\theta_W}{\sin\theta_W} + \frac{1}{2}\delta Z_{HH} - \sin\beta\cos\beta\,\frac{\sin(\beta-\alpha)}{\cos(\beta-\alpha)}\delta\tan\beta\right) \\ & + \frac{1}{2}\frac{ieM_W}{\sin\theta_W}\sin(\beta-\alpha)\delta Z_{hH}\end{aligned} \tag{3.93}$$

Similarly, for the coupling of the CP even Higgs bosons to a pair of Z bosons

$$\Gamma^0_{hZZ} = \frac{ieM_W \sin(\beta-\alpha)}{\sin\theta_W \cos^2\theta_W} \tag{3.94}$$

$$\Gamma^0_{HZZ} = \frac{ieM_W \cos(\beta-\alpha)}{\sin\theta_W \cos^2\theta_W} \tag{3.95}$$

$$\begin{aligned}\Gamma^{CT}_{hZZ} = {} & \frac{ieM_W}{\sin\theta_W}\sin(\beta-\alpha)\left(\delta Z_e + \frac{1}{2}\frac{\delta M_W^2}{M_W^2} + \delta Z_{WW}\right. \\ & \left. + \frac{\delta \sin\theta_W}{\sin\theta_W} + \frac{1}{2}\delta Z_{hh} + \sin\beta\cos\beta\,\frac{\cos(\beta-\alpha)}{\sin(\beta-\alpha)}\delta\tan\beta\right) \\ & + \frac{1}{2}\frac{ieM_W}{\sin\theta_W}\cos(\beta-\alpha)\delta Z_{Hh}\end{aligned} \tag{3.96}$$

$$\begin{aligned}\Gamma^{CT}_{HZZ} = {} & \frac{ieM_W}{\cos\theta_W}\cos(\beta-\alpha)\left(\delta Z_e + \frac{1}{2}\frac{\delta M_W^2}{M_W^2} + \delta Z_{WW}\right. \\ & \left. + \frac{\delta \sin\theta_W}{\sin\theta_W} + \frac{1}{2}\delta Z_{HH} - \sin\beta\cos\beta\,\frac{\sin(\beta-\alpha)}{\cos(\beta-\alpha)}\delta\tan\beta\right) \\ & + \frac{1}{2}\frac{ieM_W}{\sin\theta_W}\sin(\beta-\alpha)\delta Z_{hH}\end{aligned} \tag{3.97}$$

These are the counterterms needed to study Higgs production via weak boson fusion at the LHC. If we consider weak boson fusion and Higgsstrahlung at a linear collider (see Chapter 4), we also need counterterms for the vertices between a gauge boson and a pair of leptons. Firstly, for the Z bosons,

$$\Gamma^0_{\bar{l}lZ} = \left\{ \begin{array}{c} g_{Ll} \\ g_{Rl} \end{array} \right\} \tag{3.98}$$

$$\Gamma^{CT}_{\bar{l}lZ} = \left\{ \begin{array}{l} \frac{g_{Ll}}{2}\delta Z_{ZZ} + \delta g_{Ll} + \frac{Q_l}{2}\delta Z_{AZ} + \frac{1}{2}g_{Ll}\left(\delta Z_{fL}(l) + \delta Z^*_{fL}(l)\right) \\ \frac{g_{Rl}}{2}\delta Z_{ZZ} + \delta g_{Rl} + \frac{Q_l}{2}\delta Z_{AZ} + \frac{1}{2}g_{Rl}\left(\delta Z_{fR}(l) + \delta Z^*_{fR}(l)\right) \end{array} \right\} \tag{3.99}$$

Here l can represent either an electron e or an electron neutrino ν_e, Q_l is the lepton l charge and the g functions are given by:

$$g_{R\nu} = 0 \tag{3.100}$$

$$g_{Re} = -\frac{\sin\theta_W}{\cos\theta_W} \tag{3.101}$$

$$g_{L\nu} = -\frac{1}{2\sin\theta_W\cos\theta_W} \tag{3.102}$$

$$g_{Le} = -\frac{1}{\sin\theta_W\cos\theta_W}\left(-\frac{1}{2} + \sin^2\theta_W\right) \tag{3.103}$$

and

$$\delta g_{R\nu} = 0 \tag{3.104}$$

$$\delta g_{Re} = -\frac{\sin\theta_W}{\cos\theta_W}\left(\delta Z_e - \frac{1}{\sin\theta_W\cos^2\theta_W}\delta\sin\theta_W\right) \tag{3.105}$$

$$\delta g_{L\nu} = -\frac{1}{2\sin\theta_W\cos\theta_W}\left(\delta Z_e - \left(\frac{\sin^2\theta_W - \cos^2\theta_W}{\sin\theta_W\cos^2\theta_W}\right)\delta\sin\theta_W\right) \tag{3.106}$$

$$\begin{aligned}\delta g_{Le} = {} & \frac{1}{2\sin\theta_W\cos\theta_W}\left(\delta Z_e - \left(\frac{\sin^2\theta_W - \cos^2\theta_W}{\sin\theta_W\cos^2\theta_W}\right)\delta\sin\theta_W\right) \\ & -\frac{\sin\theta_W}{\cos\theta_W}\left(\delta Z_e - \frac{1}{\sin\theta_W\cos^2\theta_W}\delta\sin\theta_W\right)\end{aligned} \tag{3.107}$$

The tree level and counterterm couplings between a neutrino, an electron and a W boson are given by

$$\Gamma^0_{e\bar{\nu}_e W} = \left\{ \begin{array}{c} \frac{-ie}{\sqrt{2}\sin\theta_W} \\ 0 \end{array} \right\} \tag{3.108}$$

$$\Gamma^{CT}_{e\bar{\nu}_e W} = \left\{ \begin{array}{c} \frac{-ie}{\sqrt{2}\sin\theta_W}\left(\delta Z_e + \frac{\delta\sin\theta_W}{\sin\theta_W} + \frac{1}{2}\delta Z_{WW} + \frac{1}{2}\left(\delta Z^*_{fL}(\bar{\nu_e}) + \delta Z_{fL}(e)\right)\right) \\ 0 \end{array} \right\} \tag{3.109}$$

This coupling describes the process $e + \bar{\nu} \rightarrow W^+$, and the corresponding vertex $\nu\bar{e}W$ is found by conjugating the fermion field renormalisation constants – i.e. the only difference is that the electron field renormalisation constant is conjugated, rather than the neutrino field renormalisation constant.

Finally, if we are considering Z production via weak boson fusion (see Chapter 7), we also need to study the coupling between a pair of W bosons and a Z boson.

$$\Gamma^0_{ZWW} = -\frac{ie\cos\theta_W}{\sin\theta_W} \tag{3.110}$$

$$\begin{aligned}\Gamma^{CT}_{ZWW} = {} & -\frac{ie\cos\theta_W}{\sin\theta_W}\left(\delta Z_e + \frac{\delta\sin\theta_W}{\sin\theta_W\cos^2\theta_W} + \delta Z_{WW} + \frac{1}{2}\delta Z_{ZZ} + \right. \\ & \left. \frac{\sin\theta_W}{2\cos\theta_W}\delta Z_{AZ}\right)\end{aligned} \tag{3.111}$$

3.6 Soft and collinear divergences

In this section, we will focus on the QED corrections to weak boson fusion, as the QCD corrections are already part of the public `VBFNLO`. Since weak boson fusion involves charged external particles, bremsstrahlung processes (where a photon is attached to one of the external legs) need to be considered. If the photon is soft (i.e. the photon momentum $k \to 0$, and we cannot experimentally distinguish a process with the photon from one without the photon), the integral over the phase space contains an infra-red (IR) logarithmic divergence proportional to $\alpha \ln(m_\gamma)$ for a small regulating photon mass m_γ. The Bloch-Nordsieck theorem (Ref. [107]) states, however, that these singularities are cancelled in the cross section order-by-order in perturbation theory by IR singularities arising from the virtual photonic corrections.

Another type of singularity that can occur in weak boson fusion happens when a collinear photon is emitted, if the external quarks are regarded as having vanishing mass (as is the case throughout this work). The singular limit in this case is $p_f \cdot k \to 0$, where p_f is the emitting quark's momentum.

Although these divergences vanish in the total cross section when the real and virtual corrections are combined, in practice there is still the problem of numerically integrating over the singular regions of phase space. There are two principle methods commonly used to achieve this.

3.6.1 Phase space slicing

The phase space slicing method involves introducing a cut-off in the energy E (for soft divergences) or the emission angle θ (for the collinear divergences) and only performing the numerical integration over phase space up to that cut-off[11]. The soft or collinear parts are then calculated analytically. This is possible as these divergent pieces factorise from the Born cross section. For example, in the soft photon approximation, the bremsstrahlung diagrams are proportional to the Born level diagrams, as is seen from this relation for the bremsstrahlung (denoted with the subscript $soft, brem$) and Born (denoted with the subscript $Born$) matrix elements (derived, for example, in Ref. [85]):

$$\mathcal{M}_{soft,brem} = -e\, \mathcal{M}_{Born} \sum_i (\sigma_i Q_i)\, \frac{\varepsilon \cdot p_i}{k \cdot p_i} \tag{3.112}$$

[11]This method is described in Ref. [108], and was developed in [109].

where

$$\begin{aligned} Q_i &= \text{charge on } i^{\text{th}}\text{external particle} \\ p_i &= \text{momentum of } i^{\text{th}} \text{ external particle} \\ \varepsilon &= \text{polarisation vector of } \gamma \\ k &= \text{momentum of } \gamma \\ \sigma_i &= \text{sign factor for particle } i \end{aligned}$$

Owing to this form of the IR-divergent parts of the matrix element, a factor can be calculated (using Equation 3.112) that, when multiplied with the Born element, will contain all of the singular pieces. This is then included in the complete calculation, thus eliminating the divergences.

3.6.2 Dipole subtraction

An alternative to phase space slicing is known as the subtraction method, which is outlined in Ref. [68, 110]. In this procedure, we add and subtract the integral of a subtraction function $|\mathcal{M}_{sub}|^2$ (Equation 3.113) to our calculation in order to avoid any singular numerical integration.

$$\int d\phi_1 \sum_{\lambda_\gamma} |\mathcal{M}_1|^2 = \int d\phi_1 \left(\sum_{\lambda_\gamma} |\mathcal{M}_1|^2 - |\mathcal{M}_{sub}|^2 \right) + \int d\phi_1 |\mathcal{M}_{sub}|^2 \qquad (3.113)$$

Note that ϕ_1 represents the phase space of the diagram with a radiated photon. The subtraction function is chosen such that it has the same behaviour as the sum over all photon polarisations (λ_γ) of the loop matrix element $\sum_{\lambda_\gamma} |\mathcal{M}_1|^2$ in the singular limits – i.e.

$$|\mathcal{M}_{sub}|^2 \text{ behaves like } \sum_{\lambda_\gamma} |\mathcal{M}_1|^2 \text{ for } k \to 0 \text{ or } p_i \cdot k \to 0 \qquad (3.114)$$

Consequently, the divergences cancel in the first integral on the right hand side of Equation 3.113, which means it can be performed numerically (with no regulatory quark or photon masses). All of the singularities reside in the second integral, which

can be analysed analytically ($\mathcal{M}_{sub}$ is chosen specifically so that it is simple enough to be integrated in this fashion).

The phase space integral for the process with a radiated photon ($\int d\phi_1$) is factorised into the photon phase space integral ($\int [dk]$) and an integral of a phase space closely related to the Born phase space ($\int d\tilde{\phi}_{Born}$), where $\bigotimes$ symbolises that the "multiplication" also involves convolutions and summations:

$$\int d\phi_1 = \int d\tilde{\phi}_{Born} \bigotimes \int [dk] \tag{3.115}$$

As we have seen previously, in the singular limits the loop level matrix squared element is proportional to the Born level matrix squared element, i.e.

$$|\mathcal{M}_1(\phi_1)|^2_{\text{singular limit}} \sim |\mathcal{M}_{Born}(\phi_{Born})|^2 \tag{3.116}$$

Here ϕ_{Born} represents the phase space of the tree level diagram. This relation means that the subtraction term can be factorised into two parts – one of which depends on the momenta in the phase space ϕ_{Born}, and the second of which depends on the integration variables of $\int [dk]$. Thus, Equation 3.113 can be re-written as

$$\begin{aligned} \int d\phi_1 \sum_{\lambda_\gamma} |\mathcal{M}_1|^2 \;\; = \;\; & \int d\phi_1 \left(\sum_{\lambda_\gamma} |\mathcal{M}_1|^2 - |\mathcal{M}_{sub}|^2 \right) + \\ & \int d\tilde{\phi}_{Born} \bigotimes \left(\int [dk] \, |\mathcal{M}_{sub}|^2 \right) \end{aligned} \tag{3.117}$$

Only the integral over $[dk]$ contains any singular pieces. This integral is completely process-independent, which means that the analytical integration need only be performed once (and has been calculated in Ref. [110]).

The subtraction function itself is constructed from auxiliary functions g^{sub}, which are labelled by pairs of different fermions ($f \neq f'$), in the following manner

$$|\mathcal{M}_{sub}|^2 = - \sum_{f \neq f'} Q_f \sigma_f Q_{f'} \sigma_{f'} e^2 g^{(sub)}_{ff',\tau} (p_f, p_{f'}, k) \, |\mathcal{M}_{Born}|^2 \tag{3.118}$$

Only the kinematics of the fermion f lead to divergent contributions in the subtraction function, so f is termed the emitter and f' the spectator. The subscript τ is summed

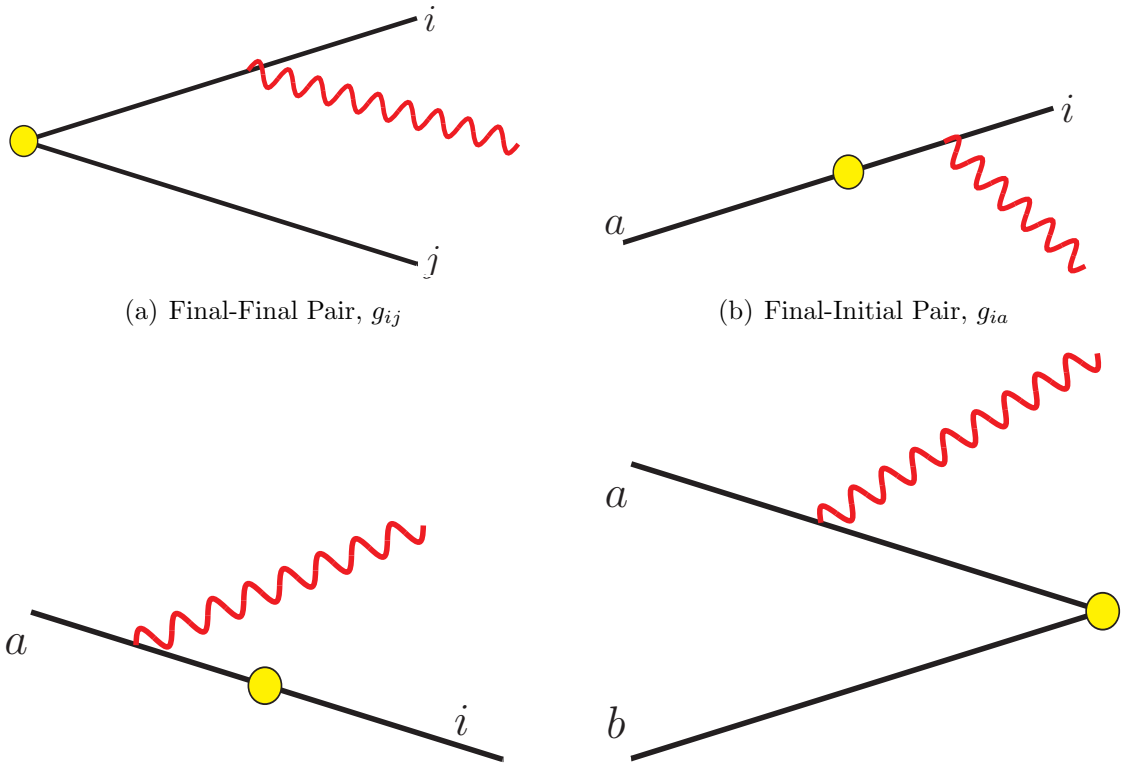

(a) Final-Final Pair, g_{ij}

(b) Final-Initial Pair, g_{ia}

(c) Initial-Final Pair, g_{ai}

(d) Initial-Initial Pair, g_{ab}

Figure 3.3: Possible combinations of emitter–spectator pairs.

over and represents a helicity flip of the emitter. The integral of the auxiliary function $g_{ij,\tau}^{(sub)}$ over the photonic phase space is $G_{ij,\tau}^{(sub)}$.

Applying the dipole subtraction method to weak boson fusion is relatively simple. The first step is to group the external fermions (i.e. the charged legs) into pairs of one emitter and one spectator. There are four categories, shown in Fig. 3.3. The subscripts a, b always refer to initial state fermions, and i, j to final state fermions.

For weak boson fusion, there are thus eight diagrams that need to be considered. In the first category of diagrams, there are two initial-initial contributions (Fig. 3.4).

In this case, the subtraction factor (which multiplies the Born matrix element squared) for an emitter a and a spectator b is given by

$$\delta_{sub}^{ab} = \frac{-\alpha}{2\pi} Q_a Q_b \sigma_a \sigma_b \left(G_{ab,+}^{sub}(s) + G_{ab,-}^{sub}(s) \right) \tag{3.119}$$

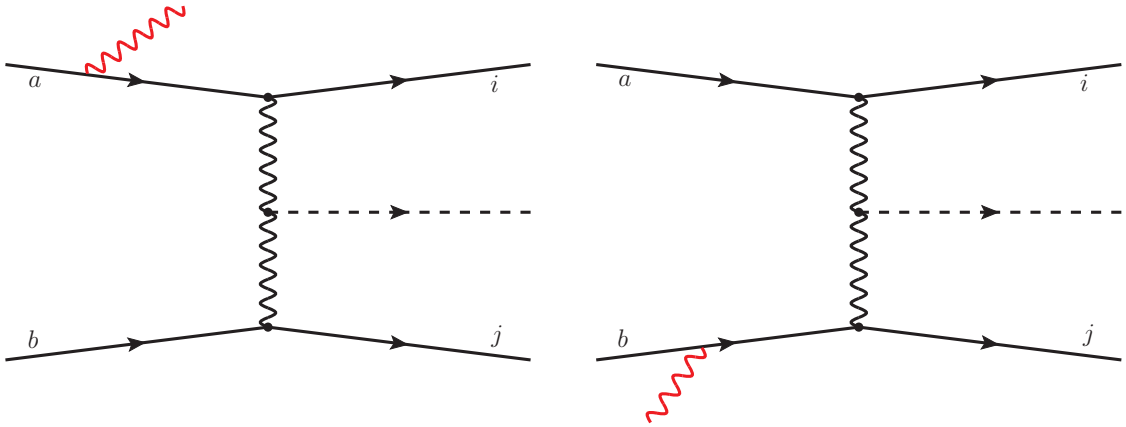

Figure 3.4: The initial–initial photon radiation pairs for weak boson fusion.

where the integrals of the auxiliary functions are [110]

$$\begin{aligned} G^{sub}_{ab,+}(s) &= \mathcal{L}(s, m_a^2) - \frac{\pi^2}{3} + \frac{3}{2} \\ G^{sub}_{ab,-}(s) &= \frac{1}{2} \\ m_a &= \text{mass of fermion } a \\ s &= \text{centre of mass energy} = (p_a + p_b)^2 = 2p_a \cdot p_b \end{aligned} \tag{3.120}$$

The function $\mathcal{L}$ is given by

$$\mathcal{L}(r, m^2) = \ln\left(\frac{m^2}{r}\right) \ln\left(\frac{m_\gamma^2}{r}\right) - \frac{1}{2}\ln^2\left(\frac{m^2}{r}\right) + \frac{1}{2}\ln\left(\frac{m^2}{r}\right) \tag{3.121}$$

Since there are two cases (see Fig. 3.4), ab and ba, then

$$\delta^{init-init}_{sub} = -\frac{\alpha}{2\pi} Q_a Q_b \sigma_a \sigma_b \left(2\mathcal{L}(2p_a \cdot p_b, m_a^2) - \frac{2\pi^2}{3} + 4\right) \tag{3.122}$$

Note that the auxiliary functions (and, indeed, the whole subtraction procedure) are considerably simplified as we assume that the external quarks have vanishing mass.

The second category of diagrams consists of initial-final and final-initial pairs of emitters and spectators, as shown in Fig. 3.5.

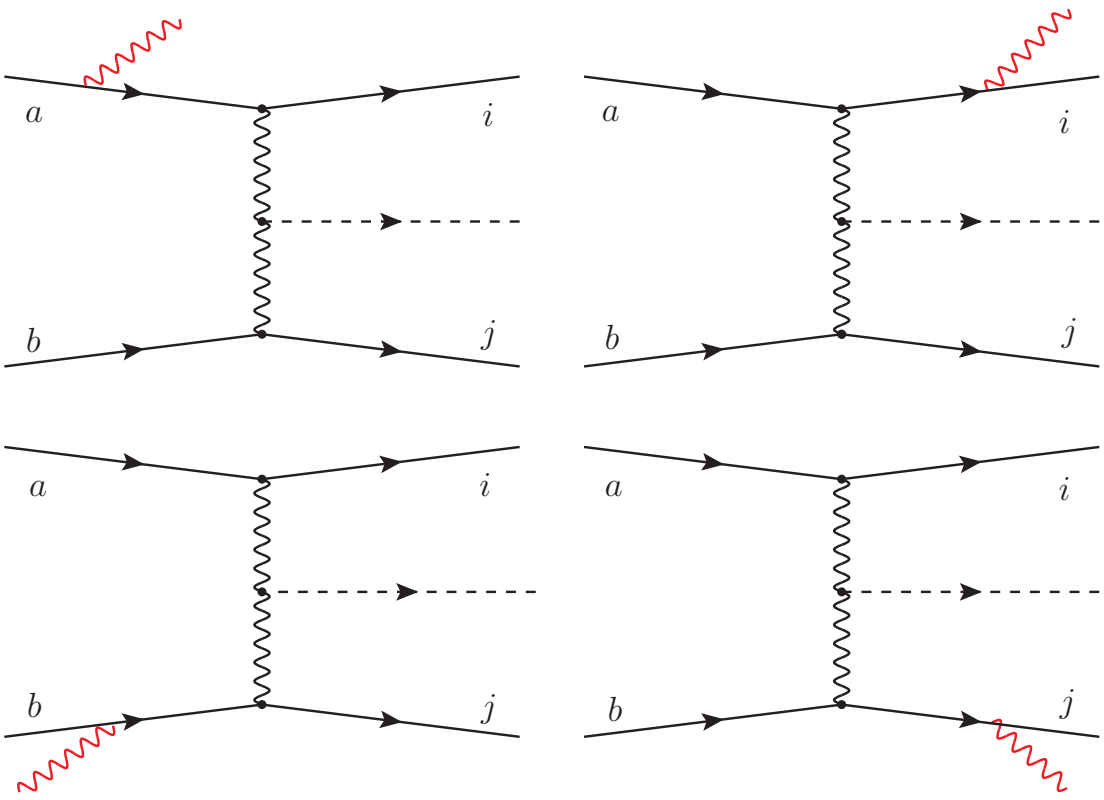

Figure 3.5: The initial–final and final–initial photon radiation pairs of emitters and spectators for weak boson fusion.

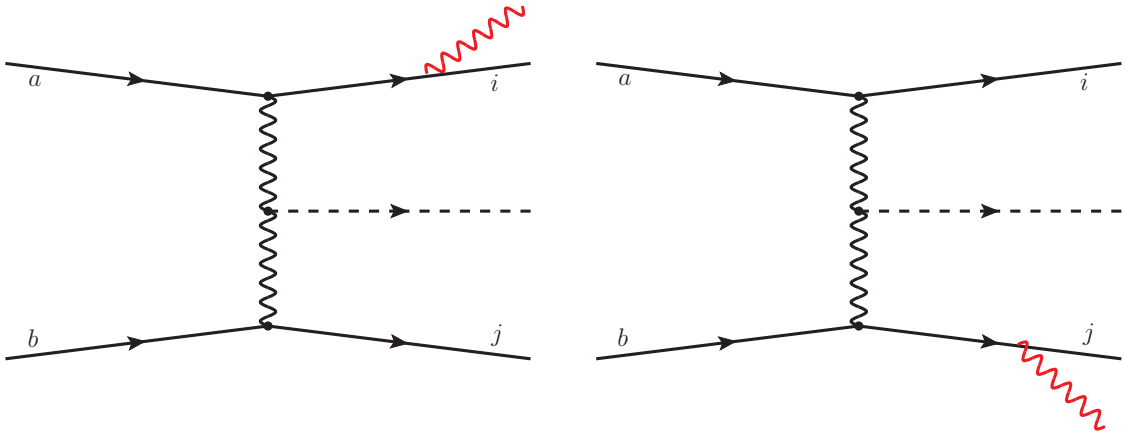

Figure 3.6: The final–final photon radiation pairs of emitters and spectators for weak boson fusion.

This gives the contributions ai, ia, bi, ib, aj, ja, bj and jb. In this case the integrals of the auxiliary functions are given by

$$\begin{aligned} G^{sub}_{ia,+}(P^2_{ia}) &= \mathcal{L}(|P^2_{ia}|, m_i^2) - \frac{\pi^2}{2} + 1 \\ G^{sub}_{ai,+}(P^2_{ia}) &= \mathcal{L}(|P^2_{ia}|, m_i^2) + \frac{\pi^2}{6} - \frac{3}{2} \\ G^{sub}_{ii,-}(P^2_{ia}) &= G^{sub}_{ii,-}(P^2_{ia}) = \frac{1}{2} \\ \text{where} & \\ P_{ia} &= p_i - p_j \Rightarrow |P^2_{ia}| = 2p_i \cdot p_j \end{aligned} \tag{3.123}$$

Thus, the total initial-final and final-initial contribution to the subtraction factor is given by

$$\begin{aligned} \delta^{ini-fin}_{sub} = & -\frac{\alpha}{2\pi}\left(Q_a Q_i \sigma_a \sigma i \left[2\mathcal{L}(2p_i \cdot p_a, m_q^2) - \frac{\pi^2}{3} + \frac{1}{2}\right]\right. \\ & + Q_a Q_j \sigma_a \sigma j \left[2\mathcal{L}(2p_a \cdot p_j, m_q^2) - \frac{\pi^2}{3} + \frac{1}{2}\right] \\ & + Q_b Q_i \sigma_b \sigma i \left[2\mathcal{L}(2p_b \cdot p_i, m_q^2) - \frac{\pi^2}{3} + \frac{1}{2}\right] \\ & \left. + Q_b Q_j \sigma_b \sigma j \left[2\mathcal{L}(2p_b \cdot p_j, m_q^2) - \frac{\pi^2}{3} + \frac{1}{2}\right]\right) \end{aligned} \tag{3.124}$$

The third category of contributions comprises the final-final emitter-spectator pairs (Fig. 3.6).

The two diagrams give contributions ij and ji. Here, the integrated auxiliary functions are

$$G^{sub}_{ij,+} = \mathcal{L}(P^2_{ij}, m^2_i) - \frac{\pi^2}{3} + 1 \tag{3.125}$$

$$G^{sub}_{ij,-} = \frac{1}{2} \tag{3.126}$$

where

$$P^2_{ij} = (p_i + p_j)^2 \to 2p_i \cdot p_j \tag{3.127}$$

Thus, the subtraction factor is given by

$$\delta^{fin-fin}_{sub} = \frac{-\alpha}{2\pi} Q_i Q_j \sigma_i \sigma_j \left(2\mathcal{L}(2p_i \cdot p_j, m^2_q) - \frac{2\pi^2}{3} + 3 \right) \tag{3.128}$$

These contributions are added together to give the total subtraction factor

$$\delta_{sub} = \delta^{ini-ini}_{sub} + \delta^{ini-fin}_{sub} + \delta^{fin-fin}_{sub} \tag{3.129}$$

The dipole subtraction formalism has been shown [55] to be more numerically stable for the process of weak boson fusion than phase space slicing, with an integration error which is an order of magnitude smaller. In addition, it is less computationally expensive, and is consequently used for all of the results presented here.

3.7 Implementation in VBFNLO

The results obtained in this work have been implemented into the public Monte Carlo code VBFNLO. The total cross section and a range of distributions are calculated, although in this thesis we focus exclusively on the azimuthal angle distribution. The modified code is set up such that the user can choose whether to work in the Standard Model or the MSSM, and which higher order contributions they want to be included. The code can be used to study either the third generation quark (and squark) contributions, corrections for all fermions (and sfermions), the full set of Standard Model diagrams, or the dominant SUSY corrections supplemented by the SM type boxes and pentagons.

The various types of corrections to weak boson fusion are implemented in different ways in the adapted VBFNLO code. Firstly, the corrections to the weak boson self energy

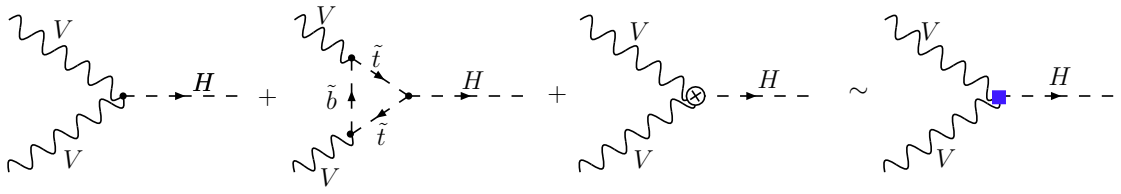

Figure 3.7: An "effective coupling" $T_{\mu\nu}$ for the Higgs vertex, symbolised by the blue square. The circle with a cross in it signifies the counterterm contribution.

and the Higgs vertex are interpreted as an effective coupling $T^{\mu\nu}$ between the Higgs and the weak bosons, as is shown in Fig. 3.7.

All loop and counterterm diagrams in these categories are calculated using code derived from `FormCalc` and the result is separated into its component formfactors a_1, a_2 and a_3, according to Equation 2.13. Appendix C details an example calculation of the corrections to the HVV vertex in the top / bottom quark sector, to demonstrate the origin of each of the formfactors that are involved in the effective coupling.

In this manner formfactors are calculated and fed into `VBFNLO`. This is a much simpler (and computationally more efficient) method than calculating the full matrix squared element for each phase space point. Since these subroutines are self-contained, it is also possible to run them separately and perform fast scans over the parameter space (which can be very useful in the MSSM). As the corrections contained within the formfactors are where we would expect interesting Higgs phenomenology to occur, interesting regions of parameter space can be identified quickly.

The method used to implement the corrections to the quark vertex depends on the sector in which we are working. If only fermion and sfermion contributions are being considered, there are no loop diagrams to calculate, only a counterterm. This counterterm is used as an effective coupling in the `VBFNLO` code. If, however, the full Standard Model is needed, the loop diagrams change the structure of the qqV coupling from its tree level configuration. In this case, we have calculated the full matrix element squared.

The pentagon and box diagram contributions are also included by calculating the full $2 \to 3$ matrix element squared (summed over all allowed helicity combinations). All of the matrix elements are coded in a suitably general manner, so that the same code can be used to calculate each different pattern of external quarks and anti-quarks.

Each of the three options commonly used for parametrising the lowest order electromagnetic coupling ($\alpha(0), \alpha(M_Z^2)$, via G_F) are included in the modified code and, in the MSSM, Higgs propagator corrections can be included.

There is a second version of the code that studies only the corrections to the Higgs vertex in the MSSM, and has been specially tuned in order to compare our results with results presented in the literature (Ref. [56]). In this version, the loop contributions from the Standard Model particles and those from the SUSY particles can be studied separately, as well as the complete set of MSSM diagrams, in each of the sectors described above (i.e. (s)top / (s)bottom corrections, (s)fermion corrections, and full corrections). This is described in more detail in Section 6.4.1.

Appendix B contains details of the structure and options in the modified `VBFNLO`.

3.8 Checks

Once the renormalisation procedure has been carried out, the results must of course be UV-finite. In order to ensure this, a variety of checks have been performed at every stage of the calculation. The renormalisation and regularisation parameters (the UV divergence, the photon mass and the external quark mass) can all be manually varied, to confirm that the final result yielded by the code is not dependent on them (indicating a finite result).

If only fermions (and sfermions) are considered, each type of correction (i.e. corrections to the qqV vertex, the VV self energy and the HVV vertex – see Section 3.2) should be separately finite[12]. It has been explicitly verified that the corrections to the qqV vertex, the weak boson self energy corrections, and the Higgs vertex corrections are all finite. Additionally, in this sector the gauge boson field renormalisation constants drop out, and have no effect on the final result, which has been checked by altering the values of the renormalisation constants δZ_{WW} and δZ_{ZZ} by hand.

These checks have been performed for the formfactors, at the partonic level, and for the total cross section results produced by `VBFNLO`. The top / bottom (and stop

[12] When moving beyond the purely (s)fermionic corrections, these are not gauge invariant quantities, and the virtual corrections need to be combined with the real corrections in order to achieve an IR finite result.

/ sbottom) corrections to the Higgs vertex have also been studied analytically using `Mathematica` [111], and all divergences have been shown to cancel.

The modified `VBFNLO` can either regularise the IR divergences using the phase space slicing approach or the dipole subtraction method, both of which have been checked numerically and found independent of the photon mass. The default mode of the code uses dipole subtraction.

To check internal consistency, the tree level cross section and the corrections to the Higgs vertex (in the top / bottom sector) have been calculated using both the formfactor method, as well as by calculating the full matrix squared elements, to ensure that the results agree.

The wavefunction normalisation factors (the Z factors) were implemented in two ways: first, the `FeynHiggs` output was used, and secondly the value of each Z factor was calculated at one loop level using only `FeynArts` and `FormCalc` (with Equations 3.67 and 3.66) in the MSSM with real parameters, and the two results were compared.

These checks were all successful, obtaining agreement to within the numerical accuracy of the code.

Chapter 4

Weak boson fusion at linear colliders

"A journey of a thousand miles begins with a single step."
— Lao Tzu

4.1 Higgs production at a linear collider

The LHC is expected to be able to find a Higgs boson if it is Standard Model like. Discovering a Higgs candidate is, however, only the first step. In order to understand the Higgs sector, and the mechanism of electroweak symmetry breaking, we also need to determine the properties of the particle. For instance, by measuring the coupling of the Higgs candidate to the gauge bosons, we can experimentally verify the mass relations described in Chapter 1. It is also vital to determine the spin and CP properties of the particle, as well as the number of Higgs states that exist. While the LHC should be able to start studying these properties, the greater precision that can be obtained at a future linear collider will enable us to make further progress in the complete determination of the Higgs sector. The LHC and a linear collider should complement one another in various ways, and combining the data obtained from each experiment could lead to great advantages.

For instance, in the MSSM, the CP violation in the Higgs sector comes solely from loop effects and so can depend strongly on the particle content of the theory. By combining high precision measurements of the Higgs sector from a linear collider with information gathered at the LHC regarding the SUSY particle spectrum, we can study the

CP structure of the Higgs sector. For a review of this and other synergies between the LHC and a linear collider see, for instance, References [112, 113].

At a linear collider, the principle Higgs production channels in the Standard Model are W boson fusion and the Higgsstrahlung process, described in Section 4.2, as well as $t\bar{t}H$ production. In the MSSM, associated Higgs pair production ($e^+e^- \to h(H)A$) and Yukawa processes can also be important. One of the principle advantages of a linear collider is that it is able to detect a Higgs boson independently of the Higgs decay mode by studying the Higgsstrahlung process where the Z boson decays into a pair of leptons (e^+e^- or $\mu^+\mu^-$), because the distribution of the invariant mass (of the recoil against the Z) peaks at the Higgs mass [114]. Both the Higgsstrahlung process and W boson fusion provide direct access to the important coupling between the gauge bosons and the Higgs. Additionally, the W boson fusion channel can be used to determine the total Higgs width with both a high level of accuracy and – crucially – a low model dependence (see Reference [115] for a discussion of the evaluation of the Higgs width).

4.2 Corrections to the process $e^+e^- \to \nu_e\overline{\nu}_e H$

The corrections to the process $e^+e^- \to \nu_e\overline{\nu}_e H$ have been investigated in the literature [116–119]. In particular, Ref. [119] studied the fermionic and sfermionic corrections to the process $e^+e^- \to \nu_e\overline{\nu}_e H$ via the combined W boson fusion and Higgsstrahlung channels in the MSSM. These corrections include contributions from the Higgs vertex and the weak boson self energy, as well as a counterterm contribution at the lepton–weak boson vertex (this is analogous to the case for weak boson fusion with external quarks at the LHC, described in Section 3.2, Fig. 3.2). We first successfully reproduce the results presented in Ref. [119], and then go on to study each separate contribution in detail. This also provides us with an additional check of our renormalisation procedures, as well as investigating the simpler case where we have leptonic external particles, rather than hadronic.

Following Ref. [119], in this chapter we consider not only weak boson fusion itself, but also the Higgsstrahlung process, both of which are shown in Fig. 4.1 for a linear collider.

At low energies the Higgsstrahlung diagrams will give the dominant contribution to the combined process, owing to the enhanced cross section at the threshold $\sqrt{s} \sim$

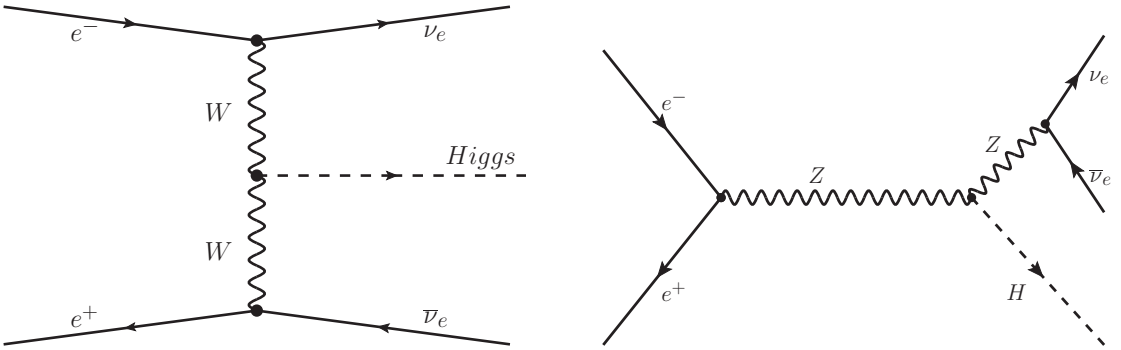

(a) The weak boson fusion process.

(b) The Higgsstrahlung process.

Figure 4.1: Principle leading order diagrams for Higgs production at a linear collider.

$M_H + M_Z$ (when the second Z boson goes on shell). As the centre of mass energy rises, however, the $\frac{1}{s}$ suppression in the Higgsstrahlung process, combined with the $\ln(s)$ enhancement of the WBF channel, means that the W boson fusion becomes dominant. In this (high energy) limit, the combined process yields, at leading order, a cross section of [120]

$$\sigma \to \frac{G_F^3 M_W^4}{4\sqrt{2}\pi^3} \left[\left(1 + \frac{M_H^2}{s}\right) \ln\left(\frac{s}{M_H^2}\right) - 2\left(1 - \frac{M_H^2}{s}\right) \right] \tag{4.1}$$

4.2.1 Finite width

There is an additional issue that needs to be considered when calculating the Higgsstrahlung process. As mentioned previously, the second Z boson (that is connected to the two neutrinos) will become resonant when we integrate over phase space. We therefore need to include a width Γ into the Z boson propagator, as follows:

$$\frac{1}{s - M_Z^2} \to \frac{1}{s - M_Z^2 - i\Gamma M_Z} \tag{4.2}$$

In this work, we include a running width (Γ_{run}), which incorporates the known kinematic dependences and the experimentally measured finite width Γ_{fin} (the value of which is taken from the Particle Data Book [87]).

$$\Gamma_{fin} = 2.4952 \text{ GeV} \tag{4.3}$$

$$\Gamma_{run} = \left(\frac{s}{M_Z^2}\right) \Gamma_{fin} \tag{4.4}$$

We also disregard all imaginary parts of the contributions from the light fermions to the Z boson self energy, in order to avoid double counting. This is the procedure followed by Ref. [119].

4.3 Results in the Standard Model

As a starting point, we discuss the total cross section, at tree level and with corrections from the third generation fermions or from all fermions, of the combined W boson fusion and Higgsstrahlung channels in the Standard Model. Note that no cuts have been performed on these partonic cross sections. The parameters used are set to match those of Ref. [119] – in particular, the top mass is set to $m_t = 174.3$ GeV, and the electromagnetic coupling constant is parametrised via the Fermi constant (with the appropriate renormalisation – see Section 3.3.2). The graphs are shown in Figures 4.2 and 4.3, as a function of the centre of mass energy, $\sqrt{s}$, and the Higgs mass, M_H respectively. These results compare well to the results presented in Ref. [119]. As can be seen, for a Higgs mass of $M_H = 115$ GeV (Fig. 4.2), there is a threshold behaviour at $\sqrt{s} \sim 210$ GeV, which is caused by the Z boson that couples to the two neutrinos going on shell in the Higgsstrahlung process. The cross section increases with centre of mass energy, following the form of Equation 4.1. Looking at the percentage loop corrections as a function of energy (Fig. 4.2(b)), we can see that in the threshold region the corrections cause a quite significant enhancement in the cross section, whereas for higher centre of mass energies, above ~ 300 GeV, the loop corrections reduce the total cross section. The contributions from the third generation fermions are significant, especially away from the threshold region, but they are not dominant.

The cross section in Fig. 4.3, at a high centre of mass energy, shows the expected behaviour – production decreases smoothly as the Higgs mass increases (again, following Equation 4.1). The threshold observed in the percentage loop correction at a Higgs mass of $M_H \approx 350$ GeV (see Fig. 4.3) stems from the Higgs field renormalisation in the HVV counterterm, when the two top quarks in the Higgs self energy go on shell.

The interference between the two processes involved can play an important rôle in the final cross section, as can be seen from Fig. 4.4. This interference is most relevant in the region where the cross section of weak boson fusion becomes larger than that of Higgsstrahlung. The spikes seen in Fig. 4.4(d) are of course at centre of mass energies where the total loop correction, $\Delta\sigma$, becomes zero as the corrections from weak boson

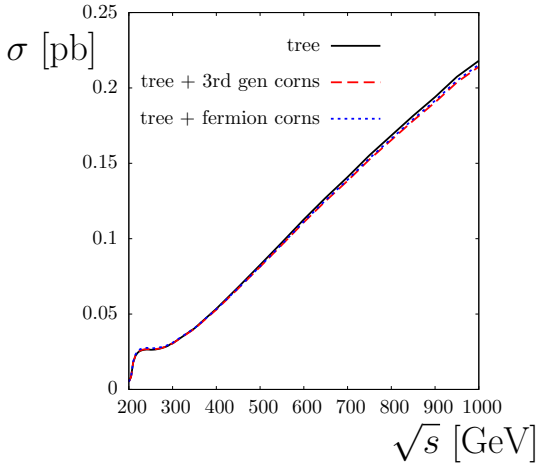

(a) Total cross section at tree (black curve) and loop level (red and blue curves).

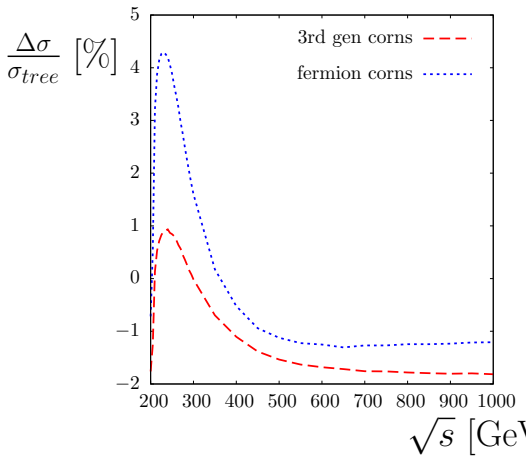

(b) Percentage loop corrections from the 3rd generation (red curve) and all fermion (blue curve) contributions.

Figure 4.2: Cross section for the process $e^+e^- \to \nu_e\bar{\nu}_e H$ at a linear collider in the Standard Model with $M_H = 115$ GeV. The red and blue curves show the loop corrections from third generation fermions and all fermions respectively.

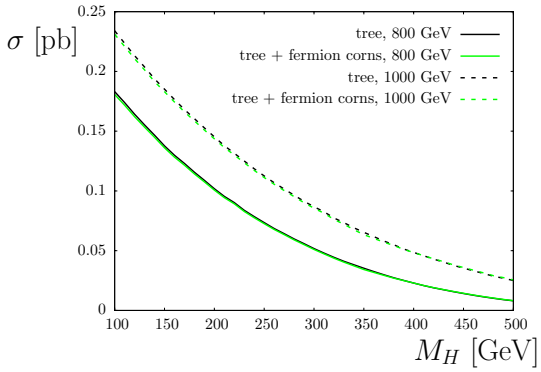

(a) Total cross section at tree and loop level.

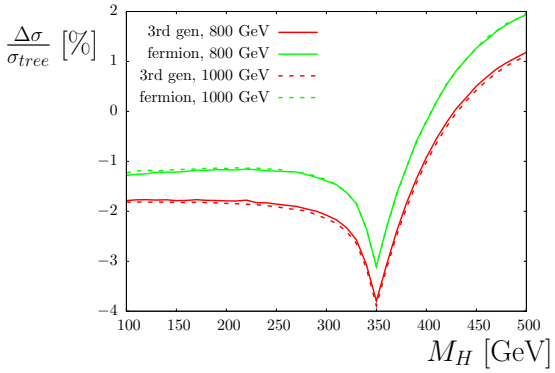

(b) Percentage loop corrections from the 3rd generation (red curve) and all fermion (blue curve) contributions.

Figure 4.3: Cross section for the process $e^+e^- \to \nu_e\bar{\nu}_e H$ at a linear collider in the SM as a function of M_H, with $\sqrt{s} = 800$ GeV (solid lines) and 1000 GeV (dotted lines).

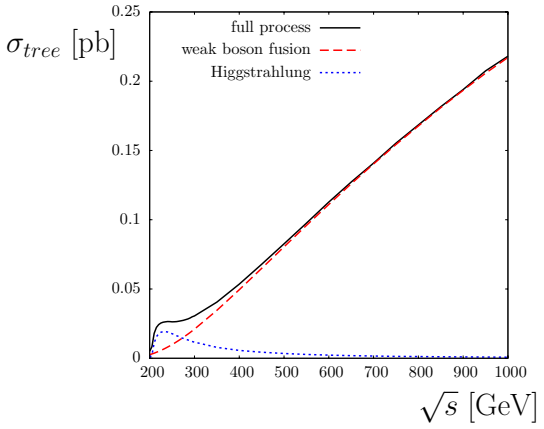

(a) Tree level cross sections for weak boson fusion, Higgsstrahlung and the combined process.

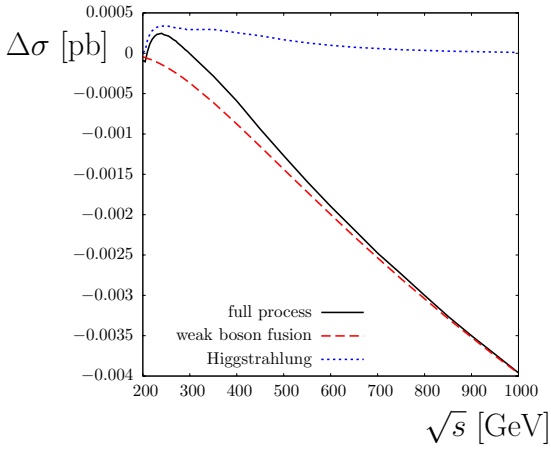

(b) Loop correction for weak boson fusion, Higgsstrahlung and the combined process.

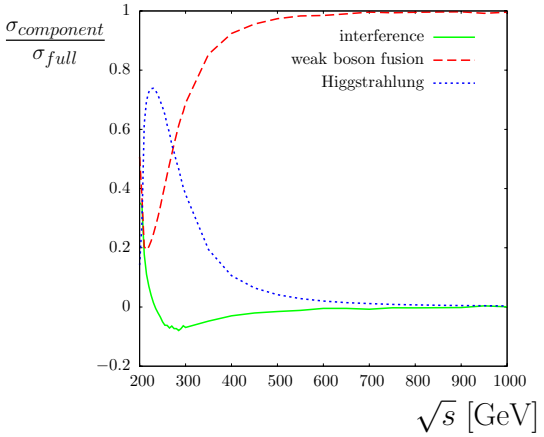

(c) Tree level cross sections for weak boson fusion, Higgsstrahlung and the interference, as a fraction of the total tree level cross section.

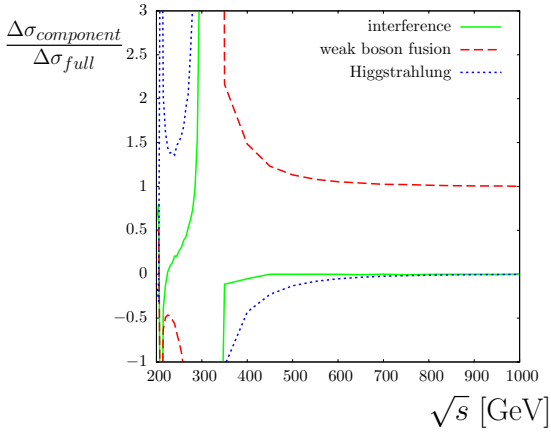

(d) Loop correction for weak boson fusion, Higgsstrahlung and the interference as a fraction of the total loop correction.

Figure 4.4: Cross section graphs showing the relative effect of weak boson fusion, Higgsstrahlung, and interference in the process $e^+e^- \to \nu_e\bar{\nu}_e H$ at $M_H = 115$ GeV when corrections from third generation fermions are included. $(\Delta)\sigma_{component}$ is the contribution to the total $(\Delta)\sigma_{full}$ from either WBF, Higgsstrahlung or interference. Plots (a) and (c) are at tree level, (b) and (d) show loop effects.

fusion, Higgsstrahlung and the interference cancel out. Fig. 4.4 shows the corrections arising from third generation fermion loops – adding in the complete fermion corrections does not alter the general shape of the graphs, although it does slightly shift the value of the centre of mass energy where the corrections to weak boson fusion become more important than the corrections to Higgsstrahlung (by ~ 50 GeV). This is because, as we will see (Fig. 4.6), the first and second generation fermion loop corrections have a bigger impact on Higgsstrahlung processes than they do on WBF processes.

At a high fixed centre of mass energy of $\sqrt{s} = 1000$ GeV, we can see (Fig. 4.5) that, as expected, the weak boson fusion process completely dominates the Higgsstrahlung process. As a function of the Higgs mass, we can once more see a pronounced dip at $M_H = 350$ GeV, and the contribution from the interference is very small. (Again, the kinks occur when the sign of the loop corrections – from all fermion contributions in the case of Fig. 4.5 – switches from positive to negative.) The lower centre of mass energy of 800 GeV was also investigated, and displays the same features as seen at 1000 GeV – the only differences are a smaller cross section and a slightly larger relative contribution from the Higgsstrahlung process. Fig. 4.4 and 4.5 show that, if we choose a high enough centre of mass energy, the effects of the Higgsstrahlung process can be neglected.

Since each of the three types of corrections considered here (the Higgs vertex HVV, the weak boson self energy VV and lepton–weak boson vertex llV) are separately finite, we consider each one individually, in order to see where the dominant contribution to the total loop correction originates[1]. Fig. 4.6 studies the HVV, llV and VV contributions for weak boson fusion, Higgsstrahlung and the combined process for a Higgs of mass $M_H = 115$ GeV as a function of the centre of mass energy.

Fig. 4.6 shows that, for low energies, the most important contribution to the loop correction is the result of the counterterm correction at the lepton vertex. The Higgs vertex correction and the weak boson self energy corrections are seen to cancel one another out to a large extent in the threshold region when only third generation fermion loop diagrams are considered. When all fermions are included in the loops, the size of the corrections increases at low energies and we no longer see this cancellation at resonance. As the energy moves above the Z resonance, the Higgs vertex correction increases in importance until it is the dominant contribution for third generation fermion corrections. When all fermions are included in the loop, the Higgs vertex loses importance (even at high energies). For all contributions except the Higgs vertex loop (and the renormalisation constants δZ_H and $\delta \sin\theta_W$), the large top quark mass suppresses the correction, so the Higgs vertex (which is, of course, enhanced by the large Higgs–top coupling) is the dominant piece. The light fermions' contributions to (for instance) the W / Z boson self energy correction is larger than the contribution from the top quark, and we therefore see an increase in the size of this correction when we include all fermions (instead of only the third generation). Note that the llV vertex corrections to WBF and Higgsstrahlung are of course independent of the centre of mass energy $\sqrt{s}$ – the small fluctuations seen

[1] In general, of course, this is not gauge invariant, but there is no issue here as we are working solely in the (s)fermion sector.

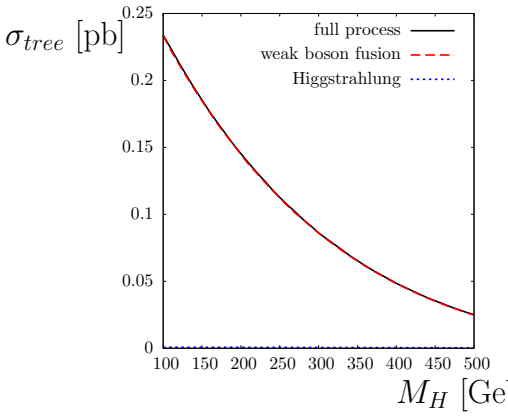

(a) Tree level cross sections for weak boson fusion, Higgsstrahlung and the combined process.

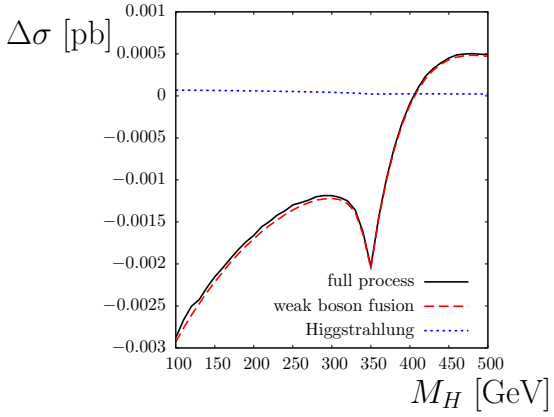

(b) Loop correction for weak boson fusion, Higgsstrahlung and the combined process.

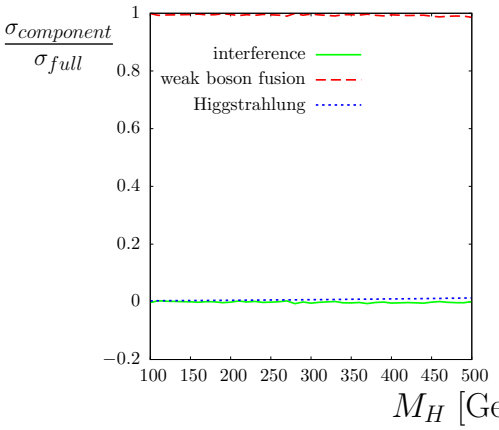

(c) Tree level cross sections for weak boson fusion, Higgsstrahlung and the interference, as a fraction of the total cross section.

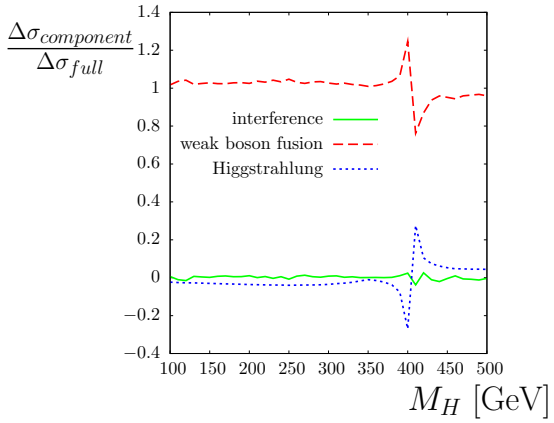

(d) Loop correction for weak boson fusion, Higgsstrahlung and the interference as a fraction of the total loop correction.

Figure 4.5: Cross section graphs showing the relative effect of the weak boson fusion, Higgsstrahlung, and interference contributions in the process $e^+e^- \to \nu_e\bar{\nu}_e H$ at a centre of mass energy $\sqrt{s} = 1000$ GeV as a function of the Higgs mass when corrections from all fermions are included. The first column, Graphs (a) and (c), shows the tree level cross sections, and the second column (Graphs (b) and (d)) shows the relative loop effects.

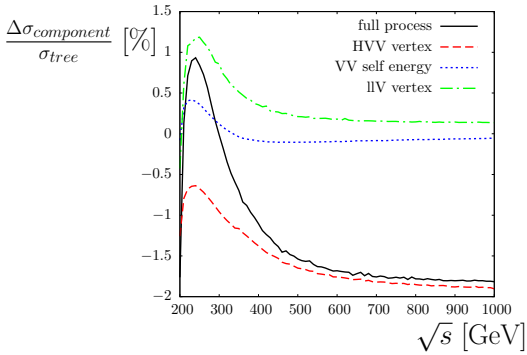

(a) Percentage loop corrections for the combined process when third generation fermions are considered.

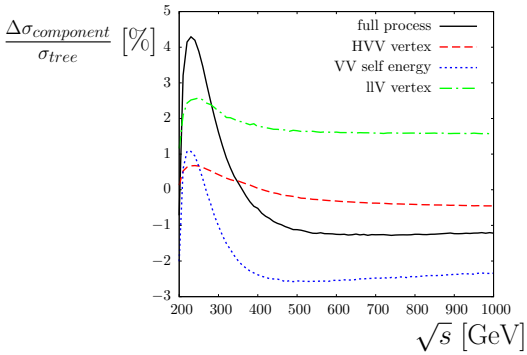

(b) Percentage loop corrections for the combined process when all fermions are considered.

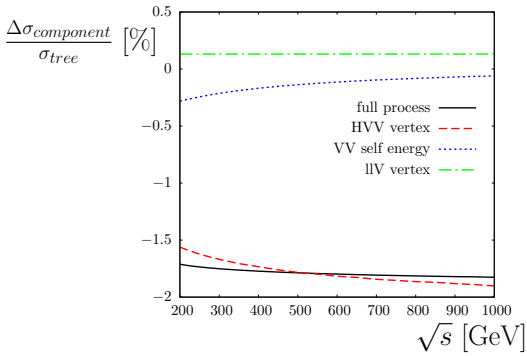

(c) Percentage loop corrections for WBF when third generation fermions are considered.

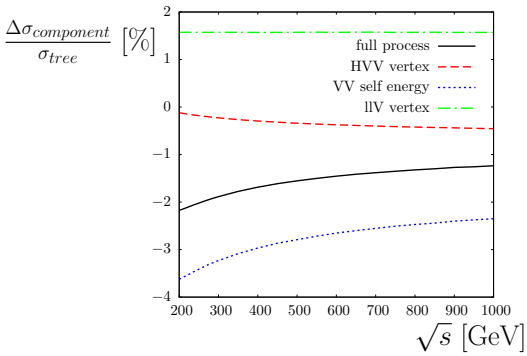

(d) Percentage loop corrections for WBF when all fermions are considered.

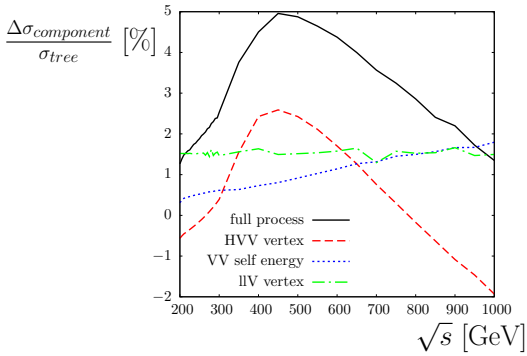

(e) Percentage loop corrections for Higgsstrahlung when third generation fermions are considered.

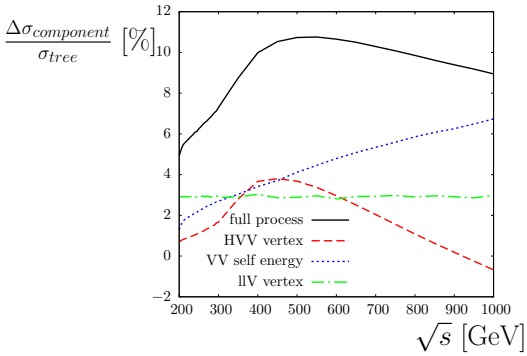

(f) Percentage loop corrections for Higgsstrahlung when all fermions are considered.

Figure 4.6: Percentage loop corrections for the individual HVV, VV and llV contributions for $M_H = 115$ GeV. The top row contains the full process $e^+e^- \to \nu_e\bar{\nu}_e H$, the second row presents results from weak boson fusion, and the third row focuses on Higgsstrahlung.

for this correction in the Higgsstrahlung process (Fig. 4.6 (e) and (f)) are the result of numerical instability. In the combined process, the relative weights of the llV vertex corrections to weak boson fusion and Higgsstrahlung is dependent on the centre of mass energy, resulting in the energy dependence of the llV vertex correction seen in Fig. 4.6 (a) and (b).

For weak boson fusion, the dominant piece in the third generation fermion approximation is the Higgs vertex at all energies, although its importance again decreases when the contributions from the light fermions are included. For Higgsstrahlung, on the other hand, although always an important correction, the Higgs vertex is never truly dominant. For the Higgsstrahlung process, the Z boson self energy corrections increase with energy. With increasing energy, the Higgs vertex corrections go from negative to positive between energies of $\sim$ 200 GeV and $\sim$ 450 GeV, before decreasing and becoming negative once again.

Fig. 4.7 again looks at these individual contributions, but for a fixed centre of mass energy (of $\sqrt{s} = 800$ GeV, where weak boson fusion is the dominant contribution rather than Higgsstrahlung) as a function of the Higgs mass.

The self energy corrections and corrections to the vertex between the weak boson and the external leptons do not depend on the mass of the Higgs boson. The Higgs vertex correction, however, does vary with Higgs mass, as it enters via the Higgs field renormalisation constant. The threshold behaviour in the loop correction at $M_H = 350$ GeV $\sim 2m_t$ is now clearly seen to originate from the Higgs vertex correction. For weak boson fusion (and hence, at this high centre of mass energy, for the full $e^+e^- \to \nu_e\bar{\nu}_e H$ process), the Higgs vertex correction is the dominant contribution, although it does become less important when all fermions are included in the loop diagrams. This dominance is enhanced by the fact that the self energy corrections are cancelled out, to a large extent, by the lepton vertex corrections. For the Higgsstrahlung contribution, on the other hand, the Higgs vertex corrections only become dominant at relatively high Higgs masses when third generation quarks are considered, and when all fermions are included in the loop diagrams the HVV corrections are never truly dominant. Additionally, for the Higgsstrahlung diagrams there is no cancellation between the Z boson self energy diagrams and the lepton vertex diagrams.

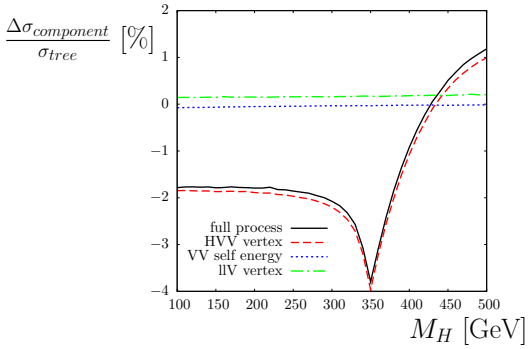

(a) Percentage loop corrections for the combined process when third generation fermions are considered.

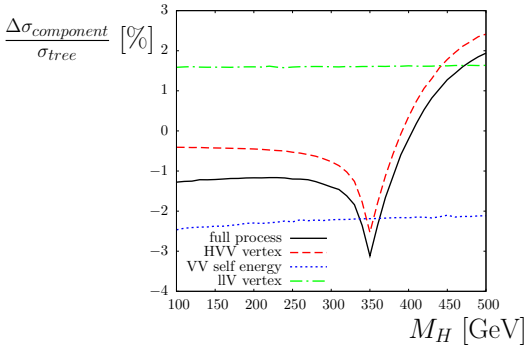

(b) Percentage loop corrections for the combined process when all fermions are considered.

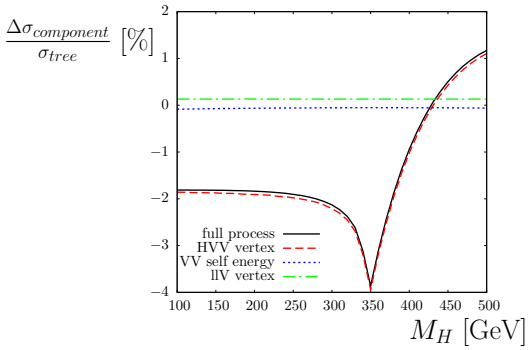

(c) Percentage loop corrections for WBF when third generation fermions are considered.

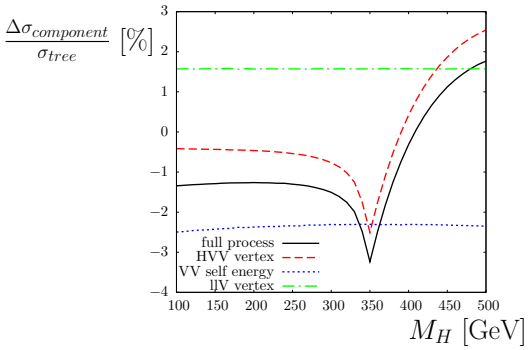

(d) Percentage loop corrections for WBF when all fermions are considered.

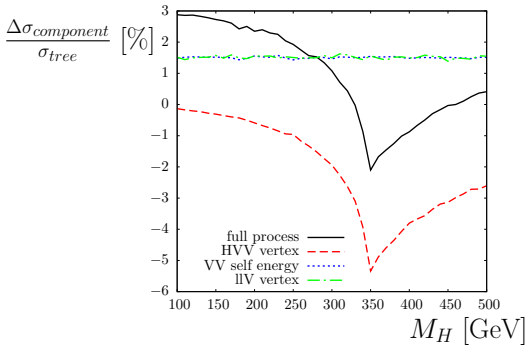

(e) Percentage loop corrections for Higgsstrahlung when third generation fermions are considered.

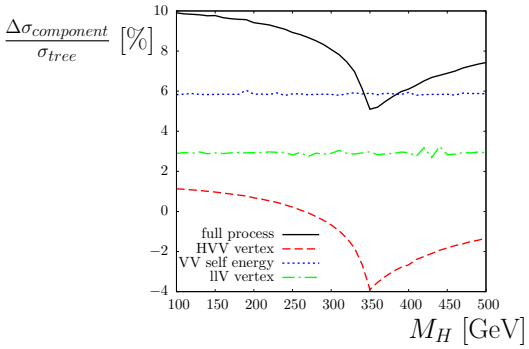

(f) Percentage loop corrections for Higgsstrahlung when all fermions are considered.

Figure 4.7: Percentage loop corrections for the individual HVV, VV and llV contributions for $\sqrt{s} = 800$ GeV. The first row shows the combined process, the second row shows weak boson fusion, and the third row shows Higgsstrahlung.

Table 4.1: Fixed parameters of the benchmark scenarios in the MSSM

	$M_h^{\max}$	no-mixing	gluophobic	small α_{eff}
M_{SUSY}	1 TeV	2 TeV	350 GeV	800 GeV
μ	200 GeV	200 GeV	300 GeV	2.5 M_{SUSY}
M_2	200 GeV	200 GeV	300 GeV	500 GeV
X_t	2 M_{SUSY}	0	-750 GeV	-1100 GeV
$m_{\tilde{g}}$	0.8 M_{SUSY}	0.8 M_{SUSY}	500 GeV	500 GeV

4.4 Results in the MSSM

The parameter space in the MSSM is obviously far larger than in the Standard Model, with many more free parameters. Consequently, when studying cross sections in the MSSM, we investigate the four benchmark scenarios described in Ref. [121], where M_A (the mass of the CP odd Higgs boson) and $\tan\beta$ (the ratio of the Higgs VEVs) are taken as input parameters, and all other parameters are fixed. We consider four benchmark scenarios: the $M_h^{\max}$ scenario, the no-mixing scenario, the gluophobic scenario and the small α_{eff} scenario, described in Table 4.1. Note that M_2 is the SU(2) gaugino mass parameter, X_t is related to the trilinear Higgs–$\tilde{t}$ couping A_t by Equation 1.21 and $A_t = A_b = A_\tau$. For simplicity, the same trilinear couplings are used for all generations and M_{SUSY} – a common soft SUSY breaking parameter – is used in the diagonal entries of the sfermion mass matrix of Equation 1.21.

We study the effect of the centre of mass energy, as well as varying $\tan\beta$ and M_A. In this Section we define our leading order (LO) result by including the Higgs propagator corrections (see Section 3.4) at Born level – i.e. the interference term between the loop level diagrams and Born level diagrams is as is shown in Fig. 4.8. This means that graphs of the loop correction percentages do not include the effect of propagator corrections, but are instead the genuine vertex corrections.

As in the Standard Model, we first study the production process for the light Higgs boson (including both vector boson fusion contributions and Higgsstrahlung diagrams) as a function of the centre of mass energy $\sqrt{s}$. In Fig. 4.9, as in Ref. [119], we examine the cross section (and, additionally, the percentage loop corrections) with a fixed CP odd Higgs mass ($M_A = 500$ GeV) at $\tan\beta = 3$ and 40. Note that this value of the CP

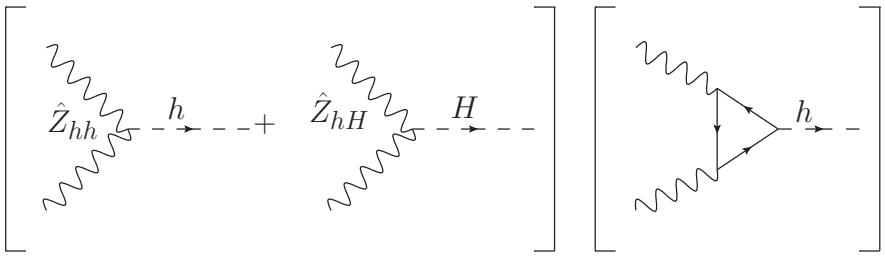

Figure 4.8: Corrections to the Higgs propagator are included at leading order.

odd Higgs mass is well within the decoupling regime, and so we expect to see Standard Model like behaviour. All fermion loop corrections are included.

The comparison of Fig. 4.9 with the results presented in Ref [119] shows good agreement. It can also be seen that, as expected, the threshold region where the Z boson is produced on shell shifts to higher energies with higher values of $\tan\beta$ as this – for these benchmarks at any rate – causes the mass of the light Higgs, M_h, to increase. It can be seen that the value of $\tan\beta$ has a larger effect in the small α_{eff} scenario than in the other benchmarks. This is because, owing to the large value of μ, the higgsino mass parameter, the masses of the sfermions are more affected by $\tan\beta$, causing the loop corrections to change more drastically with altered $\tan\beta$.

Fig. 4.10 compares the loop corrections obtained considering only third generation (s)fermions with those obtained when all fermions are included. The behaviour seen in the Standard Model – where light fermion corrections are as important as third generation fermion corrections at resonance – is seen to be repeated. The small α_{eff} scenario's dependence on the first and second generation sfermions is far more pronounced than the other scenarios', even at high centre of mass energies.

Fig. 4.11 focuses on the M_h^{max} scenario, showing the behaviour of the total cross section and loop corrections as functions of $\tan\beta$ and M_A. These graphs show the leading order and corrected cross section at $\sqrt{s} = 800$ GeV as a function of M_A and $\tan\beta$, and compare the percentage corrections at $\sqrt{s} = 800$ GeV and $\sqrt{s} = 1000$ GeV. Due to this high energy, although both Higgsstrahlung and weak boson fusion diagrams are included, the weak boson fusion process is dominant, as is the case in the Standard Model. The cross section and loop corrections depend on M_A in the manner that we would expect. At large values of the CP odd Higgs mass, the loop corrections are fairly constant at approximately -2%. This is in the decoupling regime (where the light Higgs becomes Standard Model like), where the light Higgs mass is ~ 129 GeV. By looking

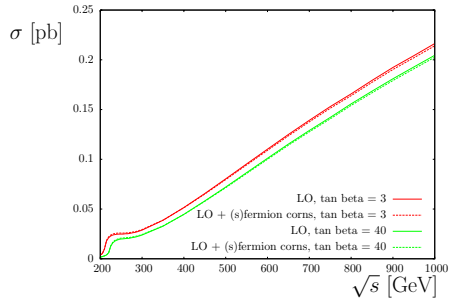

(a) Total cross section at leading order and loop level for the M_h^{max} scenario.

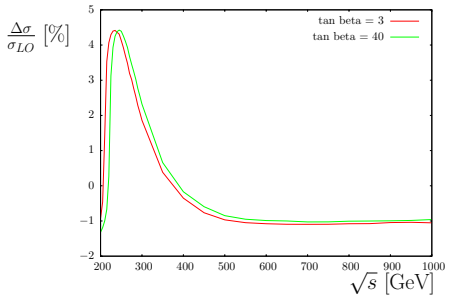

(b) Percentage loop corrections for the M_h^{max} scenario.

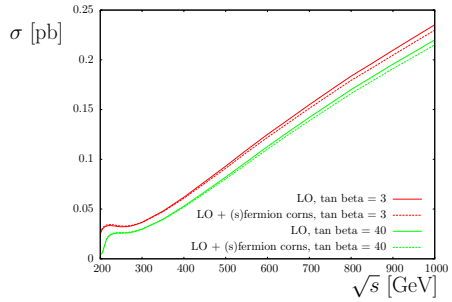

(c) Total cross section at leading order and loop level for the no-mixing scenario.

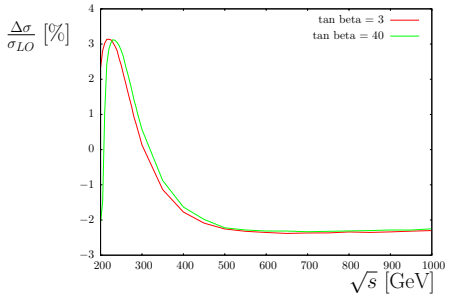

(d) Percentage loop corrections for the no-mixing scenario.

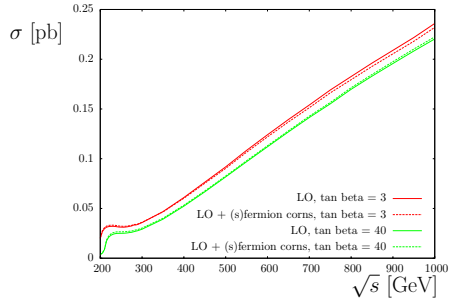

(e) Total cross section at leading order and loop level for the small α_{eff} scenario.

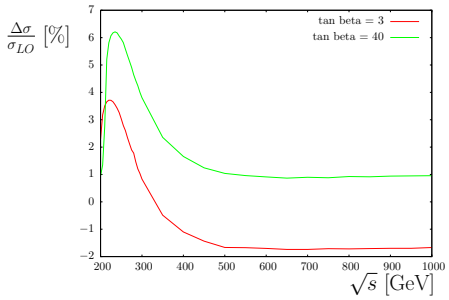

(f) Percentage loop corrections for the small α_{eff} scenario.

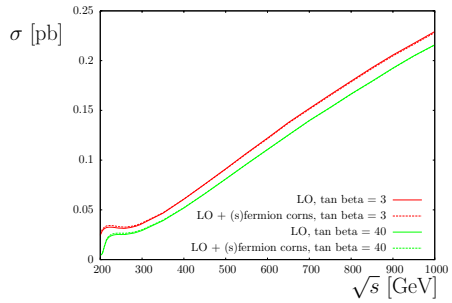

(g) Total cross section at leading order and loop level for the gluophobic scenario.

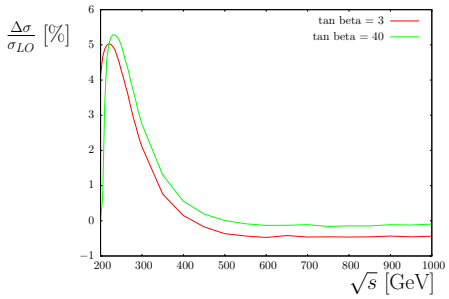

(h) Percentage loop corrections for the gluophobic scenario.

Figure 4.9: Production of the light CP even Higgs boson for process $e^+e^- \to \nu_e\bar{\nu}_e H$ at a linear collider in the MSSM with $M_A = 500$ GeV at $\tan\beta = 3$ (red curve) and $\tan\beta = 40$ (blue curve). All (s)fermion corrections are included.

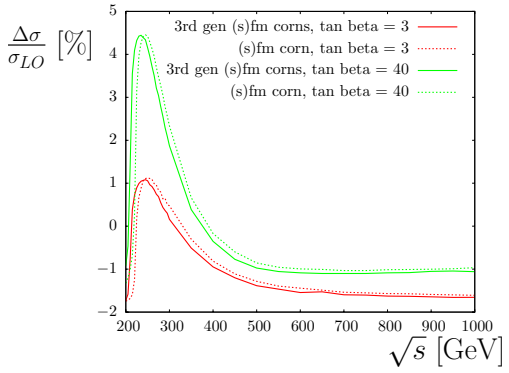

(a) Percentage loop corrections in the M_h^{max} scenario.

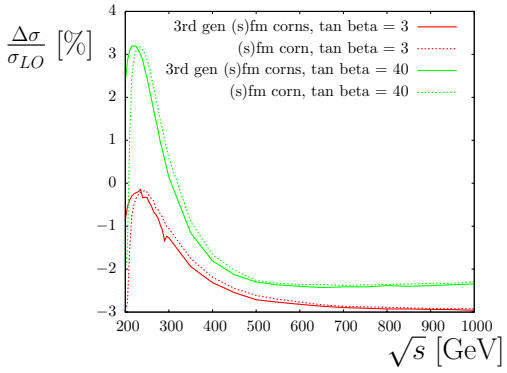

(b) Percentage loop corrections in the no-mixing scenario.

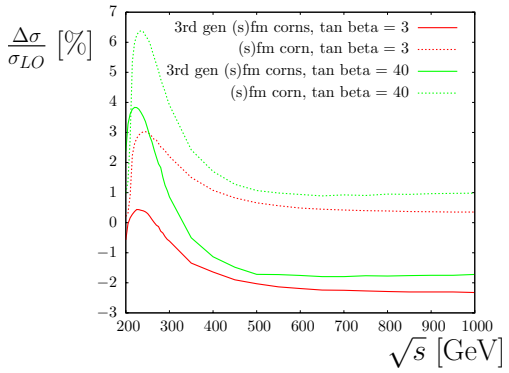

(c) Percentage loop corrections in the small α_{eff} scenario.

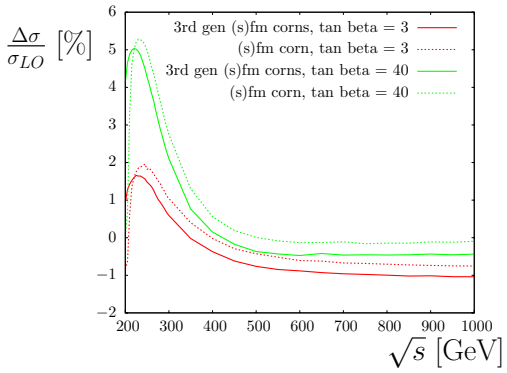

(d) Percentage loop corrections in the gluophobic scenario.

Figure 4.10: A comparison of loop corrections obtained from third generation (s)fermions with those from all (s)fermions in the benchmark scenarios as a function of the centre of mass energy. The CP odd Higgs mass is set to 500 GeV, and $\tan\beta = 3$ (red curve) or $\tan\beta = 40$ (blue curve).

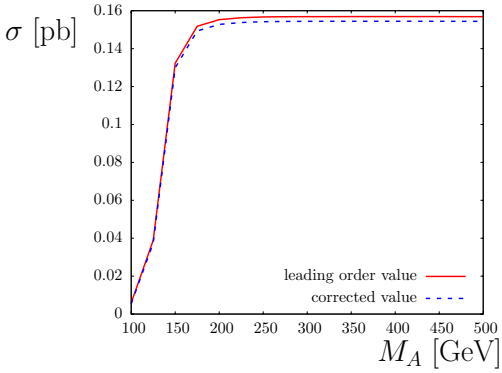

(a) Total cross section at leading order and loop level as a function of M_A, with $\tan\beta = 10$ for $\sqrt{s} = 800$ GeV.

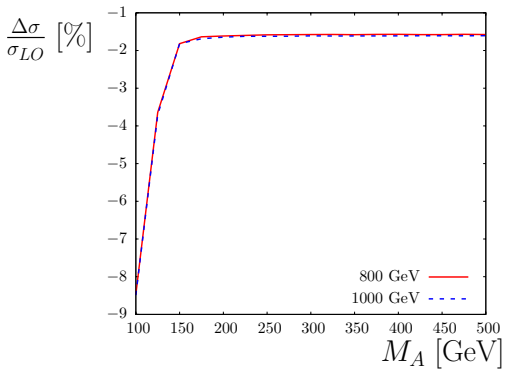

(b) Percentage loop corrections as a function of M_A, with $\tan\beta = 10$: a comparison between $\sqrt{s} = 800$ GeV and $\sqrt{s} = 1000$ GeV.

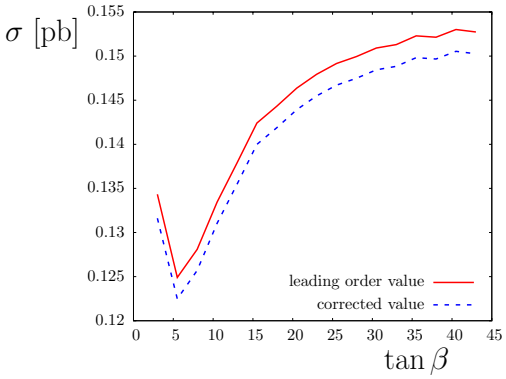

(c) Total cross section at leading order and loop level as a function of $\tan\beta$, with $M_A = 150$ GeV for $\sqrt{s} = 800$ GeV.

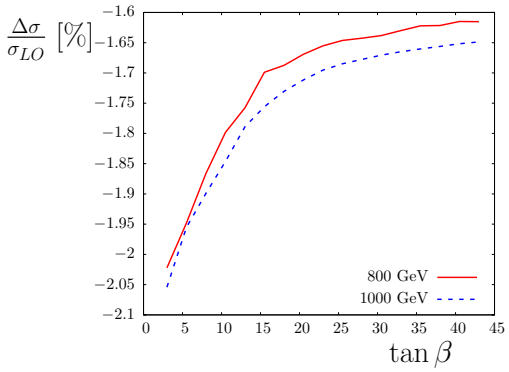

(d) Percentage loop corrections as a function of $\tan\beta$, with $M_A = 150$ GeV.

Figure 4.11: Cross sections and loop corrections for the combined process at a linear collider in the M_h^{max} scenario, with third generation fermion corrections included in the loop diagrams.

at Fig. 4.3, we can see that in the Standard Model at $\sqrt{s} = 800$ GeV for this value of M_H, the loop corrections are also $\sim -2\%$. In the non–decoupling regime, with low M_A, the corrections can reach up to $\sim -8\%$. The percentage corrections increase slightly at higher centre of mass energies.

The $\tan\beta$ behaviour is less intuitive. The dip we observe in the cross section at $\tan\beta \sim 5$ is caused by a combination of two effects. As $\tan\beta$ increases, the mass of the light Higgs boson, M_h, also increases, causing the term in square brackets of Equation 4.1 (containing the mass and energy dependence) to decrease. The hVV coupling, however, is proportional to the factor $\sin(\beta-\alpha)$ in the MSSM (see Section 3.5, Equations 3.86 and 3.90). Thus, in the MSSM, the right hand side of Equation 4.1 needs to be multiplied by $\sin^2(\beta-\alpha)$. This additional factor increases with $\tan\beta$ and – for values of $\tan\beta$ over ~ 5 – it is this behaviour that dominates at high energies of $\sqrt{s} = 800$ GeV or 1000 GeV. Percentage loop corrections range from $\sim -2\%$ to $\sim -1.6\%$ over this range of $\tan\beta$ with $M_A = 150$ GeV.

Chapter 5

Results for WBF Higgs production at the LHC in the Standard Model

In this Chapter we present an analysis of weak boson fusion Higgs production in the Standard Model. The Chapter starts by examining the W and Z boson fusion channels at the partonic level, and examining the dominant sources of loop corrections when all fermions and only top / bottom quarks are considered. Results for the formfactors are then examined as a function of the Higgs mass, and compared to the partonic results. We go on to the complete results, obtained by implementing our result for the complete electroweak one loop contributions (including QED contributions) to weak boson fusion into the Monte Carlo program `VBFNLO`, yielding in this way a theoretical prediction incorporating the full electroweak and QCD one loop corrections in the Standard Model. We first compare our results with the available literature [55] and then present both total cross sections and the important azimuthal angle distributions discussed in Chapter 2.

5.1 Parameters

The Standard Model parameters used in this chapter are those found in the Particle Data Book [87] unless specifically stated otherwise, excepting the top quark mass, where $m_t = 172.6$ GeV has been used, as reported in [122]. The default cuts imposed upon the cross sections are described in Section 2.2, Equation 2.5, and the PDF set MRST2004QED [123] is used as this includes distributions for the photon, allowing photon-induced processes to be considered in the calculations[1]. The electromagnetic

[1] Where an alternative PDF set is used, the entry for the photon is set to zero, thus neglecting photon induced processes.

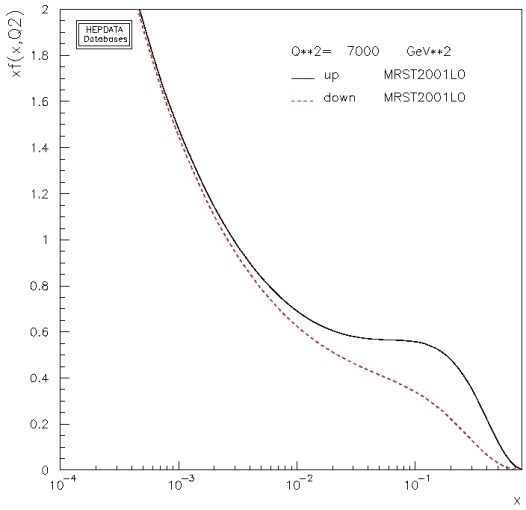

Figure 5.1: MRST2001lo PDF for up and down quarks, produced with the online HEPDATA [125] tool.

coupling α is parametrised in terms of the Fermi constant (Equation 3.46), yielding a shift in the charge renormalisation constant of $\frac{1}{2}\Delta r$.

5.2 Partonic cross sections

We investigate the partonic cross section and percentage loop correction for Higgs production via weak boson fusion[2], for the leading subprocess

$$u + d \to d + H + u \tag{5.1}$$

This process includes both Z and W boson fusion (the Z fusion is a u-channel process, while the W fusion is in the t-channel). In contrast to Chapter 4, the Higgsstrahlung contribution is neglected here.

A partonic centre of mass energy of $\sqrt{\hat{s}} = 500$ GeV is used for this and all subsequent partonic cross sections. This energy sits on the "plateau" region of the PDF of the up quark, which is shown in Fig. 5.1 (which also shows the PDF of the down quark) for MRST2001lo [124]. This energy also allows us (kinematically) to create a Higgs boson, and is high enough that we know (from the results of Chapter 4) that we can safely neglect the Higgsstrahlung contribution, even without imposing cuts.

[2]Note that no cuts are implemented on the partonic cross sections.

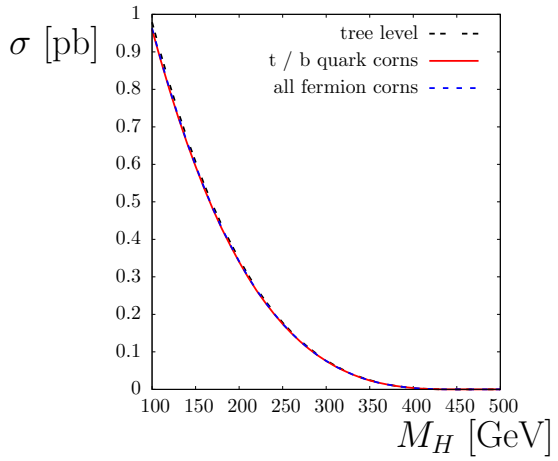

(a) Total cross section at tree and loop level.

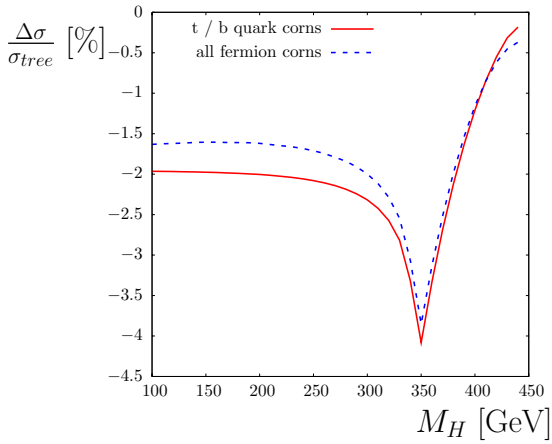

(b) Percentage loop corrections from the 3rd generation quarks and from all fermion contributions.

Figure 5.2: Partonic cross section for H production via weak boson fusion in the SM at $\sqrt{\hat{s}} = 500$ GeV. Corrections from the top / bottom quarks are shown in red, with the full fermionic corrections shown in blue.

Fig. 5.2 shows the partonic cross section and percentage loop correction for Higgs production via weak boson fusion. It can be seen that the production cross section of the Higgs boson decreases quite rapidly as the Higgs mass increases, until it becomes practically zero. Loop correction percentages range from $\sim -0.5\% \rightarrow -4\%$, but are reasonably constant between $M_H = 100 \rightarrow 300$ GeV at -1.5% for all fermion contributions and -2% for third generation quark contributions. A threshold in the loop correction percentage is again seen at $M_H \sim 350$ GeV ($\sim 2m_t$) (in Fig. 5.2) stemming from the Higgs field renormalisation constant, as in WBF at the linear collider (Chapter 4, see Fig. 4.3).

The dominant contribution is from the W boson fusion process, as can be seen in Fig. 5.3, where all fermion contributions are included[3]. The interference between W and Z boson fusion is minimal, and will in any case be greatly suppressed by the WBF cuts (because the interference is a crossed diagram), as described in Section 2.2 and 2.6.

Looking in more detail at the contributions to the loop correction (Fig. 5.4), we can see that, when only top / bottom quark contributions are considered, the dominant correction arises from the Higgs vertex, as is expected (due to the large Higgs–top coupling). When all fermion corrections are included, however, the diagrams involving the weak boson self energy and the quark vertex become far more important. Since the

[3]The relative contributions from W and Z fusion when only top and bottom quarks are considered are practically identical to the case shown here when all fermions are considered.

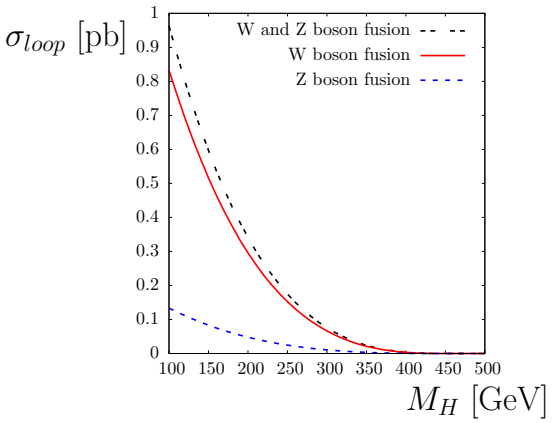

(a) Corrected partonic cross section for W (red curve), Z (blue curve) and weak boson fusion (black curve).

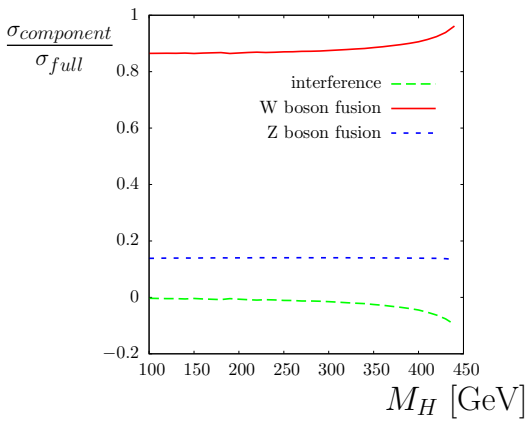

(b) Fraction of cross section from W and Z boson fusion. $\sigma_{component}$ is the cross section contribution from either W or Z boson fusion, or the interference between them.

Figure 5.3: A comparison of W (red curve) and Z (blue curve) boson fusion contributions to the corrected cross section for H production via weak boson fusion at $\sqrt{\hat{s}} = 500$ GeV when corrections from all fermions are considered.

weak boson self energy and the renormalisation constants (and hence counterterms) do not experience any enhancement to their couplings caused by the top mass (except for the Higgs field renormalisation constant and $\delta \sin\theta_W$), they are actually suppressed by the large top mass and so receive larger contributions from the lighter fermions. For the Z boson fusion process, the Higgs vertex contribution is less important than for the W fusion case, although it is still the dominant contribution when only third generation quarks are considered.

5.3 Formfactors

As explained in Section 3.7, the formfactor calculations can be performed separately in order to obtain a "first approximation" to the size and behaviour of the loop corrections. They are also useful since they provide an additional check on the procedures used. Fig. 5.5 shows the formfactors a_1, a_2 and a_3 for the couplings HWW and HZZ as a function of the Higgs mass. The general form of the effective coupling $T^{\mu\nu}$ is given in Equation 2.13.

The momenta q, which need to be input into these calculations, are given generic values generated by `VBFNLO`, which pass all of the weak boson fusion cuts. Note that the coupling HZZ has no a_3 component as terms involving the Levi-Civita ϵ tensor from

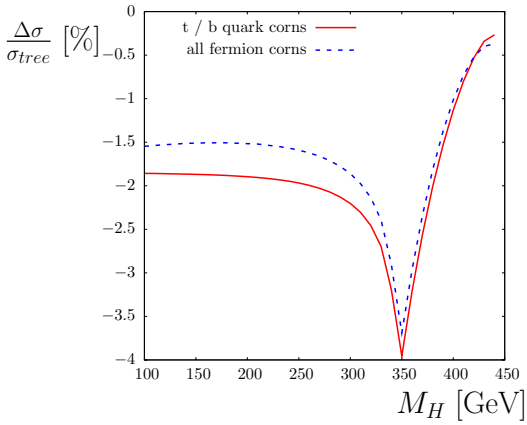

(a) Percentage loop corrections from top / bottom and all fermion contributions for W fusion.

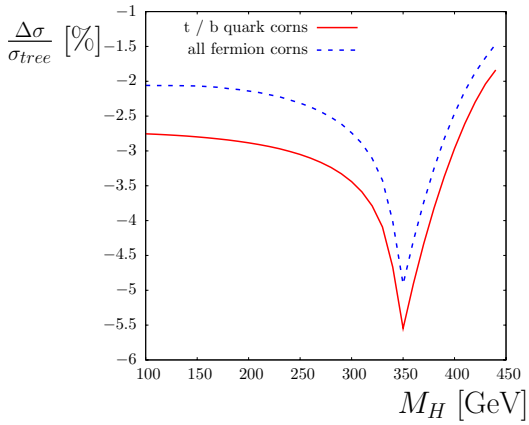

(b) Percentage loop corrections from top / bottom and all fermion contributions for Z fusion.

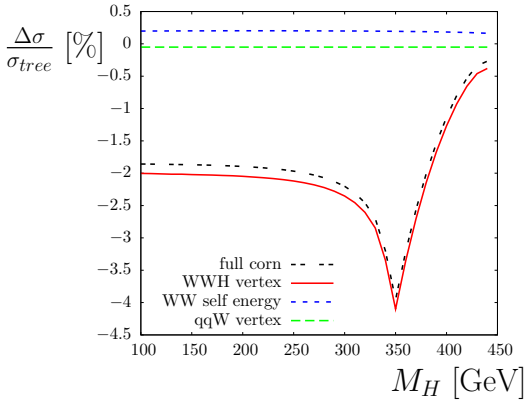

(c) Percentage individual loop corrections from top / bottom contributions for W fusion.

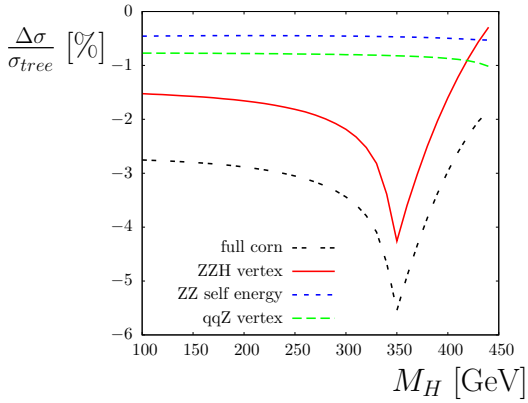

(d) Percentage individual loop corrections from top / bottom contributions for Z fusion.

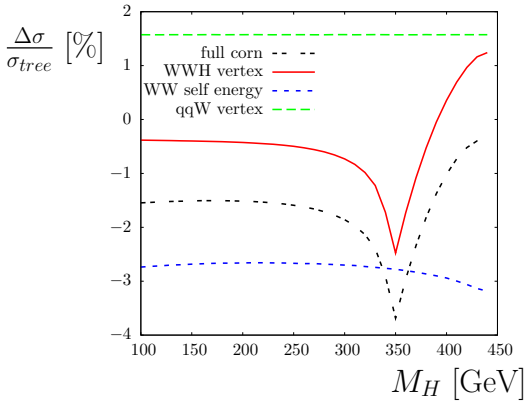

(e) Percentage individual loop corrections from all fermion contributions for W fusion.

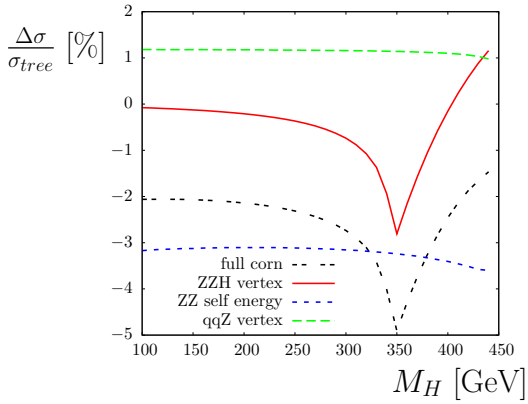

(f) Percentage individual loop corrections from all fermion contributions for Z fusion.

Figure 5.4: A comparison of individual contributions to loop corrections for H production via weak boson fusion at $\sqrt{\hat{s}} = 500$ GeV in the Standard Model.

the two diagrams with opposite fermion flow involving (for instance) the top quark will cancel one another out (this is shown explicitly in the calculation in Appendix C). The formfactors for HWW with the full Standard Model loop contribution are not shown as these are IR divergent (as the W field renormalisation enters them) and need to be combined with the other virtual and real corrections in order to achieve a finite result[4].

The relative effects of the corrections for the HZZ formfactor are larger than those for the HWW formfactor (due to the increased importance of the Z boson self energy) when only top and bottom quark loops are considered. The corrections to the formfactor a_1 are seen to be larger when all fermions are considered, although a significant proportion of the contribution does come from the third generation quarks. The anomalous formfactors a_2 and a_3 are seen to be extremely small in the Standard Model – smaller than the level that is expected to be observable at the LHC (see Section 2.4.3). At tree level, $a_1^{HWW} \approx 52$ and the loop correction Δa_1 is $\mathcal{O}(1)$ – i.e. a_2 and a_3 are smaller than Δa_1 by approximately 5 and 10 orders of magnitude respectively.

Fig. 5.6 shows the relative importance of the self energy and vertex corrections to the formfactor a_1. As can be seen, the relative importance of the Higgs vertex corrections decreases when all fermions are included in the loop diagrams, as the weak boson self energy contributions (as well as the counterterm at the Higgs vertex) for light fermions are not suppressed by the large top mass. The familiar threshold behaviour at $\sim 2m_t$ is joined in the full corrections by two more features at $\sim 2M_W$ and $\sim 2M_Z$, which are similarly the result of the W / Z boson going on shell in the calculation of the Higgs field renormalisation constant.

When comparing these formfactor results with the partonic cross sections shown in Section 5.2, and the total cross section in Section 5.4, it is important to remember that the formfactor correction should be (as indeed it is) approximately half of the cross section correction, because:

$$\Delta\sigma = 2\mathrm{Re}\left[\mathcal{M}^*_{\mathrm{tree}}\mathcal{M}_{\mathrm{loop}}\right] \tag{5.2}$$

Another significant point is that the corrections to the quark vertex are obviously not included in the formfactor calculations. When only the top / bottom quark contributions are considered this does not make a large difference (due to the dominance of the HVV

[4]Since the formfactor calculation and the squared matrix elements (which are calculated completely independently) need to be combined to give an IR finite result, we have a stringent check on the implementation of our renormalisation procedures.

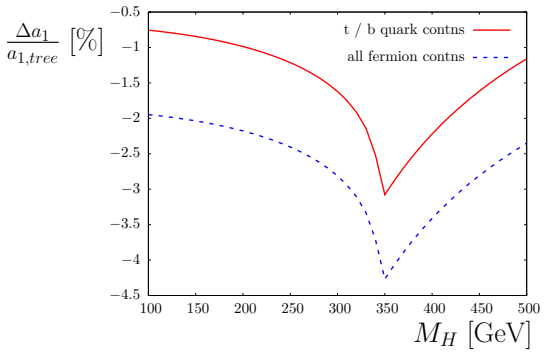

(a) Percentage corrections to the formfactor a_1 from t/b and all fermion contributions for HWW.

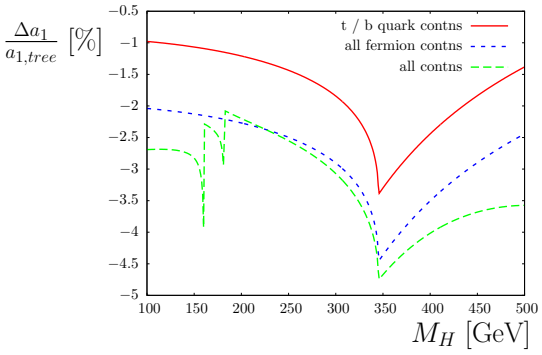

(b) Percentage corrections to the formfactor a_1 from t/b, all fermion and all contributions for HZZ.

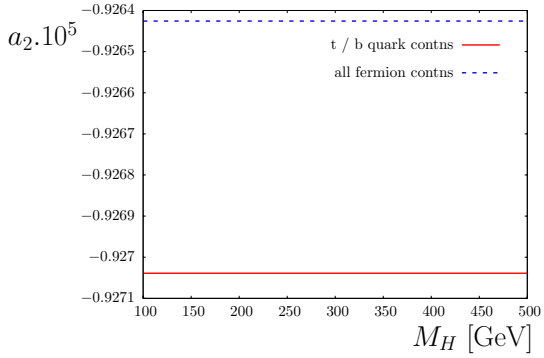

(c) Corrections to the formfactor a_2 from t/b and all fermion contributions for HWW.

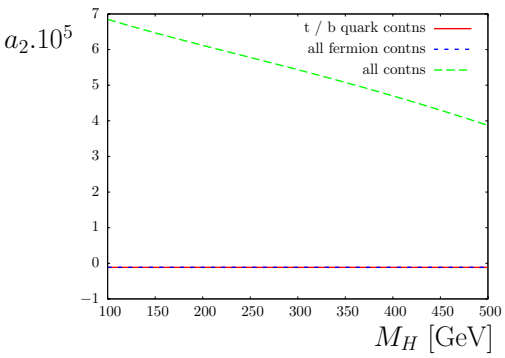

(d) Corrections to the formfactor a_2 from t/b, all fermion and all contributions for HZZ.

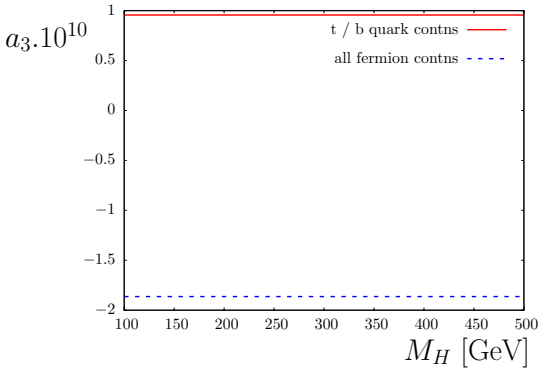

(e) Corrections to the formfactor a_3 from t/b and all fermion contributions for HWW.

Figure 5.5: HVV formfactors for W and Z boson fusion in the Standard Model. For comparison, note that $a_{1,tree}^{HWW} \approx 52$ and $a_{1,tree}^{HZZ} \approx 68$ – i.e. Δa_1 is $\mathcal{O}(1)$. The red curves are the top / bottom quark contributions, the blue curves show the fermion contributions and the green curves display the full SM correction.

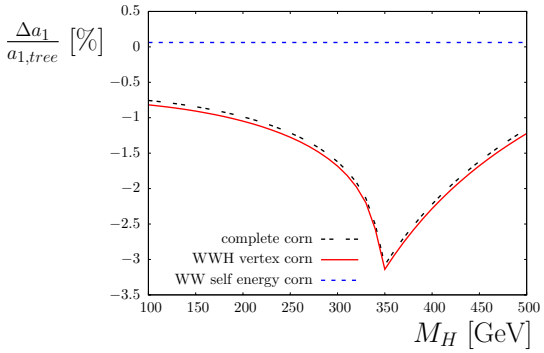

(a) Vertex and self energy corrections to the formfactor a_1 from t/b contributions for HWW.

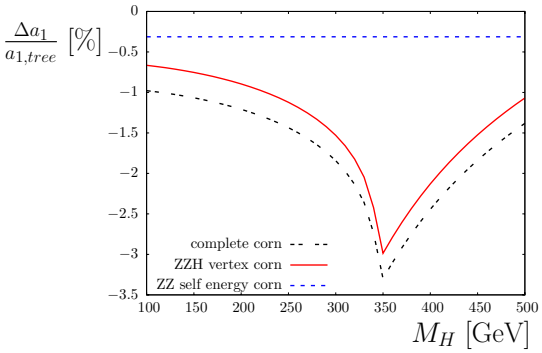

(b) Vertex and self energy corrections to the formfactor a_1 from t/b contributions for HZZ.

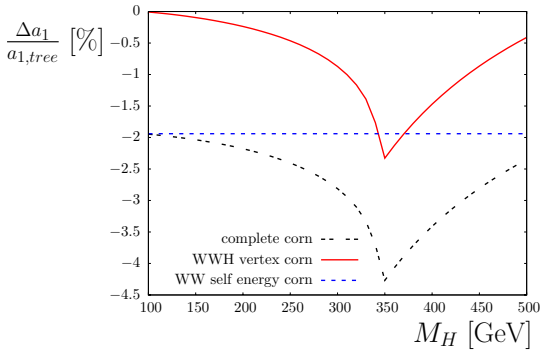

(c) Vertex and self energy corrections to the formfactor a_1 from all fermion contributions for HWW.

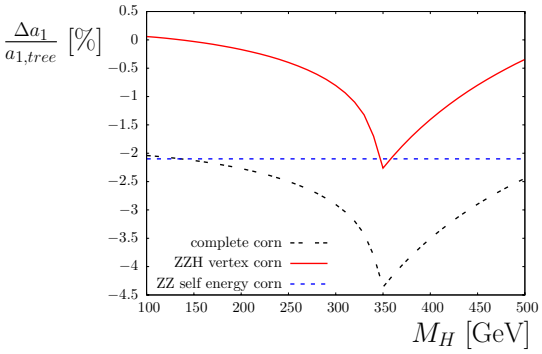

(d) Vertex and self energy corrections to the formfactor a_1 from all fermion contributions for HZZ.

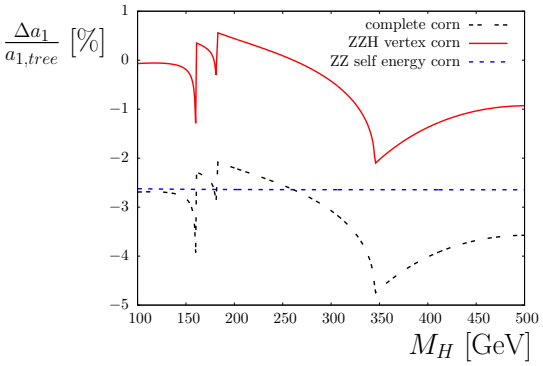

(e) Vertex and self energy corrections to the formfactor a_1 from all contributions for HZZ.

Figure 5.6: Vertex and self energy contributions to the formfactor a_1 in the Standard Model for HWW and HZZ. The first row concentrates on top / bottom quark corrections, the second row displays all fermion corrections and the third row shows the full corrections. The red curves show the correction from the Higgs vertex HVV, the blue curves show the VV self energy contribution and the black curves are the combined correction (HVV plus VV).

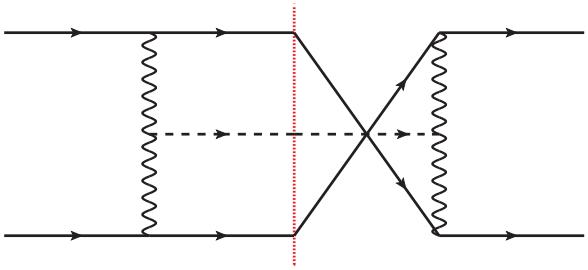

Figure 5.7: Feynman diagram of t-u channel interference.

corrections), but when the lighter fermions are included the size of the quark vertex correction increases and partially cancels out the increased correction from the weak boson self energy.

5.4 Total cross sections

5.4.1 Comparison with the literature

Reference [55] studied the electroweak and QCD corrections to Higgs production via vector boson fusion in the Standard Model. The results of our modified `VBFNLO` were compared with the results presented in Ref. [55] and found to be in agreement to within the numerical accuracies of the code.

The basic method used in Ref. [55] is to consider the QCD and electroweak corrections to the decay $H \to q\bar{q}q\bar{q}$ (as detailed in Ref. [126, 127]), and relate the amplitudes found in that process to the weak boson fusion Higgs production process using crossing symmetries. The calculation in Ref. [55] includes several of the NLO contributions that are customarily neglected (and are neglected in our calculation using `VBFNLO`). Principally, both s-channel (Higgsstrahlung) diagrams and t-u interference diagrams (shown in Fig. 5.7) are considered.

The parameters we use for the comparison are set to match those of Ref. [55]. In particular, a top mass $m_t = 174.3$ GeV is used, and the cuts differ slightly from our default set (Equation 2.5), in that no cut is made on the dijet mass. For the comparison,

we use the cuts:

$$\begin{aligned} p_{T_j} &> 20 \text{ GeV} \\ |\eta_j| &< 5 \\ R_{jj} &> 0.8 \\ \Delta\eta_{jj} = |\eta_{j_1} - \eta_{j_2}| &> 4 \\ \eta_{j_1} \cdot \eta_{j_2} &< 0 \end{aligned} \tag{5.3}$$

The electromagnetic coupling constant is defined using the Fermi constant (Equation 3.46) and the renormalisation and factorisation scales are set to M_W^2.

Another difference between the approaches in `VBFNLO` and Ref. [55] is the manner in which the produced Higgs boson is treated. In `VBFNLO`, an isotropic decay of the Higgs boson into two massless particles is generated (see [47]). The matrix element is evaluated with an invariant Higgs mass given by a Breit-Wigner distribution. Ref. [55] evaluates the matrix element for an on shell Higgs boson and our code has been modified so that it is capable of reproducing this at leading order.

Table 5.1 compares the results presented in Ref. [55] with those obtained using the modified `VBFNLO`. Note that the results quoted here are a combination of the results presented in Ref. [55] – their total cross section after WBF cuts have been applied (Table 2 in Ref. [55]) and the contribution from s-channel and t-u channel interference diagrams (given in Table 4, Ref. [55]). Since we do not include these contributions, the results we give here are the total cross section of Ref. [55] minus these s and t-u diagram types. At NLO, the correction caused by Higgsstrahlung and crossing suppressed diagrams is always less than 0.55% of the NLO cross section.

5.4.2 New results and distributions

We now move on to examine the results obtained using our modified `VBFNLO` in the Standard Model using our default settings. Figure 5.8 shows the total cross section as a function of the Higgs mass at a collider energy of 14 TeV (the "design energy" of the LHC). The cross section is shown at leading order and with various NLO corrections: QCD corrections (which have been checked against results obtained using the public `VBFNLO`), QCD corrections plus virtual corrections involving top and bottom quark loops, QCD corrections plus loop contributions from all fermions and the full QCD and

Table 5.1: Comparison of our results with those presented in Ref. [55] for the weak boson fusion channel only. Note that the errors quoted here are numerical uncertainties. We compare results for the LO cross section (with both our default settings – labelled "Breit-Wigner", and the on shell variant of our code – labelled "on shell"), for the QCD corrections at NLO, and for the full result (containing both QCD and electroweak corrections).

M_H [GeV]	120	150	200
σ_{LO}, Ref [55] [fb]	1876.42±0.5	1589.89±0.4	1221.16±0.3
σ_{LO}, `VBFNLO` [fb] (Breit-Wigner)	1872.27±0.93	1586.63±0.77	1218.95±0.58
σ_{LO}, `VBFNLO` [fb] (on shell)	1876.25±0.93	1590.00±0.77	1221.31±0.58
σ_{QCD}, Ref [55] [fb]	1787.18 ± 0.75	1507.61 ± 0.64	1151.99 ± 0.49
$\frac{\Delta\sigma_{QCD}}{\sigma_{LO}}$[%], Ref [55]	-4.75 ± 0.04	-5.17 ± 0.04	-5.66 ± 0.04
σ_{QCD}, `VBFNLO` [fb]	1783.24 ± 3.07	1505.41 ± 3.08	1152.17 ± 1.70
$\frac{\Delta\sigma_{QCD}}{\sigma_{LO}}$[%], `VBFNLO`	-4.76 ± 0.16	-5.12 ± 0.19	-5.48 ± 0.14
σ_{NLO}, Ref [55] [fb]	1656.3 ± 1	1402.12 ± 0.8	1088.21 ± 0.5
σ_{NLO}, `VBFNLO` [fb]	1653.93±5.96	1407.69±5.09	1091.76±5.98

electroweak corrections. Also shown is the corrected cross section (with QCD and full electroweak corrections) at 10 TeV, the energy that the LHC will (hopefully) run at in the near future. Very recently it was announced [128] that the collider will initially run at an energy of 7 TeV, which will cause a further reduction in the cross section shown in Figure 5.8.

The QCD corrections are seen to be nearly independent of the Higgs mass, remaining at a value of $\sim -5\%$ over the entire range considered here, as are the fermion corrections. As was seen in the partonic cross section, the percentage loop corrections for top and bottom quark diagrams is greater than that when all fermions are included. The total electroweak corrections are, on average, about the same size as the QCD corrections – they are larger than the QCD corrections for $M_H \sim 100 \to 150$ GeV and smaller at higher masses. The thresholds at $M_H \sim 2M_W$ and $M_H \sim 2M_Z$, which were seen previously in the formfactor calculations for the HZZ coupling (Fig. 5.5), are visible here as well – the curve is more jagged here as the cross section was calculated for far fewer Higgs masses than the formfactor, as the cross section calculation naturally takes more time to run than the simpler formfactor calculation. We have explcitly verified that our partonic cross sections, our formfactors, and our total cross sections are consistent

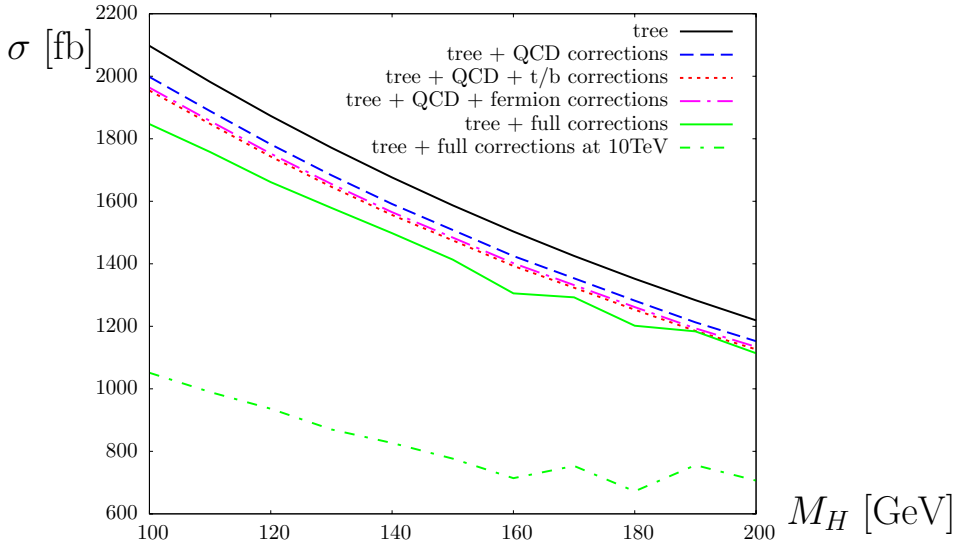

(a) Total cross section.

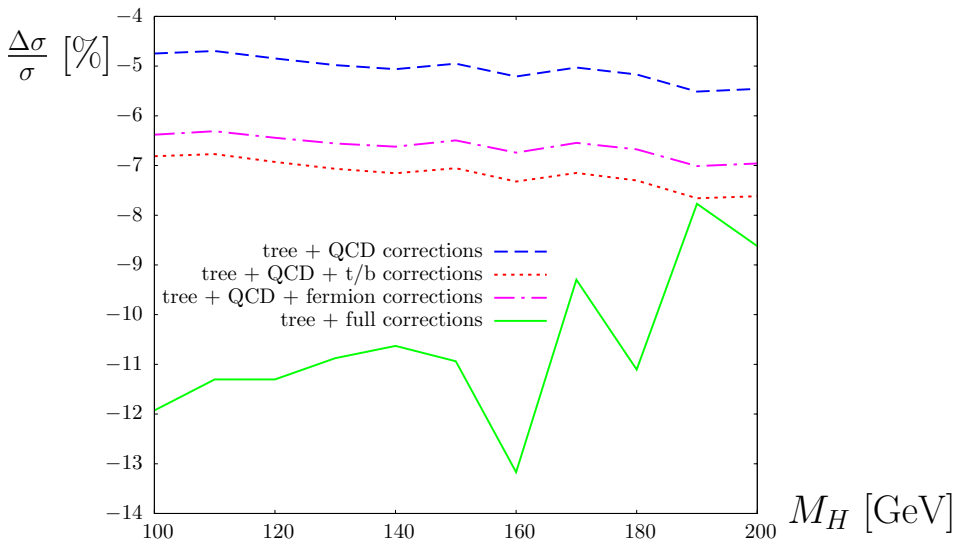

(b) Percentage higher order corrections.

Figure 5.8: Higgs production via WBF in the Standard Model at 14 TeV and 10 TeV at leading order and with QCD, t/b, fermion and full electroweak corrections.

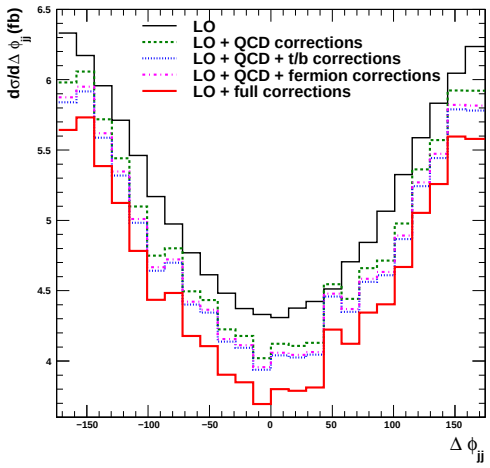

Figure 5.9: Azimuthal angle distribution for Higgs production via WBF in the Standard Model, at $\sqrt{\hat{s}} = 14$ TeV with $M_H = 120$ GeV.

for both W and Z boson fusion individually, and each of the correction types (HVV, VV and qqV).

Figure 5.9 shows the azimuthal angle distribution of WBF for $M_H = 120$ GeV. As can be seen, although the corrections alter the value of the distribution, the shape remains unaffected by the higher order corrections. This is as expected, considering the small values of the formfactors a_2 and a_3 that were calculated in Section 5.3.

Chapter 6

Results for WBF Higgs production at the LHC in the MSSM

In this Chapter we study the weak boson fusion process in the MSSM with both real and complex parameters. As in the previous Chapter, we start by examining the leading partonic subprocess, and then move on to look at the formfactors, as a function of both $\tan\beta$ and M_A (or $M_{H^\pm}$ for the case of the complex MSSM). We then turn to the full results obtained by implementing the dominant SUSY loop corrections, supplemented by the full SM result, into the Monte Carlo program `VBFNLO`. These results include the complete MSSM corrections to the Higgs vertex and weak boson self energy, as well as the sfermion corrections to the quark–weak boson vertex. We first compare our results with the "pure SUSY" corrections available for the real MSSM in the literature [56], before studying the results in the MSSM – both the total cross sections and the important azimuthal angle distribution.

6.1 Parameters

As in the previous Chapter, unless otherwise stated the Standard Model parameters used are from the Particle Data Book, the top mass is 172.6 GeV, the cuts of Section 2.2 are imposed and the PDF set MRST2004QED is employed. If we are working solely in the fermion / sfermion sector, the electromagnetic coupling is parametrised in terms of the Fermi constant, G_F. If, however, we are going beyond this sector and including the full MSSM corrections, we express our result in terms of $\alpha(M_Z^2)$.

Table 6.1: Parameters of the CPX scenario

M_{SUSY}	μ	$\lvert m_{\tilde{g}}\rvert$	$\phi_{m_{\tilde{g}}}$	M_2	$\lvert A_t\rvert$	ϕ_{A_t}
500 GeV	2000 GeV	1000 GeV	$\frac{\pi}{2}$	200 GeV	900 GeV	$\frac{\pi}{2}$

As in Chapter 4, in the MSSM we study the so-called benchmark scenarios, as described in Ref. [121] and Table 4.1, and take M_A and $\tan\beta$ as our input parameters. In this Chapter, we also investigate the MSSM with complex parameters. The complex benchmark – the CPX scenario (originally proposed in [129], we use the parameters as described in [33], which are shown in Table 6.1) – is especially interesting as it leads to the so-called "LEP hole": an area of MSSM parameter space leading to a light Higgs of mass ~ 40 GeV, which the experimental searches at LEP could not exclude [130]. In this scenario, the gluino mass parameter and the trilinear couplings are entirely imaginary, leading to large CP violation. Note that, in the complex MSSM, the physical Higgs bosons are no longer CP eigenstates – they are referred to as h_1, h_2 and h_3, and are combinations of all three neutral Higgs particles. We also investigate weak boson fusion for the SPS benchmark points (described in Ref. [131]).

Typically, in this Chapter we define our leading order cross section to be the tree level cross section combined with the well known effect of the Higgs propagator corrections (Z factors – see Section 3.4).

6.2 Partonic cross sections

Partonic cross sections were generated using `FeynArts`, `FormCalc`, `LoopTools`, and `FeynHiggs` for the leading partonic subprocess

$$u + d \to d + h + u \tag{6.1}$$

Processes involving both Z and W boson exchange were included, and loop diagrams involving all (s)fermions or only third generation (s)quarks were considered. Corrections to the Higgs propagator are included at tree level – consequently, the loop correction percentages shown below do not include the well known propagator effects, but are instead the genuine vertex corrections.

Fig. 6.1 shows the corrected cross section of light Higgs production via weak boson fusion in the four real MSSM benchmarks, for fixed $\tan\beta = 10$ as a function of M_A, and for fixed $M_A = 150$ GeV as a function of $\tan\beta$. We can see that, at high values of the (input) CP odd Higgs mass (over $M_A \sim 180$ GeV), the cross section and loop corrections are reasonably flat. This is because at large M_A the light Higgs becomes Standard Model like, and the ratio of the MSSM hWW coupling to the Standard Model coupling $\sin(\beta - \alpha) \approx 1$ (see Section 3.5). At low M_A, the differences between the benchmarks are more pronounced, and the cross sections and loop corrections vary more dramatically. Loop corrections in the non-decoupling regime can be up to $\mathcal{O}(10\%)$.

Studying the sensitivity of the cross section and loop corrections to $\tan\beta$ (the right hand plot of the first row, and the third row respectively), we see that the cross section decreases up to $\tan\beta \sim 5$ before beginning to increase. This behaviour was also seen when considering weak boson fusion at a linear collider, with external electrons and neutrinos rather than quarks (see Section 4.4), and is due to the combination of an enhancement caused by the increasing factor $\sin^2(\beta - \alpha)$ and a suppression due to the increasing Higgs mass. For the benchmarks other than the small α_{eff} scenario, the loop corrections are reasonably insensitive to the value of $\tan\beta$. In the small α_{eff} scenario, however, because the masses of the sfermions are more strongly dependent on $\tan\beta$, the loop corrections are also more sensitive to variations of this input parameter.

Figure 6.1 shows that, although the contribution from third generation (s)quarks is important, the loop diagrams involving other fermions and sfermions are not negligible and should be included in higher order calculations. The corrections when all (s)fermion contributions are included are smaller than the corrections when only third generation (s)quarks are considered.

6.3 Formfactors

As in the Standard Model, we examine the formfactors (the Standard Model like a_1, and the anomalous a_2 and a_3), before calculating the total cross sections and distributions. We scan over the two input parameters that describe the tree level Higgs sector ($\tan\beta$ and M_A or $M_{H^\pm}$). We also run a further check on the renormalisation procedures.

The Higgs propagator corrections are included at tree level (see Figure 4.8), where they form part of the a_1 formfactor. At loop level triangle diagrams at the Higgs vertex

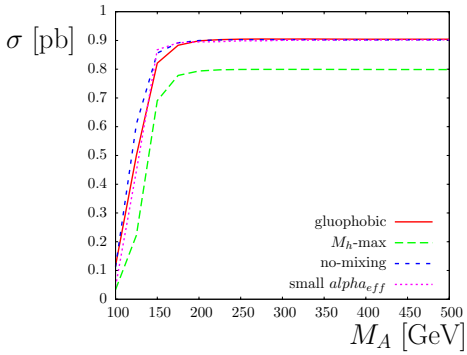

(a) Corrected partonic cross section, with $\tan\beta = 10$. All (s)fermion diagrams are included.

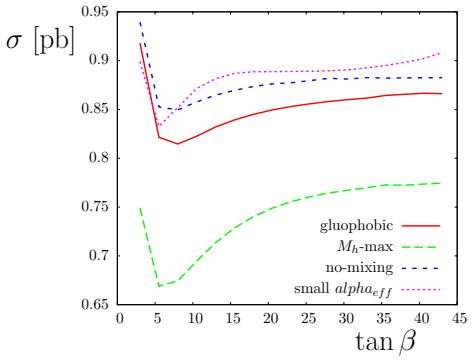

(b) Corrected partonic cross section, with $M_A = 150$ GeV. All (s)fermion diagrams are included.

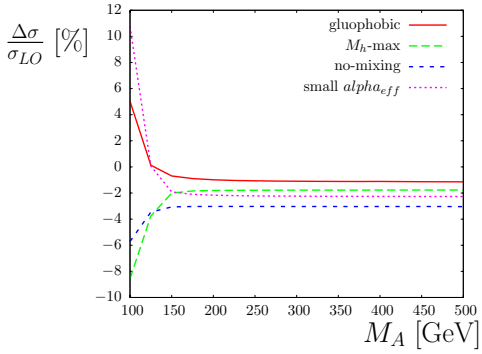

(c) Percentage correction when only (s)top / (s)bottom loops are included, with $\tan\beta = 10$.

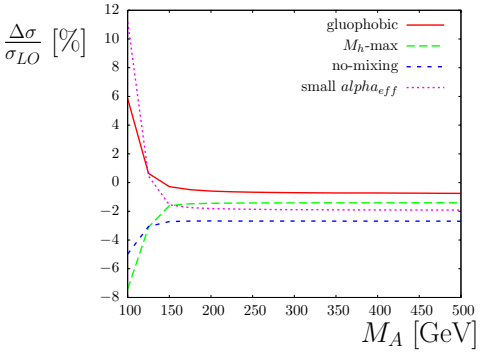

(d) Percentage correction when all (s)fermions are included in the loops, with $\tan\beta = 10$.

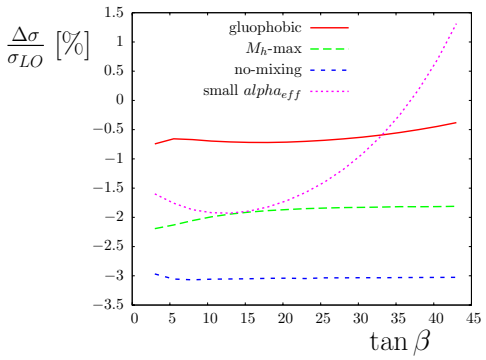

(e) Percentage correction when only (s)top / (s)bottom loops are included, with $M_A = 150$ GeV.

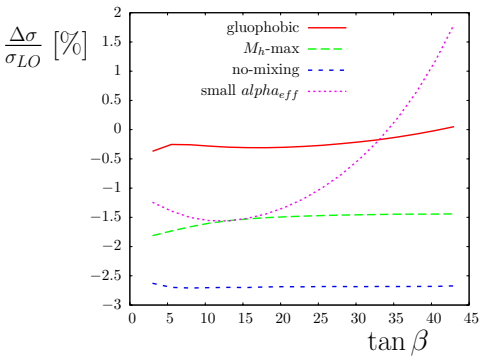

(f) Percentage correction when all (s)fermions are included in the loops, with $M_A = 150$ GeV.

Figure 6.1: Partonic cross section of h production in the MSSM with real parameters at $\sqrt{\hat{s}} = 500$ GeV. The first row shows the loop corrected cross section, the second row shows the loop correction percentages as a function of M_A, and the third row shows the loop correction percentages as a function of $\tan\beta$.

and weak boson self energy diagrams are included in the formfactors, along with the corresponding counterterms.

First, in Fig. 6.2, we examine the formfactor a_1 for the vertices hWW and hZZ in the four benchmarks in the MSSM with real parameters, as a function of $\tan\beta$. As was seen in the earlier partonic cross sections, the small α_{eff} scenario displays the highest sensitivity to the value of $\tan\beta$, owing to greater changes in the masses of the sfermions – for the other benchmarks, the percentage corrections to a_1 are nearly independent of $\tan\beta$. For the values of $\tan\beta$ shown here, the light Higgs mass varies from ~ 90 GeV to ~ 120 GeV (or ~ 130 GeV in the M_h^{max} scenario). Comparing the percentage corrections shown in Fig. 6.2 to those obtained in the Standard Model for a Higgs of this mass (see Fig. 5.5), we see that there is very little deviation between the MSSM formfactors and the SM formfactors. The corrections to the formfactors are larger when contributions from all (s)fermions are considered than when only third generation (s)quarks are included, and again, the percentage corrections to the hZZ formfactor are slightly larger than those for the hWW formfactor.

The formfactors a_2 and a_3 are – as in the Standard Model – much smaller than a_1. Values of these formfactors corresponding to the results for a_1 in Fig. 6.2 are shown in Fig. 6.3 and Fig. 6.4 respectively.

We observe larger discrepancies between the MSSM and the Standard Model when studying the anomalous formfactors a_2 and a_3. The formfactor a_2 in the gluophobic scenario is smaller than in the other benchmarks, which are more SM like here. a_2 also has a stronger dependence on $\tan\beta$ than a_1, changing fairly rapidly below $\tan\beta \sim 10$. This behaviour is repeated by the formfactor a_3, which doubles in value between $\tan\beta = 3$ and $\tan\beta = 10$. The sign of a_3 is different in the MSSM than in the SM for the (s)top / (s)bottom contributions, and is larger by a factor of 2 in the MSSM[1]. These differences in the anomalous formfactors, however, are still very small compared to the size of the SM like formfactor a_1.

The formfactor a_1 is shown in Fig. 6.5 for the case where $\tan\beta$ is constant and M_A is allowed to vary. The expected decoupling behaviour can be clearly seen – at low values of M_A, the corrections are generally large and change rapidly. When we move to heavier CP odd Higgs bosons, the corrections become practically constant, as the

[1]Note that the value of a_3 (which is only non-zero for the coupling between the W bosons and the Higgs – see Appendix C) does not depend on the benchmark we are studying. This is because the additional sfermion loops have no effect on the value of a_3 and – since we use the tree level value of the Higgs mixing angle α – the value of $\sin(\beta - \alpha)$ does not alter between benchmarks.

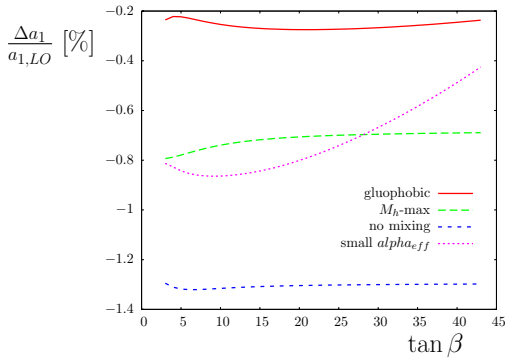

(a) Percentage correction to a_1 for the coupling hWW when only (s)tops and (s)bottoms are included in the loops.

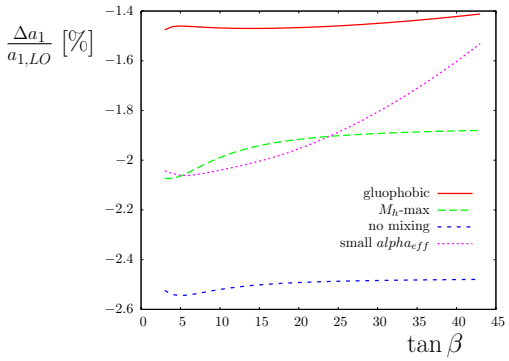

(b) Percentage correction to a_1 for the coupling hWW when all (s)fermions are included in the loops.

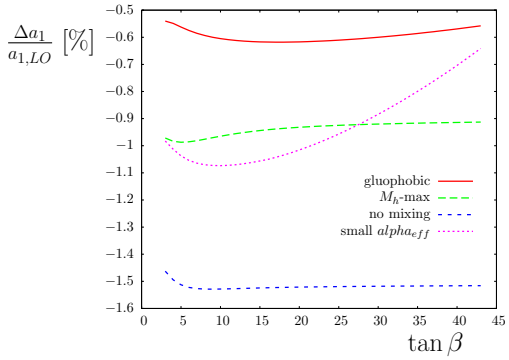

(c) Percentage correction to a_1 for the coupling hZZ when only (s)tops and (s)bottoms are included in the loops.

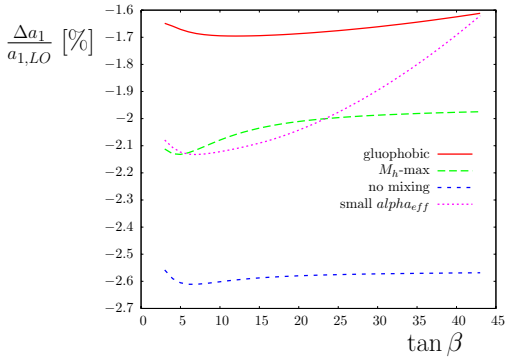

(d) Percentage correction to a_1 for the coupling hZZ when all (s)fermions are included in the loops.

Figure 6.2: Correction to the formfactor a_1 as a percentage of the leading order formfactor with $M_A = 150$ GeV in the MSSM with real parameters. The first row contains the formfactors for the coupling hWW, the second for the coupling hZZ.

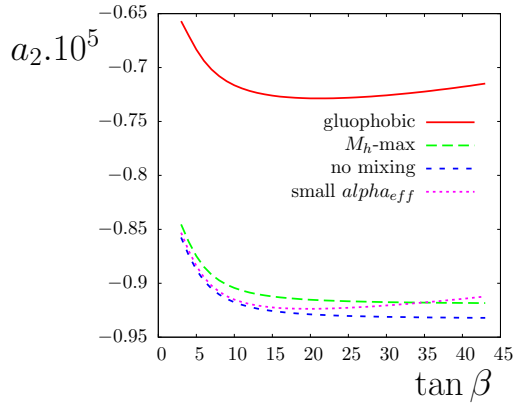

(a) The formfactor a_2 for the coupling hWW when only (s)tops and (s)bottoms are included in the loops.

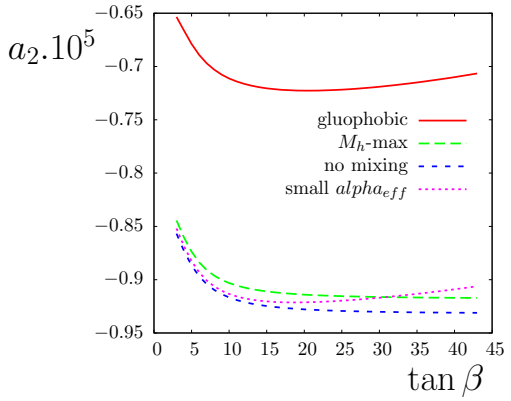

(b) The formfactor a_2 for the coupling hWW when all (s)fermions are included in the loops.

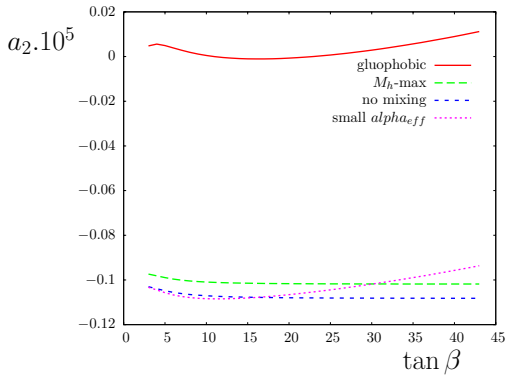

(c) The formfactor a_2 for the coupling hZZ when only (s)tops and (s)bottoms are included in the loops.

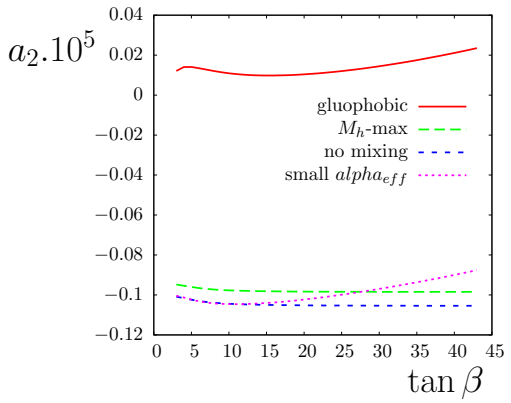

(d) The formfactor a_2 for the coupling hZZ when all (s)fermions are included in the loops.

Figure 6.3: Corrections to the formfactor a_2 with $M_A = 150$ GeV in the MSSM with real parameters. Results for the hWW and hZZ couplings are presented in the first and second rows respectively.

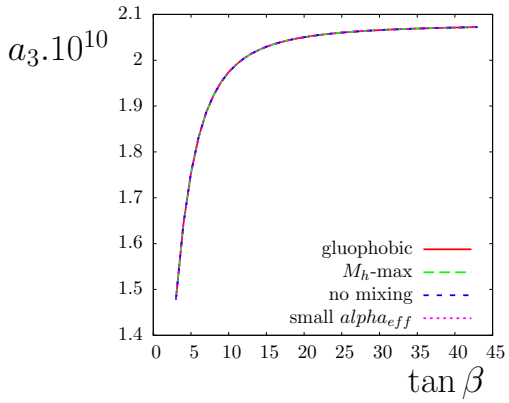

(a) The formfactor a_3 for the coupling hWW when only (s)tops and (s)bottoms are included in the loops.

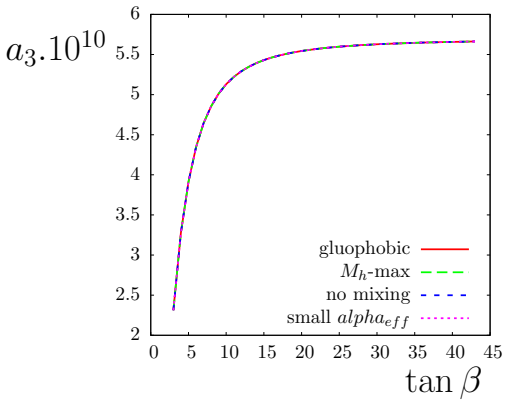

(b) The formfactor a_3 for the coupling hWW when all (s)fermions are included in the loops.

Figure 6.4: Corrections to the formfactor a_3 with $M_A = 150$ GeV in the MSSM with real parameters.

model becomes more SM like. Generally, the largest corrections occur in the no-mixing scenario, and the smallest in the gluophobic scenario.

Turning to the production of the heavy CP even Higgs boson H, Fig. 6.6 and 6.7 show the formfactors for the coupling HWW. In Fig. 6.6 the first row shows the leading order values of the formfactor a_1, and the decoupling behaviour at high M_A is shown clearly here – $a_{1,LO}$ becomes negligible for large $M_A > 200$ GeV. In this region, the light Higgs becomes more Standard Model like and the factor $\sin(\beta - \alpha)$ (which modifies the light Higgs coupling in the MSSM) approaches 1. This means that the factor $\cos(\beta - \alpha)$ (which modifies the heavy Higgs coupling in the MSSM) approaches 0, so the production of heavy Higgs bosons becomes negligible. The formfactors a_2 and a_3 (the second row of Fig. 6.6 show different behaviour as a function of $\tan\beta$ when describing the heavy and light CP even Higgs bosons, but since the size of a_2 does not change, and a_3 only increases by one order of magnitude, this behaviour is (in this scenario) unlikely to produce an observable effect.

Since in the decoupling regime a_1 is extremely small, the loop correction becomes the dominant contribution – consequently, in Fig. 6.7 we show the loop correction as a percentage of the leading order value for $M_A = 100 \rightarrow 200$ GeV. The loop percentage correction also becomes very large in the small α_{eff} scenario for high $\tan\beta$, but again this is due to the leading order value of a_1 approaching zero (see Fig. 6.6(b)). The first and second generation (s)fermions have a very large effect on a_1.

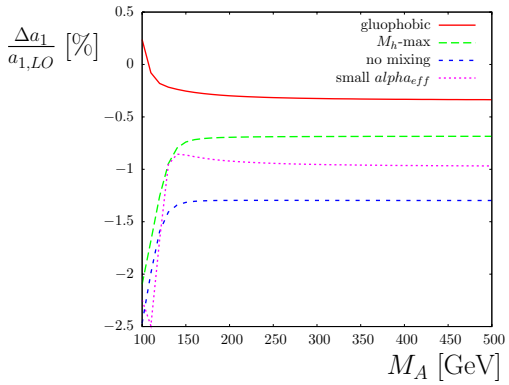

(a) Percentage correction to a_1 for the coupling hWW when only (s)tops and (s)bottoms are included in the loops.

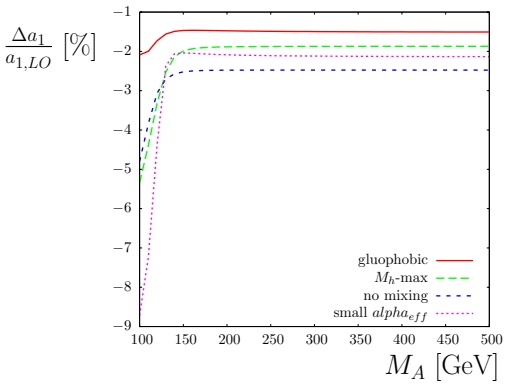

(b) Percentage correction to a_1 for the coupling hWW when all (s)fermions are included in the loops.

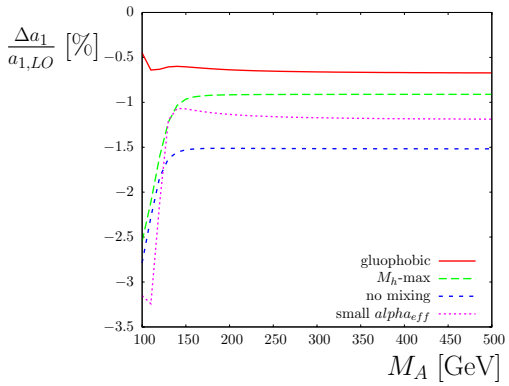

(c) Percentage correction to a_1 for the coupling hZZ when only (s)tops and (s)bottoms are included in the loops.

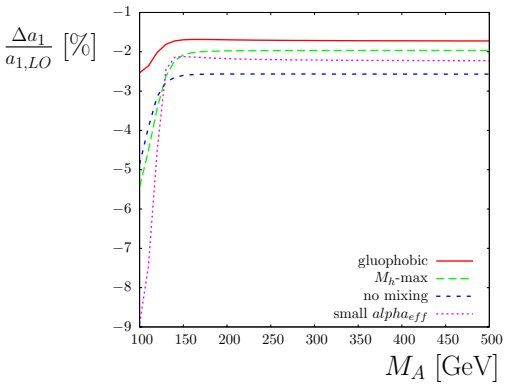

(d) Percentage correction to a_1 for the coupling hZZ when all (s)fermions are included in the loops.

Figure 6.5: Correction to the formfactor a_1 as a percentage of the leading order formfactor with $\tan\beta = 10$ for the benchmark scenarios in the MSSM with real parameters. The first row contains the formfactors for the coupling hWW, the second for the coupling hZZ.

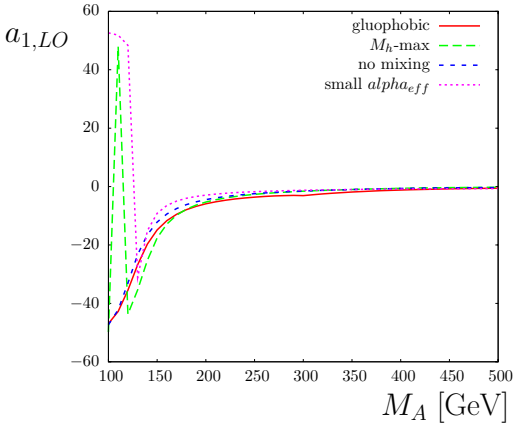

(a) Leading order value of the formfactor a_1, with $\tan\beta = 10$.

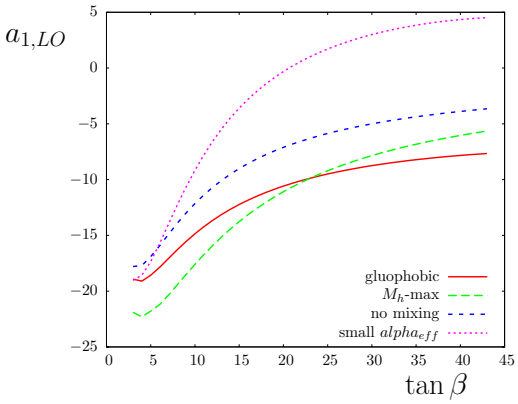

(b) Leading order value of the formfactor a_1, with $M_A = 150$ GeV.

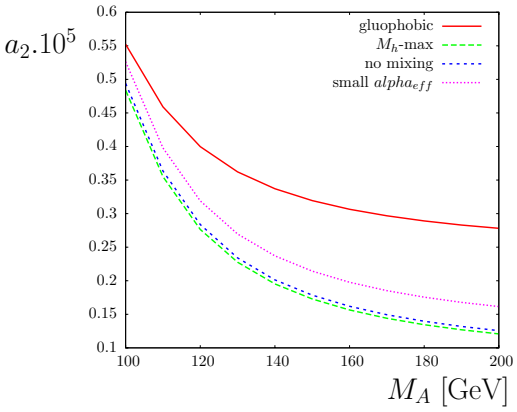

(c) Formfactor a_2 from all (s)fermions, with $\tan\beta = 10$.

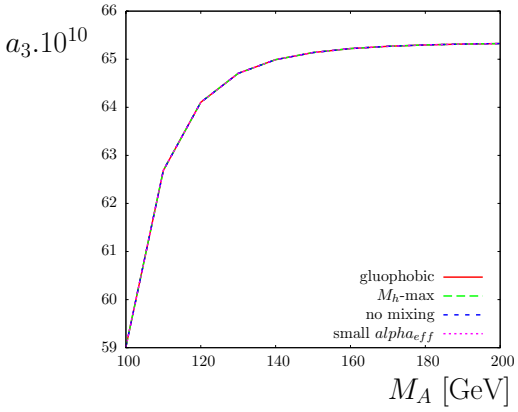

(d) Formfactor a_3 from all (s)fermions, with $\tan\beta = 10$.

Figure 6.6: Formfactors for the coupling HWW for the heavy CP even Higgs in the MSSM with real parameters. The first row shows the leading order value of a_1 and the second row shows the formfactors a_2 and a_3 with $\tan\beta = 10$.

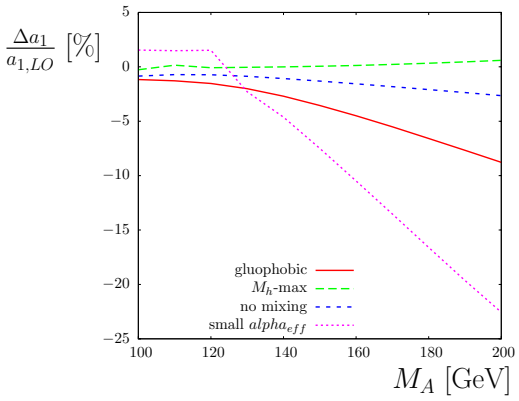

(a) Percentage correction to formfactor a_1 from (s)tops / (s)bottoms, with $\tan\beta = 10$.

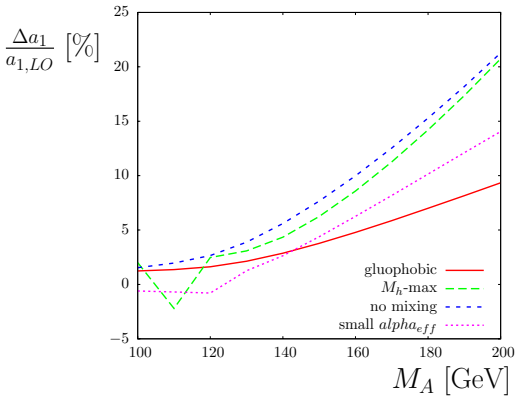

(b) Percentage correction to formfactor a_1 from all (s)fermions, with $\tan\beta = 10$.

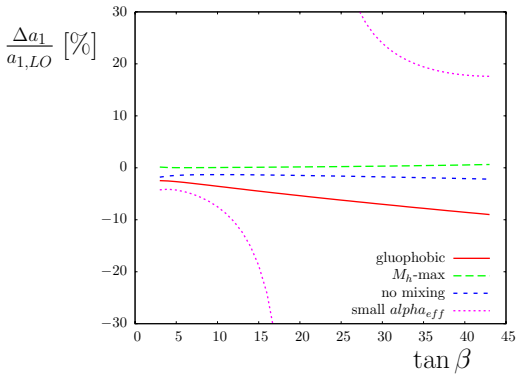

(c) Percentage correction to formfactor a_1 from (s)tops / (s)bottoms, with $M_A = 150$ GeV

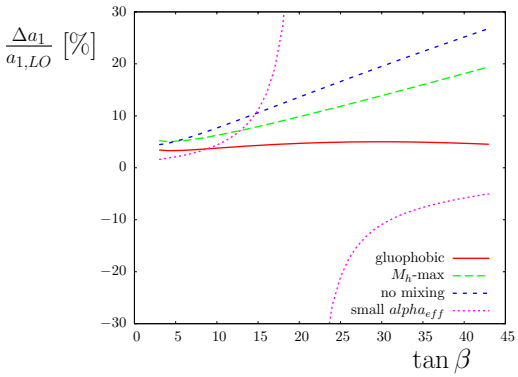

(d) Percentage correction to formfactor a_1 from all (s)fermions, with $M_A = 150$ GeV.

Figure 6.7: Formfactors for the coupling HWW for the heavy CP even Higgs in the MSSM with real parameters. The first and second rows show percentage corrections to a_1 for $\tan\beta = 10$ and $M_A = 150$ GeV respectively.

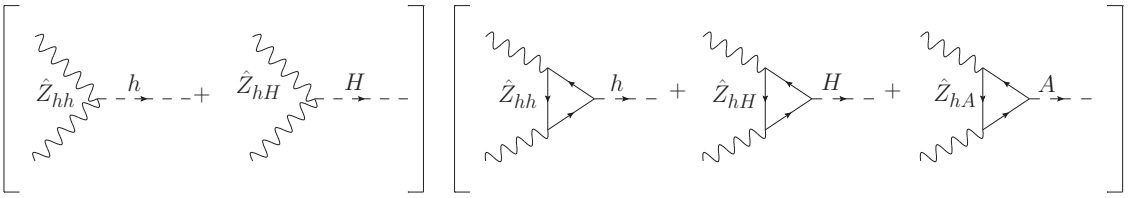

Figure 6.8: Inclusion of the corrections to the Higgs propagator at loop level as well as at Born level.

Since the leading order values of a_1 (and hence the cross sections) are so small in the decoupling regime, in the calculation of the matrix squared elements we do not neglect the term $|\mathcal{M}_{loop}|^2$, i.e. the loop correction term is

$$\Delta\sigma \;=\; 2\,\mathrm{Re}\,[\mathcal{M}^*_{LO}\mathcal{M}_{loop}] + |\mathcal{M}_{loop}|^2 \tag{6.2}$$

6.3.1 The inclusion of higher order corrections in the MSSM with complex and real parameters

The above results comprise the leading order – which includes the tree level and the propagator corrections – and the corrected level, which is the leading order plus the genuine vertex corrections. This is described in Chapter 4, Figure 4.8. A more complete picture may be obtained by applying the propagator Z factors to *both* the tree level and one loop level. This will incorporate more of the known higher order corrections, and is illustrated in Fig. 6.8, which shows the diagram content of the NLO virtual corrections (i.e. the term $2\,\mathrm{Re}\,[\mathcal{M}^*_{LO}\mathcal{M}_{loop}]$). This does not give rise to double counting – these corrections are formally of higher order but, since they're universal (and one knows that they will also appear in the next order), they can be included here.

We use the formfactor calculations as a simple way to look at the effect of these higher order corrections. Figure 6.9 compares each formfactor for h_1WW and h_1ZZ in the CPX scenario, both with and without the inclusion of wave function normalisation factors at the loop level according to Fig. 6.8. The effect of also incorporating the Z factors at loop level is, for the CPX scenario, quite large in the non-decoupling regime of low $M_{H^\pm}$ (below ~ 200 GeV) – deviations exist in all of the formfactors. The correction to a_1 changes sign when the new effects are included, changing by a value of $\sim 1.5\%$. The formfactor a_2 for the effective coupling of h_1WW also changes sign as the result of these higher order corrections. The effect of including Z factors at loop level is most

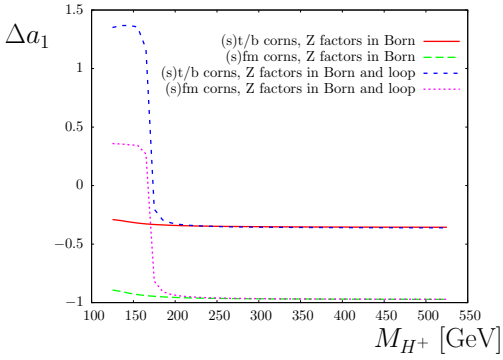

(a) Correction to a_1 for the coupling h_1WW.

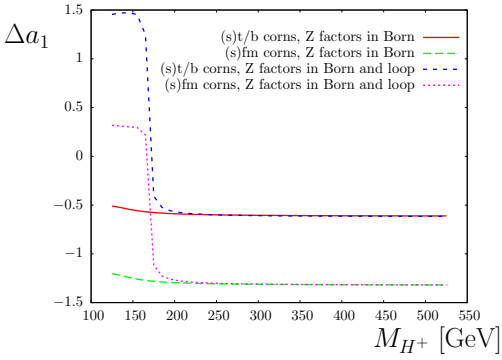

(b) Correction to a_1 for the coupling h_1ZZ.

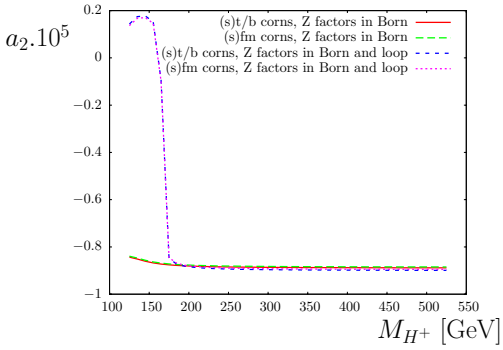

(c) Formfactor a_2 for the coupling h_1WW.

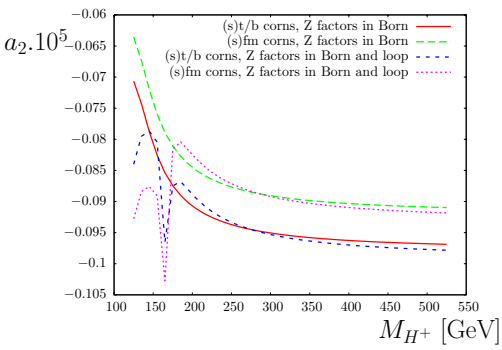

(d) Formfactor a_2 for the coupling h_1ZZ.

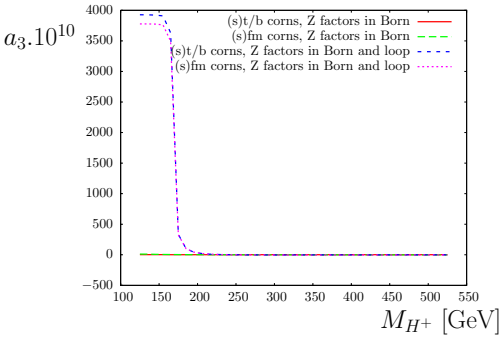

(e) Formfactor a_3 for the coupling h_1WW.

Figure 6.9: Effect on the formfactors of incorporating wavefunction normalisation factors at both loop level and tree level for the CPX scenario, with $\tan\beta = 10$.

significant, however, in the formfactor a_3, for the h_1WW coupling, which is greatly enhanced[2].

In the MSSM with real parameters, the effect of including the Z factors at loop level is not as dramatic, as the mixing between the neutral Higgs bosons is not as extreme as in the CPX scenario, since no mixing occurs between the CP even Higgs bosons h and H and the CP odd Higgs boson A. As an example, Figure 6.10 shows the formfactors for the coupling hWW with the extra corrections included. (This should be compared to Figures 6.2 – 6.4, which show the same formfactors without the additional propagator corrections.) For a_1 the inclusion of Z factors at loop level has the largest effect for the small α_{eff} scenario, but even here the alteration is less than $\sim 2\%$. The effect is more significant for the anomalous formfactors a_2 and a_3: a_2 is "shifted" by $\sim 10\%$, and a_3 changes by an order of magnitude.

6.4 WBF Higgs production cross sections and distributions

6.4.1 Comparison with the literature

In the literature, an examination of the "pure SUSY" loop contributions to the total cross section of h production with two forward jets in the MSSM with real parameters has been carried out in Ref. [56]. In order to compare with these results, we have produced a special version of our code to study these SUSY corrections, which we can tune to fit the procedure followed by [56].

In the fermion / sfermion sector, it is simple to separate the Standard Model corrections from their supersymmetric counterparts at the one loop level, as R-parity ensures that there is no mixing between fermions and sfermions within the loops. Moving beyond the (s)fermion contributions, however, this distinction is not so clear-cut owing to the increased complexity of the Higgs sector in the MSSM. The authors of Ref. [56] define the SUSY corrections as follows for production of the light CP even Higgs boson h:

$$\sigma_{SUSY} = \sigma_{MSSM} - \sin^2(\beta - \alpha)\, \sigma_{SM} \tag{6.3}$$

[2]It should be noted, however, that the value of a_3 is still very small, even after the enhancement of ~ 4 orders of magnitude.

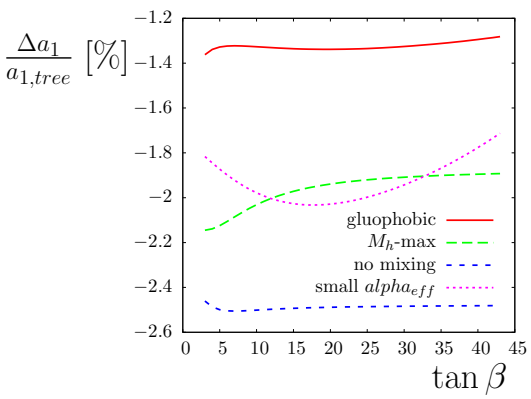

(a) Correction to the formfactor a_1 as a percentage of the leading order value.

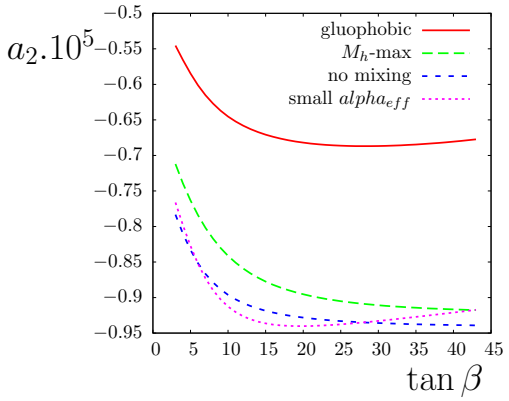

(b) Formfactor a_2.

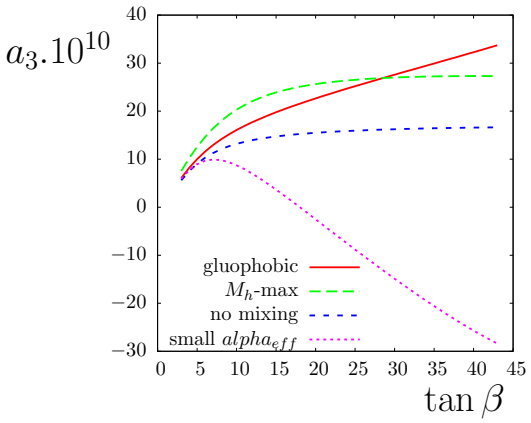

(c) Formfactor a_3.

Figure 6.10: Corrections to the formfactors for the case where the wavefunction normalisation factors are incorporated both at tree level and at loop level for the coupling hWW in the real MSSM. The loop corrections contain contributions from all (s)fermions.

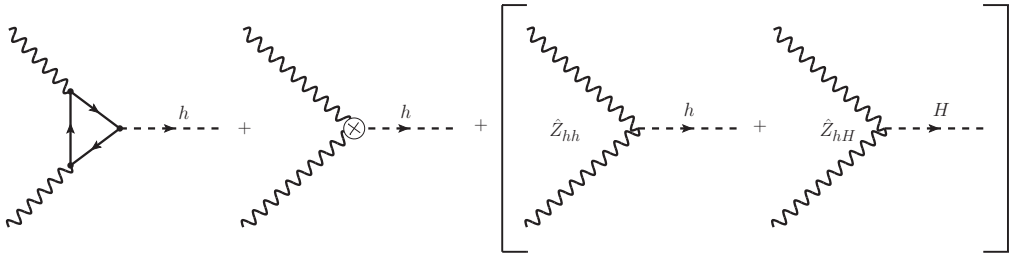

Figure 6.11: SUSY corrections to weak boson fusion.

The factor $\sin^2(\beta - \alpha)$ is the ratio of the squared lowest order coupling of the light CP even Higgs to two weak bosons over the corresponding coupling of a Standard Model Higgs. This definition of the SUSY corrections ensures that σ_{SUSY} contains only IR-finite virtual contributions. The bremsstrahlung contributions and the IR-divergent pieces of the virtual corrections are proportional to the squared lowest order matrix element, which in turn depends on the coupling of the Higgs to two weak bosons. Thus, the inclusion of the factor $\sin^2(\beta - \alpha)$ leads to a cancellation of these IR divergent terms between the MSSM and the SM in Equation 6.3. Using this definition, the authors of Ref. [56] find a value that estimates the effect of the supersymmetric corrections to WBF without having to calculate the full set of diagrams in the MSSM (e.g. the real corrections – Fig. 3.1 – do not need to be calculated).

It is obvious that the simple proportionality with $\sin^2(\beta - \alpha)$ between the SM cross section and the MSSM cross section is modified once loop corrections to the Higgs–weak boson vertex are taken into account. The procedure adopted in Ref. [56] for extracting the pure SUSY loop corrections can therefore be considered only as an approximation of the full result. For the SPS scenarios considered in Ref. [56] this is unlikely to have a large effect as they are all in the decoupling limit of large M_A, where the couplings of the light Higgs become Standard Model like and $\sin^2(\beta - \alpha) \approx 1$, but the approximation may be less well motivated when more extreme scenarios are studied.

For the purposes of studying the pure SUSY contributions (and comparing with Ref. [56]), we do not incorporate the Z factors into the lowest order contribution, as is done elsewhere in this thesis, but instead we consider the Z factors as an additional NLO correction. In other words, the correction to the cross section is taken to be the sum of the loop diagrams, the counterterm and the propagator correction (Z factors), as shown in Fig. 6.11. The Z factors $\hat{Z}_{hh}$ and $\hat{Z}_{hH}$ are defined in Section 3.4 and are taken at two loop level from `FeynHiggs`.

The parameters used in Ref. [56] differ from our standard set of parameters. The PDF set MRST2002nlo [132] is used, with the following cuts [133]:

$$\begin{aligned} y_j &< 4.5 \\ p_{T_j} &> 20 \text{ GeV} \\ y_{j_1} \cdot y_{j_2} &< 0 \\ \Delta y_{jj} = |y_{j_1} - y_{j_2}| &> 4.5 \\ M_{jj} &> 600 \text{ GeV} \end{aligned} \tag{6.4}$$

Additionally, no jet algorithms have been used in Ref. [56] – it is assumed that the final partons are jets. We have written a variation of our modified `VBFNLO` that performs the cuts specified in Equation 6.4 on the final state partons, rather than using the k_T algorithm and then imposing the cuts, as is our standard practice.

For comparison with Ref. [56] the electromagnetic coupling constant used is $\alpha(0) = (137.0359895)^{-1}$, and the appropriate charge renormalisation is employed (see Section 3.3.2). The third generation quark masses are taken to be $m_t = 170.9$ GeV and $m_b = 4.7$ GeV – all other quark and lepton masses are set to zero. Reference [56] takes the high energy definitions of the SPS points and then evolves them down using `SOFTSUSY` [134] to arrive at low energy parameters. These low energy parameters [133] are used throughout this comparison. The Higgs masses and mixings are, as usual, calculated by `FeynHiggs`[3].

There are several differences between our approach to evaluating WBF and that followed by Ref. [56]. We use the tree level Higgs mixing angle α in all couplings, as this allows for the compensation of the UV divergences in the renormalised self energies, whereas Ref. [56] uses corrected couplings obtained from `FeynHiggs`. The masses of the internal Higgs bosons (present in the loop correction diagrams) are, in this work, at tree level, but Ref. [56] always uses the higher order corrected value of the Higgs mass. An especially important difference is the way in which the Higgs propagator corrections are implemented: we take the Z factors from `FeynHiggs` at two loop level, while Ref. [56] calculates them independently, as described below. Using both the corrected couplings *and* the Z factors (in the diagrams in square brackets in Fig. 6.11) leads to double counting (see Section 3.4).

[3]Note, however, that different versions of `FeynHiggs` have been used in this work and in Ref. [56], which will lead to slight deviations.

Additionally, Ref. [56] includes top / bottom loops in both the MSSM and SM cross sections of Equation 6.3, but we do not include these contributions in our calculation of the "pure SUSY" corrections. For the SPS parameters, this is unlikely to cause large deviations as the Higgs–top and Higgs–bottom couplings are Standard Model like in the decoupling limit, and so the top / bottom contributions in σ_{MSSM} will, to a large extent, be cancelled by the top / bottom contributions in $\sin^2(\beta-\alpha)\sigma_{SM}$. Difficulties may arise, however, if we move into more extreme scenarios. Finally, our calculations focus on purely weak boson fusion, whereas the authors of [56] also include Higgsstrahlung contributions and t-channel photons (as opposed to purely W or Z boson fusion). This is unlikely to cause large discrepancies, however, as the WBF cuts should substantially reduce the extra contributions.

Our code has been tuned as far as possible to resemble the procedure followed in Ref. [56]. In Ref. [56] `FeynHiggs` has been used to determine the value of all the couplings, employing the function `FHCouplings`. These higher order, corrected values are used for every coupling. For the purposes of comparing with Ref. [56], our tuned `VBFNLO` was further altered to include the U_{Higgs} matrix (see Section 3.4) in the couplings at both Born and loop level, except when evaluating the propagator type corrections (the diagrams in square brackets), thus avoiding any double counting. For the tuned version of our code we also use the corrected Higgs masses everywhere, following the procedure of Ref. [56]. In our tuned code, we include third generation quark loops in both the Standard Model and the MSSM corrections of Equation 6.3 (as in [56]).

As stated, the propagator corrections to the external Higgs are calculated in a different manner in Ref. [56] to that which we normally use (see Section 3.4). To examine the differences between the two approaches, we first define

$$A = -\mathrm{Re}\Sigma'_{hh}(M_h^2) \tag{6.5}$$

$$B = \frac{2}{M_H^2 - M_h^2}\left(\mathrm{Re}\Sigma_{hH}(M_h^2) - \delta m_{hH}\right) \tag{6.6}$$

The Higgs field renormalisation constants δZ_{hh} and δZ_{hH} are taken in Ref. [56] to be the divergent parts of A and B respectively. Consequently, these renormalisation constants agree with those defined earlier, in Chapter 3.

The propagator Z factors (which we usually take from `FeynHiggs` and are defined according to Equation 3.67) in Ref. [56] involve the finite parts of the terms A and B, as follows (recall that a hat, $\hat{\Sigma}$, signifies the renormalised self energy, defined in Equations

3.55 – 3.58, and a prime, Σ' indicates the derivative of a self energy with respect to the external momentum squared):

$$Z_h = \left(1 + \frac{1}{2}A^{fin}\right)^2 = \left(1 - \frac{1}{2}\hat{\Sigma}'_{hh}(M_h^2)\right)^2 \tag{6.7}$$

$$Z_{hH} = B^{fin} = \frac{2}{M_H^2 - M_h^2}\hat{\Sigma}_{hH}(M_h^2) \tag{6.8}$$

The propagator corrections (i.e. the diagrams in the square bracket of Fig. 6.11) are then described in Ref. [56] by:

$$\Gamma_{prop} = \Gamma_{born}\left(\sqrt{Z_h} - 1 + \frac{1}{2}\frac{\cos(\beta-\alpha)}{\sin(\beta-\alpha)}\sqrt{Z_h}Z_{hH}\right) \tag{6.9}$$

$$= \Gamma_h\left(\sqrt{Z_h} - 1\right) + \frac{1}{2}\sqrt{Z_h}Z_{hH}\Gamma_H \tag{6.10}$$

$$= \frac{1}{2}\Gamma_h A^{fin} + \frac{1}{2}\Gamma_H\left(1 + \frac{1}{2}A^{fin}\right)B^{fin} \tag{6.11}$$

$$= -\frac{1}{2}\Gamma_h \mathrm{Re}\hat{\Sigma}'_{hh}(M_h^2) - \frac{\Gamma_H}{M_h^2 - M_H^2}\mathrm{Re}\hat{\Sigma}_{hH}(M_h^2) - \frac{1}{2}\frac{\Gamma_H}{M_H^2 - M_h^2}\mathrm{Re}\hat{\Sigma}_{hH}(M_h^2)\mathrm{Re}\hat{\Sigma}'_{hh}(M_h^2) \tag{6.12}$$

These propagator corrections have been implemented into the tuned version of our code. Since the Z factors are finite by construction, we cannot simply check our code by ensuring that the final result is finite. We have therefore explicitly checked that the divergent parts of the new Z factors agree with the divergent parts of the Higgs field renormalisation[4].

If we look at the strictly one loop part of Equation 6.12 only the first two terms survive:

$$\Gamma_{prop} = -\frac{1}{2}\Gamma_h \mathrm{Re}\hat{\Sigma}'_{hh}(m_h^2) - \frac{\Gamma_H}{m_h^2 - m_H^2}\mathrm{Re}\hat{\Sigma}_{hH}(m_h^2) \tag{6.13}$$

This is equal to a strict, one-loop expansion of our standard propagator corrections, which can be arrived at using Equation 3.67 together with Equation 3.65.

A summary of the differences between our default code for this comparison, which produces our best results, with our tuned code (which we use in order to reproduce the

[4]For this check, in order to ensure UV-finiteness, tree level Higgs masses and mixing angle need to be used for the particles appearing in the loops.

Table 6.2: Summary of the procedures used in our tuned code (used for the comparison with Ref. [56]) with those used in our default code, which gives our best results.

	Default code	**Tuned code**
Couplings	Couplings are defined at tree level – i.e. the Higgs mixing angle α_{tree} is used.	Couplings incorporate higher order corrections using the U_{Higgs} matrix. Couplings in the propagator corrections are taken to be at tree level.
Higgs masses in loops	Tree level masses	Corrected masses
t/b in loops	Not included	Included
Higgs propagator corrections	2 loop Z factors from `FeynHiggs`	Calculated from Equation 6.12

results of [56]) is given in Table 6.2. Note that, even in our tuned code, we use tree level couplings in the propagator correction pieces (the diagrams in square brackets, Fig. 6.11), as to do otherwise leads to double counting. We have, however, explicitly verified that, in the SPS points considered here, the effect of this is negligible. It is also important to note that in the "Default code" column, the settings are not quite the same as those used in the rest of this thesis. In particular, elsewhere we incorporate the Z factors into the Born level cross section.

Table 6.3 compares the percentage SUSY loop corrections to WBF using our default code with the tuned version of our code and the values reported in Ref. [56]. As can be seen, good agreement is found between the tuned code and the results in the literature. The remaining differences are likely due to a combination of small factors (such as the extra diagrams in [56], and slightly different values for Higgs sector parameters) and numerical uncertainties in the integration procedures. The differences between our tuned code and our best results are partially the result of the higher order contributions to the Z factors that are included in our best results, as well as the use of different values of the Higgs mass for internal particles in the loops[5].

[5]Using corrected Higgs masses in the loops will in general spoil the UV finiteness of the renormalised self energies.

Table 6.3: Comparison of percentage loop corrections for the pure SUSY contributions calculated here with those presented in Ref. [56]. The first results column give our best results, using `FeynHiggs` Z factors to incorporate Higgs propagator corrections (as described by Column 2, Table 6.2). The second column gives the result we obtain using our tuned code (described in Column 3, Table 6.2). The final column reproduces the results presented in Ref. [56].

SPS	This work	Tuned result	**Ref. [56]**
1a	-0.184	-0.362	**-0.329**
1b	-0.057	-0.202	**-0.162**
2	-0.026	-0.220	**-0.147**
3	-0.004	-0.211	**-0.146**
4	-0.074	-0.271	**-0.258**
5	-0.526	-0.612	**-0.606**
6	-0.087	-0.277	**-0.226**
7	-0.058	-0.244	**-0.206**
8	-0.010	-0.214	**-0.157**
9	-0.051	-0.189	**-0.094**

Table 6.4 presents our result for the leading order cross sections calculated for all the SPS parameter points, along with a comparison of the mass of the lightest CP even Higgs boson used in our result and in Ref. [56]. Note that Ref. [56] reports a leading order cross section of 706 fb for SPS1a. We have checked our leading order result with the results produced by `MadGraph` [135] at SPS1a and found agreement to within the numerical accuracies of the code. We also checked that the LO cross section in the Standard Model for an equivalent Higgs mass was very close to our MSSM LO cross section (as it should be, since it is in the decoupling regime). This SM result was found to be in agreement with the value produced in the Standard Model using `MadGraph`, as well as the results presented in [55]. The difference we observe in the leading order cross section is unlikely to affect the percentage loop corrections by a large amount. The (typically small) differences between the Higgs masses are probably due to the different versions of `FeynHiggs` being used to calculate M_h.

Table 6.4: Leading order cross sections and Higgs masses at the SPS points.

SPS	LO σ [fb]	M_h [GeV]	M_h [GeV] Ref [56, 133]
1a	1247.56	110.789	111.000
1b	1224.86	114.112	114.196
2	1238.31	112.149	112.173
3	1231.52	113.135	113.260
4	1238.11	112.178	112.192
5	1265.90	107.970	108.397
6	1243.90	111.382	111.487
7	1259.16	109.144	109.237
8	1248.76	110.641	110.719
9	1211.73	116.054	116.114

6.4.2 New results

We now move on to results obtained using our full code, which includes both Standard Model and SUSY particles. Fig. 6.12 shows the total cross section of the production of a light Higgs boson, h, via WBF in the M_h^{max} scenario as a function of both the CP odd Higgs mass (left plot) and the light CP even Higgs mass (right plot). Here we include the propagator type corrections at leading order, meaning that the loop effects we observe are the genuine vertex corrections. For comparison, the Standard Model cross section with a Higgs mass equal to that in the M_h^{max} scenario is also shown. This plot clearly demonstrates the decoupling behaviour of the MSSM scenario. At low values of the CP odd Higgs mass, the cross section in the MSSM is very different from that in the Standard Model: it is much smaller, owing to mixing between the three neutral Higgs bosons. As M_A increases, the Standard Model and MSSM cross sections become close – at $M_A = 400$ GeV, the difference between them is less than a percent of the total cross section. Also shown in Fig. 6.12 are the loop correction precentages for the QCD corrections, the QCD plus (s)top / (s)bottom corrections and the QCD plus (s)fermion corrections. The (s)top / (s)bottom corrections and full (s)fermion loop corrections are $\sim -2\%$ and $\sim -1.5\%$ respectively in the decoupling regime, but these rise to almost $\sim -9\%$ at very low values of M_A. These loop corrections differ from the Standard Model loop corrections by $\sim -0.2\%$ in the decoupling regime, and $\sim -4.5\%$ in the non-decoupling regime. The behaviour of the total cross section obtained using Monte Carlo

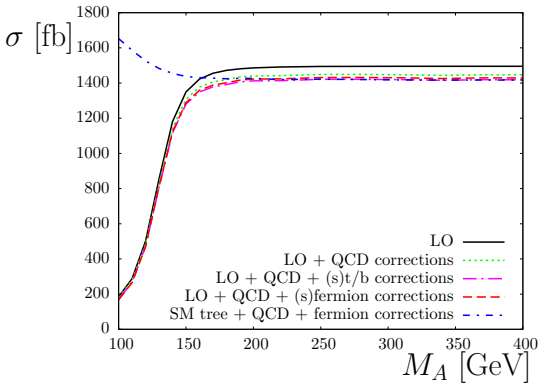

(a) Total cross section of light Higgs production as a function of M_A.

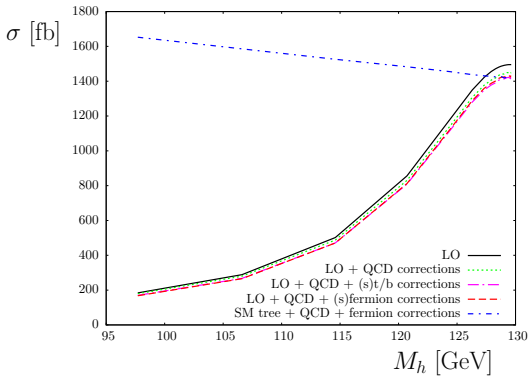

(b) Total cross section of light Higgs production as a function of M_h.

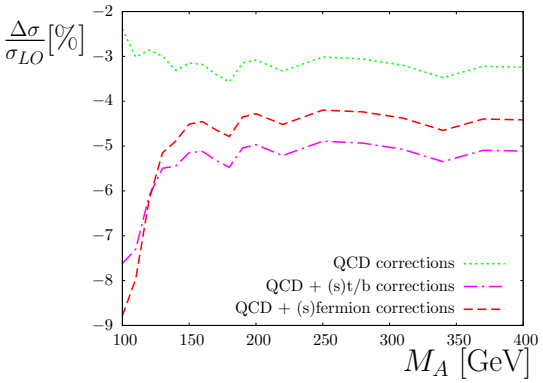

(c) Percentage loop corrections for light Higgs production as a function of M_A.

Figure 6.12: Cross sections of light Higgs production via weak boson fusion in the M_h^{max} scenario with $\tan\beta = 10$, and in the Standard Model, at leading order and with QCD, third generation (s)quark and all (s)fermion corrections.

techniques is very similar to that of the partonic cross sections presented earlier (see Fig. 6.1), demonstrating that the cuts (which are applied to these total cross sections, but not to the partonic cross sections) have little effect on these loop corrections.

In addition, Figure 6.13 shows the azimuthal angle distribution in the decoupling regime (with large M_A – Plots (a) and (b)), where the distribution is similar to that in the Standard Model (as is, of course, expected), and in the non-decoupling regime (with low M_A) where large deviations from the SM occur (Plots (c) and (d)). In the non-decoupling regime, the distribution can be seen to be much smaller (although the shape is not significantly altered here) due to a suppression of the coupling between the Higgs and the pair of weak bosons. Note that Plots (c) and (d) of Fig. 6.13 present the same MSSM data – the axis scale has been altered in Plot(d) to provide an enlarged version of the MSSM results.

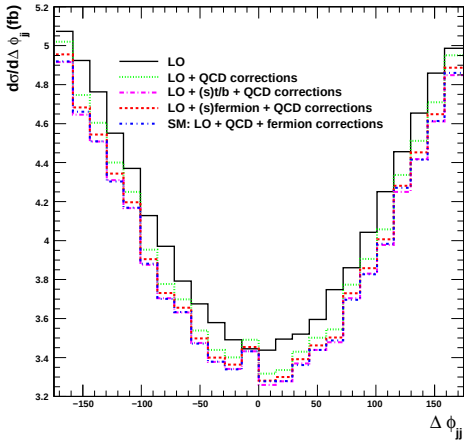

(a) Azimuthal angle distribution with $M_A = 250$ GeV, compared with the distribution in the Standard Model for a Higgs of equal mass.

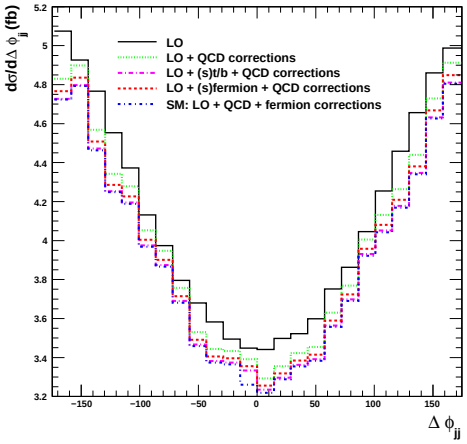

(b) Azimuthal angle distribution with $M_A = 400$ GeV, compared with the distribution in the Standard Model for a Higgs of equal mass.

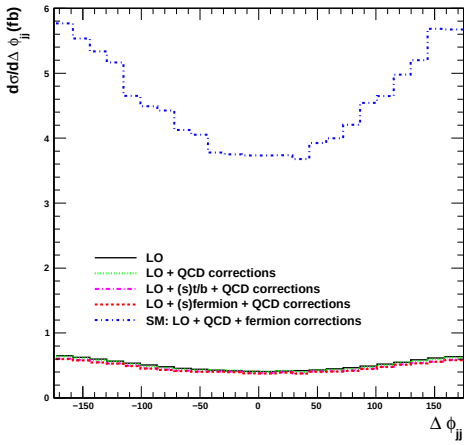

(c) Azimuthal angle distribution with $M_A = 100$ GeV, compared with the distribution in the Standard Model for a Higgs of equal mass.

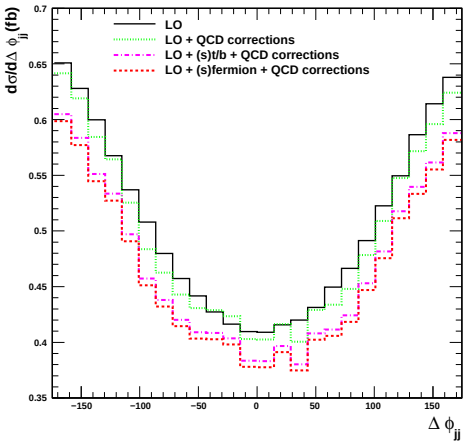

(d) Azimuthal angle distribution with $M_A = 100$ GeV.

Figure 6.13: Azimuthal angle distributions in the M_h^{max} scenario with $\tan\beta = 10$, at leading order and with QCD, third generation (s)quark and all (s)fermion corrections in the decoupling regime (Plots (a) and (b)) and in the non-decoupling regime (Plots (c) and (d)). For comparison, the Standard Model distributions (with equivalent Higgs mass) are also shown in blue (except in Plot (d), which reproduces only the MSSM results of Plot(c)).

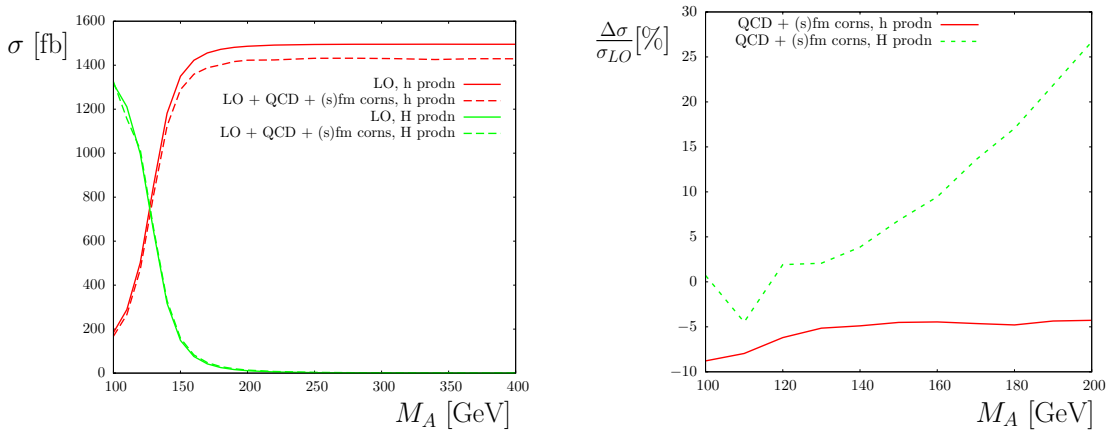

(a) Total cross section for h and H production.

(b) Percentage corrections for h and H production.

Figure 6.14: A comparison of light and heavy CP even Higgs boson production in the M_h^{max} scenario with $\tan\beta = 10$, with QCD plus (s)fermion loop corrections.

Figure 6.14 shows a comparison of the production cross sections in the M_h^{max} scenario of a light and a heavy CP even Higgs, as a function of the mass of the CP odd Higgs, with $\tan\beta = 10$. As can be seen, at low values of M_A, in the non-decoupling regime, production of the heavy Higgs is the dominant process. This cross section rapidly decreases with increasing M_A, and becomes close to zero in the decoupling regime as the light Higgs h becomes SM like. Due to this near-zero leading order cross section, the percentage corrections to heavy Higgs production become very large in the decoupling regime, although the total cross section is still, of course, small[6]. For the heavy Higgs the loop corrections act to increase the cross section and there is a cancellation between the electroweak loop corrections and the QCD corrections (leading to a very small combined correction at $M_A = 100$ GeV). The feature at $M_A = 110$ GeV for the heavy Higgs stems from the behaviour of the propagator corrections at this point in parameter space.

The azimuthal angle distributions for production of the heavy Higgs boson are shown in Fig. 6.15, for two values of M_A. As expected from studying the total cross section graphs (Fig. 6.14), the distribution is far more Standard Model like for low M_A in the non-decoupling regime. In the decoupling regime the scale of the distribution is reduced and the loop effects are seen to be large, although they do not alter the distribution's shape.

[6]Note that the left plot of Fig. 6.14 only presents percentage loop corrections for the range $M_A = 100 \rightarrow 200$ GeV, where the production cross section of the heavy Higgs is non-negligible.

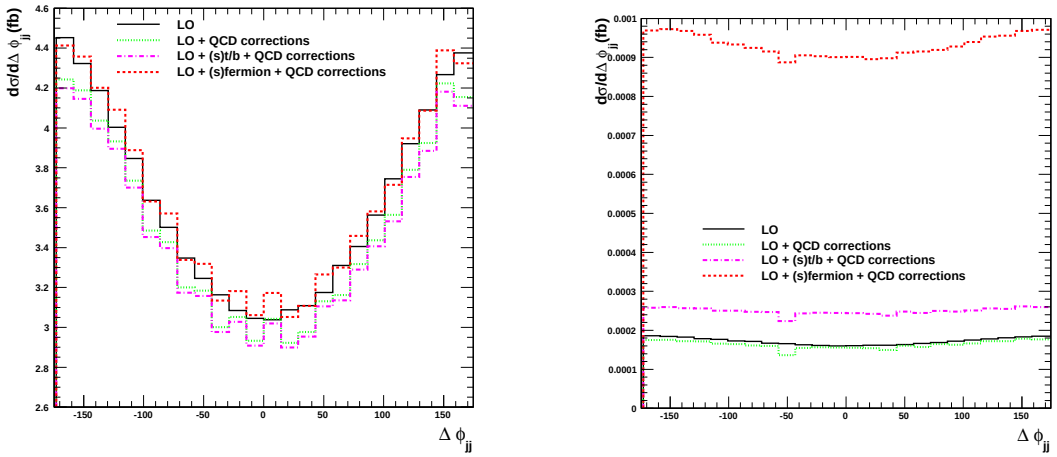

(a) Azimuthal angle distribution with $M_A = 100$ GeV.

(b) Azimuthal angle distribution with $M_A = 400$ GeV.

Figure 6.15: Azimuthal angle distribution for production of the heavy CP even Higgs boson in the M_h^{max} scenario with $\tan\beta = 10$ for QCD, (s)top / (s)bottom and (s)fermion loop corrections.

Moving on to the MSSM with complex parameters, the situation in the CPX scenario is different to that seen above in the M_h^{max} scenario, as is expected since CPX was designed to describe an "extreme" region of MSSM parameter space in which the effects of complex phases are maximised. Figure 6.16 shows the light Higgs (h_1) production cross section as a function of the charged Higgs mass[7] M_{H^+} for $\tan\beta = 10$. In this scenario, the behaviour at low values of $M_{H^\pm}$ is more extreme than in the real MSSM – mixing can now occur between all three neutral Higgs bosons (in the real MSSM, only the CP even states h and H mix), and at low $M_{H^\pm}$ the values of the Z factors mean that principle component of the lightest Higgs is the CP odd state, which does not couple to weak bosons. Consequently, the leading order cross section for values of $M_{H^\pm} < 170$ GeV is practically zero, leading to extremely large percentage loop corrections.

The azimuthal angle distribution found for production of the lightest Higgs h_1 in the CPX scenario is presented in Figure 6.17. The distributions in the CPX scenario deviate from those expected in the Standard Model in the non-decoupling regime, just as the total cross sections are different. The shape of the azimuthal angle distribution, however, is not significantly affected. While at this low value of $M_{H^\pm}$ the lightest Higgs

[7] Recall that, when working in the complex MSSM, we use $M_{H^\pm}$ as an input parameter, as M_A is not a mass eigenstate at higher orders. We also refer to the neutral Higgs bosons as h_1, h_2 and h_3 (in order of lightest to heaviest mass), rather than h, H and A, because the physical Higgs bosons are not CP eigenstates in the complex MSSM.

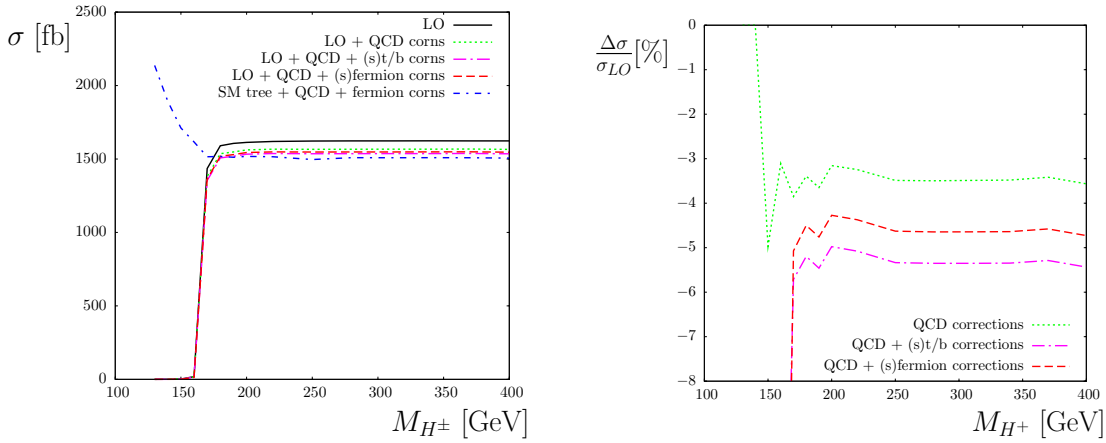

(a) Total cross section for h production in the CPX scenario.

(b) Percentage higher order corrections for h production in the CPX scenario.

Figure 6.16: Production of the lightest Higgs boson h_1 in the CPX scenario with $\tan\beta = 10$ with QCD, (s)top / (s)bottom and (s)fermion loop corrections.

is primarily composed of the CP odd A Higgs boson (and one might therefore naively expect a shift towards the purely a_3 behaviour of the azimuthal angle distribution, as shown in Fig. 2.6), because the lowest order coupling AVV is zero, the mixing manifests itself principally as a decrease in the leading order cross section, rather than a change in the shape of the azimuthal angle distribution.

Figure 6.18 shows the production of the Higgs boson h_2 in the CPX scenario, and compares it to production of the lightest Higgs h_1. Between charged Higgs masses of ~ 130 GeV and ~ 170 GeV, production of h_2 has a larger cross section than production of the lighter Higgs boson h_1, rising to its maximum value at $M_{H^\pm} \approx 160$ GeV, where the loop corrections (from QCD plus (s)fermion loops) are $\sim -5\%$. As the charged Higgs mass increases, the loop corrections become positive, causing an enhancement of the cross section.

As with the formfactors, we now consider applying Higgs propagator corrections (Z factors) to the loop diagrams, as well as to the tree level (as shown in Fig. 6.8). These additional, higher order corrections have been implemented into the modified `VBFNLO`. Figure 6.19 compares two cases (where propagator corrections are included at loop and Born level, and only at Born level) for the M_h^{max} scenario, and includes the cross section as a function of M_A as well as azimuthal angle distributions. In this scenario, the additional corrections are seen to make very little difference, even for low values of M_A.

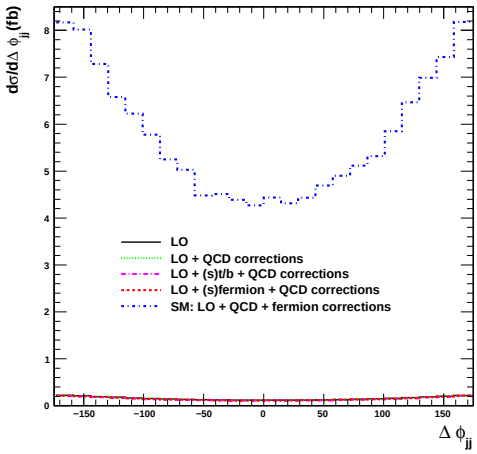

(a) Azimuthal angle distribution with $M_{H^\pm} = 160$ GeV: a comparison of the CPX distribution with the corresponding Standard Model distribution.

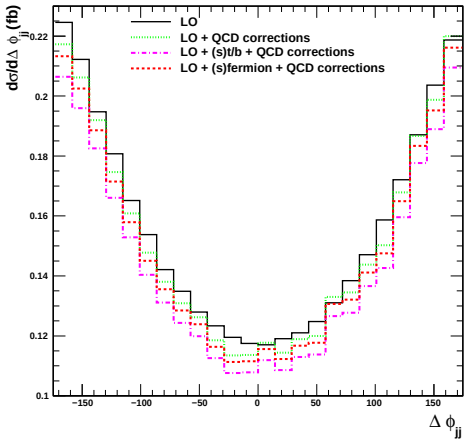

(b) Azimuthal angle distribution with $M_{H^\pm} = 160$ GeV in the CPX scenario.

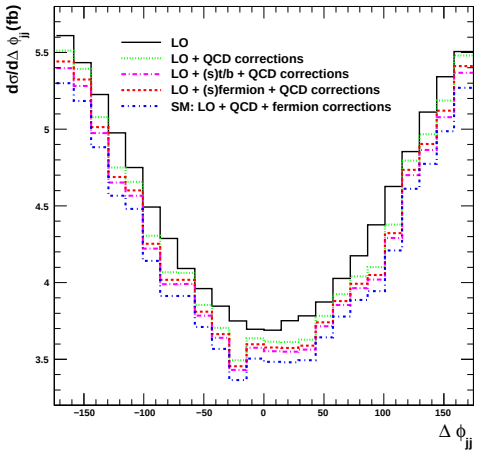

(c) Azimuthal angle distribution with $M_{H^\pm} = 400$ GeV: a comparison of the CPX distribution with the corresponding Standard Model distribution.

Figure 6.17: Azimuthal angle distributions for light Higgs production in the CPX scenario at the LHC, with $\tan\beta = 10$.

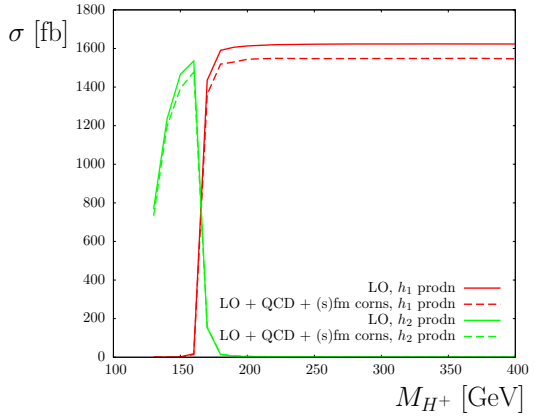

(a) Total cross section for h_1 and h_2 production with QCD plus (s)fermion loop corrections.

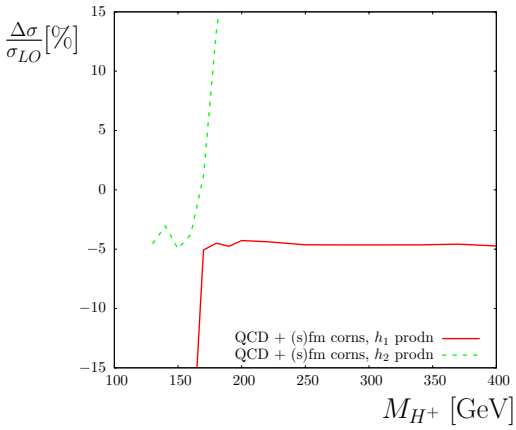

(b) Percentage loop corrections for h_1 and h_2 production for QCD plus (s)fermion loop corrections.

Figure 6.18: Production of the Higgs boson h_2 in the CPX scenario with $\tan\beta = 10$, and a comparison with light Higgs production.

Figure 6.20 examines the effect of incorporating the Z factors at loop level (as well as at Born level) in the MSSM with complex parameters, in the CPX scenario. Here, the effects of the additional corrections are far more noticeable. At low values of the charged Higgs mass, the total cross section is increased by these additional contributions (relative to the corrected cross section when propagator corrections are only applied at Born level). The azimuthal angle distribution undergoes some change as well – for small $M_{H^\pm}$, the shape of the distribution changes owing to the importance of the loop connecting to a CP odd Higgs boson. Despite these enhancements, however, the cross sections remain small. It must also be kept in mind that in the region of parameter space described by the CPX scenario, the theoretical uncertainties remain relatively large, even with the inclusion of higher order corrections.

6.4.3 Full result: supplementing the MSSM cross section with Standard Model corrections

We now combine all of our previous results to arrive at our best predictions for MSSM Higgs production via weak boson fusion at the LHC. Moving beyond the (s)fermion corrections, the full MSSM contributions to the VVh vertex and the VV self energy have been calculated. These are supplemented by the MSSM sfermion corrections to the qqV vertex, and the complete Standard Model contributions to the qqV vertex as well as the SM boxes and pentagons, and the real photon radiation. The SM contributions

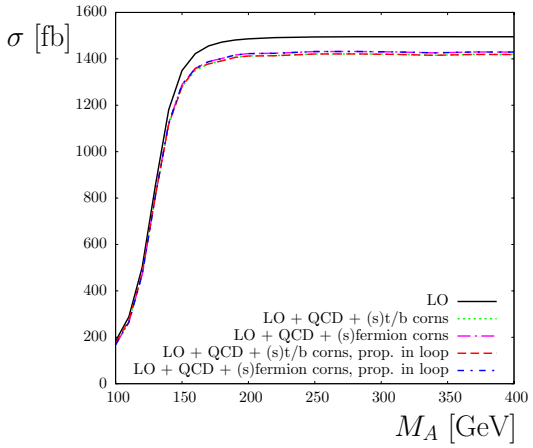

(a) Total cross section for QCD plus (s)top / (s)bottom or (s)fermion loop corrections, with and without Z factors applied at loop level.

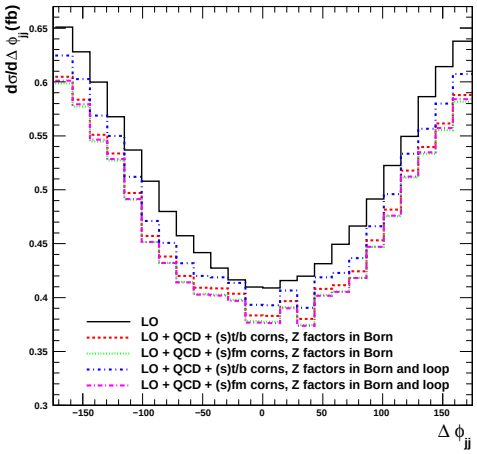

(b) Azimuthal angle distributions with $M_A = 100$ GeV including QCD plus (s)top / (s)bottom or (s)fermion loop corrections, with and without Z factors applied at loop level.

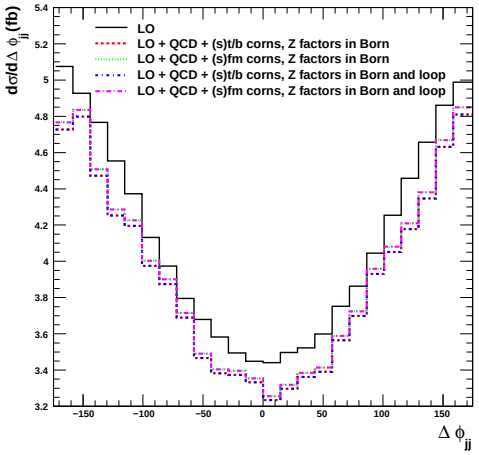

(c) Azimuthal angle distributions with $M_A = 400$ GeV including QCD plus (s)top / (s)bottom or (s)fermion loop corrections, with and without Z factors applied at loop level.

Figure 6.19: Total cross section and aximuthal angle distributions in the M_h^{max} scenario with $\tan\beta = 10$ for h production, demonstrating the effect of including Z factors at both loop level and tree level.

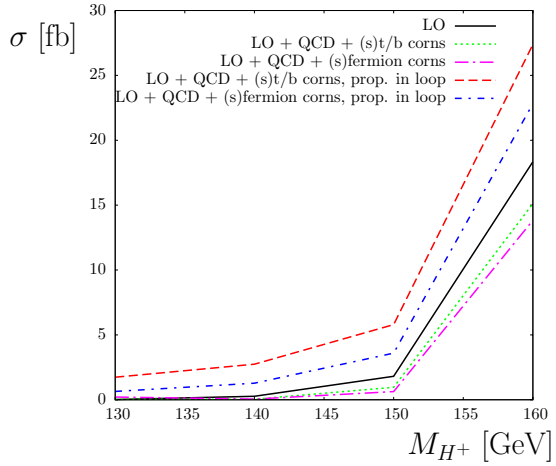

(a) Cross sections for LO plus QCD and (s)top / (s)bottom and (s)fermion loop corrections, with and without Z factors applied at loop level.

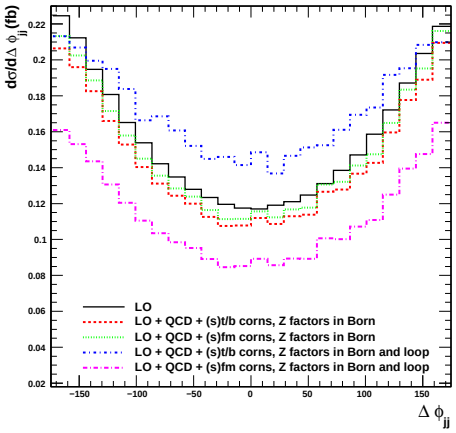

(b) Azimuthal angle distributions with $M_{H^\pm} = 160$ GeV including QCD plus (s)top / (s)bottom or (s)fermion loop corrections.

Figure 6.20: Results in the CPX scenario with $\tan\beta = 10$ for h_1 production, demonstrating the effect of including Z factors at loop level as well as at tree level.

are modified by a factor $\sin^2(\beta - \alpha)$ to account for the different value of the VVh coupling – see Section 3.5. Special care must be taken here to ensure that the sign of the SU(2) covariant derivative is consistent. It is important to note that in this section we parametrise the electromagnetic coupling using $\alpha(M_Z^2)$, rather than G_F, as has been our practice previously.

There is an approximation involved in this procedure as we are neglecting boxes and pentagons involving charginos and neutralinos. No diagrams involving Higgs or Goldstone bosons coupling to the external quarks are present, as we assume our external quarks to be massless. Consequently, using the multiplicative factor $\sin^2(\beta-\alpha)$ (for the SM boxes etc.) is not an approximation here, as the only couplings involved in these diagrams that change between the SM and the MSSM are modified by exactly this factor.

In Fig. 6.21 we present our full results[8]: the complete SM type one loop corrections (including real photon radiation and NLO QCD corrections), supplemented by the sfermion loop corrections and the remaining MSSM contributions for the Higgs vertex and the weak boson self energy. We compare the cross section when the complete VVh and VV corrections are included with the cross section that includes sfermion and SM type (i.e. all particles except charginos and neutralinos) contributions, as well as the

[8]Note that the cuts used to produce this graph are not our default cuts, but are rather those described in Section 5.4.1.

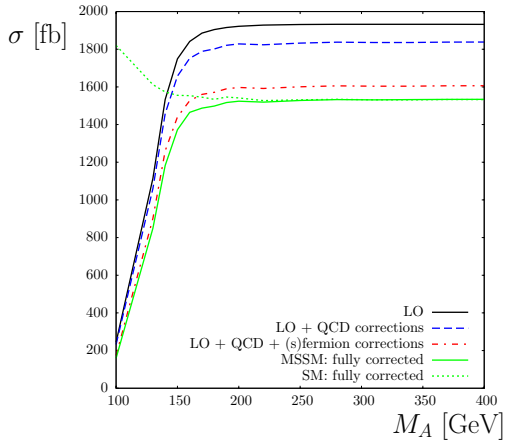

(a) Total cross section in the MSSM (including corrections), compared with total cross section in the SM with full corrections

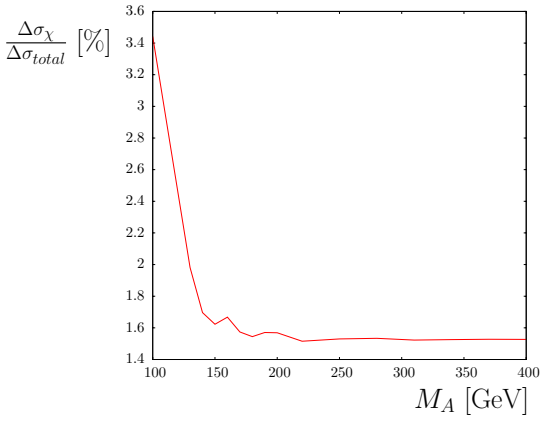

(b) Percentage of total loop correction contributed by charginos and neutralinos

Figure 6.21: Light Higgs boson h production as a function of M_A in the M_h^{max} scenario, with $\tan\beta = 10$, with MSSM corrections supplemented with SM type corrections.

Standard Model cross section, and the cross section with NLO QCD corrections. When including the loop effects from SUSY particles other than the sfermions, it is difficult to gauge the effect of these additional particles when compared to the Standard Model, because – as explained in Section 6.4.1 – beyond the (s)fermion sector there is no clear separation between SM and SUSY particles. We gauge the effect of the SUSY contributions by comparing the percentage loop corrections in the MSSM with those in the SM, for a Standard Model Higgs mass equal to the light MSSM Higgs mass[9]. In the decoupling regime, the difference between the SM loop corrections and the MSSM loop corrections is small ($\sim -0.3\%$), but in the non-decoupling regime this difference rises to $\sim -5\%$.

The right hand plot of Fig. 6.21 shows the contribution of the charginos and neutralinos as a percentage of the total loop correction $2\,\mathrm{Re}\,[\mathcal{M}_{LO}^{*}\mathcal{M}_{loop}]$. As can be seen, the effect of these SUSY particles is small – they contribute only $\sim 3.5\%$ of the total correction in the non-decoupling regime, and this decreases to $\sim 1.5\%$ in the decoupling regime. Since the charginos and neutralinos only have a small effect on the loop corrections at the Higgs vertex and weak boson self energy, it is reasonable to assume that they will have a similarly small effect on the boxes and pentagons. The calculation and implementation of the full result in the MSSM is in progress, but we believe the result presented here to be a good approximation of the complete result.

[9]We must of course be careful not to choose an MSSM parameter point with a vanishingly small LO cross section.

Chapter 7

Z production via weak boson fusion at the LHC

"Only show me where to stand ..."
— Archimedes

7.1 The practicality and desirability of a calibration process

Although Higgs production via weak boson fusion has many helpful properties that should allow us to identify and study it at the LHC, the success of our investigations will of course depend not only on our knowledge of the process itself, but also on our understanding of backgrounds and the detector's behaviour. It would therefore be helpful if we were able to study a well understood process that would allow us to verify that the methods we plan to use to isolate weak boson fusion Higgs production are effective.

A promising process is Z boson production via weak boson fusion, shown at tree level in Fig. 7.1. This seems an ideal process with which to "calibrate" Higgs production because, for one thing, the Feynman diagrams involved are analogous for Z and Higgs boson production, and for another if $M_H \sim M_Z$, as the precision data from LEP seems to indicate [32], the kinematics of the tagging jets will be similar. If we further study Z production with subsequent leptonic decay, there is a clean resonance in the dilepton

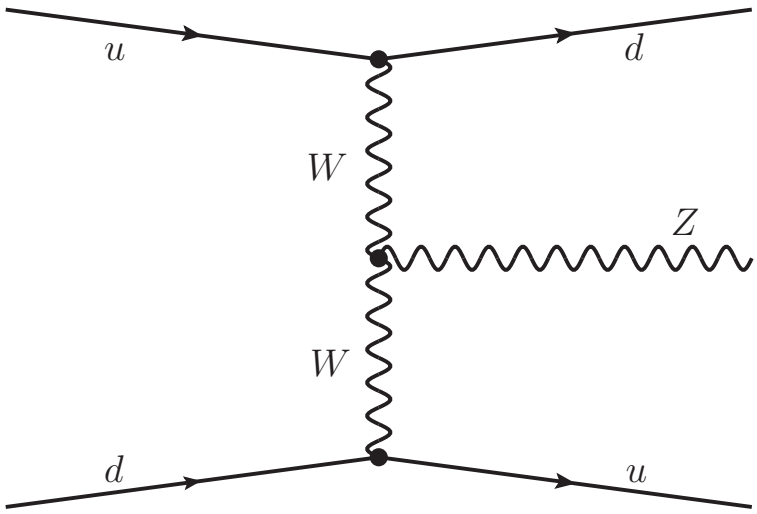

Figure 7.1: Leading order Z boson production via weak boson fusion.

spectrum to assist with identification as well. By comparing Z and Higgs production, we can confirm that the theoretical uncertainties are well under control.

In order to assess whether this method of Z boson production will be useful as a calibration process, however, we need to ascertain whether the weak boson fusion production of Z plus two jets can be separated from the various backgrounds to this final state. This question was studied in Ref. [136][1], which considered four major background processes, examples of which are shown in Fig. 7.2.

With no cuts, the weak boson fusion channel is lost in the backgrounds, having a smaller cross section by a factor ~ 2000. By imposing a set of four cuts, however, the signal to background ratio can be improved to approximately 1. These cuts (as for the Higgs process) include a rapidity cut (which improves the signal to background by ~ 10) and a cut on the invariant mass of the tagging jets. The invariant mass cut, for all backgrounds except the scattering of two valence quarks – Fig. 7.2(b) – improves the signal to background ratio further by a factor of ~ 100, as the momentum of the t-channel W boson from the external quarks is soft, so the tagging jets' kinematics are very similar to those of the initial quarks. There is also a cut ensuring that the Z boson is well separated from the final jets, as well as a cut on the transverse momentum of the Z boson (in WBF, the Z boson receives a large amount of transverse momentum, whereas the background processes involve the Z radiating from low mass partons). The specific details of the cuts used here are slightly different to the cuts used elsewhere in

[1]The program CompHEP [137,138] was used to generate cross sections at leading order, assuming the final state partons were jets.

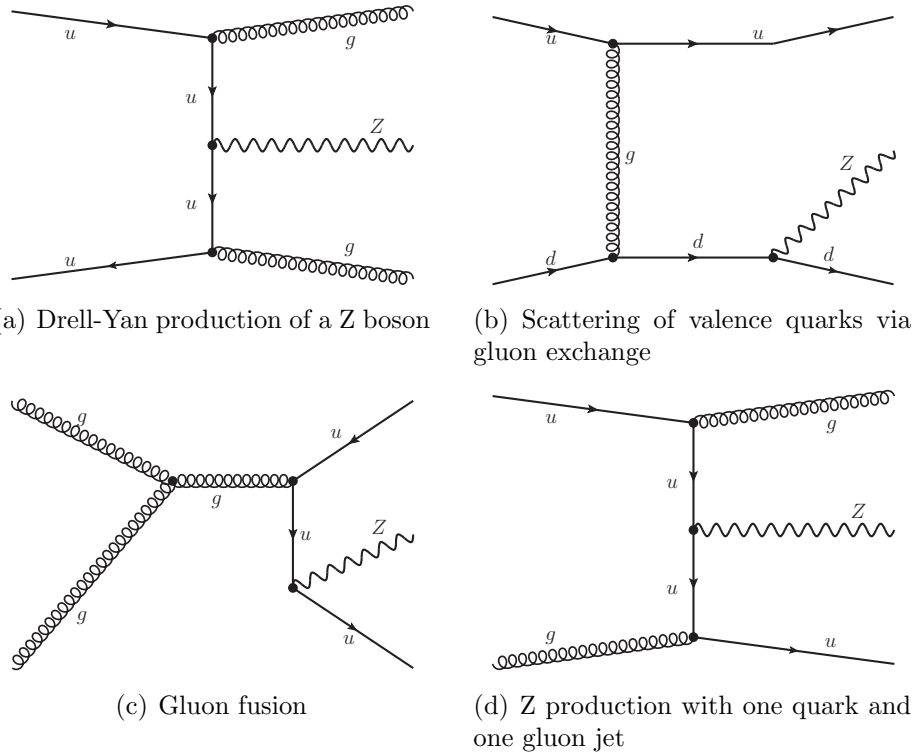

(a) Drell-Yan production of a Z boson

(b) Scattering of valence quarks via gluon exchange

(c) Gluon fusion

(d) Z production with one quark and one gluon jet

Figure 7.2: Major backgrounds to Z production via weak boson fusion.

Table 7.1: Leading order cross sections for Z + 2 jet production for WBF and background processes before and after cuts, from Ref. [136].

Process	Fig. 7.2(a)	Fig. 7.2(b)	Fig. 7.2(c)	Fig. 7.2(d)	**WBF**
Uncut σ [pb]	3000	20,000	340	1700	**13.4**
Cut σ [pb]	0.15	1.3	0.91	0.20	**2.4**

this thesis for Higgs production (see Equation 2.5). Here, there is no cut on R_{jj} (the separation of the jets in the azimuthal angle versus rapidity plane), and the cuts on the dijet mass and transverse momentum of the tagging jets are significantly more stringent. The cut on the rapidity gap, however, is less stringent here than in our standard cuts. The leading order cross sections calculated in Ref. [136] before and after cuts are shown in Table 7.1.

As can be seen from Table 7.1, the most persistent background is the strong scattering of initial valence quarks (Fig. 7.2(b)), since this leads to very forward emission of the final state partons, which of course to some extent mimics the weak boson fusion signal.

At leading order, the cuts described reduce the background to manageable levels, which means that this process has the potential to provide a good calibration against which to measure Higgs production.

The rapidity gap cuts described here and in Section 2.2 significantly improve the signal to background ratio (for both the Higgs and the Z boson). It is important to be certain, however, that we have properly accounted for the possibility that another pair of initial partons will interact in the same event. This interaction could cause more QCD radiation and fill the rapidity gap. Although the probability that the gap will survive can in theory be calculated, confirming these predictions with observations of Z boson production will help decrease uncertainty when Higgs production is being studied. The idea of measuring the rapidity gap survival probability using Z production via WBF was proposed in References [139, 140], and studied in detail in Ref [48].

In this Chapter we will study the (s)fermionic (and specifically third generation (s)quark) corrections to the partonic cross section for Z boson production via WBF in both the Standard Model and the MSSM, and compare these to the Higgs production case as a function of $\tan\beta$. We will also briefly discuss an anomalous WWZ coupling, and the alterations needed to include electroweak corrections to Z production in `VBFNLO`.

7.2 Partonic cross sections

As in the previous chapters, here we use masses from the Particle Data Book [87] with the exception of $m_t = 172.6$ GeV, and parametrise the electromagnetic coupling α by the Fermi constant. In the MSSM, we study the benchmark scenarios described in Ref. [121], varying $\tan\beta$ (varying M_A will have no effect on the cross sections studied here, as we only consider (s)fermionic corrections to WBF). Note that no cuts have been performed on the partonic cross sections.

7.2.1 Results in the Standard Model

We investigate the production of a Z boson through the WBF process

$$u + d \to d + Z + u \tag{7.1}$$

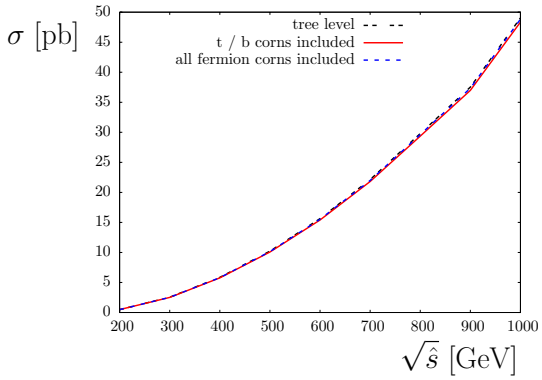

(a) Total cross section at tree and loop level.

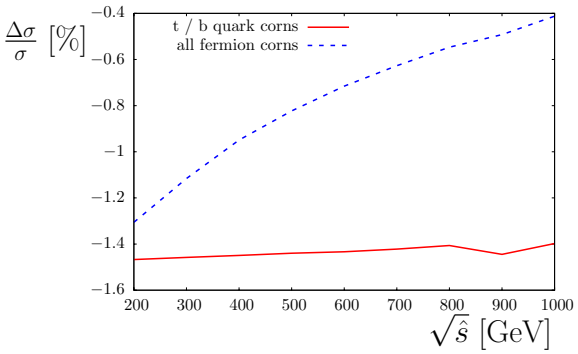

(b) Percentage loop corrections from the 3rd generation quark and all fermion contributions.

Figure 7.3: Cross section for Z production via WBF in the Standard Model.

Note that, in contrast to the Higgs production case, only W bosons mediate this process as (in the Standard Model and MSSM) there is no tree level triple Z boson vertex. The corrections are studied in detail for the cases where all fermions are included in the loops, and where only contributions from top and bottom quarks are considered. Fig. 7.3 shows the partonic cross section at a Higgs mass $M_H = 120$ GeV in these two cases, as well as the percentage loop corrections as a function of the centre of mass energy[2].

Fig. 7.3 shows that the cross section for Z boson production is larger than that for Higgs boson production in the WBF channel (compare Fig. 7.3 to Fig. 5.2) and increases with the centre of mass energy. The loop corrections when only the top and bottom quark loops are included have a larger effect than the corrections when all fermions are considered, and are nearly independent of the centre of mass energy. The size of the full fermion corrections, on other hand, decrease with increasing centre of mass energy.

Fig. 7.4 shows the individual contributions to the total loop correction from the WWZ vertex, the WW self energy and the qqW vertex, again as a function of $\sqrt{\hat{s}}$ with $M_H = 120$ GeV. Unlike the situation with Higgs production described in Chapter 5, the third generation quarks receive no enhancement from a large coupling value, and consequently all corrections increase in magnitude when light fermions are included. As with Higgs production, however, these corrections largely cancel one another out (due in part to the W boson field renormalisation constant, which naturally acts in opposite directions in the different contributions, so that overall it has no effect), and we are

[2]We use the centre of mass energy as the variable here because the partonic cross section for Z boson production via WBF is independent of the Higgs mass if only fermion loops are included in the corrections.

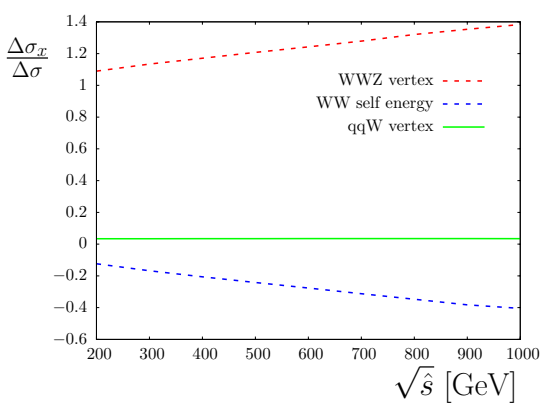

(a) Individual contributions to $\Delta\sigma$ from t/b contributions.

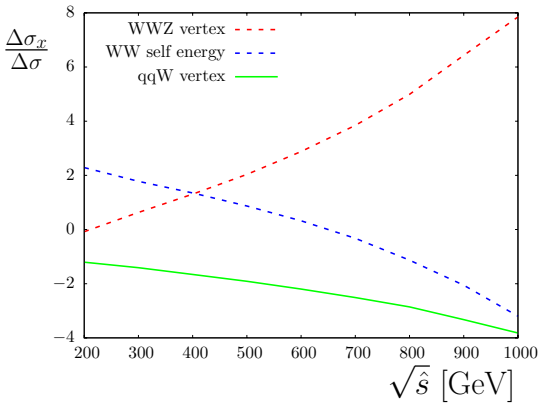

(b) Individual contributions to $\Delta\sigma$ from all fermion contributions.

Figure 7.4: Individual contributions for Z production via WBF in the Standard Model. $\Delta\sigma_x$ signifies either the corrections to the WWZ vertex (in red), the corrections to the WW self energy (in blue) or the quark–weak boson qqW vertex corrections (in green).

left with a smaller total loop correction when all fermions are taken into account than when only top and bottom quarks are considered. Corrections to the WWZ vertex are dominant at all energies when only top and bottom quark corrections are considered, but if we include all fermions in our loop diagrams at low energies this WWZ contribution is practically zero.

Fig. 7.5 compares the corrections to Higgs and Z boson production via weak boson fusion. As can be seen, the cross section for Z production is approximately 10 times larger than that for Higgs production, and has no dependence on the Higgs mass. The loop corrections to Higgs production are (for Higgs masses of less than $\sim$ 380 GeV) larger than those for the calibration process, but both sets of corrections reduce their respective cross sections.

7.2.2 Results in the MSSM

We also studied the production of Z bosons via weak boson fusion in the MSSM, as a function of $\tan\beta$. Although the WWZ coupling is the same in both the Standard Model and the MSSM, the new SUSY particles that are present in the loop corrections mean that different correction patterns are observed, as can be seen in Fig. 7.6, which presents

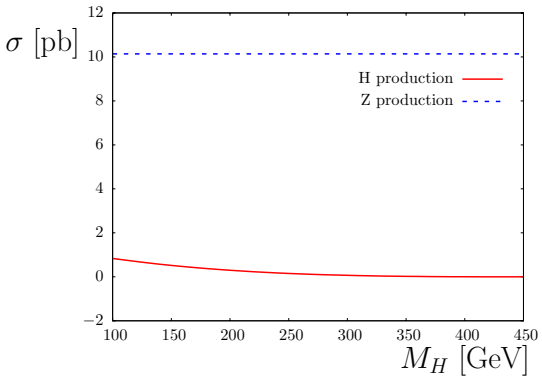

(a) Loop corrected partonic cross section of H and Z production via W boson fusion, with all fermion contributions considered.

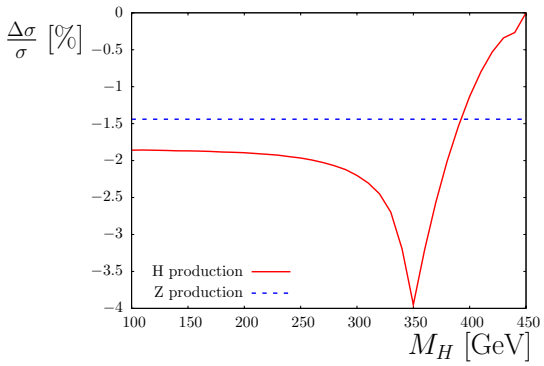

(b) Percentage loop corrections when only t / b quark contributions are included.

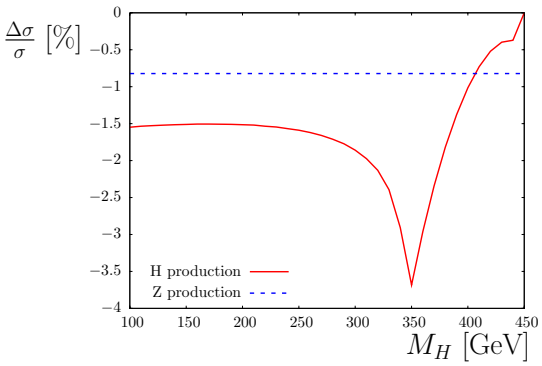

(c) Percentage loop corrections when all fermion contributions are included.

Figure 7.5: Comparison of Higgs and Z boson production via weak boson fusion at a centre of mass energy $\sqrt{\hat{s}} = 500$ GeV in the Standard Model.

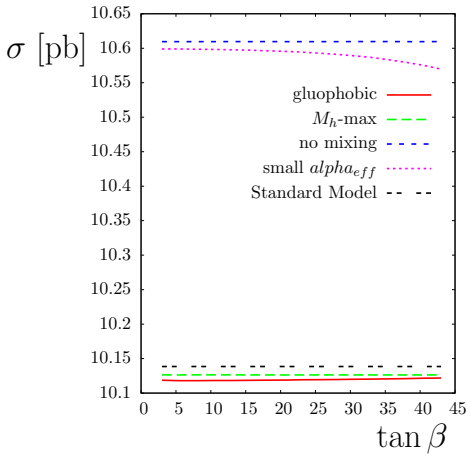

(a) Loop corrected partonic cross section of Z production as a function of $\tan\beta$, with all fermion corrections included.

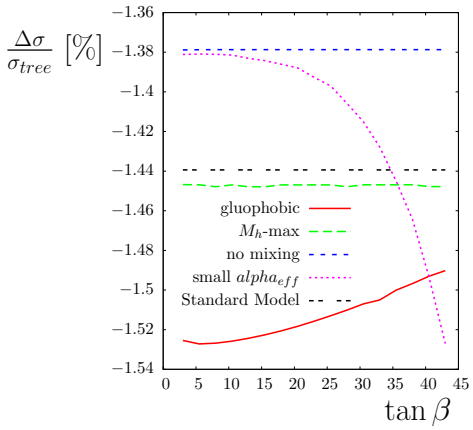

(b) Loop corrections from t / b quark contributions, as a function of $\tan\beta$.

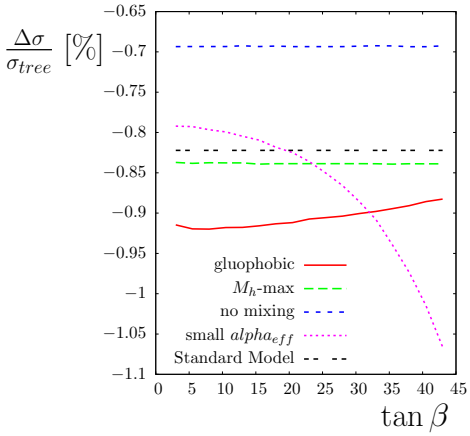

(c) Loop corrections from all fermion contributions, as a function of $\tan\beta$.

Figure 7.6: Z boson production via W boson fusion at $\sqrt{\hat{s}} = 500$ GeV for the Standard Model and the benchmark scenarios in the MSSM with real parameters.

the loop corrected partonic cross section and percentage loop corrections for

$$u + d \to d + Z + u$$

For comparison, the Standard Model cross section and loop corrections are also shown. As was the case for Higgs production in the MSSM, the small α_{eff} scenario demonstrates the greatest sensitivity to $\tan\beta$, owing to the stronger dependence of the sfermion masses on $\tan\beta$ in this benchmark. The M_h^{max} scenario is seen to most closely resemble the Standard Model, and the inclusion of all fermions and sfermions in the loop corrections results in smaller corrections than if only third generation quarks are considered.

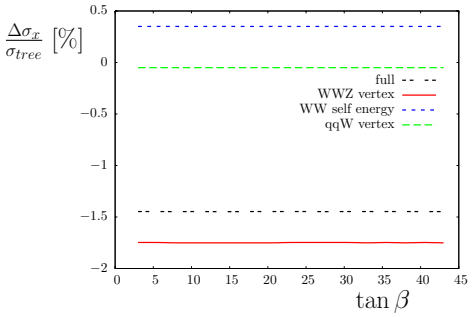

(a) Individual corrections from t / b quark contributions in the $M_h^{\max}$ scenario.

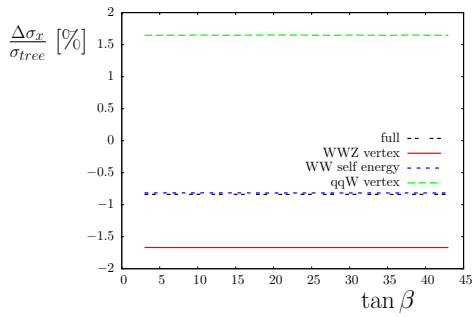

(b) Individual corrections from all fermion contributions in the $M_h^{\max}$ scenario.

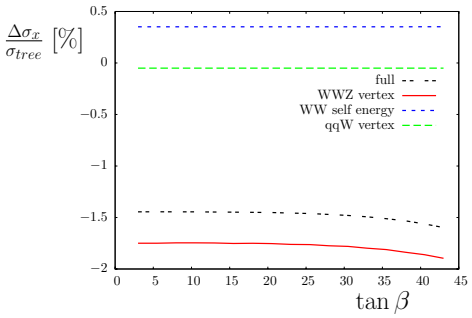

(c) Individual corrections from t / b quark contributions in the small α_{eff} scenario.

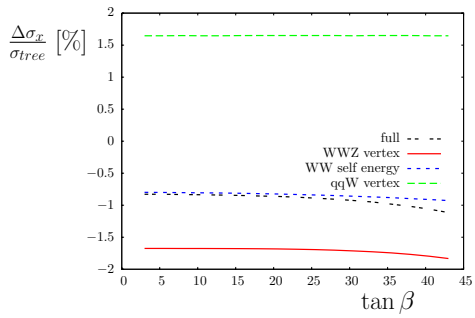

(d) Individual corrections from all fermion contributions in the small α_{eff} scenario.

Figure 7.7: Individual contributions to Z boson production via W boson fusion as a function of $\tan\beta$ with $M_A = 150$ GeV at $\sqrt{\hat{s}} = 500$ GeV in the MSSM. Here, $\Delta\sigma_x$ signifies the either the WWZ, the WW or the qqW correction.

Fig. 7.7 shows the individual contributions for the WW self energy, the ZWW vertex and the qqW vertex for the small α_{eff} scenario and the $M_h^{\max}$ scenario. In both the gluophobic and the no-mixing benchmarks, the relative contributions from each type of correction are very similar to those in the $M_h^{\max}$ scenario. The pattern of contributions can be seen to be similar to that found in the Standard Model (see Fig. 7.4). When all (s)fermions are included in the calculation of the loop corrections, the corrections to the WW self energy are seen to be a good approximation of the full correction, whereas if only top and bottom quarks are considered, the WWZ vertex gives the dominant contribution to the loop correction.

Finally, Fig. 7.8 compares the production of a light Higgs boson, h, with a Z boson in the small α_{eff} and $M_h^{\max}$ benchmarks[3], as a function of either M_A (with a fixed $\tan\beta = 10$) or a function of $\tan\beta$ (with $M_A = 150$ GeV). As in the Standard Model, the cross section for Z boson production is larger than that for h production, by a factor

[3]The no-mixing scenario and the gluophobic scenario are similar to the $M_h^{\max}$ scenario.

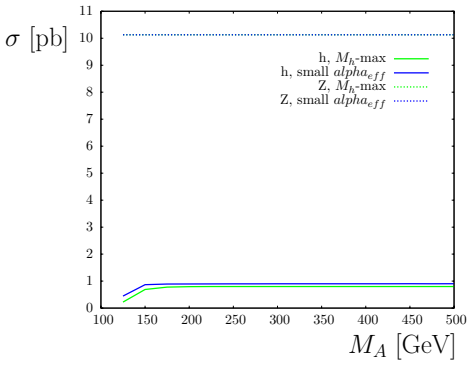

(a) Partonic cross section for h and Z production via weak boson fusion. All (s)fermion diagrams are included in the loop corrections, and $\tan\beta = 10$.

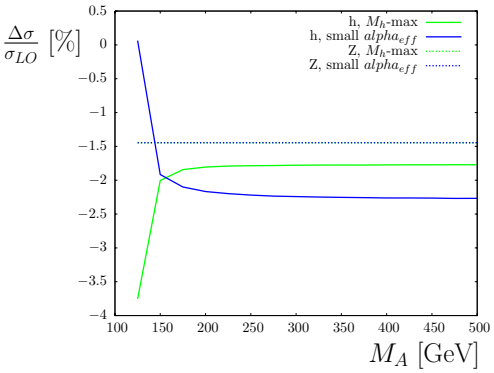

(b) Loop corrections for 3rd generation (s)quark contributions, with $\tan\beta = 10$.

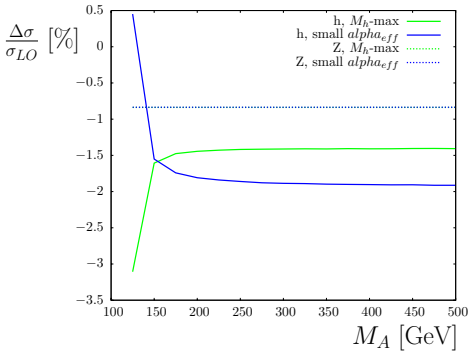

(c) Loop corrections for all (s)fermion contributions, with $\tan\beta = 10$.

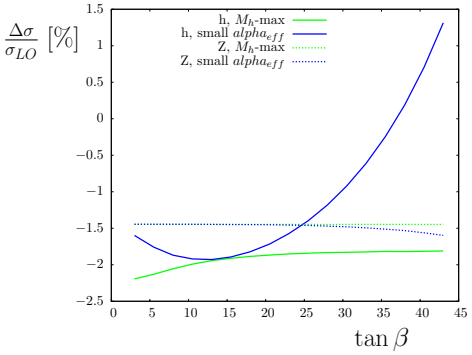

(d) Loop corrections for 3rd generation (s)quark contributions, with $M_A = 150$ GeV.

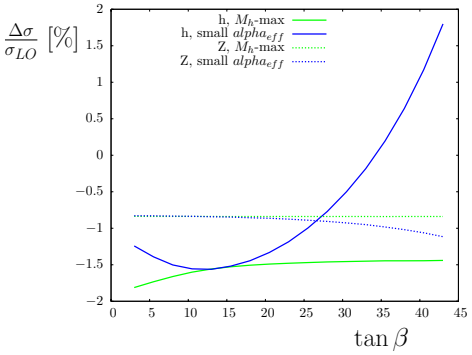

(e) Loop corrections for all (s)fermion contributions, with $M_A = 150$ GeV.

Figure 7.8: Comparison of h (solid lines) and Z (dotted lines) production via weak boson fusion at $\sqrt{\hat{s}} = 500$ GeV in the MSSM.

of ~ 10. The loop corrections are, in general, larger for light Higgs production in the MSSM and are (as expected) more sensitive to the parameters M_A and $\tan\beta$.

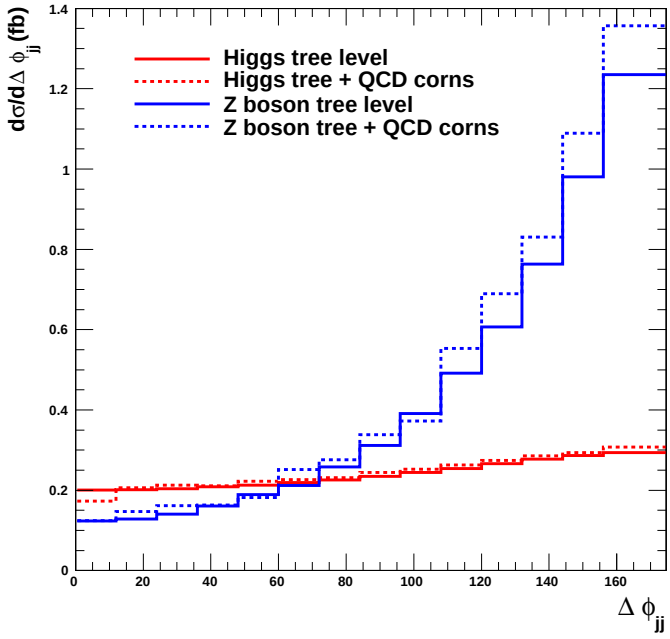

Figure 7.9: Azimuthal angle distribution for Higgs and Z boson production via weak boson fusion, with subsequent decay into a pair of τ leptons, produced with the public `VBFNLO`.

7.3 Outlook: Implementation of higher order corrections to Z production into `VBFNLO`

As has been mentioned, `VBFNLO` is capable of simulating the production of a Z boson plus two jets via WBF, incorporating the NLO QCD corrections to this possible calibration process. For example, Fig. 7.9 shows the azimuthal angle distributions for the Standard Model processes

$$p + p \to H/Z + j + j \to \tau^+ + \tau^- + j + j$$

This was produced at leading order and with QCD NLO corrections using the public `VBFNLO`, with our usual set of parameters and cuts (Equation 2.5). For this analysis, however, the PDF set is different – here we use CTEQ6L [72]. A Higgs mass of $M_H = 120$ GeV was chosen (this of course does not affect the Z boson production). The

corresponding cross sections are

$$\begin{aligned}
\sigma_{LO}(pp \to Hjj \to \tau^+\tau^- jj) &= 87.48 \pm 0.02 \text{ pb} \\
\sigma_{NLO}(pp \to Hjj \to \tau^+\tau^- jj) &= 90.13 \pm 0.09 \text{ pb} \\
\sigma_{LO}(pp \to Zjj \to \tau^+\tau^- jj) &= 186.54 \pm 0.39 \text{ pb} \\
\sigma_{NLO}(pp \to Zjj \to \tau^+\tau^- jj) &= 200.22 \pm 1.42 \text{ pb}
\end{aligned}$$

As can be seen, the process of Z production has a larger total cross section than Higgs production, and the azimuthal angle distribution shown in Fig. 7.9 covers a wider range. At low values of $\Delta\phi$, however, the Higgs boson distribution is larger than Z production. The large difference between the partonic cross sections for Higgs and Z production (Fig. 7.5) is reduced here – partly because the branching ratio for $H \to \tau^+\tau^-$ is larger than that for $Z \to \tau^+\tau^-$, and partly because the cuts (which are applied here but not to the partonic cross sections) have a greater effect on Z production than on Higgs production.

Anomalous couplings between the weak bosons have received considerable study – both theoretical and experimental – in the literature (see, for instance Ref. [141–143]). As when studying anomalous HVV couplings, we describe the anomalous interaction in terms of an effective Lagrangian. For the WWZ vertex that we are interested in here, the effective Lagrangian is given by [143]

$$\begin{aligned}
\mathcal{L}_{\text{eff}}^{WWZ} = -\frac{ie\cos\theta_W}{\sin\theta_W}\Big(\Delta g_1^Z \left[W^+_{\mu\nu}W^{-\mu} - W^{+\mu}W^-_{\mu\nu}\right] Z^\nu + \kappa_Z W^+_\mu W^-_\nu Z^{\mu\nu} + \\
\frac{\lambda_Z}{M_W^2} W^+_\mu W^{-\rho}_\nu Z_\rho{}^\mu\Big)
\end{aligned} \tag{7.2}$$

In the Standard Model, $\Delta g_1^Z = \kappa_Z = 1$ and $\lambda_Z = 0$. These will, however, be modified by the loop diagrams. The terms Δg_1^Z and κ_Z are involved in the second parametrisation of the HVV effective Lagrangian detailed in Section 2.4.3.

`VBFNLO` can also produce predictions for Z boson production via WBF when the trilinear coupling WWZ is not described by the Standard Model coupling, but rather by some anomalous coupling, in terms of the Lagrangian in Equation 7.2. Consequently, it will be possible to include the electroweak corrections to Z production via weak boson fusion into `VBFNLO` in the same way as the Higgs production corrections were included. This would mean that one could compare the signal and calibration processes at the same high level of accuracy. Although new code would have to be developed to calculate the parameters of the anomalous WWZ coupling (or alternatively, to implement the matrix

squared elements for the WWZ corrections), as well as the box and pentagon diagrams, the W self energy, quark vertex and real (photonic) corrections are all the same for Z and Higgs production and could be re-used. An additional set of corrections, however, may need to be considered for Z production – diagrams where the Z boson is radiated from one of the external quark lines. For Higgs production, this contribution was neglected as we work in the approximation of massless external quarks (which consequently have zero coupling to the Higgs boson). It is unlikely that this contribution would have a large effect of Z boson production either, as the kinematics are different and consequently the WBF cuts will suppress these diagrams.

Z boson production via weak boson fusion, besides being interesting in its own right, has the potential to be useful as a calibration process for Higgs production. Implementing Standard Model and MSSM loop corrections for this process into `VBFNLO` would provide the community with a useful tool with which to perform comparisons. This would be possible using the methods developed here, but the actual implementation is beyond the scope of this thesis.

Chapter 8

Conclusions

"While the Universe is under no obligation to make sense, students in pursuit of a PhD are."
— Robert Kishner

The search for the Higgs boson, and for supersymmetry, has been underway for decades and – with the advent of the LHC – we may soon receive confirmation of our theories. This thesis has looked at a very promising channel of Higgs boson production, weak boson fusion (WBF), which could not only serve as a discovery channel, but could also shed light on the properties of the Higgs, and through them on electroweak symmetry breaking as well. The techniques that need to be employed in order to calculate the electroweak corrections to weak boson fusion are described in detail in this work.

Initially, in this work, the process of weak boson fusion (including the Higgsstrahlung contribution) at a linear e^+e^-collider was studied in the Standard Model and MSSM. The fermion / sfermion one loop corrections were calculated, combined with propagator type corrections in the Higgs sector up to two loop level. Results previously reported in the literature [119] were confirmed, and the individual contributions to the complete process were studied in detail. It was found that (as expected), the Higgsstrahlung process is dominant at low centre of mass energies, while at high centre of mass energies weak boson fusion is dominant. The interference between the two processes is also important at low energies – particularly in the region where the cross sections from WBF and Higgsstrahlung are equal. While the (s)top / (s)bottom loop diagram contributions were seen to be a significant part of the corrections, they are not completely dominant, especially at the threshold centre of mass energy. Here, the corrections resulting from

the first and second generation (s)fermions were seen to be equally important, owing to the significance of the weak boson self energy and lepton–weak boson vertex corrections.

We then moved on to the main topic of this thesis: weak boson fusion Higgs production at the LHC. In the Standard Model, the full one loop electroweak corrections to WBF at the LHC have been calculated. We used formfactors describing an effective coupling $T^{\mu\nu}$ between the Higgs and a pair of weak bosons to include weak boson self energy corrections and Higgs vertex corrections. This is a simpler – and computationally more efficient – method than calculating these corrections in the full $2 \to 3$ process. The effective coupling was combined with the complete calculation of box and pentagon type diagrams, the corrections to the quark–weak boson vertex in the full $2 \to 3$ process, the corrections from real photon radiation and the (already existing) NLO QCD contributions. The complete one loop result was implemented into the public Monte Carlo event generator `VBFNLO` so that cross sections can be studied, as well as a range of distributions. The electroweak corrections were found to be $\sim \mathcal{O}(-5\%)$ for Higgs masses of between 100 GeV and 200 GeV. This is approximately the same size as the QCD NLO corrections in this region of parameter space, leading to a full NLO correction of $\sim -10\%$. We found good agreement with the available literature [55].

We also examined the relative importance of the loop corrections from third generation quarks and from all fermions to the WBF process. These were seen to give corrections of $\sim -2\%$ and $\sim -1.5\%$ respectively. While certainly a significant proportion of the total correction, the contribution from the top loop diagrams is not as dominant as is often seen in Higgs processes. In this case, the corrections from the weak boson self energy, and the quark–weak boson vertex become more important as we include more particles in the loops.

Weak boson fusion production of a neutral Higgs was studied in the MSSM, for the general case where the parameters are allowed to be complex. Our result consists of the complete one loop corrections to the Higgs vertex HVV and the weak boson self energy VV, supplemented by the two loop propagator type corrections in the Higgs sector (which are included in the Born level), the sfermion corrections to the quark–weak boson vertex qqV and the Standard Model boxes, pentagons, and full SM type corrections to the qqV vertex (i.e. we neglect only the effects of charginos and neutralinos in the box, pentagon and quark vertex diagrams). Implementation of these additional diagrams is in progress, but – as we have shown that the charginos and neutralinos have very little effect on the Higgs vertex and weak boson self energy corrections, and there is no reason

to suppose that this will be any different for the boxes – it is expected that the result presented here is a good approximation of the complete one loop result in the MSSM.

While studying the "pure SUSY" corrections to weak boson fusion we found differences $\mathcal{O}(0.5\%)$ between our results and the values reported in the literature [56]. We believe this difference to be partially caused by the implementation of the propagator type corrections in the Higgs sector – we use Z factors at the two loop level, obtained from `FeynHiggs`, to give the most complete result available. Using a specially tuned version of our code we followed the procedure used in [56], and found good agreement.

We investigated the formfactors, cross sections and distributions for the light CP even Higgs boson in the MSSM (i.e. including both SM particles and their superpartners). In general – as is expected – in the decoupling regime the differences between the MSSM predictions for the light Higgs production and the SM prediction for production of a Higgs with the same mass are small. When we move out of the decoupling regime into more extreme regions of parameter space, the differences between the MSSM and SM predictions can be sizeable. In the decoupling regime, the difference between the SM loop corrections and MSSM loop corrections is typically $\mathcal{O}(-0.3\%)$, but in the non-decoupling regime, with low M_A, this difference was found to be up to $\mathcal{O}(-5\%)$ in our most complete study of the $M_h^{\max}$ scenario.

Production of the other two neutral Higgs bosons was also studied in the MSSM with real and complex parameters. Although generally these have much smaller cross sections than the lightest Higgs boson, there are regions of parameter space where they make a sizeable (or even dominant) contribution – here, loop corrections from the QCD and (s)fermion corrections vary between $\sim \pm 5\%$ in the $M_h^{\max}$ scenario. This is due in large part to the mixing that occurs between the Higgs bosons, which we include at Born level via propagator corrections. Applying these propagator corrections at loop level was found to produce significant effects in the CPX scenario, even altering the shape of the azimuthal angle distribution in some regions of parameter space.

The results obtained in this thesis have been implemented into the public Monte Carlo code `VBFNLO`, and the modified program will be made available to the community. Using the new code, production of a Standard Model Higgs can be simulated including the full QCD and electroweak next to leading order corrections. In addition, various approximations can be made in order to speed up the running of the code – the electroweak corrections can be set to include only top and bottom quark loops, or only fermion loops, or the full correction.

The new code has also been designed to study the production of neutral Higgs bosons in the MSSM with complex parameters. The dominant SUSY one loop corrections have been included in the program, and these can be supplemented with the two loop level propagator type corrections in the Higgs sector, as well as the contribution from the Standard Model box and pentagon type diagrams. The results obtained go beyond those available in the literature, as they include loop corrections from both SUSY and SM particles, implemented in a Monte Carlo event generator that produces cross sections and a range of distributions. Included with the full Monte Carlo code are separate subroutines that calculate the formfactors involved in the effective coupling between a Higgs and a pair of weak gauge bosons. Restricting the calculation to just these formfactors is much quicker than calculating the full $2 \to 3$ process, and the results of such a calculation are often sufficient to identify interesting regions of parameter space in the MSSM.

The process of Z boson production via weak boson fusion was also studied at the partonic level in both the Standard Model and the MSSM. This process could be used for calibration of Higgs production (and possibly background suppression), as it will provide us with information about the detector performance, and the extent to which we can identify a clear weak boson fusion signal. Electroweak corrections to Z boson production were found to be generally smaller than those for Higgs production, although in both cases the NLO contributions reduce the cross section.

Weak boson fusion is an interesting and important process to study for the LHC and a future e^+e^- linear collider as not only does it have potential as a Higgs discovery channel, but it also could allow us to study the properties of the Higgs boson, as well as the mechanism of electroweak symmetry breaking. It is important that precise theoretical predictions for this process are made, such as those presented in this thesis, to match the expected experimental accuracy of the LHC.

Appendix A

Renormalisation constants and counterterms in the Standard Model

As explained in Chapter 3, the sign conventions used in this thesis (following the `FeynArts` conventions) for the SU(2) covariant derivative (Equation 1.3) differ between the Standard Model and the MSSM. Chapter 3 describes the renormalisation constants and counterterms using (in most cases) the MSSM convention. For completeness, in this Appendix we briefly state the necessary counterterms and constants using the other, Standard Model, convention.

A.1 Renormalisation constants

The renormalisation constants for the field and mass of the gauge bosons and fermions are not affected by the sign of the SU(2) covariant derivative. The constant $\delta \sin\theta_W$, however, becomes

$$\delta \sin\theta_W = \frac{1}{2}\frac{\cos^2\theta_W}{\sin\theta_W}\left(\frac{\delta M_Z^2}{M_Z^2} - \frac{\delta M_W^2}{M_W^2}\right) \tag{A.1}$$

Note that Chapter 3 explicitly states the necessary renormalisation constants for the Higgs field in both the Standard Model and MSSM conventions, and so they do not need to be stated again here.

A.1.1 Charge renormalisation

In Chapter 3 the section describing charge renormalisation (Section 3.3.2) uses the Standard Model convention for the SU(2) covariant derivative, due to the inclusion of the full, Standard Model calculation of the quantity Δr. Consequently, in this section we state the necessary constants using the MSSM convention.

When parametrising the lowest order coupling by $\alpha(0)$, the form of the charge renormalisation constant δZ_e is

$$\delta Z_e = \frac{1}{2}\Pi^{\gamma}(0) + \frac{\sin\theta_W}{\cos\theta_W}\frac{\sum_{\gamma Z}^{T}(0)}{M_Z^2} \tag{A.2}$$

The procedure for parametrising the electromagnetic coupling by $\alpha(M_Z^2)$, thereby shifting the renormalisation constant by $\Delta\alpha$, and avoiding difficulties encountered whilst calculating $\Pi^{\gamma}(0)$, is not altered by the change in conventions.

In this thesis, when working in the MSSM the lowest order coupling is parametrised via the Fermi constant G_F in the special case when only loop contributions from (s)fermions are considered. In this case, the charge renormalisation constant is

$$\delta Z_e^{G_F,(s)fermion} = -\frac{\delta\sin\theta_W}{\sin\theta_W} - \frac{1}{2}\left(\frac{\sum_{WW}^{T}(0) - \delta M_W^2}{M_W^2}\right) \tag{A.3}$$

A.2 Counterterms

In this section we give the counterterms needed in this work using the SM conventions for the SU(2) covariant derivative. Note that the counterterms for the HVV vertex are given in Chapter 3 for both the Standard Model and the MSSM (as the form of these terms is different owing to the increased complexity of the MSSM Higgs sector) and so are not stated here. The VV counterterm coupling is also not presented in this Appendix, as it is unaffected by the change in convention.

Looking first at the qqV coupling between the external quarks and the weak boson, the structure of the coupling (given in Equation 3.73) is of course unchanged, but the

left and right handed parts of the qqW coupling are now given by

$$\Gamma^{0}_{u\bar{d}W} = \left\{ \begin{array}{l} \frac{ie}{\sqrt{2}\sin\theta_W} \\ 0 \end{array} \right\} \tag{A.4}$$

$$\Gamma^{CT}_{u\bar{d}W} = \left\{ \begin{array}{l} \frac{ie}{\sqrt{2}\sin\theta_W}\left(\delta Z_e - \frac{\delta\sin\theta_W}{\sin\theta_W} + \frac{1}{2}\delta Z_{WW} + \frac{1}{2}\left(\delta Z^{*}_{fL}(\bar{d}) + \delta Z_{fL}(u)\right)\right) \\ 0 \end{array} \right\} \tag{A.5}$$

The coupling between the external quarks and a Z boson is still of the form given in Equation 3.77, but the quantities $g_R, \delta g_R$ etc. are now seen to be

$$g_{Ru} = -\frac{2}{3}\frac{\sin\theta_W}{\cos\theta_W} \tag{A.6}$$

$$g_{Rd} = \frac{1}{3}\frac{\sin\theta_W}{\cos\theta_W} \tag{A.7}$$

$$g_{Lu} = \frac{1}{\sin\theta_W\cos\theta_W}\left(\frac{1}{2} - \frac{2}{3}\sin^2\theta_W\right) \tag{A.8}$$

$$g_{Ld} = \frac{1}{\sin\theta_W\cos\theta_W}\left(-\frac{1}{2} + \frac{1}{3}\sin^2\theta_W\right) \tag{A.9}$$

and

$$\delta g_{Ru} = -\frac{2\sin\theta_W}{3\cos\theta_W}\left(\delta Z_e + \frac{1}{\sin\theta_W\cos^2\theta_W}\,\delta\sin\theta_W\right) \tag{A.10}$$

$$\delta g_{Rd} = \frac{\sin\theta_W}{3\cos\theta_W}\left(\delta Z_e + \frac{1}{\sin\theta_W\cos^2\theta_W}\,\delta\sin\theta_W\right) \tag{A.11}$$

$$\delta g_{Lu} = \frac{1}{2\sin\theta_W\cos\theta_W}\left(\delta Z_e + \left(\frac{\sin^2\theta_W - \cos^2\theta_W}{\sin\theta_W\cos^2\theta_W}\right)\delta\sin\theta_W\right) - \frac{2\sin\theta_W}{3\cos\theta_W}\left(\delta Z_e + \frac{1}{\sin\theta_W\cos^2\theta_W}\,\delta\sin\theta_W\right) \tag{A.12}$$

$$\delta g_{Ld} = -\frac{1}{2\sin\theta_W\cos\theta_W}\left(\delta Z_e + \left(\frac{\sin^2\theta_W - \cos^2\theta_W}{\sin\theta_W\cos^2\theta_W}\right)\delta\sin\theta_W\right) + \frac{\sin\theta_W}{3\cos\theta_W}\left(\delta Z_e + \frac{1}{\sin\theta_W\cos^2\theta_W}\,\delta\sin\theta_W\right) \tag{A.13}$$

Similarly, for the coupling $\bar{l}lZ$, the form remains as in Equation 3.99, but the terms $g_{L\nu}$ etc. are affected by the change in convention.

$$
\begin{aligned}
g_{R\nu} &= 0 && \text{(A.14)}\\
g_{Re} &= \frac{\sin\theta_W}{\cos\theta_W} && \text{(A.15)}\\
g_{L\nu} &= \frac{1}{2\sin\theta_W\cos\theta_W} && \text{(A.16)}\\
g_{Le} &= \frac{1}{\sin\theta_W\cos\theta_W}\left(-\frac{1}{2}+\sin^2\theta_W\right) && \text{(A.17)}
\end{aligned}
$$

and

$$
\begin{aligned}
\delta g_{R\nu} &= 0 && \text{(A.18)}\\
\delta g_{Re} &= \frac{\sin\theta_W}{\cos\theta_W}\left(\delta Z_e+\frac{1}{\sin\theta_W\cos^2\theta_W}\,\delta\sin\theta_W\right) && \text{(A.19)}\\
\delta g_{L\nu} &= \frac{1}{2\sin\theta_W\cos\theta_W}\left(\delta Z_e+\left(\frac{\sin^2\theta_W-\cos^2\theta_W}{\sin\theta_W\cos^2\theta_W}\right)\delta\sin\theta_W\right) && \text{(A.20)}\\
\delta g_{Le} &= -\frac{1}{2\sin\theta_W\cos\theta_W}\left(\delta Z_e+\left(\frac{\sin^2\theta_W-\cos^2\theta_W}{\sin\theta_W\cos^2\theta_W}\right)\delta\sin\theta_W\right)+ \\
&\quad \frac{\sin\theta_W}{\cos\theta_W}\left(\delta Z_e+\frac{1}{\sin\theta_W\cos^2\theta_W}\,\delta\sin\theta_W\right) && \text{(A.21)}
\end{aligned}
$$

The tree level and counterterm couplings between a neutrino, an electron and a W boson are also affected by the sign convention for the SU(2) covariant derivative and in the Standard Model are given by

$$
\begin{aligned}
\Gamma^0_{e\bar{\nu}_eW} &= \left\{\begin{array}{c}\frac{ie}{\sqrt{2}\sin\theta_W}\\ 0\end{array}\right\} && \text{(A.22)}\\
\Gamma^{CT}_{e\bar{\nu}_eW} &= \left\{\begin{array}{c}\frac{ie}{\sqrt{2}\sin\theta_W}\left(\delta Z_e-\frac{\delta\sin\theta_W}{\sin\theta_W}+\frac{1}{2}\delta Z_{WW}+\frac{1}{2}\left(\delta Z^*_{fL}(\bar{\nu}_e)+\delta Z_{fL}(e)\right)\right)\\ 0\end{array}\right\} && \text{(A.23)}
\end{aligned}
$$

Finally, the coupling between a pair of W bosons and a Z boson with the Standard Model convention is

$$\Gamma^{0}_{ZWW} = \frac{ie\cos\theta_W}{\sin\theta_W} \tag{A.24}$$

$$\Gamma^{CT}_{ZWW} = \frac{ie\cos\theta_W}{\sin\theta_W}\left(\delta Z_e - \frac{\delta\sin\theta_W}{\sin\theta_W\cos^2\theta_W} + \delta Z_{WW} + \frac{1}{2}\delta Z_{ZZ} - \frac{\sin\theta_W}{2\cos\theta_W}\delta Z_{AZ}\right) \tag{A.25}$$

Appendix B

Implementation of the higher order electroweak corrections into the Monte Carlo program VBFNLO

"It's not a bug, it's a feature."
— David Lubar

In this Appendix, we briefly describe the additions made to the existing VBFNLO code in order to incorporate the higher order corrections. To make these additions more transparent (and to facilitate debugging!), the additions are contained within entirely separate subroutines and files that are simply added to the existing code's structure. All modifications to the existing code have been kept to a minimum, and the original structure of the code is not affected. As has been explained previously (see Chapter 2, Section 2.5), VBFNLO is already able to analyse WBF with anomalous couplings between a Higgs and a pair of weak bosons (see Ref. [52] and [59]), by using the formfactor formalism described in Section 2.4. This pre-existing structure was used in order to incorporate the loop corrections to the Higgs vertex and the weak boson self energy. Other corrections are included by calculating the matrix squared element.

Several options are provided for the evaluation of the NLO electroweak corrections to Higgs production via WBF, which are detailed in Table B.1.

The user can, of course, choose whatever supersymmetric parameters they wish. For ease of use, however, the benchmark scenarios (described in Ref. [121]) have been pre-

Table B.1: Description of inputs to the version of VBFNLO including the results of this thesis.

input name	**input value**	**description**
susy		*Choice of which model* VBFNLO *will work in*
	1	Standard Model
	2	MSSM
ivirt		*Choice of whether to include electroweak corrections*
	0	Leading order calculation only
	1	Electroweak corrections included in the calculation
charge		*Method of parametrising the electromagnetic coupling constant α (see Section 3.3.2)*
	1	Parametrised by $\alpha(0)$
	2	Parametrised by $\alpha(M_Z^2)$
	3	Parametrised by G_F
sector		*Choice of which set of corrections the code will calculate*
	1	Only (s)top and (s)bottom corrections
	2	All (s)fermion corrections
	3	All corrections (not yet available in MSSM)
bench		*Choice of pre-defined parameter points*
	1	Gluophobic Higgs benchmark
	2	$M_h^{\max}$ benchmark
	3	No-mixing benchmark
	4	Small α_{eff} benchmark
	5	CPX scenario
	6	User defined scenario
	7 – 16	SPS points 1a - 9, as defined in Ref. [144]
HiggsType		*Choice of which of the neutral Higgs bosons is produced*
	1	Light CP even Higgs h (or h_1 in the complex MSSM)
	2	Heavy CP even Higgs H (or h_2 in the complex MSSM)
	3	CP odd Higgs A (or h_3 in the complex MSSM)
prop		*Choice of propagator corrections*
	0	No propagator corrections are included
	1	U matrix is used at Born level
	2	Z matrix is used at Born level
	4	Z matrix is used at Born and loop level

programmed into the code. The first four benchmarks – gluophobic, $M_h^{\max}$, no-mixing, and small α_{eff} – are all for the real MSSM. The mass of the CP odd Higgs boson M_A and the value of $\tan\beta$ are not set in these scenarios, but are input values to be chosen by the user. All other parameters are fixed. The fifth benchmark is the CPX scenario, which has been designed as an "extreme" scenario in the complex MSSM (Ref. [129]). Here, $\tan\beta$ and the mass of the charged Higgs $m_{H^\pm}$ are taken as free parameters, and the other parameters have been chosen to maximise the effects of complex phases. Also, the SPS benchmark points [131], as described in Ref. [144], have been included as options in the modified `VBFNLO`. When working in the Standard Model, if a set of supersymmetric parameters has been defined, the Higgs sector is calculated by `FeynHiggs` (see Section 3.4) and the Standard Model Higgs mass and width are set to equal those of the chosen MSSM Higgs. Alternatively, the Standard Model Higgs mass and width can be input straight into the code, bypassing `FeynHiggs` entirely.

As stated earlier, the additions to the code are primarily in the form of new, separate subroutines, which are called from the main, original code. These new subroutines are contained in the following files.

`parameters.F` contains subroutines that set and calculate all the parameters of the chosen parameter point (defined by the input `bench`). These parameters (and in particular those of the Higgs sector – the masses of each Higgs boson and the matrix containing propagator corrections) are calculated using calls to `FeynHiggs`. This file also contains subroutines that calculate all necessary renormalisation constants in either the Standard Model or the MSSM, for whichever particles the user has chosen to include (using the input `sector`), and whichever parametrisation of the electromagnetic coupling has been input. It is here that the renormalisation and regularisation parameters (the UV divergence, and the regulatory quark and photon masses - see Chapter 3) are set, and can be varied in order to check that the final result is finite.

The file `virtual.F` is the interface to the subroutines that calculate the loop corrections. It calls and combines the individual parts of the formfactors for either the Standard Model or the MSSM, and feeds these values back into the main code. It also provides the connection to subroutines calculating the matrix element squared values for the boxes and pentagons, converting the necessary momentum information into a suitable format. Importantly, both procedures for treating the IR divergences are stored in this file (see Chapter 3, Section 3.6). By default (as stated in the text), the subtraction method is used, but this can be (manually) altered to the phase space slicing method in order to provide an additional check on the procedures.

Finally, the file `formfactors.F`, together with `mat_elNC+.F` and `mat_elCC+.F`, calculates the formfactors and the matrix elements for the boxes and pentagons for neutral and charged currents respectively. `formfactors.F` also contains the calculation of the counterterm coupling between the external quarks and the internal weak boson, which is used if only the contribution arising from (s)fermions are being considered (if the complete one loop corrections.are being studied, these are implemented via 2 Re$|\mathcal{M}^*_{tree}\mathcal{M}_{loop}|$).

Appendix C

Example formfactor calculation

In this Appendix we explicitly calculate the top quark loop diagrams (involving the coupling $t\bar{t}H$) to the $V + V \rightarrow H$ interaction in order to see where each component of the anomalous coupling $T^{\mu\nu}$ originates, recalling that:

$$\begin{aligned} T^{\mu\nu}(q_1, q_2) &= a_1(q_1, q_2)g^{\mu\nu} + \\ & a_2(q_1, q_2)\left(q_1.q_2 g^{\mu\nu} - q_1^{\mu} q_2^{\nu}\right) + \\ & a_3(q_1, q_2)\epsilon^{\mu\nu\rho\sigma} q_{1\rho} q_{2\sigma} \end{aligned} \tag{C.1}$$

The formfactors for the HVV coupling involve Feynman diagrams of the type shown in Figure C.1 for the W and Z bosons.

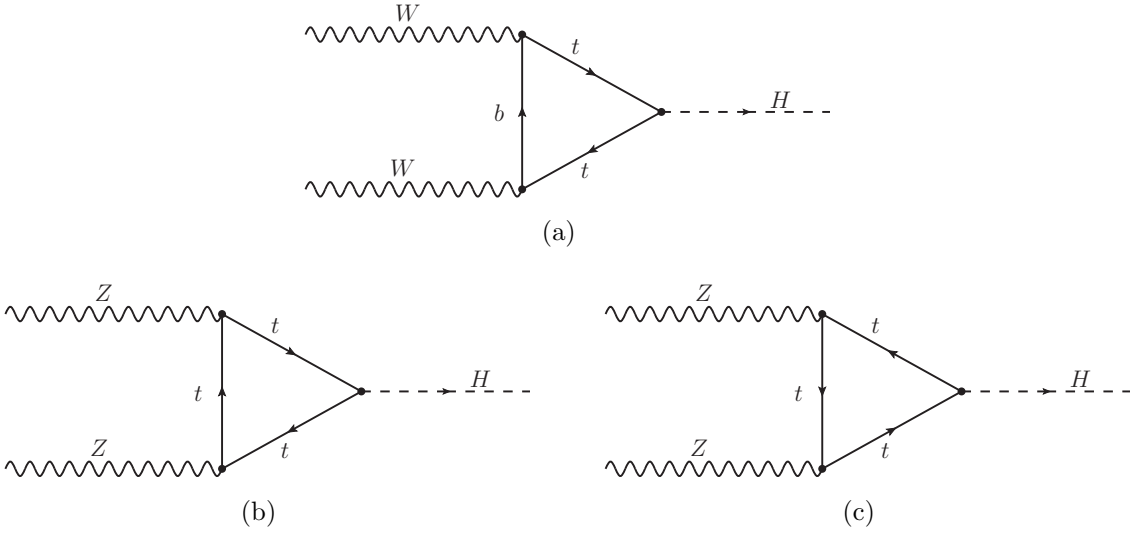

Figure C.1: Top quark loop correction diagrams to the HVV coupling.

These all have the same general form, for which the relevant part (for the formfactor calculation) is the trace:

$$\begin{aligned}\mathrm{Tr}[X] &= \mathrm{Tr}\left[(m_t+\not{k})\left(\frac{-iem_t}{M_W\sin\theta_W}\right)(m_t+\not{q})\,\gamma^\mu\,(A+B\gamma_5)\,(m_x+\not{Q})\right.\\ &\quad\left.\gamma^\nu\,(A+B\gamma_5)\right]\end{aligned}$$

Here, m_x signifies the mass of the bottom quark m_b for the HWW coupling, and the mass of the top quark m_t for HZZ. k, q and Q are the momenta of the three particles in the loop. Additionally, A and B are the left- and right-hand pieces of the coupling $q\bar{q}V$ (i.e. $\Gamma_{q\bar{q}V} = A\gamma^\mu + B\gamma^\mu\gamma_5$). Discarding the constant coefficients, this leads to

$$\begin{aligned}\mathrm{Tr}[X] &= \mathrm{Tr}\left[\left(m_t^2 + m_t(\not{k}+\not{q}) + \not{k}\not{q}\right)(A\gamma^\mu + B\gamma^\mu\gamma_5)\,(m_x\gamma^\nu + \not{Q}\gamma^\nu)\,(A+B\gamma_5)\right]\\ &= \mathrm{Tr}\left[\left(Am_t^2\gamma^\mu + Bm_t^2\gamma^\mu\gamma_5 + Am_t(\not{k}+\not{q})\gamma^\mu + Bm_t(\not{k}+\not{q})\gamma^\mu\gamma_5 + \right.\right.\\ &\qquad \left.\left. A\not{k}\not{q}\gamma^\mu + B\not{k}\not{q}\gamma^\mu\gamma_5\right)(Am_x\gamma^\nu + Bm_x\gamma^\nu\gamma_5 + A\not{Q}\gamma^\nu + B\not{Q}\gamma^\nu\gamma_5)\right]\\ &= \mathrm{Tr}\left[A^2m_t^2m_x\gamma^\mu\gamma^\nu + ABm_t^2m_x\gamma^\mu\gamma_5\gamma^\nu + \right.\\ &\qquad A^2m_tm_x\,(\not{k}+\not{q})\,\gamma^\mu\gamma^\nu + ABm_tm_x\,(\not{k}+\not{q})\,\gamma^\mu\gamma_5\gamma^\nu +\\ &\qquad A^2m_x\not{k}\not{q}\gamma^\mu\gamma^\nu + ABm_x\not{k}\not{q}\gamma^\mu\gamma_5\gamma^\nu +\\ &\qquad BAm_t^2m_x\gamma^\mu\gamma^\nu\gamma_5 + B^2m_t^2m_x\gamma^\mu\gamma_5\gamma^\nu\gamma_5 +\\ &\qquad BAm_tm_x\,(\not{k}+\not{q})\,\gamma^\mu\gamma^\nu\gamma_5 + B^2m_tm_x\,(\not{k}+\not{q})\,\gamma^\mu\gamma_5\gamma^\nu\gamma_5 +\\ &\qquad BAm_x\not{k}\not{q}\gamma^\mu\gamma^\nu\gamma_5 + B^2m_x\not{k}\not{q}\gamma^\mu\gamma_5\gamma^\nu\gamma_5 +\\ &\qquad A^2m_t^2\gamma^\mu\not{Q}\gamma^\nu + ABm_t^2\gamma^\mu\gamma_5\not{Q}\gamma^\nu +\\ &\qquad A^2m_t\,(\not{k}+\not{q})\,\gamma^\mu\not{Q}\gamma^\nu + ABm_t\,(\not{k}+\not{q})\,\gamma^\mu\gamma_5\not{Q}\gamma^\nu +\\ &\qquad A^2\not{k}\not{q}\gamma^\mu\not{Q}\gamma^\nu + AB\not{k}\not{q}\gamma^\mu\gamma_5\not{Q}\gamma^\nu +\\ &\qquad BAm_t^2\gamma^\mu\not{Q}\gamma^\nu\gamma_5 + B^2m_t^2\gamma^\mu\gamma_5\not{Q}\gamma^\nu\gamma_5 +\\ &\qquad BAm_t\,(\not{k}+\not{q})\,\gamma^\mu\not{Q}\gamma^\nu\gamma_5 + B^2m_t\,(\not{k}+\not{q})\,\gamma^\mu\gamma_5\not{Q}\gamma^\nu\gamma_5 +\\ &\qquad \left.BA\not{k}\not{q}\gamma^\mu\not{Q}\gamma^\nu\gamma_5 + B^2\not{k}\not{q}\gamma^\mu\gamma_5\not{Q}\gamma^\nu\gamma_5\right]\end{aligned}$$

where, as is normal, $\not{q} = q_\rho \gamma^\rho$. Recalling the standard relations for the traces of the gamma matrices:

$$\begin{aligned}
\mathrm{Tr}\left[\gamma^\mu \gamma^\nu\right] &= 4g^{\mu\nu} \\
\mathrm{Tr}\left[\gamma^\mu \gamma^\nu \gamma_5\right] &= 0 \\
\mathrm{Tr}\left[\text{odd number of } \gamma\right] &= 0 \\
\left\{\gamma_5, \gamma^\mu\right\} &= 0 \\
\gamma_5^2 &= 1 \\
\mathrm{Tr}\left[\gamma^\mu \gamma^\nu \gamma^\rho \gamma^\sigma\right] &= 4\left(g^{\mu\nu} g^{\rho\sigma} - g^{\mu\rho} g^{\nu\sigma} + g^{\mu\sigma} g^{\nu\rho}\right) \\
\mathrm{Tr}\left[\gamma^\mu \gamma^\nu \gamma^\rho \gamma^\sigma \gamma_5\right] &= -4i\epsilon^{\mu\nu\rho\sigma}
\end{aligned} \tag{C.2}$$

we see that most of the terms in the trace vanish and we are left with

$$\begin{aligned}
\mathrm{Tr}[X] = \mathrm{Tr}\Big[&m_t^2 m_x \left(A^2 - B^2\right) \gamma^\mu \gamma^\nu + \left(A^2 - B^2\right) m_x \not{k} \not{q} \gamma^\mu \gamma^\nu + \\
&\left(A^2 + B^2\right) m_t \left(\not{k} + \not{q}\right) \gamma^\mu \not{Q} \gamma^\nu + 2AB m_t \left(\not{k} + \not{q}\right) \gamma^\mu \not{Q} \gamma^\nu \gamma_5\Big]
\end{aligned} \tag{C.3}$$

Focussing first on the HWW loop diagrams, the coupling $b\bar{t}W$ is given by (ignoring universal constant factors)

$$\begin{aligned}
A &= 1 \\
B &= -1
\end{aligned}$$

This means that, for momenta p^ρ, q^σ and Q^α the trace reduces to:

$$\mathrm{Tr}[X] = \sum_{\beta=\rho,\sigma} 8m_t \left(g^{\mu\beta} g^{\alpha\nu} - g^{\beta\alpha} g^{\mu\nu} + g^{\beta\nu} g^{\mu\alpha} - i\epsilon^{\beta\mu\alpha\nu}\right) j_\beta Q_\alpha$$

This expression can clearly be seen to lead to the three components of the general coupling $T^{\mu\nu}$: the second term (in red) leads to contributions to the formfactor a_1, the first and third terms (in blue) contribute to a_2, and the final term (in green) to a_3.

Moving on to the calculation of the ZZH loop, the coupling $t\bar{t}Z$ for Figure C.1(b) is defined by:

$$\Gamma_{t\bar{t}Z} = \frac{2ie \sin\theta_W \gamma^\mu}{3\cos\theta_W}\left(1 - \gamma_5\right) - \frac{ie}{\sin\theta_W \cos\theta_W}\left(\frac{1}{2} - \frac{2\sin^2\theta_W}{3}\right)\gamma^\mu\left(1 + \gamma_5\right)$$

This leads to (again, ignoring universal factors)

$$\begin{aligned} A &= \frac{4\sin\theta_W}{3} - \frac{1}{2\sin\theta_W} \\ B &= -\frac{1}{2\sin\theta_W} \end{aligned}$$

When adding the diagrams in Figure C.1(b) and C.1(c) together, we must remember that the fermion flow in Fig. C.1(b) is opposite to that in Fig. C.1(c) – this means that the final AB term in Equation C.2 vanishes when Figures C.1(b) and C.1(c) are added together. See also the `FeynArts` manual and Ref. [145].

Substituting these values into the general form of the trace (Equation C.2), we arrive at

$$\begin{aligned} \mathrm{Tr}[X] &= 2\mathrm{Tr}\left[m_t^3 \left(\frac{16\sin^2\theta_W}{9} + \frac{1}{2\sin^2\theta_W} - \frac{4}{3} \right) \gamma^\mu\gamma^\nu + m_t \left(\frac{16\sin^2\theta_W}{9} - \frac{4}{3} \right) \not{k}\not{q}\gamma^\mu\gamma^\nu \right. \\ &\qquad \left. m_t \left(\frac{16\sin^2\theta_W}{9} + \frac{1}{2\sin^2\theta_W} - \frac{4}{3} \right) (\not{k} + \not{q})\gamma^\mu\not{Q}\gamma^\nu \right] \\ &= 8m_t^3 \left(\frac{16\sin^2\theta_W}{9} + \frac{1}{2\sin^2\theta_W} - \frac{4}{3} \right) g^{\mu\nu} + \\ &\quad 8m_t \left(\frac{16\sin^2\theta_W}{9} - \frac{4}{3} \right) k_k q_q \left(g^{kq}g^{\mu\nu} + g^{k\mu}g^{q\nu} - g^{k\nu}g^{q\mu} \right) + \\ &\quad 8m_t \left(\frac{16\sin^2\theta_W}{9} + \frac{1}{2\sin^2\theta_W} - \frac{4}{3} \right) k_k Q_Q \left(g^{k\mu}g^{Q\nu} + g^{kQ}g^{\mu\nu} - g^{k\nu}g^{\mu Q} \right) + \\ &\quad 8m_t \left(\frac{16\sin^2\theta_W}{9} + \frac{1}{2\sin^2\theta_W} - \frac{4}{3} \right) q_q Q_Q \left(g^{q\mu}g^{Q\nu} + g^{qQ}g^{\mu\nu} - g^{q\nu}g^{\mu Q} \right) \end{aligned} \tag{C.4}$$

The contribution to a_3 from quark loops at the HZZ vertex is thus exactly zero, as the opposite fermion flow around the loops in the two diagrams causes the a_3 terms to have opposite signs.

Colophon

This thesis was made in LaTeX, using the hepthesis class [146]. Graphs were produced using gnuplot [147] and Compare [148], a ROOT [149] interface.

Bibliography

[1] M. Gell-Mann, Physics Letters **8**, 214 (1964).

[2] H. Fritzsch, M. Gell-Mann, and H. Leutwyler, Physics Letters B **47**, 365 (1973).

[3] D. J. Gross and F. Wilczek, Phys. Rev. Lett. **30**, 1343 (1973).

[4] S. L. Glashow, Nucl. Phys. **22**, 579 (1961).

[5] S. Weinberg, Phys. Rev. Lett. **19**, 1264 (1967).

[6] A. Salam, Originally printed in *Svartholm: Elementary Particle Theory, Proceedings Of The Nobel Symposium Held 1968 At Lerum, Sweden*, Stockholm 1968, 367-377.

[7] P. W. Higgs, Phys. Lett. **12**, 132 (1964).

[8] P. W. Higgs, Phys. Rev. Lett. **13**, 508 (1964).

[9] F. Englert and R. Brout, Phys. Rev. Lett. **13**, 321 (1964).

[10] LEP Working Group for Higgs boson searches, R. Barate *et al.*, Phys. Lett. **B565**, 61 (2003), hep-ex/0306033.

[11] CDF, (2009), arXiv:0903.4001 [hep-ex].

[12] D. Griffiths, *Introduction to Elementary Particles* (John Wiley and Sons, Inc., 1987).

[13] J. F. Gunion, H. E. Haber, G. Kane, and S. Dawson, *The Higgs Hunter's Guide* (Perseus Publishing, 1990).

[14] M. E. Peskin and D. V. Schroeder, *An Introduction to Quantum Field Theory* (Westview Press, 1995).

[15] A. Djouadi, Phys. Rept. **457**, 1 (2008), hep-ph/0503172.

[16] A. Djouadi, Phys. Rept. **459**, 1 (2008), hep-ph/0503173.

[17] F. Zwicky, Helv. Phys. Acta **6**, 110 (1933).

[18] Supernova Search Team, A. G. Riess *et al.*, Astron. J. **116**, 1009 (1998), astro-ph/9805201.

[19] WMAP, E. Komatsu *et al.*, Astrophys. J. Suppl. **180**, 330 (2009), arXiv:0803.0547 [astro-ph].

[20] U. Amaldi, W. de Boer, and H. Furstenau, Phys. Lett. **B260**, 447 (1991).

[21] M. Dine and A. Kusenko, Rev. Mod. Phys. **76**, 1 (2004), hep-ph/0303065.

[22] P. Ramond, Phys. Rev. **D3**, 2415 (1971).

[23] A. Neveu and J. H. Schwarz, Nucl. Phys. **B31**, 86 (1971).

[24] J.-L. Gervais and B. Sakita, Nucl. Phys. **B34**, 632 (1971).

[25] M. Drees, R. Godbole, and P. Roy, *Theory and Phenomenology of Sparticles* (World Scientific, 2004).

[26] R. Haag, J. T. Lopuszanski, and M. Sohnius, Nuclear Physics B **88**, 257 (1975).

[27] A. Signer, J. Phys. **G36**, 073002 (2009), arXiv:0905.4630 [hep-ph].

[28] S. Dimopoulos and H. Georgi, Nucl. Phys. **B193**, 150 (1981).

[29] L. D. Faddeev and V. N. Popov, Phys. Lett. **B25**, 29 (1967).

[30] S. Heinemeyer, Int. J. Mod. Phys. **A21**, 2659 (2006), hep-ph/0407244.

[31] M. Frank *et al.*, JHEP **02**, 047 (2007), hep-ph/0611326.

[32] LEP, J. Alcaraz *et al.*, (2007), arXiv:0712.0929 [hep-ex].

[33] K. E. Williams, *The Higgs Sector of the Complex Minimal Supersymmetric Standard Model*, PhD thesis, Durham University, Durham UK, 2008.

[34] M. A. Dobbs *et al.*, Les Houches guidebook to Monte Carlo generators for hadron collider physics (2004), hep-ph/0403045.

[35] T. Sjostrand, S. Mrenna, and P. Skands, JHEP **05**, 026 (2006), hep-ph/0603175.

[36] F. James, Rept. Prog. Phys. **43**, 1145 (1980).

[37] G. C. Blazey *et al.*, (2000), hep-ex/0005012.

[38] S. Asai *et al.*, Eur. Phys. J. C **32**, 19 (2004).

[39] The ATLAS collaboration, (2009), arXiv:0901.0512 [hep-ex].

[40] The CMS collaboration, Journal of Physics G: Nuclear and Particle Physics **34**, 995 (2007).

[41] T. Hahn, S. Heinemeyer, F. Maltoni, G. Weiglein, and S. Willenbrock, (2006), hep-ph/0607308.

[42] R. Harlander and W. Kilgore, Int. J. Mod. Phys. **A16S1A**, 305 (2001), hep-ph/0012176.

[43] C. Anastasiou and K. Melnikov, Nucl. Phys. **B646**, 220 (2002), hep-ph/0207004.

[44] V. Ravindran, J. Smith, and W. L. van Neerven, Nucl. Phys. **B665**, 325 (2003), hep-ph/0302135.

[45] V. Ravindran, J. Smith, and W. L. van Neerven, Nucl. Phys. Proc. Suppl. **135**, 35 (2004), hep-ph/0405263.

[46] M. Spira, A. Djouadi, D. Graudenz, and R. M. Zerwas, Nuclear Physics B **453**, 17 (1995).

[47] T. Figy, C. Oleari, and D. Zeppenfeld, Phys. Rev. **D68**, 073005 (2003), hep-ph/0306109.

[48] V. A. Khoze, M. G. Ryskin, W. J. Stirling, and P. H. Williams, Eur. Phys. J. **C26**, 429 (2003), hep-ph/0207365.

[49] D. Green, (2006), hep-ph/0603022.

[50] T. Figy and D. Zeppenfeld, Phys. Lett. **B591**, 297 (2004), hep-ph/0403297.

[51] T. Han, G. Valencia, and S. Willenbrock, Phys. Rev. Lett. **69**, 3274 (1992), hep-ph/9206246.

[52] K. Arnold *et al.*, (2008), arXiv:0811.4559 [hep-ph].

[53] VBFNLO is publically available from http://www-itp.particle.uni-karlsruhe.de/ vbfnloweb/.

[54] M. Spira, `vv2h`, http://people.web.psi.ch/spira/proglist.html.

[55] M. Ciccolini, A. Denner, and S. Dittmaier, Phys. Rev. **D77**, 013002 (2008), arXiv:0710.4749 [hep-ph].

[56] W. Hollik, T. Plehn, M. Rauch, and H. Rzehak, Phys. Rev. Lett. **102**, 091802 (2009), arXiv:0804.2676 [hep-ph].

[57] W. Buchmller and D. Wyler, Nuclear Physics B **268**, 621 (1986).

[58] T. Plehn, D. L. Rainwater, and D. Zeppenfeld, Phys. Rev. Lett. **88**, 051801 (2002), hep-ph/0105325.

[59] V. Hankele, G. Klamke, D. Zeppenfeld, and T. Figy, Phys. Rev. **D74**, 095001 (2006), hep-ph/0609075.

[60] K. Odagiri, JHEP **03**, 009 (2003), hep-ph/0212215.

[61] L3 Collaboration, P. Achard *et al.*, Phys. Lett. **B589**, 89 (2004), hep-ex/0403037.

[62] ALEPH Collaboration, (2005), hep-ex/0511027.

[63] C. Ruwiedel, N. Wermes, and M. Schumacher, Eur. Phys. J. **C51**, 385 (2007).

[64] T. Sjostrand, L. Lonnblad, S. Mrenna, and P. Skands, (2003), hep-ph/0308153.

[65] E. Richter-Was, D. Froidevaux, and L. Poggioli, CERN Report No. ATL-PHYS-98-131, 1998 (unpublished).

[66] K. Hagiwara and D. Zeppenfeld, Nuclear Physics B **274**, 1 (1986).

[67] K. Hagiwara and D. Zeppenfeld, Nuclear Physics B **313**, 560 (1989).

[68] S. Catani and M. H. Seymour, Nucl. Phys. **B485**, 291 (1997), hep-ph/9605323.

[69] G. P. Lepage, Journal of Computational Physics **27**, 192 (1978).

[70] M. H. Seymour, Nucl. Phys. **B513**, 269 (1998), hep-ph/9707338.

[71] M. R. Whalley, D. Bourilkov, and R. C. Group, (2005), hep-ph/0508110.

[72] J. Pumplin *et al.*, JHEP **07**, 012 (2002), hep-ph/0201195.

[73] R. V. Harlander, J. Vollinga, and M. M. Weber, Phys. Rev. **D77**, 053010 (2008), arXiv:0801.3355 [hep-ph].

[74] J. Vollinga, Nucl. Phys. Proc. Suppl. **186**, 102 (2009), arXiv:0809.3693 [hep-ph].

[75] J. R. Andersen, T. Binoth, G. Heinrich, and J. M. Smillie, JHEP **02**, 057 (2008), arXiv:0709.3513 [hep-ph].

[76] J. R. Andersen and J. M. Smillie, Phys. Rev. **D75**, 037301 (2007), hep-ph/0611281.

[77] E. B. Zijlstra and W. L. van Neerven, Nuclear Physics B **383**, 525 (1992).

[78] G. Passarino and M. Veltman, Nuclear Physics B **160**, 151 (1979).

[79] G. 't Hooft and M. Veltman, Nuclear Physics B **44**, 189 (1972).

[80] D. Stockinger, JHEP **03**, 076 (2005), hep-ph/0503129.

[81] T. Hahn and M. Perez-Victoria, Comput. Phys. Commun. **118**, 153 (1999), hep-ph/9807565.

[82] LoopTools is publically available at http://www.feynarts.de/looptools/.

[83] T. Han and S. Willenbrock, Physics Letters B **273**, 167 (1991).

[84] T. Figy, private communication.

[85] A. Denner, Fortschr. Phys. **41**, 307 (1993), arXiv:0709.1075 [hep-ph].

[86] M. Frank, S. Heinemeyer, W. Hollik, and G. Weiglein, (2002), hep-ph/0212037.

[87] Particle Data Group, C. Amsler *et al.*, Phys. Lett. **B667**, 1 (2008).

[88] M. Steinhauser, Phys. Lett. **B429**, 158 (1998), hep-ph/9803313.

[89] K. Hagiwara, A. D. Martin, D. Nomura, and T. Teubner, Phys. Rev. **D69**, 093003 (2004), hep-ph/0312250.

[90] W. J. Marciano and A. Sirlin, Phys. Rev. D **22**, 2695 (1980).

[91] A. Sirlin, Phys. Rev. D **22**, 971 (1980).

[92] W. Hollik, Fortschritte der Physik **38**, 165 (1990).

[93] P. H. Chankowski *et al.*, Nuclear Physics B **417**, 101 (1994).

[94] G. Degrassi, S. Heinemeyer, W. Hollik, P. Slavich, and G. Weiglein, Eur. Phys. J. **C28**, 133 (2003), hep-ph/0212020.

[95] S. Heinemeyer, W. Hollik, and G. Weiglein, Eur. Phys. J. **C9**, 343 (1999), hep-ph/9812472.

[96] S. Heinemeyer, W. Hollik, and G. Weiglein, Comput. Phys. Commun. **124**, 76 (2000), hep-ph/9812320.

[97] FeynHiggs is publically available at http://www.feynhiggs.de/.

[98] S. P. Martin, Phys. Rev. **D65**, 116003 (2002), hep-ph/0111209.

[99] S. P. Martin, Phys. Rev. **D71**, 116004 (2005), hep-ph/0502168.

[100] T. Hahn, Comput. Phys. Commun. **140**, 418 (2001), hep-ph/0012260.

[101] T. Hahn and C. Schappacher, Comput. Phys. Commun. **143**, 54 (2002), hep-ph/0105349.

[102] FeynArts is publically available at http://www.feynarts.de/.

[103] T. Hahn and M. Perez-Victoria, Comput. Phys. Commun. **118**, 153 (1999), hep-ph/9807565.

[104] T. Hahn, Comput. Phys. Commun. **178**, 217 (2008), hep-ph/0611273.

[105] T. Hahn and M. Rauch, Nucl. Phys. Proc. Suppl. **157**, 236 (2006), hep-ph/0601248.

[106] FormCalc is publically available at http://www.feynarts.de/formcalc.

[107] F. Bloch and A. Nordsieck, Phys. Rev. **52**, 54 (1937).

[108] B. W. Harris and J. F. Owens, Phys. Rev. **D65**, 094032 (2002), hep-ph/0102128.

[109] L. J. Bergmann, *Next-to-leading log QCD calculation of symmetric dihadron production*, PhD thesis, Florida State University, Florida, USA, 1989.

[110] S. Dittmaier, Nucl. Phys. **B565**, 69 (2000), hep-ph/9904440.

[111] I. Wolfram Research, Mathematica edition: Version 7.0, 2008.

[112] LHC/LC Study Group, G. Weiglein *et al.*, Phys. Rept. **426**, 47 (2006), hep-ph/0410364.

[113] S. Heinemeyer *et al.*, ECONF **C0508141**, ALCPG0214 (2005), hep-ph/0511332.

[114] P. Garcia-Abia and W. Lohmann, Eur. Phys. J. direct **C2**, 2 (2000), hep-ex/9908065.

[115] K. Desch and N. T. Meyer, LC-PHSM-2001-025.

[116] G. Belanger *et al.*, Nucl. Phys. Proc. Suppl. **116**, 353 (2003), hep-ph/0211268.

[117] H. Eberl, W. Majerotto, and V. C. Spanos, Phys. Lett. **B538**, 353 (2002), hep-ph/0204280.

[118] H. Eberl, W. Majerotto, and V. C. Spanos, Nucl. Phys. **B657**, 378 (2003), hep-ph/0210038.

[119] T. Hahn, S. Heinemeyer, and G. Weiglein, Nucl. Phys. **B652**, 229 (2003), hep-ph/0211204v2.

[120] W. Kilian, M. Kramer, and P. M. Zerwas, Phys. Lett. **B373**, 135 (1996), hep-ph/9512355.

[121] M. S. Carena, S. Heinemeyer, C. E. M. Wagner, and G. Weiglein, Eur. Phys. J. **C26**, 601 (2003), hep-ph/0202167.

[122] Tevatron Electroweak Working Group, (2008), arXiv:0803.1683 [hep-ex].

[123] A. D. Martin, R. G. Roberts, W. J. Stirling, and R. S. Thorne, Eur. Phys. J. **C39**, 155 (2005), hep-ph/0411040.

[124] A. D. Martin, R. G. Roberts, W. J. Stirling, and R. S. Thorne, Phys. Lett. **B531**, 216 (2002), hep-ph/0201127.

[125] HEPDATA, http://durpdg.dur.ac.uk/hepdata/.

[126] A. Bredenstein, A. Denner, S. Dittmaier, and M. M. Weber, Phys. Rev. **D74**, 013004 (2006), hep-ph/0604011.

[127] A. Bredenstein, A. Denner, S. Dittmaier, and M. M. Weber, JHEP **02**, 080 (2007), hep-ph/0611234.

[128] CERN press release PR13.09, 6 August 2009.

[129] M. S. Carena, J. R. Ellis, A. Pilaftsis, and C. E. M. Wagner, Phys. Lett. **B495**, 155 (2000), hep-ph/0009212.

[130] ALEPH, S. Schael *et al.*, Eur. Phys. J. **C47**, 547 (2006), hep-ex/0602042.

[131] B. C. Allanach *et al.*, Eur. Phys. J. **C25**, 113 (2002), hep-ph/0202233.

[132] A. D. Martin, R. G. Roberts, W. J. Stirling, and R. S. Thorne, Eur. Phys. J. **C28**, 455 (2003), hep-ph/0211080.

[133] M. Rauch, private communication.

[134] B. C. Allanach, Comput. Phys. Commun. **143**, 305 (2002), hep-ph/0104145.

[135] J. Alwall *et al.*, JHEP **09**, 028 (2007), arXiv:0706.2334 [hep-ph].

[136] D. Green, (2005), hep-ex/0502009.

[137] CompHEP, E. Boos *et al.*, Nucl. Instrum. Meth. **A534**, 250 (2004), hep-ph/0403113.

[138] A. Pukhov *et al.*, (1999), hep-ph/9908288.

[139] H. Chehime and D. Zeppenfeld, Phys. Rev. D **47**, 3898 (1993).

[140] D. Rainwater, R. Szalapski, and D. Zeppenfeld, Phys. Rev. D **54**, 6680 (1996).

[141] G. Gounaris *et al.*, (1996), hep-ph/9601233.

[142] J. Ellison and J. Wudka, Annual Review of Nuclear and Particle Science **48**, 33 (1998).

[143] K. Hagiwara, S. Ishihara, R. Szalapski, and D. Zeppenfeld, Phys. Rev. D **48**, 2182 (1993).

[144] SPS points, low energy parameters, http://www.ippp.dur.ac.uk/ georg/sps/.

[145] A. Denner, H. Eck, O. Hahn, and J. Küblbeck, Nuclear Physics B **387**, 467 (1992).

[146] A. Buckley, The hepthesis latex class.

[147] Available from the gnuplot homepage, www.gnuplot.info.

[148] Available from the Compare homepage, www.freacafe.de/compare.

[149] Available from the ROOT homepage, http://root.cern.ch/drupal/.

List of figures

List of tables